MASS TRANSFER CHARACTERISTICS OF TWO-AQUEOUS-PHASE LIQUID-LIQUID MIXTURES

HAMDAN AL-ANZI

Doctor of Philosophy

Chemical Engineering Department

The University of Aston

May, 1998

Mass Transfer Characteristics of Two-Aqueous-Phase Liquid-Liquid Mixtures

Doctor of Philosophy **Hamdan Al-Anzi** **1998**

SUMMARY

Two-aqueous-phase liquid-systems are used in the extraction and separation of biological materials. The most common system, with the potential for large scale application, consists of combinations of a polymer solution (polyethylene glycol) and a salt solution (dipotassium hydrogen ortho-phosphate) in water, which spontaneously separate into two phases. The overall aim of the author's research was to investigate the physical and mass transfer properties of such two-aqueous-phase liquid systems. The liquid-liquid system studied was PEG (polyethylene glycol) and salt (potassium hydrogen orthophosphate) in water.

The variation in viscosities, densities and interfacial tensions were determined for various concentrations of the two aqueous phase liquids. A notable feature was the low interfacial tension (i.e. from 1.28×10^{-4} to 1.11×10^{-3} N/m).

The manner in which settling rates of the dispersed phase were affected by the phase compositions and volumes was studied in batch tests. The settling rate was found to increase as the concentration of salt and polymer in the phases was increased. A fine haze was observed in both phases after sedimentation; this only cleared after a period of several days.

Mass transfer rates were studied using the falling drop method. Cibacron Blue 3 GA dye was the transferring solute from the salt phase to the PEG phase. Measurements were undertaken for several concentrations of the dye and the phase-forming solutes and with a range of different drop sizes, e.g. 2.8, 3.0 and 3.7 mm. The dye was observed to be present in the salt phase as finely dispersed solids but a model confirmed that the mass transfer process could still be described by an equation based upon the Whitman two-film model. The overall mass transfer coefficient increased with increasing concentration of the dye. The apparent mass transfer coefficient ranged from 1×10^{-5} to 2×10^{-4} m/s. Further experiments suggested that mass transfer was enhanced at high concentration by several mechanisms. The dye was found to change the equilibrium composition of the two phases, leading to transfer of salt between the drop and continuous phases. It also lowered the interfacial tension (i.e. from 1.43×10^{-4} N/m for 0.01% w/w dye concentration to 1.07×10^{-4} N/m for 0.2% w/w dye concentration) between the two phases, which could have caused interfacial instabilities (Marangoni effects). The largest drops were deformable which resulted in a significant increase in the mass transfer rate.

Drop size distribution and Sauter mean drop diameter were studied on-line in a 1 litre agitated vessel using a laser diffraction technique. The effects of phase concentration, dispersed phase hold-up and impeller speed were investigated for the salt-PEG system. An increase in agitation speed in the range 300 rpm to 1000 rpm caused a decrease in mean drop diameter, e.g. from 50 μm to 15 μm. A characteristic bimodal drop size distribution was established within a very short time. An increase in agitation rate caused a shift of the larger drop size peak to a smaller size. The minimum time required for the system to reach drop breakage steady state depended upon the Weber number of the main flow. An increase of agitation rate caused a reduction in the minimum transient time e.g. from one hour to 15 minutes. Dispersed phase hold-up had a very small effect within the range studied. System concentration had a big influence on drop size and size distribution.

Significant findings are highlighted, notably, the relatively short time to achieve a primary break of a dispersion, the extreme complexity of the mass transfer process, and the importance of temperature control.

Key Words
Liquid-liquid extraction, mass transfer in two aqueous phase systems, drop size distribution.

This thesis is dedicated to my family

ACKNOWLEDGMENTS

The author is greatly indebted to, and expresses his gratitude to, Dr. E. L. Smith for his supervision, encouragement, motivation, guidance, continual help and constructive criticism throughout the period of this research and compilation of the thesis. The author values highly the opportunity to have worked with such a stimulating individual.

The author is greatly indebted to and expresses his gratitude to Dr. C. J. Mumford for his guidance, constructive criticism, help and valuable suggestions.

The author wishes to thank the entire technical support staff of the Department of Chemical Engineering & Applied Chemistry, and the Chemistry Department at the University of Birmingham for conducting the mass spectroscopy.

This work was initiated by Dr I.P.T. Moore of the Department of Chemical Engineering, University of Birmingham. Thanks are due to him, and to all the staff of that Department, for their help during the early sections of the project.

Finally, thanks are due to the Government of Kuwait and the PAAET for sponsoring my studies.

CONTENTS

1. **Introduction** 18

1.1 Background 18

1.2 Project aim 19

2. **Two-Aqueous-Phase Liquid-Liquid Systems** 23

2.1 Process background 23

2.2 Properties determining the partition behaviour of proteins 25

2.3 Phase diagrams 28

2.4 Scale-up considerations 30

2.5 Batch settling of liquid-liquid dispersions 31

2.5.1 Phase separation characteristics 33

2.5.2 Behaviour of dispersions with sedimentation and dense-packed zones 34

2.6 Mass transfer in liquid-liquid extraction 36

2.6.1 Diffusion and mass transfer 36

2.6.1.1 Continuous phase mass transfer 38

2.6.1.2 Dispersed phase mass transfer 40

2.6.2 Interfacial phenomena and mass transfer 41

2.6.2.1 Ordered interfacial convection 42

2.6.2.2 Disordered interfacial convection 44

2.6.3 Effect of surfactants 45

2.6.4 The effect of interfacial turbulence on mass transfer 45

2.7 Drop size and size distribution 48

2.7.1 Correlations for drop size distribution 49

2.8 Conclusions 56

3. The Physical Properties of Two-Aqueous Phase Liquid-Liquid Systems 57

3.1 Preparation of the phase systems 57

3.2 Phase diagram 59

3.2.1 The construction of the binodal curve 59

3.2.2 The positioning of the tie-lines 60

3.3 Viscosity measurement 63

3.4 Temperature 66

3.5 Density measurement 68

3.6 Interfacial tension 69

4. The Effect of Phase Composition and Volume Ratios on the Settling Times of Two Aqueous-Phase Dispersions 72

4.1 Experimental methods and materials 72

4.2 Results and theoretical analysis 73

4.2.1 Characteristics of batch dispersion 74

4.2.2 Thickness of dense packed layer 76

4.2.3 Sigmoidal batch decay 78

4.2.4 Sedimentation height and drop growth 78

4.3 Batch decay experiments with the two-aqueous-phase dispersions 79

4.3.1 Settling curves 80

4.3.2 Primary break-time 84

4.3.3 Rate of sedimentation 84

5. **Mass Transfer from Single Drops** 92

5.1 Introduction 92

5.2 Experimental methods and materials 92

5.3 Theoretical methods and results 96

5.4 Discussion of the results 101

6. **Drop Size Distribution in an Agitated Vessel** 117

6.1 Introduction 117

6.2 Experimental investigation and equipment design 120

6.3 Equipment 122

6.3.1 Mixing vessel 122

6.3.1.1 Mixing vessel design I 122

6.3.1.2 Mixing vessel design II 126

6.3.2 Light scattering equipment 131

6.4 General procedure 136

6.4.1 Vessel preparation 136

6.4.2 Preparation of the phases 136

6.4.3 Filling of the vessel 136

6.4.4 De-aeration 137

6.5 Experimental procedure 137

6.6 Experimental program 138

6.6.1 Determination of time to steady state 138

6.6.2 Determination of the effect of stirrer speed 138

6.6.3 Determination of the effect of dispersed phase concentration 139

6.6.4 Determination of the effect of mixture composition 139

6.7 Experimental results 140

6.7.1 An overview 140

6.7.2 Drop size distribution 142

6.7.3 Time to steady-state 145

6.7.4 Reproducibility 146

6.7.5 Nature of the distributions 147

6.7.6 Volume, surface and number density distribution 148

6.7.7 Limitation of the operating range 150

6.8 Discussion of results 151

6.8.1 Sauter mean drop diameter 151

6.8.2 Data analysis 157

6.8.2.1 Correlation for the steady-state mean drop size 157

6.8.2.2 Time effect 161

6.8.2.3 d_{32} and d_{max} 162

6.8.2.4 Range of *We* and Re numbers 162

6.8.2.5 Drop size and scale of turbulence 163

6.8.2.6 Relative influence of viscosity and interfacial tension 166

7. Conclusions 169

7.1 Basic conclusions 169

7.1.1 Development of experimental technique 171

7.1.2 Significance of the work 172

8. **Application to Design** 173

9. **Suggestions for Future Work** 175

9.1 Additional studies 175

9.2 Application of techniques 175

References 177

Appendices 183

Appendix 1 Constants for the calculation of the viscosity for the Contraves double-gap measuring system. 183

Appendix 2 Constants for the calculation of the viscosity for the Contraves co-axial measuring system. 184

Appendix 3 Density of water at various temperatures 185

Appendix 4 Values of S=1/H, for the range from 0.33 to 0.66 186

Appendix 5 Values of S=1/H, for the range from 0.66 to 1 187

Appendix 6 Drop size distributions for various phase compositions, volume fractions and agitation speed 188

Appendix 7 Calculation of the power input per unit mass , ε , and the eddy length scale 257

Appendix 8 Power number as a function of Reynolds number for a turbine mixer 258

Publications 259

List of Tables

Table 2-1 Mean drop sizes and their application 48

Table 2-2 Correlation to predict the Sauter mean drop diameter $\bar{d}_{vs}$ 55

Table 3-1 The physical properties of the two aqueous phase systems used 66

Table 4-1 Influence of phase composition and volume ratios on break-time 85

Table 4-2 The slopes and intercepts of the line for both experiments I and II 86

Table 4-3 Rate of sedimentation comparing Stokes law and experimental data 87

Table 4-4 The slope $(1+\alpha)$ 91

Table 5-1 Interfacial tension versus dye concentration at 24 °C 107

Table 6-1 The effect of phase concentration on the slope of log d_{32} versus log N 165

List of Figures

Figure 2-1 Typical phase diagram with the tie-lines for potassium phosphate and PEG. (Data from Albertsson, 1986) 26

Figure 2-2 General phase diagram for two-aqueous phase systems 29

Figure 2-3 Typical phase diagram for (a) dextran and PEG (b) Potassium phosphate and PEG 30

Figure 2-4 Settling curve showing dispersion height changes with time 34

Figure 2-5 Schematic diagram of how the dispersion height varies during the sedimentation process 35

Figure 2-6 Diagram to illustrate the two-film theory 37

Figure 2-7 Diagram to illustrate the formation of convection cells 42

Figure 2-8 Diagram illustrating the eruption mechanism 45

Figure 3-1 Calibration curve for various salt concentrations versus conductivity 61

Figure 3-2 Binodal curve for K_2HPO_4 and PEG. 64

Figure 3-3 Viscosity measuring system (a) co-axial (b) double gap 65

Figure 3-4 Influence of temperature and phase composition on viscosity of PEG 67

Figure 4-1a Sketch of settling process 74

Figure 4-1b Typical settling curve for PEG/ salt system 75

Figure 4-2 Schematic illustration (a) Sigmoidal decay (b) Exponential decay 76

Figure 4-3 Settling curves for various compositions and volume ratios (Exp. I) 81

Figure 4-4 Settling curves for various compositions and volume ratios (Exp. II) 82

Figure 4-5 Variation of ln(x_0-x) with the sedimentation front for phase system salt/PEG with volume ratios 250 salt /(150-250) PEG 83

Figure 4-6 An overlay of ln (x_0-x) versus ln (t) for 20, 25, 30 %w/w phase systems 85

Figure 4-7 Rate of sedimentation for the experimental data 89

Figure 4-8 A typical photograph for the settling behaviour (a) before settling (b) after settling 90

Figure 5-1 Calibration curves; dye concentration versus absorbance 95

Figure 5-2 Mass transfer coefficient, K, versus dye concentration for 25 %w/w system 100

Figure 5-3 Mass transfer coefficient, K, versus dye concentration for 30 %w/w system 100

Figure 5-4 Spectrum for PEG and PEG + dye 105

Figure 5-5 Spectrum for PEG + dye a week later 106

Figure 5-6 Salt drops circulating inside (dye / PEG) drop 112

Figure 5-7 Apparent mass transfer coefficient, k_0, versus dye concentration for 25 % w/w 113

Figure 5-8 Apparent mass transfer coefficient, k_0, versus dye concentration for 30 % w/w 113

Figure 5-9 Drop internal motion. 115

Figure 5-10 Droplet behaviour following break-up. 116

a) Smaller drop within influence of wake of remaining large drop 116

b) Smaller drop behaviour independent of the remaining drop 116

Figure 6-1 Mixing vessel design I 125

Figure 6-2 Mixing vessel design II 129

Figure 6-3 Equipment 132

Figure 6-4 The effect of agitation speed, phase composition and hold-up on drop size d_{32} 141

Figure 6-5 Typical example of the drop size distribution for Salt-PEG system 143

Figure 6-6 Distribution change from trimodal to bimodal as a result of the increase of the impeller speed 144

Figure 6-7 The spread of drop size distributions (demonstrating a reduction in size as well as sharper peaks as the impeller speed increases) 144

Figure 6-8 Reproducibility of a 25 % w/w phase composition at 800 rpm 146

Figure 6-9 Reduction of distribution as a result of the increase in agitation speed 147

Figure 6-10 Volume, surface, diameter and number density distribution 149

Figure 6-11A The effect of impeller speed on drop size distribution i) 400rpm, ii)500rpm 153

Figure 6-11B The effect of impeller speed on drop size distribution iii) 600rpm,iv)700rpm 154

Figure 6-11C The effect of impeller speed on drop size distribution v) 800rpm, vi)900rpm 155

Figure 6-11D The effect of impeller speed on drop size distribution vii) 1000 156

Figure 6-12 Speed spectrum from 400-1000 rpm and the effect on the distribution 156

Figure 6-13 The effect of Weber number N_{we} on Sauter mean drop diameter d_{32} 158

Figure 6-14 Comparison of experimentally determined d_{32} values with those predicted by equation 6-2 159

Figure 6-15 Comparison plot for the theoretical correlation and other workers correlations 160

Figure 6-16 Plots of log d_{32} vs. Log N 166

List of Photographs

Photograph 6-1	Design I for the mixing vessel	124
Photograph 6-2	Ring to accommodate the lid of the vessel	127
Photograph 6-3	Lid of the mixing vessel	128
Photograph 6-4	Design II for the mixing vessel	130
Photograph 6-5	Mixing vessel design II from top view off-centre	133
Photograph 6-6	Cooling-heating unit (Malvern monitor displaying distribution in background)	134
Photograph 6-7	Experimental set-up for the laser diffraction, rig and the vessel (Emitter on left, mixing vessel, receiver on right; display on monitor)	135

Nomenclature

A	Surface area of the drop	[m^2]
a	Surface area of particles in the surface of the drop	[m^2]
b	Index for coalescence	[-]
c	The molar concentration of the solute	[mol/m^3]
c_d	Concentration of the dye in the dispersed phase	[% w/w]
c_c	Dye concentration in the continuous phase	[% w/w]
c_{ci}	Dye concentration in the continuous phase at the interface	[% w/w]
c_{di}	Dye concentration in the dispersed phase at the interface	[% w/w]
c_0, c_f	Initial and final dye concentrations in the drop	[% w/w]
C_T, C_B	Equilibrium concentrations of the partitioned compound in the top and bottom phases respectively	[mol/m^3]
c^*	Solubility of the dye in the continuous phase	[% w/w]
c'_d	Concentration of particles in the drop	[m^{-3}]
d	Diameter of the drop	[m]
d_e	Maximum diameter of the drop	[m]
d_s	Diameter of a selected cross-sectional plane located at a distance equal to d_e along the axis from the apex of the drop	[m]
d_d	Diameter of the drop in the dispersed phase	[m]
d_i	Particle diameter	[m]
$\bar{d}_{vs}$	Sauter Mean Drop Diameter (see pages 48-55)	[m]
d_{32}	Sauter Mean Drop Diameter	[m]
D	Diffusivity of the solute in the liquid	[m^2/s]
D_c	Solute diffusivity in the continuous phase	[m^2/s]
D_I	Diameter of the impeller	[m]
H	Dimensionless shape factor	
h	Dispersion height at time t	[cm]

h_s	Height of the sedimentation zone	[cm]
h_p,	Height of the dense-packed zone	[cm]
J	The flux of the solute	[m/s][%w/w]
j	Number of batches using the same continuous phase	[-]
K_m	Partition coefficient (see p. 25)	[-]
K	Overall mass transfer coefficient	[m/s]
k_c, k_d	Mass transfer film coefficient	[m/s]
k_s	Constant (Equation 4-8)	[-]
K	Constant (Equation 5-4)	[-]
k_0	Apparent mass transfer coefficient	[m/s]
m	Partition coefficient	[-]
m_0	Mass of the empty bottle	[g]
m_1	Mass of the density bottle filled with the sample	[g]
n	An exponent and empirical constant which depends on the drop Reynolds number	[-]
n_i	Number of drops counted in each batch experiment using the same continuous phase	[-]
n_i	Number of particles in the surface layer of a drop (Equation 5-16)	[-]
N	Rate of mass transfer	[m^3/s] [%w/w]
N	Total number of particles in the drop	[-]
N_{vi}	Tank viscosity group	[-]
r	A parameter in equation 4-11 and a function of Re	[-]
Re	Reynolds number $d_d U / \nu_c$	[-]
S	Amount of dye transferred to the continuous phase	[g]
S	The ratio of d_s/d_e	[-]
Sh_c	Sherwood number $k_c d_d / D_c$	[-]
Sc_c	Schmidt number ν_c / D_c	[-]
t	Time	[minutes]
U	Relative droplet velocity	[m/s]
V	Drop volume	[cm^3]

V_s	The settling velocity	[cm/min]
V_t	Volume of the sample in the density bottle at temperature (t)	[ml]
We_I	Impeller Weber Number $N^2D^3\rho_c / \sigma$	[-]
x	The coordinate normal to the area A.	
x	Height of the sedimenting interface relating to the final interface	[cm]
x_0	Initial height of the sedimenting interface	[cm]
y	Height of the coalescing interface relating to the final interface	[cm]
y_0	Initial height of the coalescing interface	[cm]

Greek Symbols

α	Exponent in the sedimentation rate equation (Equation 4-11)	[-]
δ_d, δ_c,	Thickness of the film in the dispersed and continuous phase	[m]
ε	Power input per unit mass	[W/kg]
$\bar{\varepsilon}$	Instantaneous hold-up fraction of the dispersed phase for the entire dispersion	[-]
$\bar{\varepsilon}_s$	Dispersed phase hold-up fractions in the sedimentation zone	[-]
$\bar{\varepsilon}_p$	Dispersed phase hold-up fractions in the dense-packed zone	[-]
μ	Viscosity	[mPa.s]
ν_c	Kinematic viscosity of the continuous phase	[cm^2/s], Stokes (St)
$\rho_{H_2O,t}$	Density of water	[kg/m^3]
ρ	Density	[kg/m^3]
ρ_d	Density of the dispersed phase	[kg/m^3]
ρ_l	Density of the continuous phase	[kg/m^3]
ρ_s	Density of the solid particles	[kg/m^3]
$\Delta\rho$	Density difference between the liquid used to form the drop and the continuous liquid	[kg/m^3]
σ	Interfacial tension	[N/m]
ϕ	Volume fraction of the dispersion	[-]

1. Introduction

1.1 Background

When two immiscible liquids are mixed in a stirred tank, one of the liquids normally breaks-up to form droplets suspended in the other liquid. The liquid which is in the form of droplets is termed the dispersed phase, and the continuum liquid is known as the continuous phase. Two-aqueous-phase liquid-liquid systems comprise immiscible liquid pairs in which both liquids are aqueous solutions, although of differing composition.

Aqueous two phase systems contain a high proportion of water (65-90%); they possess a very small density difference (e.g. 27 kg/m^3) and a low interfacial tension (1 x 10^{-4} - 1 x 10^{-5} N/m); this provides a favourable environment for enzymes, biologically-active proteins, cell and cell organelles (Kula,1982). They have found a number of applications in the extraction of biological products, notably protein materials, which may be sensitive to damage by the organic solvents used in conventional solvent extraction. Most of the studies reported in the literature (Hustedt et al, 1985, Kula, 1985) concentrate on the selectivity of the systems for particular product molecules, and there is very little information on either the physical properties of the mixtures or on mass transfer rates between the phases.

Typical two-aqueous-phase systems comprise combinations of polyethylene glycol (PEG) and dextran or a salt (K_2HPO_4), which spontaneously separate into two phases. The salt-rich phase is generally of lower viscosity than the PEG, which implies both a low power requirement to disperse the PEG phase and good mass transfer by diffusion in the salt solution. However, mass transfer in the PEG phase will be very much

slower and may be limiting if, as is common practice, transfer is carried out from the dispersed to the continuous phase. If the salt-rich phase is dispersed in the PEG phase, the difficulties are compounded by the increased viscosity of the PEG, which increases the power required to form the dispersion. The settling time also increases, which makes subsequent separation more difficult.

It is apparent that the dispersions form very readily, resulting in extremely small drop sizes, as a consequence of the very low interfacial tension between the phases. Thus interfacial area, which is normally a limiting factor in solvent extraction processes and which is the main factor in determining the power input necessary, will not be a problem in two-aqueous phase systems. However, separation of the phases is known to be a difficult problem, due to the small droplets, and this can cause great difficulties on scale-up if gravity settling is relied upon.

Two-aqueous phase liquid-liquid systems have been known and used for about 30 years (Verrall, 1992). They can be employed on a pilot plant scale using scaled-down industrial equipment and there appears to be no major technical obstacle to production-scale use. The problems are associated with the lack of knowledge of the physical properties, settling rate behaviour and mass transfer properties of the two aqueous phase systems.

1.2 Project aim

The aim of this project was to study the physical properties, settling rates and mass transfer properties of some of the two-aqueous-phase liquid-liquid systems. The first stage was to investigate the physical properties of the two phases, since these are important parameters in determining the dispersion behaviour. Prior to any studies on

the dispersion, the ranges of the physical properties of the phases were determined. The interfacial tension between the two liquid phases was measured using the pendant drop method. A binodal curve representing the equilibria of the two separated phases in a three component system with distilled water was constructed and the weight fraction of PEG versus the weight fraction of K_2HPO_4 plotted; the tie-lines were then found for the system used.

The viscosities of PEG and K_2HPO_4 solutions were measured for the various mixture compositions using 20 % w/w, 25 % w/w and 30 % w/w. The effect of temperature on the viscosity of the PEG phase was studied over a range of temperatures (i.e. 15°C to 30 °C).

The second stage was to investigate the settling rates of the dispersed phase in the PEG/salt liquid-liquid system and to determine how the rate changed with the composition of the phases, since the most common limiting step in the application of two-aqueous-phase systems to industrial extraction processes is the settling and separation of the two phases. As already noted, two-aqueous phase systems have very low interfacial tensions and generally produce small droplet sizes. As a result of this, and the small density difference between the two phases, separation of the phases would be expected to be difficult. The problem of phase separation is known to be a significant limitation (Nadiv et al, 1995) on the application of other liquid-liquid extraction processes in industry even where relatively large interfacial tension systems and visible drop-sizes are involved.

The third stage was to study the mass transfer between the two phases. To develop further an understanding of the mass transfer process by which solute is transferred during liquid-liquid extraction, an investigation was undertaken into the process of

extraction from single drops passing through a stationary column of solvent. The investigation of mass transfer in two-aqueous-phase systems used a coloured dye as analogue for typical biological solutes. Since the solute used was more soluble in the PEG phase than the salt phase, the experiments were carried out with a salt-in-PEG system where the salt phase was the dispersed phase and the PEG was the continuous phase using the falling drop or single drop method. The dye solute was chosen to give good partition properties to mimic, as far as possible, the properties of typical biological solutes. The measurements were all undertaken with the same two-aqueous-phase system, using various solute and phase concentrations.

Drop size distributions are an important characteristic of liquid-liquid dispersions, the physical and chemical phenomena taking place in an agitated vessel largely depending on the size of the dispersed droplets. For processes such as mass transfer, it is essential that the size distribution of the droplets, and usually some mean size can be estimated to enable the mass transfer rate to be predicted.

Several methods for the measurement of drop size distribution i.e. photographic technique, light transmission, conductivity (Coulter Electronic Counter) and light diffraction have been used by previous researchers. The photographic technique uses a microscopic camera to take a picture of the dispersion; the number of drops counted is usually about 100 for statistical reasons. The actual determination of drop sizes by the photographic technique may result in significant error especially for small drops that cannot be distinguished very clearly, as described by Chatzi et al., 1989, Chatzi et al., 1991 and Mlyneck and Resnick, 1972. The Coulter counter is an instrument which determines both the number and size of drops in an emulsion as it passes through a

small aperture between two electrodes. The resistance between the electrodes changes as a particle goes through the aperture and this change is converted to a voltage pulse in the instrument (Sprow, 1966). The light diffraction technique offers a short measuring time and permits on-line analysis with minimal possible instrumental, sampling and dispersion errors (Chatzi et al., 1991). The latter method was employed because of its accuracy, and reproducibility, and the ability of the instrument to measure a very small drop (~ 1 μm) in the dispersion. It also facilitated on-line measurement.

Several publications dealing with experimental measurements of drop size in stirred liquid-liquid systems have been reported in the literature, (Laso et. al., 1987). However, most investigations refer to systems with a high interfacial tension, i.e. in the range 0.01 -0.1 N/m and a high density difference between the phases.

In the present study the dispersion process has been studied in the essential absence of interdrop coalescence by working at very small dispersed phase fractions. A laser diffraction technique was used for the on-line measurement of the drop size distribution in an agitated vessel for salt / PEG dispersion systems. Drop size distributions were measured as a function of agitation speed, physical properties of the system and the dispersed phase hold-up. The temperature of the system studied was kept constant throughout the investigation. A theoretical treatment based on the theory of isotropic turbulence is used to correlate the data.

Finally consideration has been given to the significance of the results for the selection of practical two-aqueous-phase liquid-liquid systems and to equipment design.

2. Two-Aqueous Phase Liquid-Liquid Systems

2.1 Process background

Various liquid-liquid extraction techniques are used in biotechnology. These include: high performance liquid chromatography (HPLC), use of liquid membranes and aqueous-organic or aqueous-aqueous two phase liquid extraction (Hustedt, 1985). However their application has been limited on an industrial scale.

Two-phase liquid-liquid extraction is applied in biotechnology mainly in two fields:

1. The extraction of low-molecular weight products, mainly antibiotics, from the fermentation broth (with or without prior biomass separation) using organic solvents, which may also include carriers.

2. The extraction of proteins, mainly intracellular enzymes but also extracellular enzymes, as well as animal cell culture proteins, by using aqueous two-phase systems, which are mainly based on polyethylene glycol (PEG) and salts or dextran (Hustedt, 1986).

Liquid-liquid partition is commonly employed in biochemistry for the separation of proteins and nucleic acids in a phenol-water two phase system. However phenol, which is highly toxic, or other organic solvents will tend to denature proteins or will not dissolve proteins, so that partition in such systems is of very limited value for the purification of enzymes. Aqueous two phase systems do not have this disadvantage as they consist of up to 90% water (Kroner et.al, 1978).

Due to their very low interfacial tensions (e.g. 1×10^{-4} - 1×10^{-5} N/m), Albertsson (1971) suggests that two aqueous phase systems form a favourable environment for biologically-active proteins and cell organelles.

The results of the investigation by Kroner et al (1978) suggested that liquid-liquid separation is suited for large scale isolation of enzymes when large volumes have to be processed. Partition as a process is independent of the concentration of the desired product over a wide range. Therefore, the scale-up of a partition step can be calculated and accomplished with more precision and ease than the conventional steps in enzyme isolation and purification.

When mixed, polymer solutions, such as PEG and dextran, form two-phase systems which exhibit a variety of effects on biological material, particularly cells. Cell-cell aggregation, cell fusion, and a variety of effects on cell membrane properties have been documented for dextran and PEG under various conditions (Brooks et al., 1985).

Extractive enzyme purification using aqueous two phase systems is characterised by high capacity (the ability to handle large amounts of the materials to be separated), easy processing on any scale, high product yields, low capital investment costs, and a high potential for development as a continuous process. There is however a need to handle large volumes of chemicals (Brooks et al., 1985).

2.2 Properties determining the partition behaviour of proteins.

Partition coefficients

The partition of proteins and other compounds in aqueous two-phase systems is influenced by a number of parameters:

-the types of polymers composing the two-phase systems

- average molecular weight of the polymers

- molecular weight distribution of polymers

- length of the tie-line on the phase diagram

- pH

- temperature.

Most of these parameters do not act independently; therefore calculation or theoretical prediction of the partition coefficient for a given protein cannot be carried out at present. The effects of these parameters will be discussed in the following sections. Suitable conditions for a desired partition have to be found experimentally. The experimental reproducibility of partition coefficients is normally in the range of ±5% for any volume analysed (Kula, 1979).

The partition coefficient, K_m, is defined by equation (2-1)

$$K_m = \frac{C_T}{C_B} \qquad (2\text{-}1)$$

where C_T and C_B are the equilibrium concentrations of the partitioned compound in the top and bottom phases, respectively. The partition coefficient of enzymes is constant for a given system over a fairly wide range of phase concentrations, provided no association or dissociation of proteins takes place in one of the phases (Albertsson, 1971).

The length of the tie-line (see also Section 2.3)

The length of the tie-line (Figure 2-1) in any given system depends on the total concentration of the polymer/salt mixture and is a measure of the relative composition difference of the phases. When the tie-line length approaches zero, which is the critical point (c) on the phase diagram, the phase compositions should be identical and the partition coefficient for any third solute will be 1.

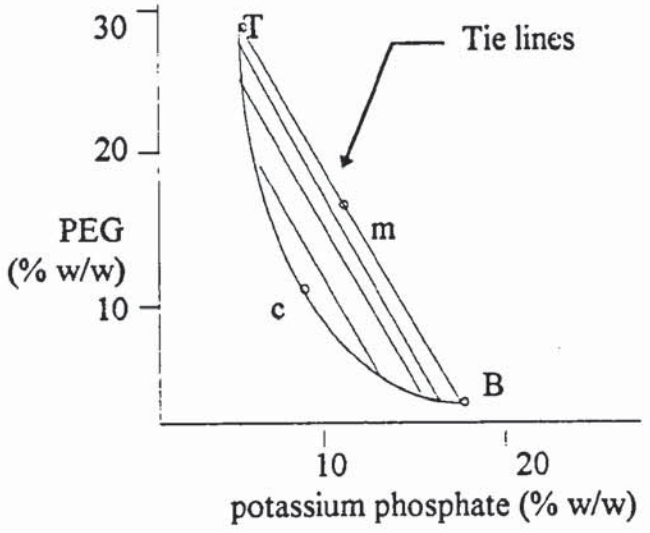

Figure 2-1 Typical phase diagram with the tie-lines for potassium phosphate and PEG. (Data from Albertsson, 1971)

The partition coefficient is equal to one if the system lies at the critical point (Figure 2-1). However, the partition coefficient deviates from one as the tie-line length increases and if the solute is a protein it may be shifted into the PEG-rich upper phase of a PEG/salt system (Kula, 1985).

pH dependence

The partitioning of a protein depends upon the pH of the system. The variation of partition coefficient of the protein in a specific system, and over a particular pH range, is influenced by the ionic composition. Altering the pH changes the net charge on the protein from positive at low values, to negative at high values of pH. At a certain pH the net charge of the protein is zero. This is the isoelectric point. It has been shown by Albertsson (1970) that at pH values very close to the isoelectric point the partition coefficient of a protein in a PEG/salt system is the same irrespective of the salt used (Johansson, 1985).

Temperature

The sensitivity of partition coefficients to changes in temperature is not very high. Large scale single stage extraction can be performed without extensive temperature regulation. Increases in temperature of 1 to 2°C in the liquid during processing have only negligible consequences for recovery of the desired protein and separation performance, provided the system is far enough from the binodal curve to ensure phase formation over this temperature interval (Kroner et al., 1978; Kula et al., 1981).

Large scale operations are usually carried out at ambient temperature (20°C) to avoid expenditure for cooling devices and energy. Two facts contribute to such desirable

operating conditions. The polymers introduced stabilise proteins and, in general, high activity yields are obtained when operating at ambient temperatures. In addition the viscosity of the dispersion will be lower at 20°C compared to 4°C, so improving the performance of the separation unit (Kula, 1985).

Polymers constituting the phase systems

Development of large scale extractions have been limited to date to systems consisting of polyethylene glycol with dextran or PEG with various non-toxic salts. Besides their general applicability, both systems are non-toxic and have been thoroughly tested and also registered for pharmaceutical and food purposes. This was a considerable advantage when developing the new technology, since most applications for enzymes and biologically active proteins were initially in the pharmaceutical and food industries. The use of other polymers to establish an aqueous phase system for the extraction of cell components is possible (Kula, 1982).

Ryden and Albertsson (1971) have measured the interfacial tension for various aqueous systems using the rotary drop method at the interface between phases and have shown that it is very small: $5x10^{-7}$- to 1 x 10^{-4} N/m. This prevents destruction of the biologically active compound due to surface denaturation at the liquid interface.

2.3 Phase diagrams

In a mixture of two polymers and water, a two-phase system will only arise when the constituents are present in a certain range of proportions. The constituent compositions at which phase separation occurs may be represented on a phase diagram. Figure 2-2 shows the concentration of polymer P plotted as the abscissa and

the concentration of polymer Q as the ordinate; the concentrations are expressed as weight per cent. The curved line separating the two areas of the plot is called a binodal curve. All mixtures which have compositions represented by points above the line give rise to phase separation, while mixtures represented by points below the line do not. Thus a composition represented by point A in Figure 1 gives a two-phase system, while a composition represented by point D gives a homogenous solution (Albertsson, 1971).

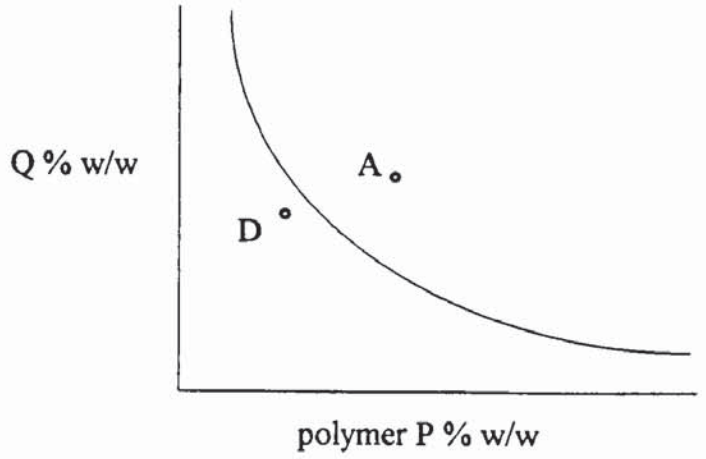

Figure 2-2 General phase diagram for two aqueous-phase systems (Albertsson, 1971).

Most polymers that are miscible with water will show phase separation in a mixture with a second polymer or with salts. Figure 2-3a shows an example of this behaviour in a commonly-used system. Polyethylene glycol (PEG) and dextran are separately miscible with water in all concentrations. However if certain concentrations are exceeded, phase separation takes place and a PEG-rich upper phase and dextran-rich lower phase are formed which are no longer miscible with each other, despite the fact that both phases contain a high proportion (more than 70%) of water (Kula, 1979).

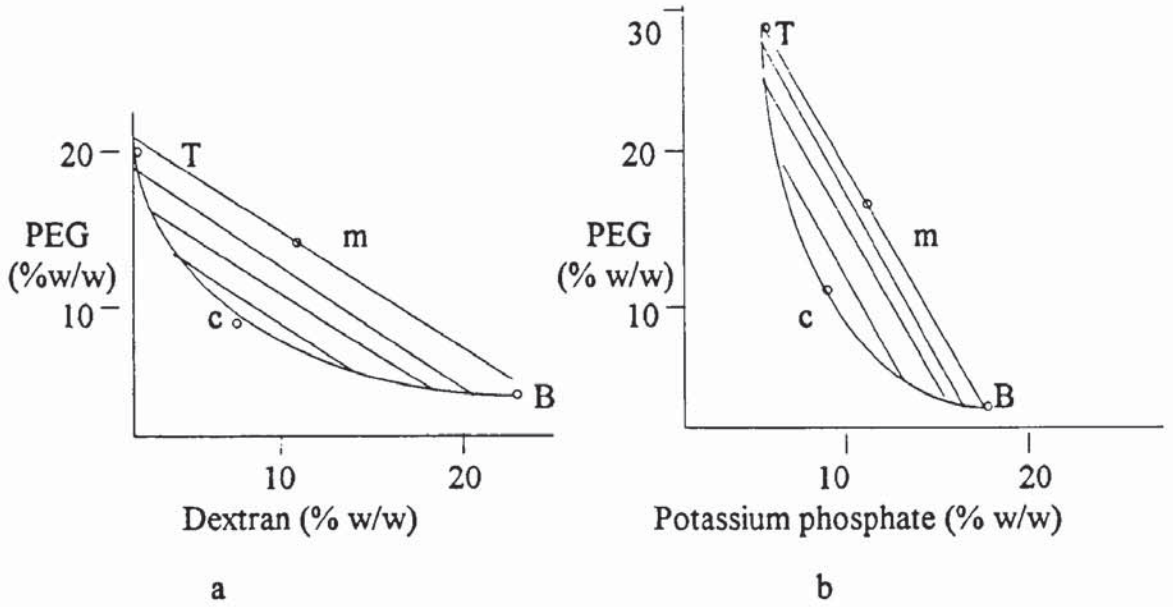

Figure 2-3 Typical phase diagram for (a) Dextran and PEG system and (b) Potassium phosphate and PEG. (Data from Albertsson, 1986)

Figure 2-3b shows similar behaviour observed with polyethylene glycol and a salt, potassium phosphate, in water. In Figure 2-3b the tie-lines connecting phase compositions on the binodal curve are steeper than for the previous system. All mixtures with compositions represented by points on the same tie-line from T through m to B will yield systems with identical compositions in the top and bottom phases but different phase volumes (Albertsson, 1986).

2.4 Scale-up considerations

Kula (1985) describes how the results of large scale separation processes could be accurately predicted from the partition coefficient of the enzyme and the volume ratio of the phase systems determined in laboratory experiments. Scale-up simply involves the linear extrapolation of concentration relative to the amount of cell homogenate included in the extraction system.

Since the enzyme or any other active protein stays in solution at all times, extraction lends itself to continuous processing. This approach represents an alternative to batchwise operation on a large scale and would allow, in addition, a decrease in process time and improve the productivity (Kula, 1985). The difficulty encountered to date in developing a continuous processing system is that large amounts of cells and material are required for experiments (Kula, 1985).

2.5 Batch settling of liquid-liquid dispersions

Liquid-liquid two phase dispersions are found in many industrial processes such as extraction of metal from solutions of their ores and removal of wax from lubricating oil (Slater, 1994). Irrespective of whether operation is stage-wise or continuous, solvent extraction is divided into two steps: firstly mixing of the two phases, secondly, separation into two bulk phases. Separation is normally carried out by settling under gravity. There are many parameters that affect this type of separation, such as the physical properties (viscosity, interfacial tension and density) of the phases. Other factors which affect the separation process are drop sizes and drop size distributions, the phase ratio, and deviation from equilibrium. In industrial systems impurities are frequently present that change the physical properties of the system; some may act as surfactants, resulting in smaller drops and inhibiting coalescence (Nadiv and Semiat, 1995).

The dispersion separation (or breaking) process usually consists of two steps, settling and coalescence of the drops, i.e. settling of the drop swarm is followed by flocculation, inter-drop coalescence and finally drop-interface coalescence. Settling by gravity depends on the drop size and the density difference between the two liquids in contact. An increase in density difference results in more rapid settling. Breaking (i.e. dispersion separation) in a batch settler can be divided into two periods: the primary break, which involves fairly rapid settling and coalescence of the majority of the dispersed phase, and may leave a fog (i.e. secondary dispersion) of very small droplets of the dispersed phase in the continuous phase; and the secondary break, which represents the slow settling of the fog. Most industrial settlers are designed for the primary break since the slow secondary break would require much longer residence times (Treybal, 1963) unless centrifugal separation, impingement aids or electrostatic forces are used.

In the separation process the drops sediment as they grow in size due to coalescence between the drops. Interdrop coalescence occurs when two drops are in contact for a sufficient period for the film of continuous phase to drain from between them. They then coalesce to form one drop. The coalescence in the separation process consists of two types: initially binary coalescence which takes place between the drops as they grow in size during settling, and then interfacial coalescence, i.e. coalescence of the large drops with their own bulk phase at the interface (Hartland, 1988).

Many authors have suggested that results from batch experiments of phase separation can be used in the design of continuous operations in order to reduce scale-up expenses.

Recently research has been undertaken by Nadiv and Semiat (1995). A physical model was suggested to allow better understanding of the liquid-liquid separation process. A mathematical model was developed to determine the relationship between final dispersion separation time, initial height of the dispersion and the initial dispersed phase hold-up. In this model there are four unknown parameters, which have to be determined from experimental data. The model was developed in order to analyse the results and to calculate parametric values such as sedimentation and coalescence velocities. However, in practice the physical properties, phase concentration, volume ratio and intensity and time of mixing also affect the separation process. In industrial situations the presence of traces of surfactants or interfacial scum may be crucial since both will retard the coalescence process.

Nadiv and Semiat (1995) concluded from their work that the overall separation time is strongly dependent on the initial dispersion height, the diameter of the batch settler, and the type of dispersion generated.

2.5.1 Phase separation characteristics

When a two-phase liquid-liquid dispersion, generated in a mixer, is poured into a cylindrical flask, the characteristic changes of dispersion height with time will be as shown in Figure 2-4. The height of the dispersion band is reduced with time until the end of the separation process, where the two layers are separated by a simple interface. The branches in Figure 2-4 describe the height of the two boundaries of the dispersion

band (Hartland and Jeelani, 1987). Since the height is plotted against time, the slopes of the lines represent the decay velocities of the two fronts.

2.5.2 Behaviour of dispersions with sedimentation and dense-packed zones

If a batch dispersion is formed in a mixing vessel and then allowed to settle, the dispersion height decreases with time due to sedimentation and interfacial coalescence. As the drops sediment, binary coalescence occurs; drops then accumulate in a thick layer (dense-packed zone) in which drop to drop (interdrop) coalescence is promoted. Finally the large drops coalesce with their homophase (own phase) at the coalescing interface (interfacial coalescence). Figure 2-4 shows a typical example of the dispersion height decaying with time, based on the author's work (see Chapter 4).

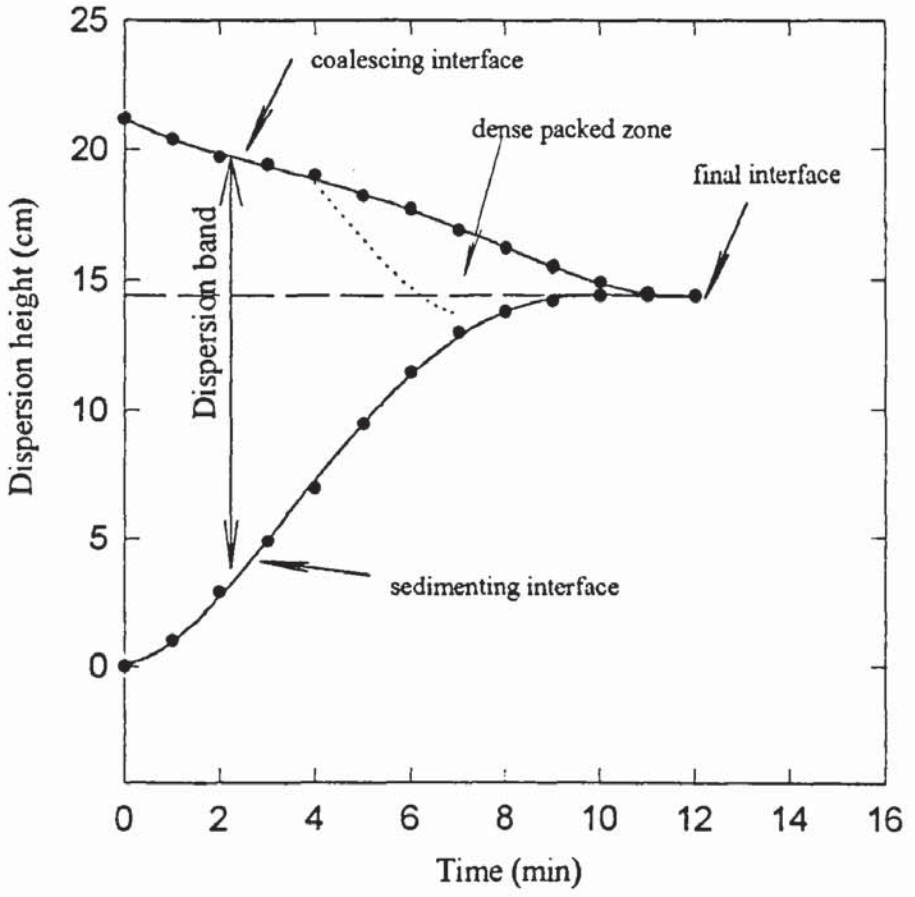

Figure 2-4 Settling curve showing dispersion height changes with time

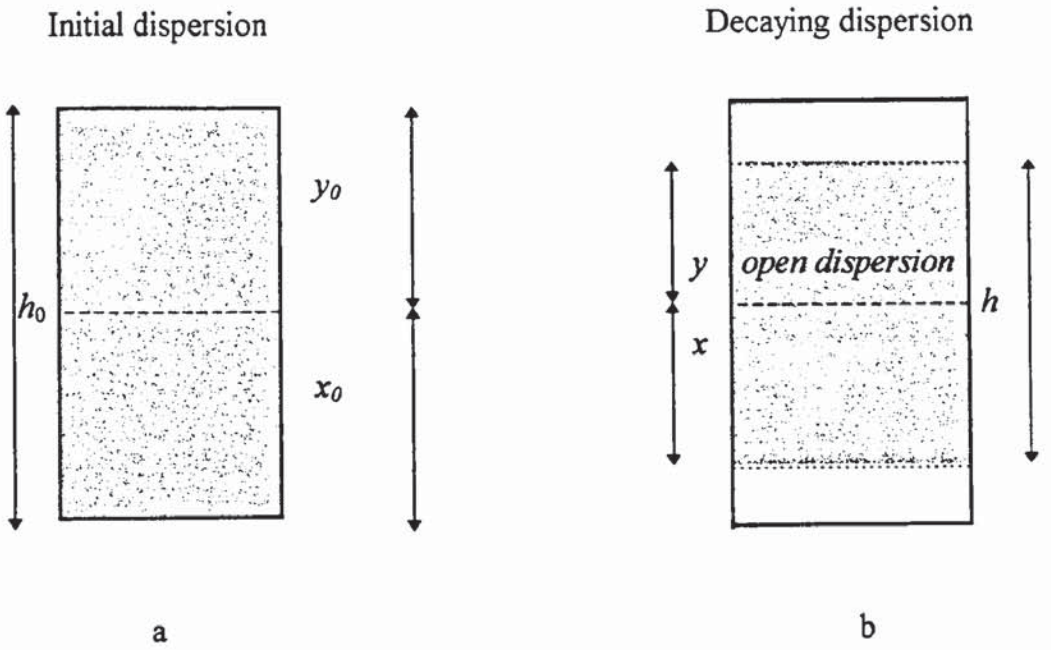

Figure 2-5 Schematic diagram of how the dispersion height varies during the sedimentation process.

The initial volume of the dispersion per unit area is equal to h_0 (Figure 2-5a), x_0 of the continuous phase and y_0 of the dispersed phase. The volume of the continuous phase per unit area in the open dispersion zone is equal to x. Therefore, as shown in Figure 2-5b, the volume of the continuous phase per unit area in the clear zone is equal to x_0-x. Similarly, the volume of the dispersed phase per unit area in the open dispersion (Figure 2-5b) is equal to y, and the dispersed phase hold-up $\bar{\varepsilon} = y / h$.

The volume rates of release of free continuous and dispersed phases per unit area in the open dispersion zone are given by the rate of sedimentation,-dx/dt, and the rate of coalescence, -dy/dt. The continuous and dispersed phase volumes are therefore proportional to x and y.

2.6 Mass transfer in liquid-liquid extraction

2.6.1 Diffusion and mass transfer

The flux of the solute J transferred across an area A in the case of unidirectional diffusion in a liquid at rest is given by Fick's first law (Bird *et al.* 1960).

$$J = -D\frac{dc}{dx} \tag{2-2}$$

where D is the diffusivity of the solute in the liquid, c is the concentration of the solute, and x is the coordinate normal to the area A.

When Fick's first law is applied to an interface between a dispersed and a continuous phase, the flux of the solute through the interface from the dispersed to the continuous phase is given, according to the two-film theory (Figure 2-6), as

$$J = k_d(c_d - c_{di}) = k_c(c_{ci} - c_c) \tag{2-3}$$

where k_d, k_c are the mass transfer coefficients of the solute in the dispersed and continuous phases, c_d, c_c are the solute concentrations in the bulk of the dispersed and continuous phases, and c_{di}, c_{ci} are the solute concentrations in the dispersed and continuous phases at the interface.

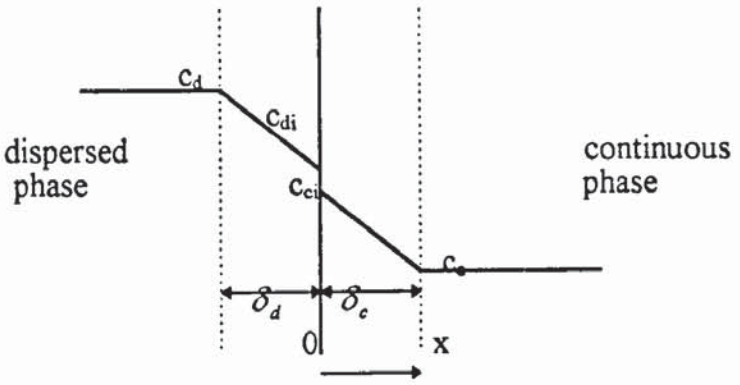

Figure 2-6 Diagram to illustrate the two-film theory

Whitman's theory (Schügerl, 1994) assumes equilibrium at the interface i:

$$m = \frac{c_{ci}}{c_{di}} \tag{2-4}$$

and that two stagnant films exist adjacent to the interface, of thickness δ_d and δ_c, in which mass transfer occurs only by molecular diffusion:

$$k_d = \frac{D_d}{\delta_d} \text{ and } k_c = \frac{D_c}{\delta_c} \tag{2-5}$$

Conveniently, c_{di}, c_{ci} can be eliminated from equation (2-3). This leads to

$$J = K(c_d - \frac{c_c}{m}) \tag{2-6}$$

where

$$\frac{1}{K} = \frac{1}{k_d} + \frac{1}{mk_c} \qquad (2\text{-}7)$$

The values of the individual dispersed and continuous phase film coefficients k_d and k_c have been shown to depend upon drop Reynolds number. For Re<10 the drops behave as rigid spheres; for 10<Re<200 they exhibit internal circulation, which enhances mass transfer; for Re>200 they oscillate (Schügerl, 1994). In the main investigation drops were <10 μm and would therefore exhibit stagnant drop behaviour.

Conventionally, process analysis is performed assuming that k_c and k_d are independent of phase concentrations and the concentration driving force. In reality however the solute concentration will affect the system physical properties and therefore the individual film coefficients. Phenomena associated with large concentration driving force are discussed in 2.6.3.

Mass transfer during drop formation

In column contactors drops may be formed initially at a distributor and, except in agitated columns where repeated coalescence and redespersion greatly enhances the mass transfer occurring during drop travel, it is necessary to compute the contribution to mass transfer during drop formation. Sherwood claimed that 40 percent of the extraction under specific conditions occurred during drop formation but West et. al., (1952) found only 14 percent; others observed no special effects.

Various correlations have been proposed for mass transfer rate during drop formation from nozzles but these are based upon laboratory data and may not extrapolate to the real case of drop swarms involving same degree of action between jets.

2.6.1.1 Continuous phase mass transfer:

From and to rigid drops:

The local mass transfer coefficient varies in value over the surface of the droplet; these differences are difficult to measure and it is usual to describe the overall process in terms of a single value for the continuous phase mass transfer coefficient.

Theoretical and empirical studies (Slater, 1994) suggest that the following form of equation is suitable for the estimation of the continuous phase mass transfer coefficient:

$$Sh_c = 2 + c_1 Re^{0.5} Sc_c^{0.33} \qquad (2\text{-}8)$$

where Sh_c, Re_c and Sc_c are the Sherwood, Reynolds and Schmidt numbers respectively, and c_1 is a constant. Attempts have been made to account for the contributions in the forward area and the wake area as well as overall. Values proposed by Garner and Suckling (1958) were c_1=1.08 for the forward area, c_1=0.67 for the wake area, and c_1=0.95 overall.

The constant c_1 has been found to range from 0.55 to 0.95 overall (Slater, 1994).

Sherwood, Reynolds and Schmidt numbers are based on the physical properties of the continuous phase:

$$Sh_c = \frac{k_c d_d}{D_c},\ Re_c = \frac{d_d U}{\nu_c},\ Sc_c = \frac{\nu_c}{D_c} \qquad (2\text{-}9)$$

where k_c is the mass transfer coefficient in the continuous phase, d_d is the diameter of the drop, D_c is the solute diffusivity in the continuous phase, U is the relative droplet velocity and ν_c is the kinematic viscosity of the continuous phase.

From and to non-rigid drops:

The mass transfer is again described via k_c and Sherwood number correlations. For non-rigid drops, the power of the Schmidt number is generally taken as 0.5 (Schügerl, 1994):

$$Sh_c = c_1 Re^{0.5} Sc_c^{0.5} \qquad (2\text{-}10)$$

It is recommended by Schügerl (1994) that the constant c_1 be 1.13.

2.6.1.2 Dispersed phase mass transfer

From and to rigid drops

Small drops, generally, < 2mm diameter, but also large drops if surfactants are present, behave as stagnant drops. Mass transfer into, or out of, the drop is by molecular diffusion and relatively simple models and correlations have been proposed for this mode of operation (Treybal, 1963).

From and to circulating drops

At Re > 200 rapid internal circulation is promoted, and the internal mass transfer film coefficient can be enhanced by a factor of 5 over that for a stagnant drop. Numerous correlations have been proposed for a film coefficient (Treybal, 1963) but few properly account for all relevant system physical properties.

From and to oscillating drops

At high Re numbers, or low continuous phase viscosities, a drop oscillates and mass transfer is considerably enhanced. Correlations for k_d must then account for frequency and amplitude of the oscillation.

2.6.2 Interfacial phenomena and mass transfer

Spontaneous interfacial convection was described in the 18th century by a number of authors. When a small drop of alcohol was gently introduced in the middle of a glass of water, a rapid rushing of the surface was found to occur outwards from the place where alcohol was introduced. It was also shown that the reduction in surface tension by the introduction of alcohol caused the outward motion of the liquid of lower surface tension. This phenomenon applies to miscible, immiscible and partially miscible liquids and is referred to as the Marangoni effect (Sawistowski, 1971).

The interfacial convection resulting from local changes in interfacial tension is exhibited in a variety of ways. Rippling of the interface, localised eruption and cellular convection are the most common types of disturbances observed. They are divided

into two main categories: ordered interfacial convection as in Figure 2-7 and disordered interfacial convection as in Figure 2-8 (Sawistowski, 1971).

2.6.2.1 Ordered interfacial convection

If a solute free phase (phase 1) is brought into contact with phase 2 containing a solute S (Figure 2-7), the mass transfer process will never be completely uniform, as a result of random external disturbances. The areas at points **a** will expand along the surface as a result of the Marangoni effect. The interfacial layer is brought thus into motion, first parallel to the interface and then turning away from it, at point **b**. The liquid at point **a** is being continuously replaced by fresh liquid from the bulk of each phase. This process leads to the formation of convection cells in both phases (Sawistowski, 1971).

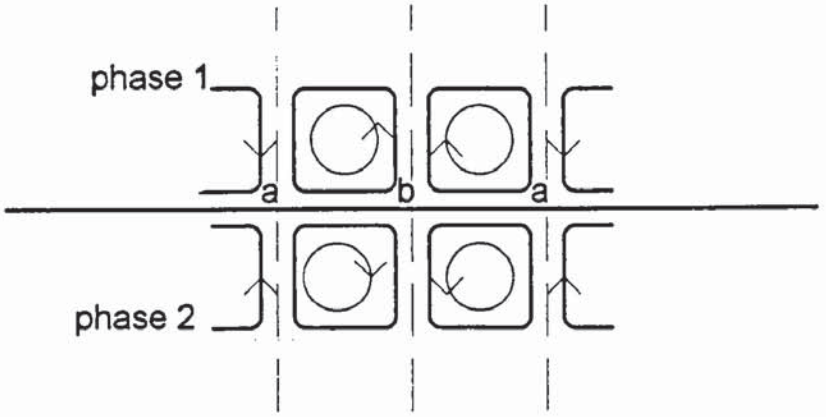

Figure 2-7 Diagram to illustrate the formation of convection cells

Since the interfacial tension is a function of solute concentration at the interface, and since the concentration of solute decreases in the lower phase and increases in the upper phase in the direction from **a** to **b**, the interfacial tension will also change along the interface.

Sternling and Scriven (1959) have discussed the origin of interfacial turbulence, i.e. spontaneous agitation of the interface between two unequilibrated liquids, in terms of classical flow, diffusion and surface processes. They discussed the conditions where a small fluctuation in surface tension during mass transfer can build up into a macroscopic eddy. Their model predicts that surface turbulence occurs if

1. there are large differences in diffusivity and also in kinematic viscosity between the phases,
2. there are high concentration gradients near the interface, and,
3. $d\sigma/dc$ is large and negative.

Maroudas and Sawistowski (1964) found that spontaneous interfacial turbulence is higher when the solute is being transferred into the phase of higher kinematic viscosity and lower diffusivity. Sternling and Scriven, however, predicted that when the transfer of solute is taking place out of the phase of higher kinematic viscosity, or out of the phase of lower diffusivity, then interfacial turbulence is promoted. Maroudas and Sawistowski (1964) concluded in their work that the theory of Sternling and Scriven is too simple to give a reliable criterion for interfacial instability. No alternative theory was proposed.

Davies (1972) also criticised the paper of Sternling and Scriven, on the grounds that they did not discuss the critical concentration of solute required just to produce surface turbulence; nor did they consider the distribution coefficient of the solute between the phases.

2.6.2.2 Disordered interfacial convection

The appearance of disordered interfacial convection is usually associated with the presence of turbulence. Consider an eddy reaching the interface from the bulk phase (Figure 2-8a) and solute transferring from the bottom phase (raffinate) to the top phase (extract). The interfacial tension is assumed to decrease with solute concentration. In Figure 2-8a the close vertical lines represent high solute concentration at the interface which lowers the interfacial tension. The affected area will expand outwards. The moving fluid at point A is not replaced by a continuous supply of solute-rich material from the bulk phase. Instead, liquid of lower subinterfacial concentration is brought to the interface at point **A** so that the interfacial tension there will become higher than at the outer part of the surface (Figure 2-8b). In the case of solutes whose rates of desorption are slow, this effect may be amplified by the compression-dilation effect. The outward movement produces a compression effect at the outer part of the surface and dilation at its centre; so the interfacial tension will be high at the centre and low at the outside. The motion will be reversed (Figure 2-8c) due to interfacial tension. The flow towards the centre will produce a jet like ejection of material rich in the transferred solute into the top phase. A similar ejection will take place into the bulk bottom phase. This ejection phenomenon is also referred to as an "eruption" (Sawistowski, 1971).

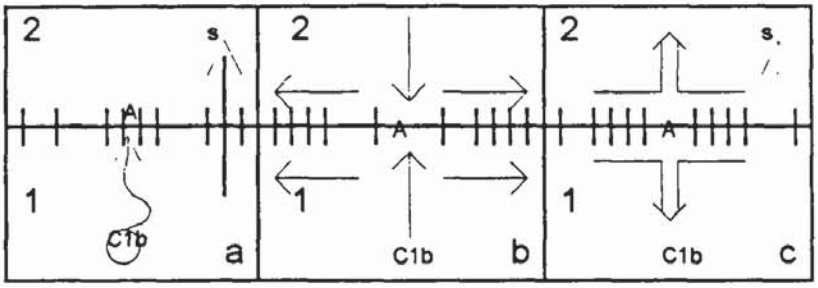

Figure-2-8 Diagram illustrating the eruption mechanism: (a) local lowering of interfacial tension, (b) outward spreading of the area of low interfacial tension, (c) reversal of direction of spreading leading to an eruption (Sawistowski, 1971).

2.6.3 Effect of surfactants

Surface active agents affect the properties of the interface in several ways if introduced in phase equilibrium. Interfacial tension will be reduced, thus becoming less dependent on solute concentration. Surfactants will also reduce the interfacial compressibility. In addition, surface viscosity will increase, slowing down any movement in the interface (Sawistowski, 1971).

Berg and Acrivos (1964) found that a small quantity of a surfactant may exert a profound stabilising effect on convection-induced by surface tension.

2.6.4 The effect of interfacial turbulence on mass transfer

Sawistowski and Goltz (1963) concluded from their experimental work that there were two main regimes of transfer. In the diffusional regime, the experimentally-determined mass transfer coefficients were in reasonable agreement with the coefficients calculated using the film theory. Mass transfer coefficients in the turbulent regime depended on

the local decrease in interfacial tension and on the concentration of the solute. They concluded that changes in interfacial tension occurring during mass transfer processes may have a significant effect on the rate of mass transfer.

Interfacial turbulence or spontaneous interfacial convection is known to increase substantially the mass transfer rates in the course of liquid-liquid extraction and has been proposed as a good way to enhance mass transfer in industrial processes (Slater, 1994). However, sufficiently high driving forces are seldom experienced in practical situations.

To make use of interfacial turbulence requires knowledge of the conditions for interfacial instability to occur, as well as a kinetic model for mass transfer accompanied by interfacial turbulence. A semi-empirical mass transfer model for liquid-liquid extraction accompanied by interfacial turbulence was presented by Golovin (1984). In framing of the model a linear dependence of mass transfer coefficient on the driving force was obtained, and this was confirmed by comparison with results from a number of experiments. Also, methods were presented which allow mass transfer rates to be predicted for extraction accompanied by interfacial turbulence in growing as well as in moving droplets. The results of Golovin showed that, in mass transfer accompanied by interfacial convection, the mass transfer coefficient values were higher than the values in the diffusional regime. Mass transfer coefficients depended on the driving force which leads to interfacial tension dependence.

The influence of interfacial turbulence on mass transfer at a mobile interface was investigated in ternary systems under well-defined conditions (Bakker *et al.*,1967).

For ternary systems without chemical reaction, the ratio between the mass transfer rates with and without interfacial movement proved to be a function of the driving force of mass transfer only and not of the contact time or the concentration level of the solute. The ratio is equal to one when there is no driving force. For a ternary system with rapid chemical reaction between the solute and a reactant R in the second phase, experimental results showed that at high concentration of the reactant R the ratio is also equal to 1, because the solute concentration at the interface becomes zero and the interfacial movement dies out. The experimental results proved that micro-scale interfacial movement is the true reason for enhanced mass transfer rates.

Lode and Heideger (1970) studied the mass transfer from a single drop augmented by interfacial instability. A photographic technique was used to evaluate mass transfer rates from a single drop in a system expected to exhibit interfacial tension-driven convection. Extremely high mass transfer coefficients were observed and this was related to the observed interfacial turbulence.

Takeuchi and Numata (1977) studied the mass transfer across liquid-liquid interfaces in a number of systems which exhibit turbulence as a result of a Marangoni effect. They used apparatus which allowed the two phases to be brought into contact with each other within a tube with no external disturbances, for a fixed time, under steady-state conditions. The phases then separated, and the amount of solute transferred was measured. The mass transfer coefficients were found to be a function of the solute concentration.

2.7 Drop size and size distribution

The process of liquid-liquid extraction involves contacting two partially miscible liquid systems, one a feed solution and the other the extracting solvent. Since the two liquids are not in chemical equilibrium, one or more solute components will transfer from the feed phase into the solvent phase. If the two liquid phases are quiescent with one on top of the other, mass transfer will occur only by molecular diffusion. The transfer flux would hence be low and an extended time would be needed to achieve chemical equilibrium. To speed-up this process the two phases are mixed together to form a dispersion of droplets of one phase (dispersed phase) in the other (continuous phase). The molar transfer rate of component i from the dispersed phase is proportional to the interfacial area between the two phases: $N_i \propto a$ (Davies, 1992).

Hence the drop size distribution is an important characteristic.

Mean drop sizes may be calculated in various ways as summarised below.

Table 2-1 Mean drop sizes and their application.

Drop size	Applications
d_{32}, Sauter mean drop size	Mass transfer application
d_{43}, Volume, moment mean diameter	Particle classification
d_{21}, Length, surface mean diameter	Hydrodynamic settling

The time to achieve chemical equilibrium can be reduced by increasing the interfacial area a. This can be done in an agitated vessel by increasing the mixing speed. The interfacial area, a, is related to the dispersed phase hold-up ϕ and the Sauter mean drop size $\bar{d}_{vs}$ thus:

$$a = \frac{6\phi}{\bar{d}_{vs}} \qquad 2\text{-}11$$

Increasing the turbulence in the mixing stage would increase the interfacial area a and result in a decrease in $\bar{d}_{vs}$. However, the effect of drop size upon the individual mass transfer coefficients, discussed in 2.6, means that in practice there is an optimum agitator speed.

Liquid-liquid extraction involves two steps, mixing and then separation of the two phases.

(a) Mixing serves to increase the interfacial area and can also, within limits, increase the dispersed and continuous phase film mass transfer coefficients.

(b) For phase separation, the two phases separate spontaneously when mixing ceases e.g. in a separate settler or at one end of a column. Gravitational forces, arising from the density difference between the two phases, promote separation. The droplets must then flocculate and coalesce. Density difference, interfacial tension and continuous phase viscosity are the critical physical properties controlling this step.

The prediction of some mean drop size enables the interfacial area for mass transfer to be estimated. Correlations for the prediction of drop size and interfacial area are discussed in Section 2.7.1.

2.7.1 Correlations for drop size

In a mixer mechanical energy is transmitted to the mixture by an impeller inducing turbulence and causing break-up of one phase into droplets. Drops are formed by

breakage in the shear field; in other parts of the flow, i.e. zones of reduced turbulence, interdrop coalescence may occur. To characterise drop size or size distribution for any given condition, a dynamic equilibrium must be achieved between break-up and coalescence.

There are extensive reports in the literature on break-up in turbulent fields. The work of Kolmogoroff describes the theory of drop break-up in isotropic turbulence (Batchelor, 1950). This is based upon the postulation that turbulent flow produces large-scale primary eddies. These eddies are unstable and dissipate energy by disintegrating into smaller and smaller eddies until, at the smallest scale, energy is dissipated by viscous flow.

Batchelor (1950) applied Kolmogoroff's theory to drop break-up. Batchelor's work assumed that two different mechanisms were responsible for break-up, depending on the dimension of the drops.

(a) If the drops are much larger than the micro-scale of turbulence, then dynamic pressure forces rather than viscous shear forces control the breakage process.

(b) If the drop diameters are of the order of, or less than, the eddy length then viscous shear forces control the breakage process.

The surface of the drop deforms due to velocity fluctuations. These shear deformations are counteracted by interfacial tension forces and viscous forces in the drop. Deformation and break-up is controlled by these three forces, the first induced by dissipative turbulence and the others acting as restoring forces. Break-up will occur when the dissipative force exceeds the restoring force. The restoring force can be represented by dimensionless groups, the Weber number, We, and a viscosity group.

Weber number represents the ratio of inertial to surface forces and is used to characterise conditions for break-up, i.e. by a critical value $(We)_{crit}$ (Hinze, 1955).

In a liquid-liquid contactor the critical Weber number defines the diameter of the largest stable drop in the dispersion

$$(We)_{crit} = \frac{\rho_c \bar{u}^2 d_{max}}{\sigma} \qquad 2\text{-}12$$

where $\bar{u}$ is the velocity difference over a distance equal to d_{max}. If d is large with respect to the smallest eddy in the flow, Kolmogoroff's first case , then from Bachelor (1951)

$$\bar{u}^2 = C_1 \varepsilon^{2/3} d^{2/3} \qquad 2\text{-}13$$

where ε is the energy dissipation per unit mass, C_1 is a constant and $\cong 2.0$. The critical Weber number then becomes

$$(We)_{crit} = K_1 \left(\frac{\rho_c}{\sigma}\right) \varepsilon^{2/3} d_{max}^{5/3} \qquad 2\text{-}14$$

on rearranging

$$d_{max} = \frac{We_{crit}^{3/5}}{K_1^{3/5}} \left(\frac{\sigma}{\rho_c}\right)^{3/5} \varepsilon^{-2/5} \qquad 2\text{-}15$$

For a fully baffled turbine mixer operating at high Reynolds number (Davies, 1992)

$$\varepsilon \propto N^3 D^2 \qquad 2\text{-}16$$

where N and D are the speed and diameter of the impeller respectively. Then applying the theory to a practical case, noting that $(We)_{crit}$ is constant, and assuming that the energy dissipation near the impeller is described by Kolmogoroff's theory

$$d_{max} = K_2 \left(\frac{\sigma}{\rho_c}\right)^{3/5} N^{-6/5} D^{-4/5} \qquad 2\text{-}17$$

Several research workers (Shinnar and Church, 1960, Chen and Middleman, 1967) have calculated Sauter mean drop diameter $\bar{d}_{vs}$ based upon equation 2.17. Use of equation 2-11, then provides information on the interfacial area available for mass transfer.

Shinnar and Church (1960), Chen and Middleman (1967) and Brown and Pitt (1970) have shown that the maximum stable drop diameter d_{max} is linearly related to the Sauter mean drop diameter $\bar{d}_{vs}$. The Sauter mean drop diameter can therefore be predicted from equation 2-18,

$$\bar{d}_{vs} = K_3 \left(\frac{\sigma}{\rho_c}\right)^{3/5} N^{-6/5} D^{-4/5} \qquad 2\text{-}18$$

When the power number, N_p, and impeller Weber number We_I are introduced into equation (2-18), as defined below

$$N_p = \frac{P}{\rho N^3 D^5} \qquad 2\text{-}19$$

where P is the power input, and

$$We_I = \frac{N^2 D^3 \rho}{\sigma} \quad , \qquad 2\text{-}20$$

then:

$$\frac{\bar{d}_{vs}}{D} \propto We_I^{-0.6} N_p^{-0.4} \left(\frac{D^3}{V}\right)^{-0.4} \qquad 2\text{-}21$$

The power number for some contactor designs varies with the impeller Reynolds number. At high Reynolds numbers i.e., ≥ 10000 the Power Number, N_p, becomes a constant value. It is in this region that most contactors operate. Equation 2-21 then reduces to:

$$\frac{\bar{d}_{vs}}{D} = K_4 We_I^{-0.6} \qquad 2\text{-}22$$

Equation 2-22 has been used at low dispersed phase hold-ups, i.e., ≤ 10 % v/v, as a basis for correlation of a wide range of experimental results for mixing in turbine contactors (Chen and Middleman 1967; Sprow 1967). Davies (1992) has listed a number of these correlations as in Table 2-2.

The physical properties of the systems for which correlations are given in Table 2-2 are in the range of 1.5 - 58.1 x 10^3 N/m for the interfacial tension; the continuous phase viscosity ranges from 1-65.5 Ns/m^2; the density of the continuous phase ranges from 693-1595 kg/m^3 and the volume fraction dispersed phase hold-up range was 0.05-48.3 v/v. By comparison, in the present work, the volume percentage dispersed phase hold-up was low, in the range 0.03-0.07 % v/v. The interfacial tension range was 1.28 x10^{-4} - 1.11 x 10^{-3} N/m, the continuous phase viscosity range 1.7 - 2.25 Ns/m^2 and the continuous phase density range 1102 - 1176 kg/m^3. Therefore, close agreement with any of these correlations would be fortuitous.

Table 2.2 Correlations to predict the Sauter mean drop diameter $\bar{d}_{vs}$

Investigator	Correlation	Range of Physical Properties					
		ρ_d (kg/m^3)	ρ_c (kg/m^3)	μ_d (Ns/m^2)	μ_c (Ns/m^2)	σ x10^3 (N/m)	X_v hold-up
Brown and Pitt	$\bar{d}_{vs} = K\left(\frac{\sigma}{\rho\varepsilon - t}\right)^{0.6}$	780-840	970-998	0.59-3.30	1.0-1.28	1.9-50	0.05
Shinnar	$\bar{d}_{vs} = K(\sigma D)^{-3/8} We^{-3/8}$			22.5	0.4		0.05
Vermeulen et al.	$\bar{d}_{vs} = KWe^{-0.6}$	683-1595	693-1595	0.52-18.4	1.81-65.4	3.1-58.1	0.1-0.4
Rodger	$\bar{d}_{vs} = KWe^{-0.36}\left(\frac{D_1}{DT}\right)^{-0.7}$	761-1101	1000	0.578-3.91	1.0	2.1-49.0	0.50
Sprow	$\frac{\bar{d}_{vs}}{D_1} = K(\rho_c\mu_c)^{-0.5}\left(\frac{\rho_c}{\sigma D_1}\right)^{-0.25} We^{-0.75}$	692	1005	0.51	1.14-3.37	1.5-1.0	0.50
Chen and Middleman	$\frac{\bar{d}_{vs}}{D_1} = 0.045We^{-0.57}$	703-1101	997-1001	0.52-25.8	0.89-1.27	4.75-48.3	4.75-48.3
Mlyneck and Resnick	$\frac{\bar{d}_{vs}}{D_1} = 0.058\ (1+5.4X_v)We^{-0.6}$	1055	1000	1.0	1.0	41	0.0245-0.34
Brown and Pitt	$\frac{\bar{d}_{vs}}{D_1} = 0.057\ (1+3.14X_v)We^{-0.6}$	783-838	972-998	0.59-3.30	1.0-1.28	1.9-5.0	0.05-0.30
Van Heuven and Beck	$\frac{\bar{d}_{vs}}{D_1} = 0.047\ (1+2.5X_v)We^{-0.6}$	-	998	-	8.5-49.5		0.04-0.35
Godfrey and Grilic	$\frac{\bar{d}_{vs}}{D_1} = 0.058\ (1+3.6X_v)We^{-0.6}$	783-829	1000	2.05-8.60	1.0	1.9-34.5	0.05-0.5

2.8 Conclusions

It may be concluded that there is a substantial body of literature on the fundamentals of liquid-liquid extraction and on the mechanisms of dispersion, sedimentation and coalescence. However, it is mainly based upon single drop hydrodynamic and mass transfer studies. It also relates to conventional two phase liquid-liquid systems generally involving drops in the size range 1mm to 3mm and interfacial tensions of 0.01 N/m upwards. There are both mathematical models for mass transfer and the coalescence process for ideal systems.

By comparison there is limited information on the fundamental physico-chemistry relating to two aqueous phase liquid-liquid systems. The fundamental differences with such systems appear to be:

a) very much smaller drop sizes; this affects both interfacial area available for mass transfer and the mechanism of mass transfer
b) low interfacial tension, (e.g. 1×10^{-4} N/m) which is essential when handling biological-active materials
c) extended settling times, since there is a small density difference between the two phases and the low interfacial tension produces very small drops e.g. 10μm.

One objective of this work was to add to knowledge as to the fundamentals, and practicalities, of two aqueous phase liquid-liquid extraction processes.

3. The Physical Properties of PEG/Salt Aqueous Phase Liquid-Liquid System

3.1 Preparation of the phase systems

Three two-phase systems were prepared using polyethylene glycol (PEG, Molecular Weight 6000) and dipotassium hydrogen ortho-phosphate (salt) as the two solutes. The PEG and salt were obtained as Analar reagents from Fisons Ltd. The required amounts of the polyethylene glycol (PEG), dipotassium hydrogen ortho-phosphate (K_2HPO_4) and water were prepared as follows:

The PEG solutions used to make a 20% w/w system consisted of 200 grams of polyethylene glycol with a relative molecular mass (RMM) of 6,000 and 800 grams of distilled water. The mixture was placed in a 1000 cm^3 glass beaker at ambient temperature and stirred using an electrically-driven agitator at 1000 RPM until all the solid had dissolved. This required approximately five minutes. 200 grams of the salt and 800 grams of distilled water were also placed in a 1000 cm^3 glass beaker and stirred until all the salt had dissolved, to form the salt solution. Both solutions were then poured into a 2 litre separating funnel at ambient temperature.
Similar procedures were used in preparing the 25% w/w and 30% w/w systems.

Once settling was completed (which normally took about 12-24 hours) the funnel contained two distinct, clear phases, with a definite interface between the two layers. The lower phase the 'salt phase', consisted of mainly salt and distilled water. The upper layer, 'the PEG phase', was predominantly PEG and distilled water.

The lower phase the 'salt phase', consisted of mainly salt and distilled water. The upper layer, 'the PEG phase', was predominantly PEG and distilled water.

The two phases were then slowly run off into separate, pre-weighed bottles. The weight of each phase was recorded.

The separating funnel was washed before use with 5% Decon solution followed by hot water, and then distilled water, to ensure that no impurities were picked-up in the freshly-prepared phases.

3.2 Phase diagrams

3.2.1 The construction of the binodal curve

The binodal curve is a plot of the weight fraction of PEG versus the weight fraction of K_2HPO_4 at the points at which two phases first separate from a single solution. It represents the equilibrium of the two separated phases in a three component system of salt, PEG and distilled water. If a mixture is prepared which separates into two phases, the compositions of these phases will lie on the binodal curve, at opposite ends of a tie-line.

To prepare the binodal curve for the system used, 40% w/w solutions of K_2HPO_4 and PEG were prepared at 20 °C by taking 40 grams of salt and 60 grams of distilled water, and 40 grams of PEG with 60 grams of distilled water.

A 100 cm^3 conical flask was weighed, and approximately 10 grams of PEG solution were placed into it. The actual weight was recorded. Salt solution was added drop-wise using a pipette whilst shaking the flask until the liquid just went cloudy. At this point, the cloud point, the flask and its contents were re-weighed and the weight percentages of the PEG and K_2HPO_4 calculated. This represented a point on the binodal curve. A small amount of water was then added dropwise until the solution clarified again. The flask was again weighed to calculate the mass of water added, and the weight was recorded. More salt solution could then be added, as before, to determine another point on the binodal curve. This procedure was repeated several

times, to give a series of points on the binodal curve. This became progressively more difficult towards the lower PEG fractions and only a small addition of water was necessary between each cloud point. Points on the binodal curve were also found by starting from the salt end of the curve, with about 10 grams of 40% w/w salt solution and gradually adding PEG solution, as described above.

The experiment was repeated to check consistency; the reproducibility of the curve was found to be ±5 %.

3.2.2 The positioning of the tie-lines

The tie-lines of the 20%, 25% and 30% w/w mixtures were required. The data for the tie-lines were found by conductivity measurements. A Jencons Scientific Ltd. conductivity meter model number 4010 with a large, clear LCD display was used. It had a capability of measuring within a conductivity range of 0.01 μS to 199.9 mS. This range can be further expanded by the use of the optional x10 and x 0.1 cells. To obtain an accurate reading, the meter was first calibrated by adjusting the digital display to the value of the cell constant (0.96) indicated on the pre-calibrated cells (probes). The accuracy of the conductivity meter is ±0.5%.

After calibration, measurement of a sample was carried out by immersing the probe in the sample, allowing the reading to stabilise and recording the result. The probe was rinsed thoroughly with deionised water between each sample to avoid contamination.

The first stage was to obtain a plot of the conductivity of the salt solution against weight concentration of the salt at 20°C ±2°C (Figure 3-1).

Several samples were made-up containing salt in the concentration range between 0 and 40 % w/w of K_2HPO_4. Their conductivities were then measured using the same cell constant (0.96) and conductivity meter. It was necessary to dilute the samples to reduce the inhibition of ion mobility which occurs in concentrated solutions. The measured conductivities of the diluted sample were multiplied by the dilution factor to obtain the apparent conductivity of the original solution.

The solutions were first diluted ten times and the conductivity measured and recorded. The solution was then diluted a hundred times and a thousand times, or even greater if necessary. This procedure was repeated until two successive values of the apparent conductivity were in agreement.

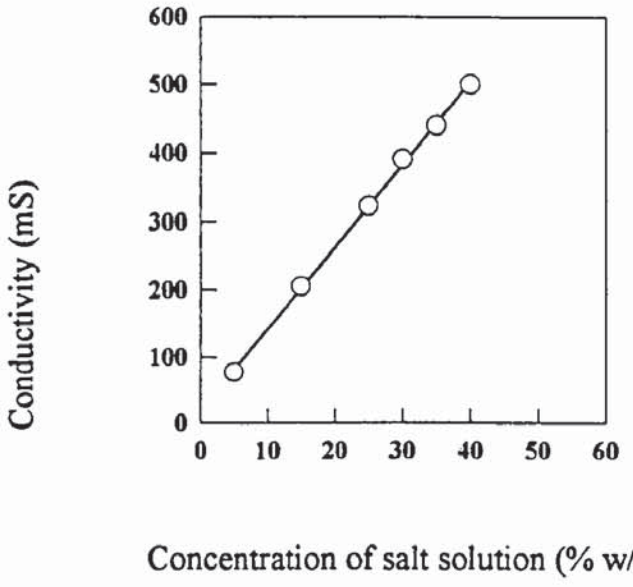

Figure 3-1 Calibration curve for various salt concentrations versus conductivity.

The separate salt phase from each of the 20% w/w, 25% w/w and 30% w/w solutions was then diluted as described above, and the conductivities were measured and recorded, using the conductivity meter. The measured conductivities were then multiplied by the dilution factor, to obtain the apparent conductivity.

From Figure 3-1 the concentration of the K_2HPO_4 in the salt phase of each mixture was then obtained. Any PEG present was assumed not to contribute to the conductivity reading, because it is effectively a non-electrolyte. The salt concentration was then plotted on the binodal curve to represent the salt end of the tie-line.

The second point plotted on the binodal diagram was the middle point of the tie-line, which represented the overall composition of the mixture i.e. 20% w/w, 25% w/w or 30% w/w, depending on the sample under test.

The composition of the PEG phase was then found by calculation, as the third point on the tie-line, where it intercepted the binodal curve near the PEG axis (Figure 3-2). The composition of the phases could be confirmed by the Lever Rule, since the ratio of the phases formed from the original mixture should be the same as the ratio of the lengths of the two parts of the tie-line.

3.3 Viscosity measurement

A Contraves Rheomat 30 rotational rheometer was used to measure the viscosities of each of the liquids. A double gap cylinder bob was used (Figure 3-3b) for very low

viscosity polyethylene glycol (PEG) and potassium hydrogen phosphate (K_2HPO_4) solutions i.e. ≤ 20% w/w. A co-axial cylinder (Figure 3-3a) measuring system was used for the more viscous PEG solutions. The use of different measuring systems for different liquids, although not ideal practice, was necessary because of the significant difference between their viscosities (Gaggero et al., 1988). Each measuring system used a different constant for calculating the viscosity as shown in Appendices 1 and 2.

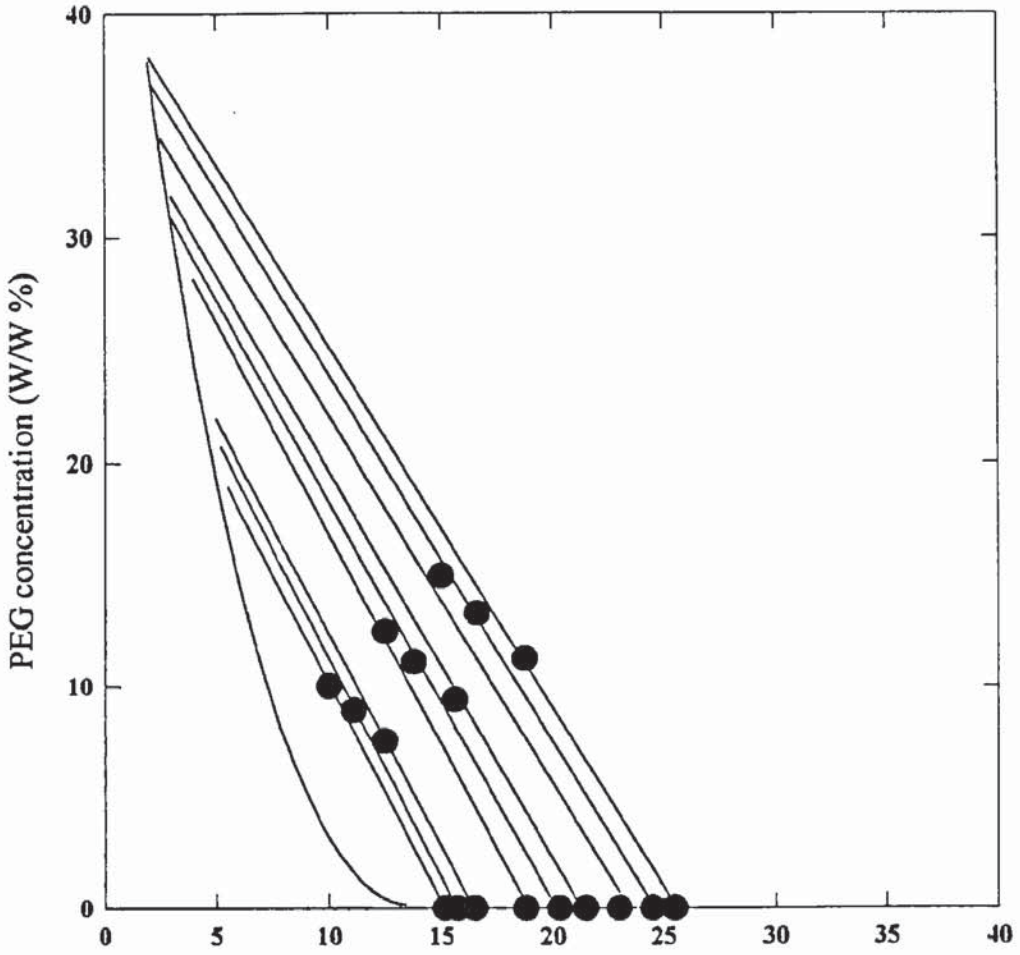

Figure-3-2 Binodal curve for K_2HPO_4 and PEG

The rotating bob was driven by a DC motor, the speed of which was precisely controlled by a programming unit incorporated in the Rheogram recorder which also plotted the speed on the y-axis of the recorder. The torque was measured and plotted on the x-axis of the recorder.

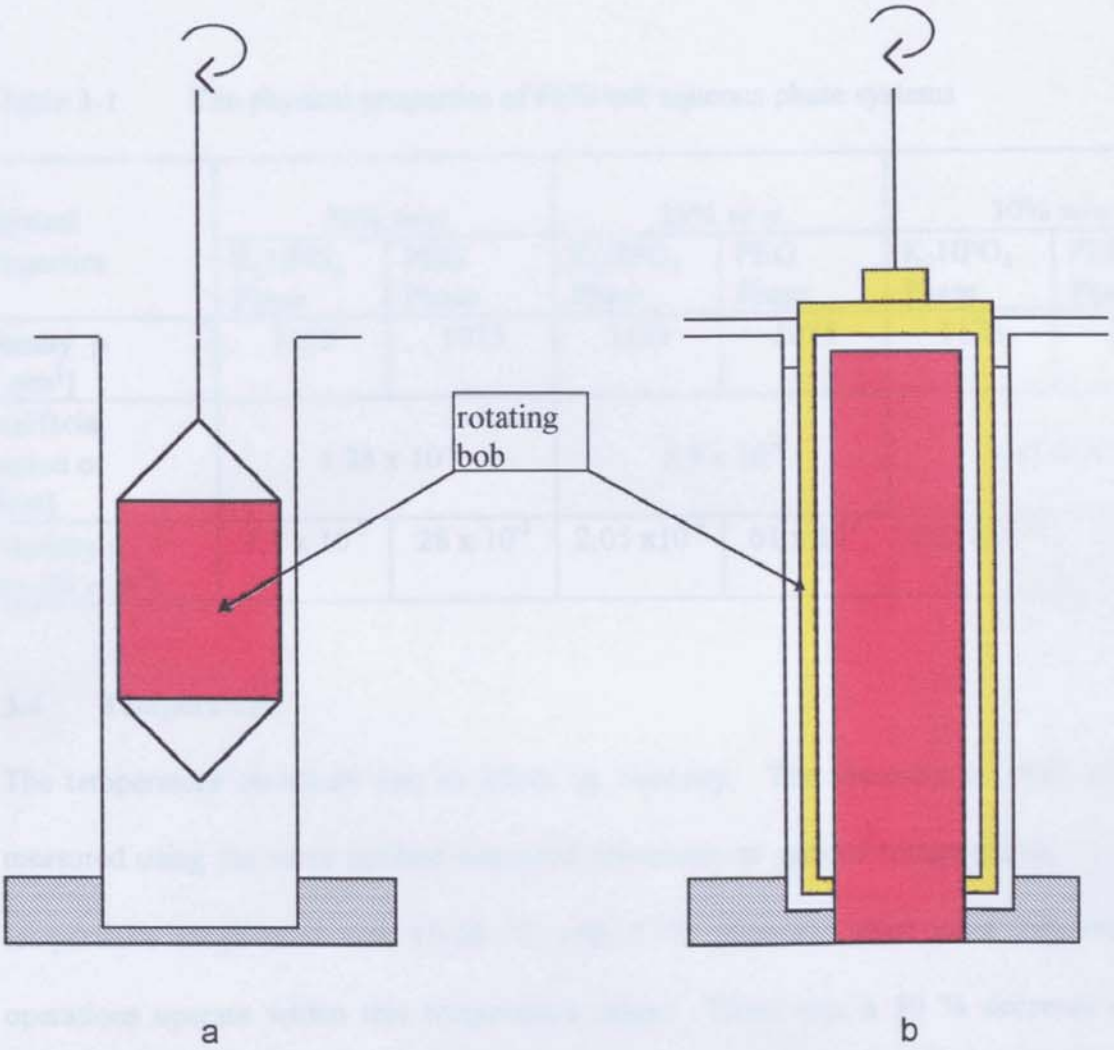

Figure-3-3 Viscosity measurement

a-Measuring system of co-axial cylinders b-Double-Gap Measuring System

There was a time-proportional speed increase gradually from zero up to the maximum speed which was set by the automatic program to be 350 RPM; the drive remained at the maximum speed for a pre-selected period of 20 seconds and the speed was then steadily reduced back down to zero. All measurements were taken at a temperature of 20°C. The viscosities of all liquids measured are listed in Table 3-1 (p. 66).

Table 3-1 The physical properties of PEG/salt aqueous phase systems

Physical Properties	20% w/w		25% w/w		30% w/w	
	K_2HPO_4 Phase	PEG Phase	K_2HPO_4 Phase	PEG Phase	K_2HPO_4 Phase	PEG Phase
Density ρ [kg/m^3]	1102	1075	1135	1074	1176	1075
Interfacial tension σ [N/m]	1.28×10^{-4}		5.9×10^{-4}		1.11×10^{-3}	
Viscosity μ Pa.s [$N\ s/m^2$]	1.7×10^{-3}	28×10^{-3}	2.05×10^{-3}	61×10^{-3}	2.25×10^{-3}	0.1

3.4 Temperature

The temperature obviously has an effect on viscosity. The viscosity of PEG was measured using the same method described previously at various temperatures. The temperature range used was 15-30 °C with 5 °C intervals, since most industrial operations operate within this temperature range. There was a 50 % decrease in viscosity of the PEG as the temperature was increased from 15 °C to 30 °C for the 30% w/w phase composition. For the 20% and 25 % w/w phase compositions there was about a 40 % decrease, as shown in Figure 3-4.

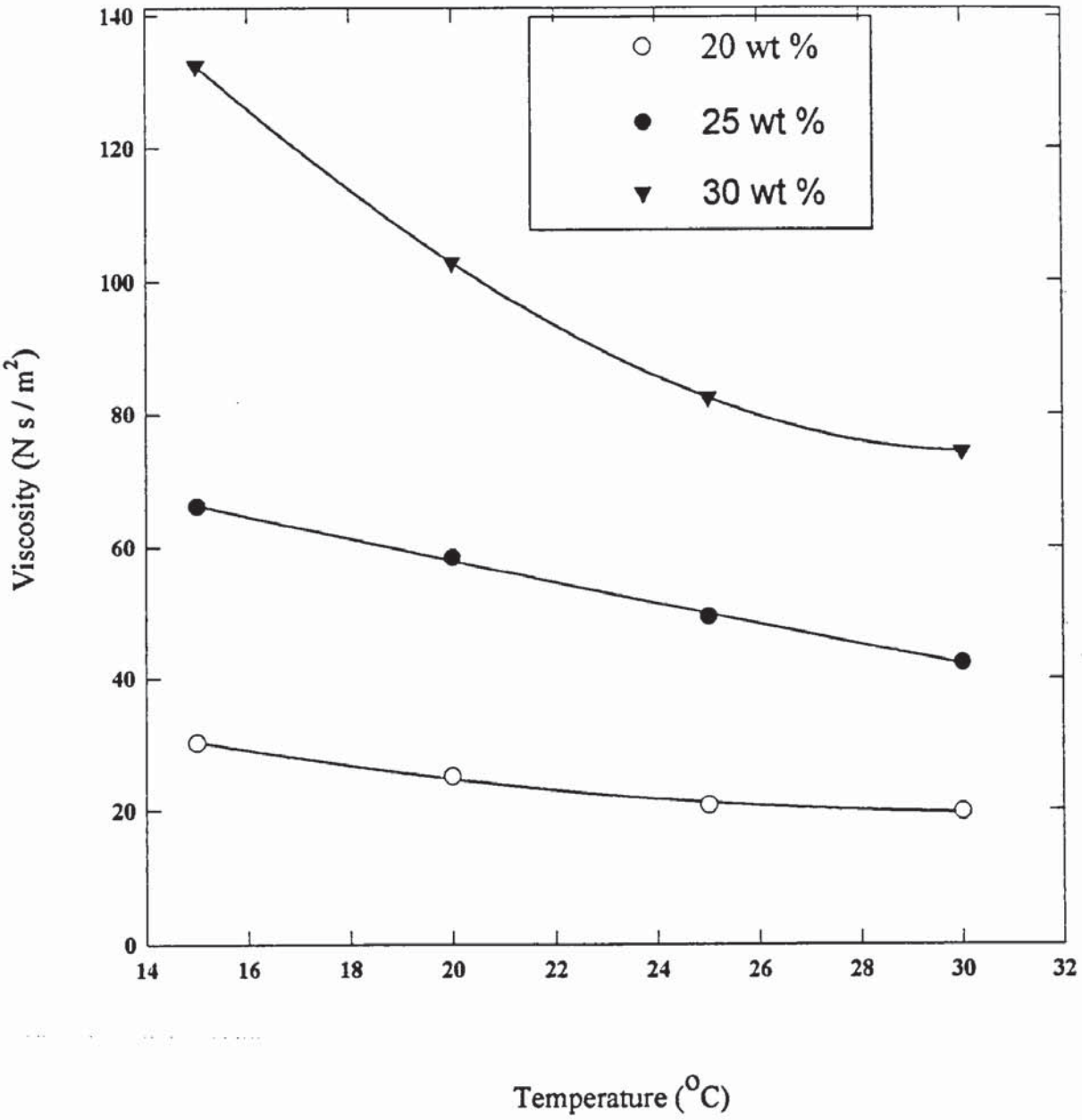

Figure 3-4 Influence of temperature and phase composition on viscosity of PEG.

3.5 Density measurement

A 100 cm^3 density bottle was cleaned thoroughly from all oils and organic materials by washing with 5% Decon solution, then hot water, distilled water and then dried in the oven at 80°C. It was then weighed and its mass m_0 recorded. The density bottle was filled with the sample and the stopper was inserted in such a way that the capillary portion was completely filled with distilled water. The temperature of the distilled water was 20 °C. The density ρ_t was simply obtained from:

$$\rho_t = \frac{m_1 - m_0}{V_t} \qquad (3\text{-}1)$$

where m_0 is the mass[g] of the empty bottle, m_1 is the mass [g], of the density bottle filled with the sample, and V_t is the volume [m*l*], of the sample in the density bottle at temperature (T) 20 °C.

Since the actual volume of the density bottle was not precisely as indicated on the bottle it was calibrated to obtain the exact volume by filling it with a sample of deionised water at a known temperature, T[°C]. Thus

$$V_t = \frac{m_1 - m_0}{\rho_{(H_2O,T)}} \qquad (3\text{-}2)$$

where $\rho_{H_2O,T}$ was the density of water at T [°C] obtained from Appendix 3. The results of the density measurements are presented in Table 3-1.

3.6 Interfacial tension

The pendant drop method of measurement of the interfacial tension of a liquid involves the determination of certain critical dimensions of a drop of the liquid whilst suspended from a suitable support, such as a glass capillary tip (Stauffer, 1965). The measurements are taken from photographs immediately before the drop detaches from the tip. The dimensions to be determined are the maximum diameter of the drop, d_e, and the diameter, d_s, of a selected cross-sectional plane located at a distance equal to d_e along the axis from the apex of the drop. By employing the table of " H-S functions " which was derived experimentally by Andreas et al., (1938), the interfacial tension of the liquid can be calculated from the measured values of d_e and d_s. A ratio S is calculated as

$$S = \frac{d_s}{d_e} = \frac{1}{H} \tag{3-3}$$

and Andreas et al. (1938) showed empirically that S maintains a fixed relationship to a parameter H defined by

$$H = \Delta\rho \frac{(d_e)^2}{\sigma} \tag{3-4}$$

so that the interfacial tension can be calculated from:

$$\sigma = \Delta\rho g \frac{(d_e)^2}{H} \qquad (3\text{-}5)$$

H is a dimensionless shape factor, σ is the interfacial tension, and $\Delta\rho$ is the density difference between the liquid used to form the drop and the density of the continuous liquid.

The original tables of Andreas et al. (1938) relating H and S were inaccurate and have been superseded by those of Niederhauser and Bartell (1948, 1949) and of Fordham (1948) for the range for S from 0.66 to 1 (Appendix 5) and by Mills (1953) and Stauffer (1965) (Appendix 4) for an extension of this range to values of S from 0.66 down to 0.30 (Padday, 1969).

In using this experimental method, certain important improvements were made to the apparatus and measurement technique. A Panasonic video camera with a microscope objective lens, equipped with a video recorder and a monitor, was used to take pictures of the drop. The magnification on each photograph was determined from the size of the capillary tip image on the picture. The glass syringe with the needle, which was used to form the drops of liquid, was mounted vertically on a micrometer. A Philips strobe flash light was mounted firmly on a stand behind the syringe to enable the camera to take a clear picture. Drops were expelled from the tip of the syringe simply by turning a screw which acted on the plunger. The plunger was restrained from

falling under gravity by winding tape around the barrel. The formation and detachment of the heavier liquid drop (salt) took place inside a 5 x 5 x 1 cm glass box filled with the lower density liquid (PEG). After the photograph was taken, a Panasonic video printer was used to make a final print image of the drop. Dividers were then used to measure the diameters d_e and d_s on the drop image.

The pendant drop method was chosen as the best method of measuring very low interfacial tensions, since the results were easily and accurately reproduced.

The video technique offers the major advantage that the video image can be selected immediately prior to detachment of the drop. In the classical photographic method, considerable trial-and-error and experience is required to operate the shutter precisely at this point.

The interfacial tension of the PEG/salt system was measured for 20% w/w, 25% w/w and 30% w/w solutions at room temperature (20±2 °C). The values for the interfacial tension of the aqueous liquid-liquid systems at room temperature are presented in Table 3-1. The resulting values of the interfacial tension for the PEG/salt system used were of the order of 10^{-4} N/m for the lower phase compositions and 10^{-3} N/m for higher phase compositions.

These values are much lower than those typically reported for pure aqueous-organic systems (Albertsson, 1982). There are few data in the literature for PEG-salt systems but Ryden and Albertsson (1971) found that the interfacial tension for aqueous liquid-liquid systems is very small e.g. 5×10^{-7} - 1×10^{-4} N/m.

4 The Effect of Phase Composition and Volume Ratios on the Settling Times of Two Aqueous-Phase Dispersions

4.1 Experimental methods and materials

Solutions of PEG (polyethylene glycol, molecular weight 6000) and salt (potassium hydrogen orthophosphate) were prepared by adding known weights of dry solid to a weighed quantity of deionised water in a flask and mixing until the solid had all dissolved. Solutions of each substance were prepared at concentrations of 20% w/w, 25% w/w and 30% w/w as described in Section 3.1. Aliquots were then taken from each prepared solution for use in the settling experiments.

Batch settling experiments were carried out at ambient temperature (20±2 °C) in glass measuring cylinders of 500 cm^3 volume and 4.9 cm diameter. Nine experiments were performed to investigate the effect of changing phase composition upon the settling time. The aliquots of each solution were poured into one of the measuring cylinders. The dispersion was allowed to collapse by sedimentation and coalescence. With the system used, two clear demarcation lines were observed at the level of the sedimenting front and the coalescing interface respectively (i.e. the bottom and the top of the dispersed band). The levels of the two fronts were recorded as a function of time, at 60 second intervals, until the dispersion had completely separated. The experimental data are shown in Figure 4-3.

The first three experiments were carried out using the 20% w/w solutions of PEG and salt. 250 cm^3 of the salt solution were used in each experiment, together with 150 cm^3, 200 cm^3, and 250 cm^3 of the PEG solution respectively. For the second set of three

experiments, the same volumes were used, but the solutions were both of 25% w/w. In the final set of three experiments, the same volumes were again used, but with 30% w/w solutions of salt and PEG.

In each case, the solutions formed an equilibrium mixture of two phases on agitation. One phase was rich in PEG, and contained only a small amount of salt, whilst the other was rich in the salt, and contained only a small amount of PEG. The volumes of each of these phases formed by mixing the pure solutions depended upon the position of the equilibrium; this may be predicted using the equilibrium diagram or "binodal curve" for the salt / PEG system. The expected volume ratios of the phases were estimated in this way for each of the experiments and are shown in Table 4-1(p. 85), together with the observed phase ratios after settling was complete.

All the settling experiments were conducted at 20±2 °C. Repeat experiments were performed, using exactly the same procedure as in the first set, to check the reliability and accuracy of the system. The accuracy was found to be within ±5% (see Table 4-4, p. 91).

4.2 Results and theoretical analysis

The settling behaviour of the two-aqueous-phase dispersions was studied using batch settling experiments, following the method of Jeelani and Hartland (1986). These experiments may be used both to predict the performance of continuous settlers, or to obtain data on the coalescence behaviour of the dispersion.

4.2.1 *Characteristics of batch dispersions*

Consider a batch dispersion in a vessel, decaying with time (Figure 4-1a) due to simultaneous sedimentation and interfacial coalescence. The two processes may be considered to occur in discrete zones. The sedimentation zone contains an open dispersion, in which the drops are free to move, and the dense-packed zone contains drops which are separated from their neighbours by only a thin film of continuous phase. In the sedimenting zone, drops sediment whilst growing in size due to inter-drop (binary) coalescence, before entering the dense-packed zone and finally coalescing with their bulk homophase at the coalescing interface.

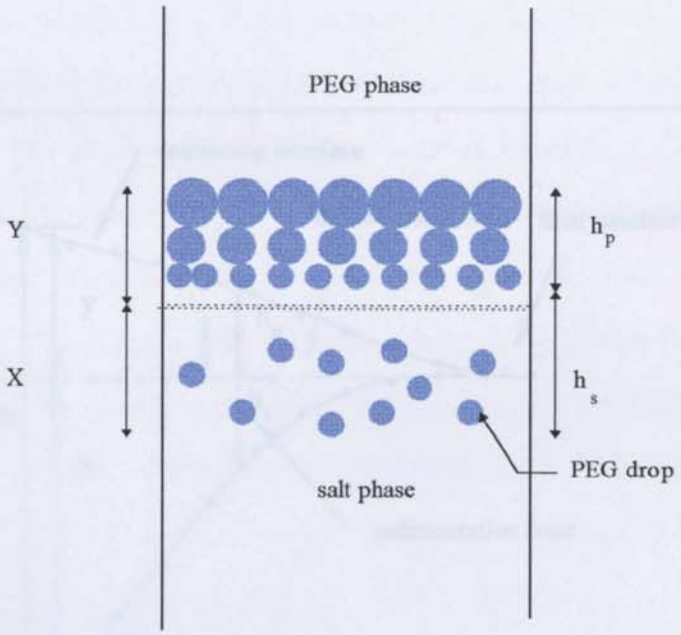

Figure 4-1a Sketch of settling process

This final process is referred to as interfacial coalescence. x and y, the levels of the lower and upper interfaces of the dispersed band, were used to estimate the height, h_p, of the dense-packed zone. The dotted line in Figure 4-1b shows the boundary of the dense-packed zone. Figure 4-1b also shows the heights of the sedimentation and

dense-packed zones which may be denoted as h_s and h_p. The heights x (continuous phase), y (dispersed phase) and h_s invariably decrease with time, but h_p may initially increase if the sedimentation rate is higher than the interfacial coalescence rate. This may result in inflection points in the variation of y and the total dispersion height h with time, t, as shown in Figure 4-2a. This batch decay is referred to as sigmoidal. Alternatively, decay of the dispersion may be exponential (Figure 4-2b) if the coalescence rate always exceeds the sedimentation rate. x_0 and y_0 (the initial values for x and y) are the total volumes per unit area of the continuous and dispersed phases, whilst (x_0-x) and (y_0-y) correspond to the free volumes per unit area of these phases (outside the dispersion band). The volume rates of release of free continuous and dispersed phases per unit area are $-\frac{dx}{dt}$ and $-\frac{dy}{dt}$.

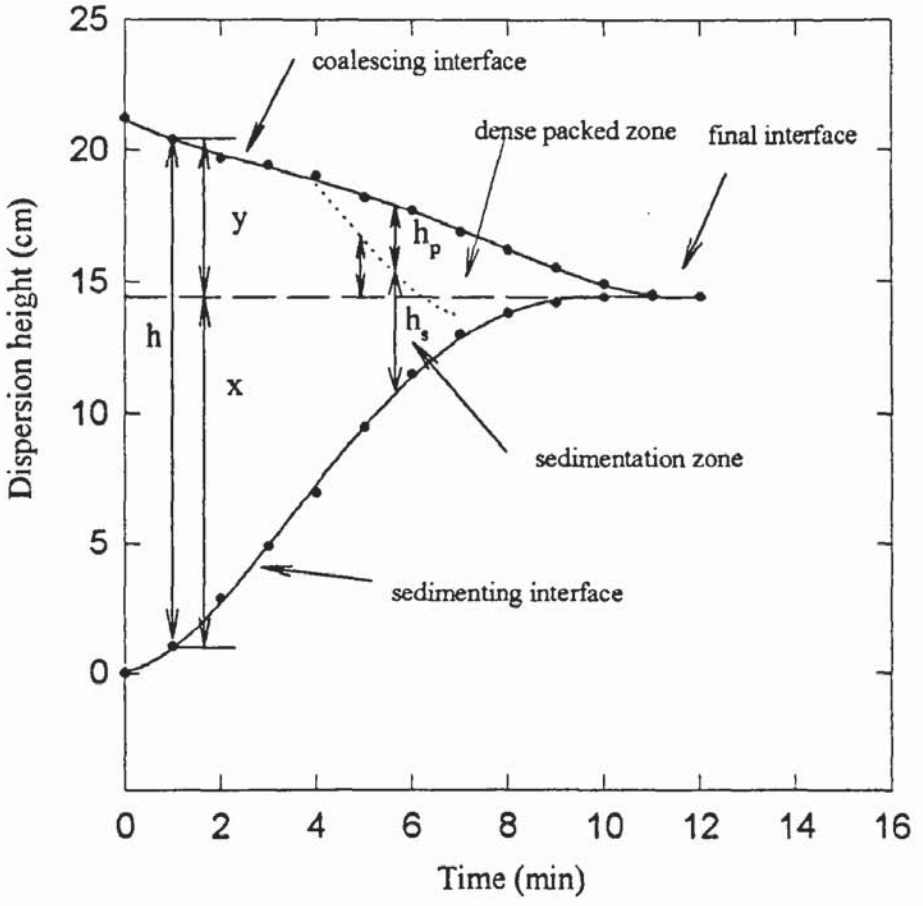

Figure 4-1b Typical settling curve for PEG/salt system

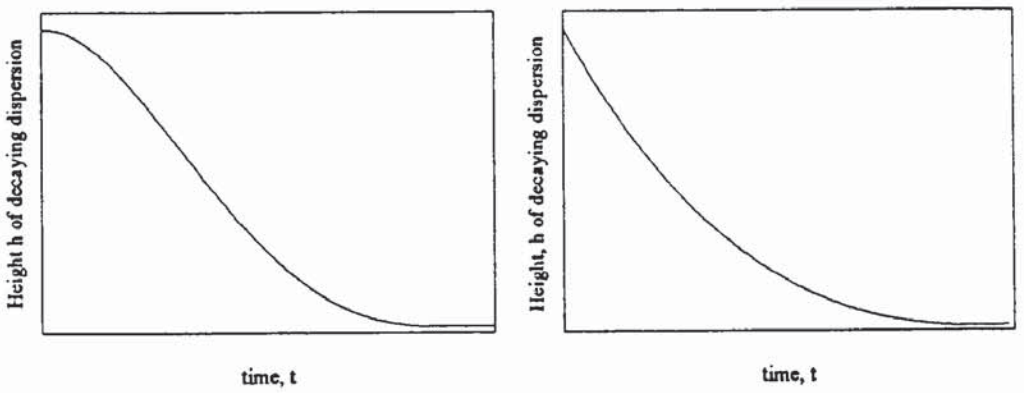

Figure 4-2 Schematic illustration: (a) sigmoidal decay (b) exponential decay of batch dispersion height h with time t.

The total volume of PEG per unit area in the column is equal to y_o. The volume of the PEG per unit area in the upper clear phase is equal to y_o-y. Therefore the volume of PEG per unit area in the open dispersion zone is equal to y. The volumes of the continuous and dispersed phase present in the dispersion are proportional to x and y, and the dispersed-phase hold-up $\bar{\varepsilon}$ equals y/h, where the total dispersion height h equals x + y. The volume rate of coalescence of the drops per unit area at the coalescing interface, which is the same as the volume rate of appearance of clear dispersed phase per unit area at the coalescing interface, is then given by $-\frac{dy}{dt}$.

4.2.2 Thickness of dense-packed layer

A decaying batch dispersion consists of a sedimenting zone of height h_s and a dense-packed zone of height h_p, so that the total dispersion height h at time t is

$$h_s + h_p = h \qquad (4\text{-}1)$$

If the dispersed phase hold-up fractions in these zones are $\bar{\varepsilon}_s$ and $\bar{\varepsilon}_p$ respectively, then a volume balance for the dispersed phase at any time t gives

$$\bar{\varepsilon}_s h_s + \bar{\varepsilon}_p h_p = \bar{\varepsilon} h \tag{4-2}$$

where $\bar{\varepsilon}$ is the instantaneous mean hold-up fraction of the dispersed phase for the entire dispersion. At any time t, the volume of coalesced dispersed phase is proportional to (y_0-y) and the volume of clear continuous phase to (x_0-x). Hence the volumes of dispersed and continuous phases in the dispersion are proportional to y and x and the dispersed phase hold-up

$$\bar{\varepsilon} = \frac{y}{x+y} \tag{4-3}$$

so that

$$\bar{\varepsilon}_s h_s + \bar{\varepsilon}_s h_p = y \tag{4-4}$$

since

$$x + y = h \tag{4-5}$$

In a decaying dispersion the boundary between the sedimentation and dense-packed zone is often hazy, making h_s and h_p difficult to determine. It is more convenient to measure the height of the dispersion as a function of time and then, once the final undisturbed interface is determined, the heights x, y of the sedimenting and coalescing interfaces relating to the final undisturbed interface are calculated. Eliminating h_s from equation 4-1 and substituting in equation 4-4 yields (Jeelani and Hartland, 1986)

$$h_p = \frac{y - \bar{\varepsilon}_s h}{\bar{\varepsilon}_p - \bar{\varepsilon}_s} \tag{4-6}$$

so that the locus $z = y\text{-}h_p$ of the boundary between the sedimentation and dense-packed zones becomes:

$$z = \frac{\bar{\varepsilon}_s x - y(1-\bar{\varepsilon}_p)}{\bar{\varepsilon}_p - \bar{\varepsilon}_s} \qquad (4\text{-}7)$$

although it was not necessary to use z, since h_p was calculated.

4.2.3 Sigmoidal batch decay

This type of curve occurs when the initial rates of drop sedimentation and coalescence are slow (Figure 4-2a). If the rate of sedimentation is higher than the rate of coalescence of drops with their own phase (homophase), a dense-packed layer is formed adjacent to the disengaging interface. The batch dispersion height h is the sum of the sedimentation and dense-packed heights, h_s and h_p, in which the average holdups are $\bar{\varepsilon}_s$ and $\bar{\varepsilon}_p$. However, it is the heights x and y of the sedimenting and coalescing interfaces relative to the final undisturbed interface that are experimentally measured. In this case, h_p can be calculated from equation 4-6 and h_s can then be calculated from equation 4-1.

4.2.4 Sedimentation height and drop growth

The method of Jeelani and Hartland (1986) assumes that the rate of sedimentation of an open dispersion will increase with time, due to binary coalescence of the drops in the sedimentation zone. In this case, a semi-empirical equation was derived by Jeelani and Hartland (1986) to describe $-\frac{dx}{dt}$,

$$-\frac{dx}{dt} = k_s t^a \qquad (4\text{-}8)$$

Here $-\frac{dx}{dt}$, the rate of movement of the sedimenting interface, is equal to the settling velocity V_s of the drops relative to the continuous phase. k_s is a constant and a function of the physical properties and dispersed phase hold-up fraction $\bar{\varepsilon}$. Integrating with the initial condition $x = x_0$ when $t = 0$ yields

$$x_0 - x = \frac{k_s}{(1+\alpha)} t^{(1+\alpha)} \qquad (4\text{-}9)$$

or in logarithmic form,

$$\ln(x_0 - x) = \ln \frac{k_s}{(1+\alpha)} + (1+\alpha) \ln t \qquad (4\text{-}10)$$

A plot of ln (x_0-x) versus ln (t) was constructed for each experiment, which then enables the values of k_s and α to be obtained from the intercept $\ln \frac{k_s}{(1+\alpha)}$ and slope $(1+\alpha)$, respectively, of the straight line region. The curved region of the plot (Figure 4-3 and 4-4) corresponding to longer times is attributable to a retardation of separation as the sedimenting interface becomes the lower edge of the dense- packed zone. This region has been ignored when estimating the rate of sedimentation.

4.3 Batch decay experiments with the two-aqueous-phase dispersions

All the results of the settling time experiments have been presented in graphical form by plotting the dispersion band height against time, for the various volume ratios and phase compositions used. A typical example of this type of plot is shown in Figure 4-1b. x and y, the levels of the lower and upper interfaces of the dispersed band, were measured for each case and used to estimate the height of the dense- packed zone, h_p, and locus, z, using equations 4-6 and 4-7. The hold-up of the dispersed phase in the sedimenting zone $\bar{\varepsilon}_s$ was assumed to be equal to the volume fraction of the dispersed phase in the initial dispersion. The hold-up of the dispersed phase in the dense packed zone $\bar{\varepsilon}_p$ was assumed to be equal to 0.7, which is the approximate value for a dense-packed array of equal-sized spherical drops (Hartland, 1988). Although these are approximations, the results obtained (Figures 4-3 and 4-4) of the height of the dense-packed zone show a consistent pattern of behaviour. The results also show the settling

curve, dense-packed zone, sedimentation zone and the heights of the dispersed (y) and continuous (x) phase for each system tested.

4.3.1 Settling curves

Batch settling curves, obtained for all the systems tested, generally show (Figures 4-3 and 4-4) a sigmoidal decay of height for both the coalescing and particularly the sedimenting interface. The coalescing interface generally fell only slowly with time, suggesting that the process of coalescence with the homophase was slow. In contrast, the sedimenting interface rose rapidly in the early stages of all the experiments and the decay was strongly sigmoidal in character. In the later stages, the sedimenting interface became the lower interface of the dense-packed region and its decay became significantly slower, as its movement was dependent on the rate of coalescence of the drops. The shape of the decay curves varied slightly with the compositions of the phases used, but generally followed the same overall pattern.

Text cut off in original

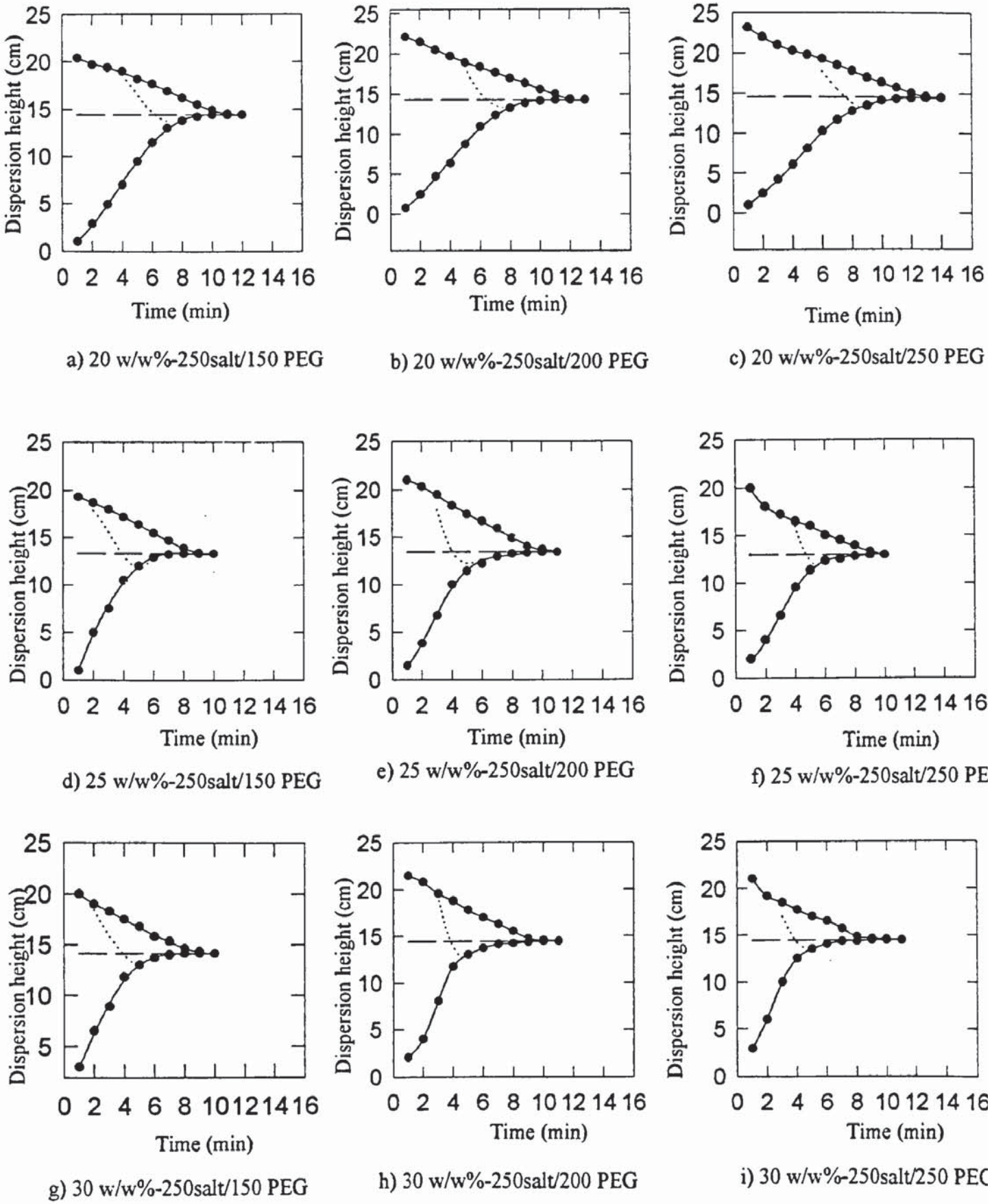

Figure 4-3 Settling curves for various compositions and volume ratios (Exp. I)

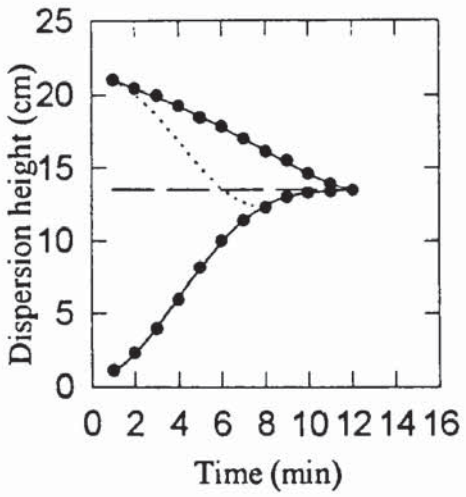

a)20 w/w%-250 salt/150 PEG

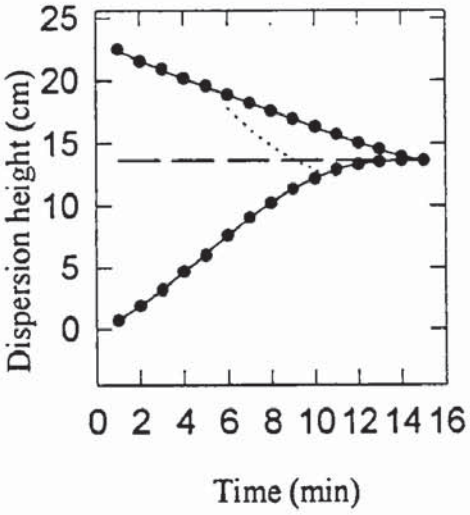

b)20 w/w%-250 salt/200 PEG

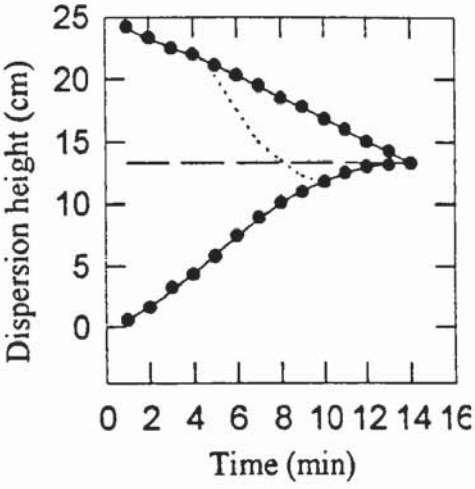

c)20 w/w%-250 salt/250 PEG

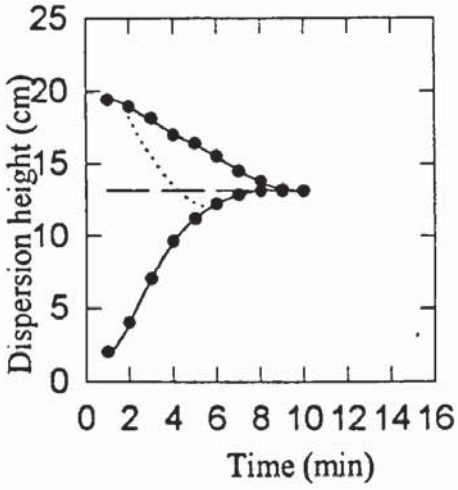

d)25 w/w%-250 salt/150 PEG

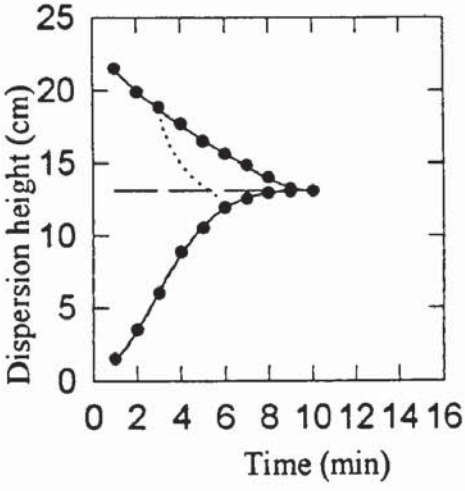

e)25 w/w%-250 salt/200 PEG

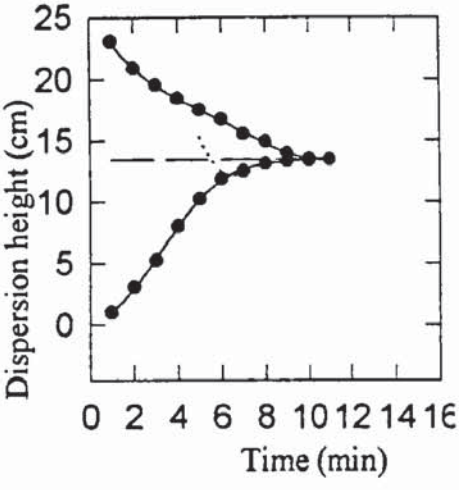

f)25 w/w%-250 salt/250 PEG

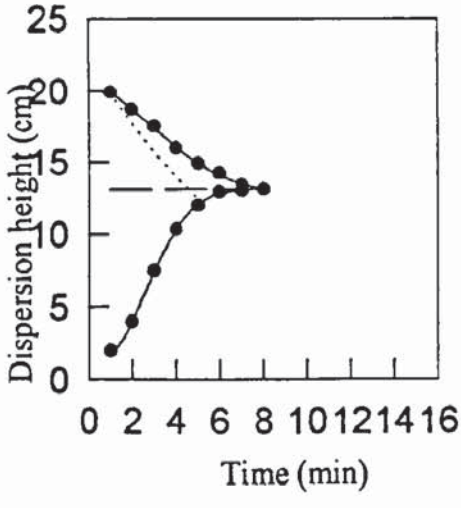

g)30 w/w%-250 salt/150 PEG

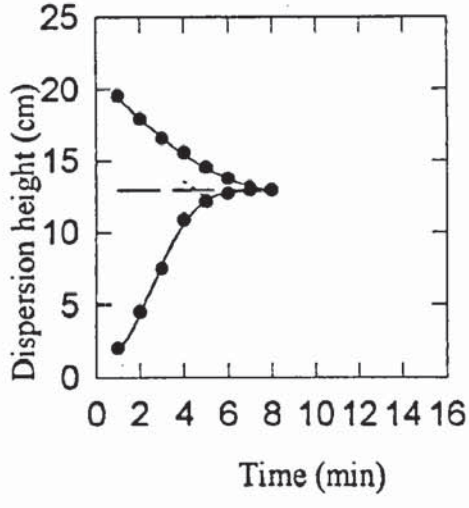

h)30 w/w%-250 salt/200 PEG

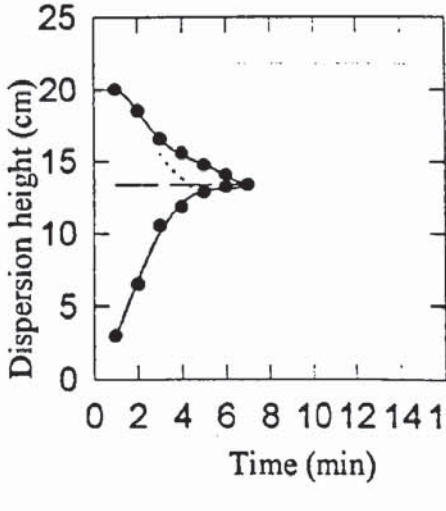

i)30 w/w%-250 salt/250 PEG

Figure 4-4 Settling curves for various compositions and volume ratios (Exp. II)

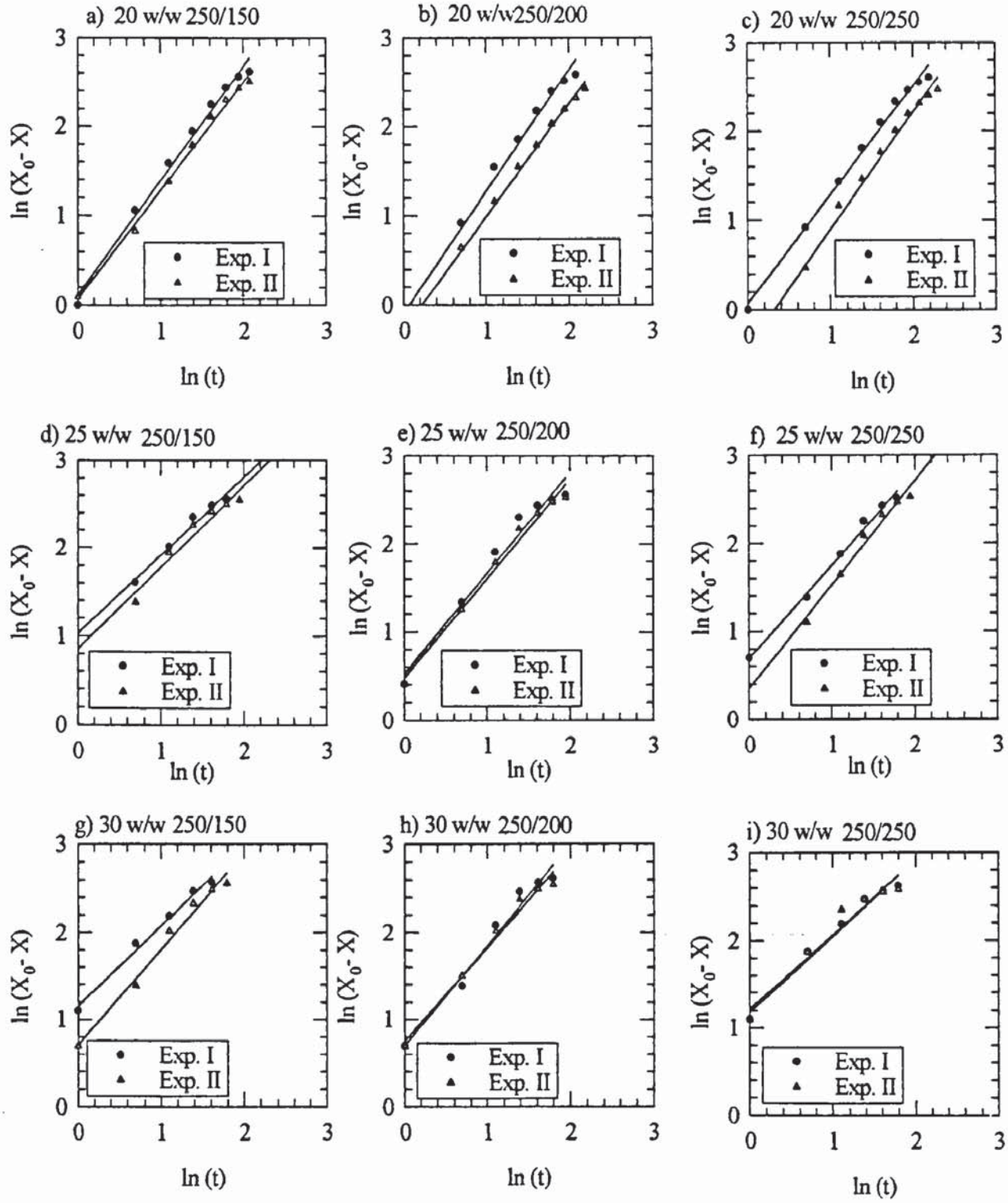

Figure 4-5 Variation of $\ln(x_0-x)$ with the sedimentation front for phase system salt/PEG with volume ratios 250 salt /(150-250) PEG

4.3.2 Primary break-time

The batch tests were first considered in terms of the primary break-time, taken as the time for the dispersion band to clear completely. The results are shown in Table 4-1. The break-time varied with both the composition and the volume ratio of the solutions used to form the dispersion. With the 20% w/w solutions, the break-time increased as the volume fraction of the PEG phase was increased. The increase was not significant, from 12 minutes with 150 cm^3 of PEG solution to 14 minutes with 250 cm^3 of PEG solution. With the 25% w/w solutions, there was again an increase in the primary break-time with increasing volume of the PEG phase, but the effect was less marked. The break-time in the dispersions formed from 30% w/w solutions was independent of the volume ratio.

The break time also decreased as the concentration of the salt and PEG solutions used to form the dispersions was increased. Hence the coalescence process apparently became faster as the concentration of each phase was increased.

4.3.3 Rate of sedimentation

A plot of ln (x_0-x) versus ln (t) was constructed for each experiment, following the method of Jeelani and Hartland (1986). Equation 4-8 assumes that the rate of sedimentation of an open dispersion will increase with time. The log plot then enables the values of k_s and α to be obtained from the intercept $\ln \frac{k_s}{(1+\alpha)}$ and slope $(1+\alpha)$, respectively, of the straight line region.

Figure 4-5 shows the log plot obtained from the experimental data and Table 4-2 gives the values of k_s and α obtained from the experiments. The results show that the

average value of α for the 20 % w/w composition was ≅0.27, and the values for 25%, 30% w/w composition were≅0.16 and ≅-0.1, respectively.

Table-4-1 Influence of phase composition and volume ratios on break time for experiments I and II.

Phase composition	20% w/w			25% w/w			30% w/w		
Batch tests No.	1	2	3	4	5	6	7	8	9
Initial volume of salt/PEG	250\ 150	250\ 200	250\ 250	250\ 150	250 \ 200	250 \ 250	250 \ 150	250 \ 200	250\ 250
Estimated volume ratio of salt/PEG from binodal curve	2.0	1.3	1	2.3	1.7	1.3	2.4	1.7	1.4
Volume ratio salt/PEG	1.9	1.1	1	2.4	1.6	1.3	2.4	1.7	1.5
Break time (Exp.I) (Minutes)	12	13	14	10	11	10	11	10	11
Break time(Exp. II)	12	14	14	10	10	11	8	8	7
Time (hr) to clear both layers	8-15	8-15	8-15	19	24-36	24-36	48-72	48-72	48-72

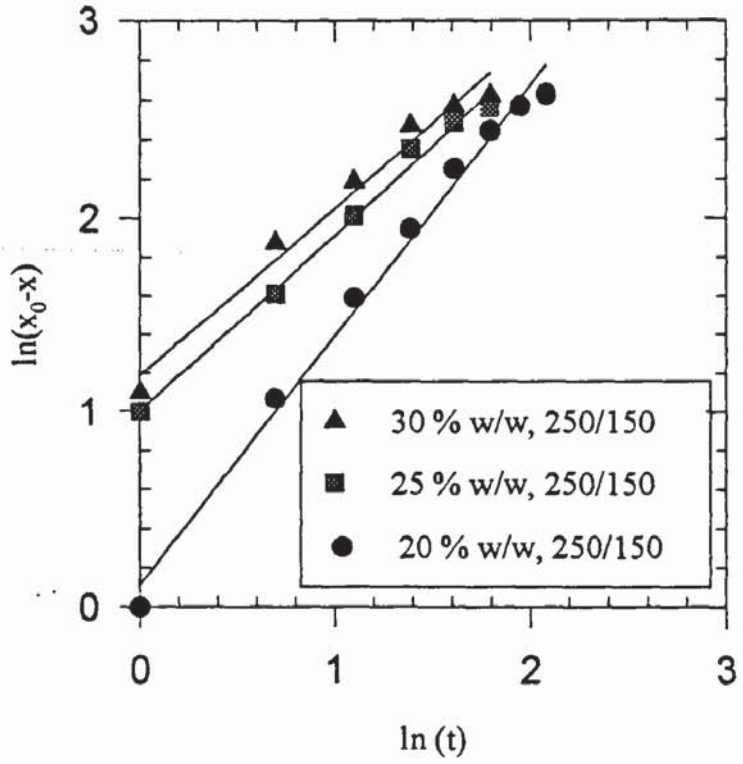

Figure 4-6 An overlay of ln (x_0-x) vs. ln t for the 20, 25 and 30% w/w phase systems.

By comparison, the value of k_s showed an increase with increasing concentration of the solutions used to form the dispersions, but did not show any consistent variation with the volume ratio of the solutions. A typical set of data (Figure 4-6) which is the overlay of the straight line resulting from ln (x_0-x) versus ln (t), for 20, 25 and 30% w/w systems, also shows that the value of k_s increased with increasing concentrations of the solutions.

Table 4-2 The slopes and the intercepts of the line for experiments I and II.

Phase	Vol.	Slope$(1+\alpha)$		$\ln(k_s/1+\alpha)$		k_s		Mean
Conc.%	Fraction	Exp. I	Exp. II	Exp. I	Exp. II	Exp. I	Exp. II	k_s
20 w/w	250/150	1.3	1.2	0.1	0.1	1.4	1.3	1.4
20 w/w	250/200	1.4	1.3	-0.1	-0.3	1.3	1.0	1.1
20 w/w	250/250	1.2	1.3	0.1	-0.3	1.3	1.0	1.1
25 w/w	250/150	0.9	0.9	1.0	0.85	2.5	2.2	2.3
25 w/w	250/200	1.1	1.1	0.5	0.5	1.8	1.8	1.8
25 w/w	250/250	1.1	1.2	0.7	0.35	2.1	1.7	1.9
30 w/w	250/150	0.9	1.1	1.2	0.7	3.1	2.2	2.6
30 w/w	250/200	1.2	1.1	0.7	0.7	2.4	2.2	2.3
30 w/w	250/250	0.9	0.8	1.2	1.2	2.9	2.8	2.8

α is an index in equation 4-8 for droplet sedimentation. In general the value of α did not show any clear pattern as a function of the variation of volume fraction. However the values of α show a slight decrease, from 0.3 to -0.1, with increasing phase composition. In fact, α, should be positive and the negative value is due to experimental error. There is a relationship between α, the binary coalescence index b and a parameter r (equation 4-11) which is a function of Reynolds number

$\mathrm{Re} = \frac{\rho_c u d}{\mu_c}$, where d is the dispersed phase drop diameter (Hartland, 1988). This relationship is expressed by:

$$\alpha = \frac{r}{b} \qquad (4\text{-}11)$$

Since the Reynolds number will increase as the phase composition increases, since ρ_c increases, the parameter r could change from 2 for laminar flow to 1/2 for turbulent flow (Kumar and Hartland, 1985). Therefore, parameter r might decrease with increase in phase composition. There are however other physical properties of obvious significance in such an analysis, e.g. ρ_d, μ_d, σ and $\Delta\rho$.

The exact relationship between index b and the phase composition is not known. Whether b increases, or decreases, with the phase composition could result in a slight decrease in the value of α . This may explain the experimental observation regarding the relationship between α and the phase composition.

Table 4-3 Rate of sedimentation comparing Stokes number and experimental data.

	20% w/w	25% w/w	30%w/w
k_s for 250/150	1.4	2.3	2.6
k_s for 250/200	1.1	1.8	2.3
k_s for 250/250	1.1	1.9	2.8
k_s mean	1.2	2.0	2.6
Stokes number	1.0	2.5	4.0
ρ salt (kg/ m^3)	1102	1135	1176
ρ PEG (kg/m^3)	1075	1074	1075
$\Delta\rho$ (kg/m^3)	27	61	101
σ (N/m)	1.28×10^{-4}	5.9×10^{-4}	1.11×10^{-3}
μ salt (mPa.S)	1.90	1.80	1.85
Assumed diameter (d) in (meters)	1.5×10^{-5}	1.5×10^{-5}	1.5×10^{-5}

The values of k_s (Tables 4-2, 4-3) show that the mean sedimentation rate increased from 1.2 for 20 % w/w to 2.6 for 30 % w/w, with increasing phase composition. This might be expected from the expression for the rise velocity of droplets (Richardson and Zaki, 1954), albeit for unhindered settling,

$$V_r = \frac{g \Delta\rho d^2}{18 \mu}(1-\phi)^n \qquad (4\text{-}12)$$

where ϕ is the volume fraction of the dispersion and exponent n is an empirical constant which depends on the drop Reynolds number.

In this case the drop diameter d is unknown, but the density difference $\Delta\rho$ between the phases increases with increasing phase composition and the viscosity μ_c is roughly constant for the continuous salt phase. Thus if the diameter of the drop d is assumed to be constant, the sedimentation rate, which is proportional to the rise velocity of the droplets, would be expected to increase with an increase in phase composition, as observed in Figure 4-7, which is based on the data in Table 4-3.

Additional observations

It was observed that, after a clear interface was formed, a haze (cloudiness) remained in both layers, with a particularly intense haze in the bottom phase (salt-rich). The haze appeared to consist of very fine drops of the salt-rich phase in the upper (PEG) layer and vice versa. These fine drops were believed to have been formed during the mixing process by spontaneous separation of the two phases of different composition

from the original solutions. They did not initially migrate to the interface under gravity and took no part in the interfacial coalescence process. The haze eventually cleared, and after a period of several days had disappeared from all parts of both layers. The height of the interface between the layers did not change before and after the haze had cleared visually (Figure 4-8), which is explainable by the very low volume fraction that the coalesced drops would occupy, e.g. 10^6 drops of 15 μm diameter ≡ 10^{-3} ml only.

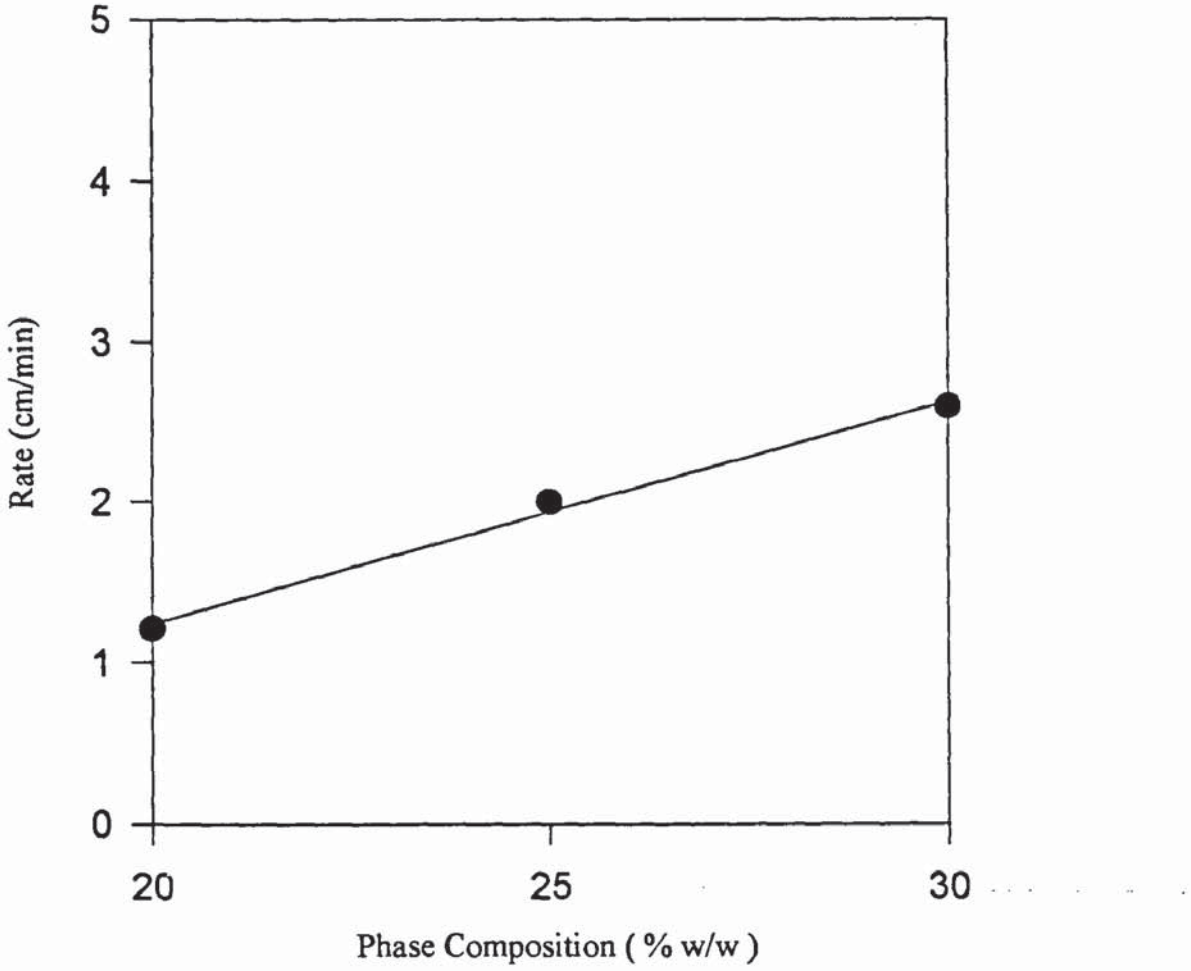

Figure 4-7 Rate of sedimentation for the experimental data.

A second set of experiments was undertaken to determine the experimental error in the settling measurements. Settling curves were plotted again for the second experiment and ln (x_0-x) vs. ln (t) curves were plotted in Figure 4-5, to demonstrate the accuracy and the reproducibility of the settling tests. The curves in Figure 4-5 show that the settling tests can be reproduced easily with a maximum deviation of ±5% and mean

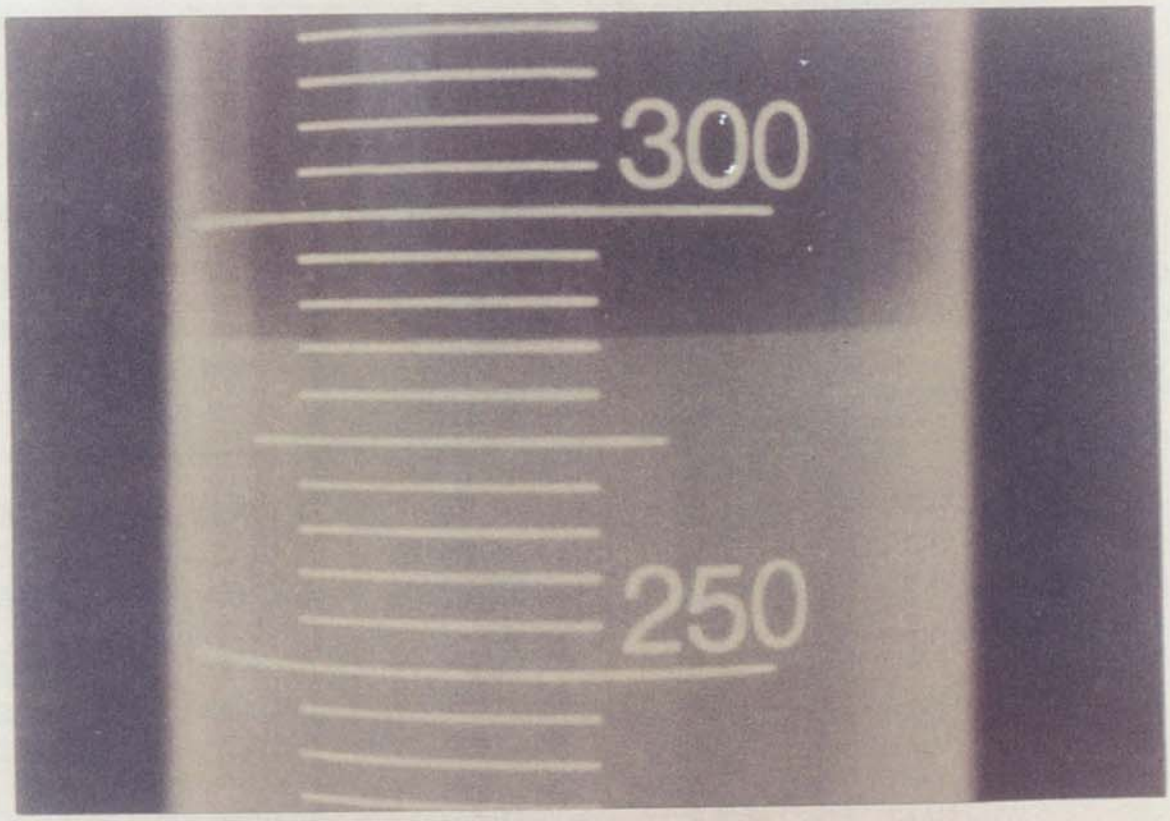
300
250

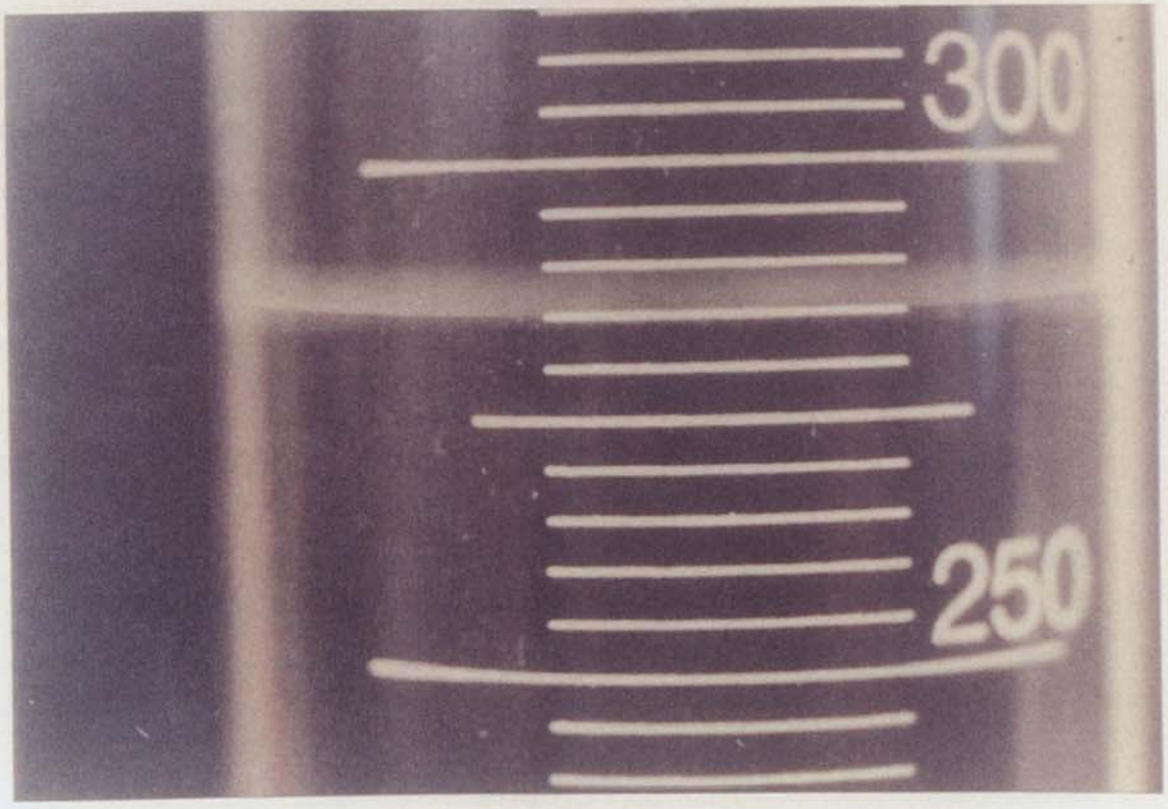
300
250

deviation of ±4%. Table 4-4 shows the slopes for both sets of experiments for various compositions and volume ratios and the mean deviation for each case.

Table 4-4 The slope $(1+\alpha)$ for experiments I and II.

Phase composition	Volume fraction Salt/PEG	Exp. I Slope $(1+\alpha)_I$	Exp. II Slope $(1+\alpha)_{II}$	Slope $(1+\alpha)_{avg}$	Mean Deviation(%) $\frac{(1+\alpha)_I-(1+\alpha)_{avg}}{(1+\alpha)_{avg}}$
20 w/w	250/150	1.3	1.2	1.25	±4
20 w/w	250/200	1.4	1.3	1.35	±4
20 w/w	250/250	1.2	1.3	1.25	±4
25 w/w	250/150	0.9	0.9	0.9	0
25 w/w	250/200	1.1	1.1	1.10	0
25 w/w	250/250	1.1	1.2	1.15	±4
30 w/w	250/150	1.0	1.1	1.05	±5
30 w/w	250/200	1.2	1.1	1.15	±4
30 w/w	250/250	0.9	0.8	0.85	±5

The significance of these results, and their application to design, are discussed in chapters 7 and 8 respectively.

5 Mass Transfer From Single Drops

5.1 Introduction

Because of the complexities involved, mass transfer studies were limited to single discrete droplets. As in previous classical studies in liquid-liquid extraction (Slater, 1994), the observations then require extrapolation to the case of swarms involving a distribution of drop sizes.

The objective was to study the effects of droplet size, phase concentration of the system and phase composition of transferring dye on the mass transfer rate. From the results it was hoped to gain some insight into mass transfer mechanisms in two aqueous phase mixtures involving small droplets.

Cibacron Blue 3GA was chosen as the transferring component because of its use as a ligand in the extraction of enzymes in PEG systems (Johansson, 1984) and its relatively high molecular weight, thus simulating the behaviour of proteins and other biochemicals.

The range of dye concentrations used was 0.01 to 0.1 % w/w. This was selected because it mimics high molecular weight solute. Since it was necessary to examine the behaviour of droplets of millimetre size, three different nozzle diameters were used. PEG/salt solutions were tested at concentrations between 20 and 30 % w/w.

5.2 Experimental methods and materials

Falling drop method

Initially it was necessary to calibrate the spectrophotometer used to measure the concentration of the transferring solute. This was carried out by preparing various

concentrations of dye (Cibacron Blue 3GA) in potassium hydrogen orthophosphate solutions. The absorbance of these samples was measured using a Perkin Elmer UV/VIS spectrophotometer at 611.5 nm. The absorbance values were plotted against concentration to generate calibration curves (Figure 5-1). The dye was used as transferring solute because it was known to partition into the PEG phase (Johansson, 1984, Kula, 1979, Kula et. al., 1982), because it should mimic the behaviour of high molecular weight protein, and to enable diffusion to be observed visually.

For the experiments involving mass transfer, discrete, single drops containing dye were allowed to fall through the continuous phase (PEG solutions) contained in a 8 cm diameter glass column of length 0.47 m. The drops were released under gravity from a glass nozzle with a needle (I.D. 0.2, 0.5 and 1.2mm), attached to a burette and then entered the continuous phase. The needle was about 3 mm above the continuous interface. Hence no solute transfer occurred during drop formation. The dispersed phase comprising between 198 and 202 drops after coalescence was collected from the bottom of the glass column. The absorbance of the dispersed phase was measured using the spectrophotometer at ambient temperature (20°C ± 2°C). The residual concentrations were then found from the calibration curve. The number of drops was counted using a hand counter, and their fall-time measured with a stop-watch. The average falling-times were 16.9 seconds, 15.2 seconds and 6.5 seconds for the needle sizes I.D. 0.2 mm, 0.5mm and 1.2 mm, respectively.

The total volume and the number of the drops released were measured from the burette to calculate the mean drop diameter. Visual observations confirmed that the drop size did not vary significantly from the mean value.

Experiments were carried out using 30% w/w, 25% w/w and 20% w/w dispersed and continuous phases, respectively. At each concentration three different needles, of 0.2mm, 0.5mm and 1.2mm internal diameter, were used to generate different drop

sizes in the approximate mean size range of 2.8mm, 3.0mm and 3.7mm. Hence there was a total of nine experimental configurations.

Absorbance measurement

A Perkin Elmer UV/VIS spectrophotometer was used to measure the absorbance of the prepared dye samples. Distilled water was used as a reference solution to calibrate the instrument to zero absorbance.

The sample cell was placed in the compartment, then "Peak Seek" mode was selected to determine precisely the wave length of an individual peak for the dye colour. The peak chosen was at 611.5 nm. The value of absorbance was then displayed on the readout.

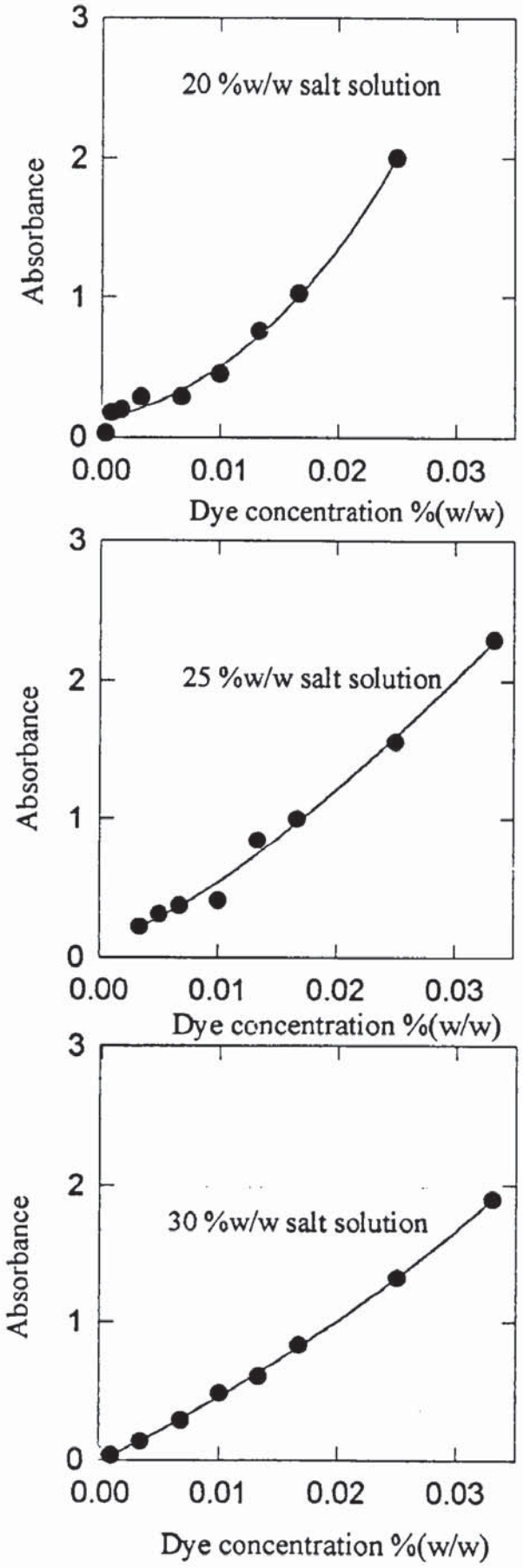

Figure 5-1 Calibration curves; dye concentration vs. absorbance.

5.3 Theoretical methods and results

Mass transfer from a single spherical drop falling under gravity through a stagnant liquid may be described by a variety of models. The simplest is the two film theory, discussed in Section 2.6 (equation 2-3). The rate of solute transfer through two films in series may be expressed by

$$N = K\,A\left(c_d - \frac{c_c}{m}\right) \qquad (5\text{-}1)$$

In this model N is the rate of mass transfer, K is the overall mass transfer coefficient, A is the surface area of the drop, c_d is the concentration of the dye in the dispersed phase, c_c is the dye concentration in the continuous phase and m is a partition coefficient.

Equilibrium at the interface is assumed, so that the partition coefficient may be expressed in terms of the interfacial concentrations as:

$$m = \frac{c_{ci}}{c_{di}} \qquad (5\text{-}2)$$

where c_{ci} is the dye concentration in the continuous phase at the interface, and c_{di} is the dye concentration in the dispersed phase at the interface.

K, the overall mass transfer coefficient, may be expressed in terms of the mass transfer coefficients k_c and k_d , corresponding to the resistances in the continuous phase and the dispersed phase respectively: [It is conventional to neglect any interfacial resistance due, in part, to the impracticality of measuring it].

Hence,

$$\frac{1}{K} = \frac{1}{mk_c} + \frac{1}{k_d} \qquad (5\text{-}3)$$

A mass balance on the dispersed phase drop gives

$$N = K A \left(c_d - \frac{c_c}{m} \right) = -V \frac{dc_d}{dt} \tag{5-4}$$

where V is the drop volume. Assuming the drop is spherical, then

$$V = \frac{\pi d^3}{6} \tag{5-5}$$

and

$$A = \pi d^2 \tag{5-6}$$

is the surface area of the spherical drop, where d is its diameter.

Thus, by substituting in equation 5-4

$$-\frac{dc_d}{dt}\frac{\pi d^3}{6} = K\pi d^2 \left(c_d - \frac{c_c}{m} \right) \tag{5-7}$$

and rearranging,

$$\frac{d}{6}\frac{dc_d}{dt} = -K(c_d - \frac{c_c}{m}) \tag{5-8}$$

Given the experimental design, i.e. the droplet contained a high concentration of dye and the continuous liquid did not, the dye concentration in the continuous phase, c_c, can be assumed to be zero. Integrating

$$\frac{1}{6}\int_{c_0}^{c_d}\frac{dc_d}{c_d} = -\frac{K}{d}\int_0^t dt \qquad (5\text{-}9)$$

$$\frac{1}{6}\ln\frac{c_d}{c_0} = -\frac{K}{d}t \qquad (5\text{-}10)$$

Rearranging gives the overall mass transfer coefficient K

$$K = \frac{d}{6t}\ln\frac{c_0}{c_d} \qquad (5\text{-}11)$$

Equation 5-11 was used to calculate K for all experiments. Results are plotted in Figures 5-2 and 5-3 as mass transfer coefficient, K, against initial dye concentration c_0. Since it was not possible to form droplets with the 20% w/w solution, because the low surface tension resulted in a jet rather than a drop, only results for the 25% and 30% w/w systems are shown.

In the absence of direct measurements of drop shape, an equivalent spherical diameter was used. This was calculated (using equation 5-5) from the mean drop size (3.7mm, 3mm, and 2.8mm from the nozzles of diameters 1.2mm, 0.5mm, 0.2mm, respectively) based on the total volume of dispersed phase used and the number of drops counted. It was assumed that the concentration of dye in the continuous phase was negligible throughout the experiments. This assumption may be tested using the following equation:

$$S = \sum_{i=1}^{j}\rho \mathrm{v} n_i \frac{c_0 - c_f}{100} \qquad (5\text{-}12)$$

where S is the amount of dye transferred to the continuous phase [g], ρ is the density of the dispersed phase [g/ml], v is the volume [cm^3] of each drop, n_i is the number of drops counted in each batch of experiments using the same continuous phase, j is the

number of batches using the same continuous phase, c_0 and c_f are the initial and final dye concentrations in the drop phase [%w/w].

To calculate the concentration of dye in the continuous phase at the end of each set of experiments (the maximum value),

$$c_c = \frac{S}{v_l \rho_l} 100 = \frac{S}{\frac{\pi}{4} D^2 H_l \rho_l} 100 \qquad (5\text{-}13)$$

where c_c is the concentration of dye in the continuous phase [%w/w], v_l is the volume of the continuous phase in the column, D is the diameter of the column, H_l is the height of the column and ρ_l is the density of the continuous phase. The final concentration of dye in the continuous phase at the end of each set of experiments, c_c, was thus about 2.0×10^{-4} %w/w, i.e. much lower than the typical dye concentration in the dispersed phase (c_d= 0.1 %w/w). Hence $\frac{c_c}{m}$ can be neglected, compared with c_d, if m is not too small (m>1).

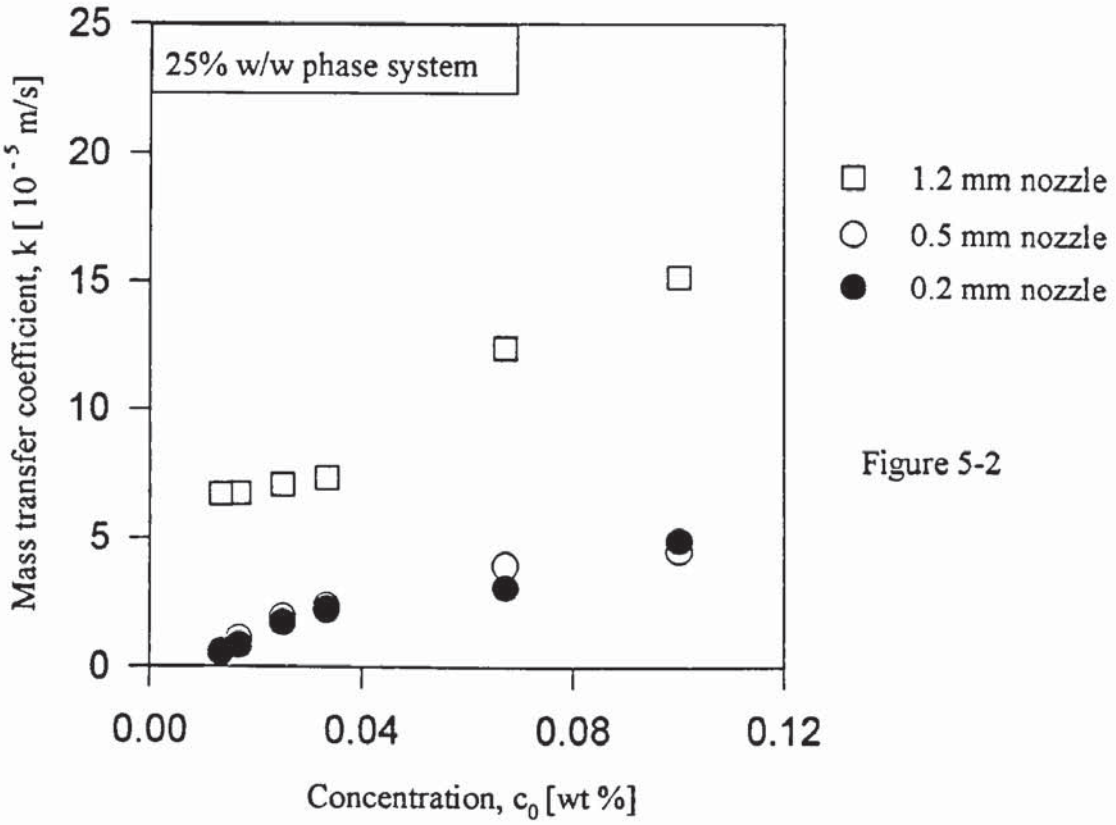

Figure 5-2

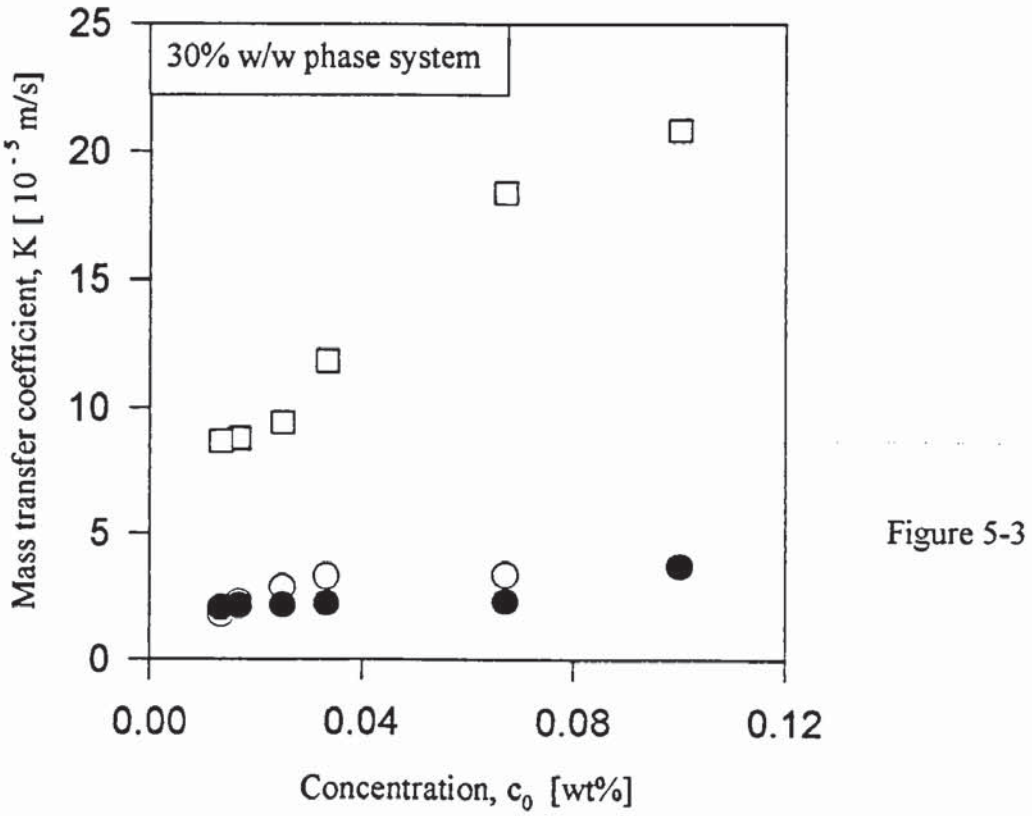

Figure 5-3

Figures 5-2 and 5-3 Mass transfer coefficient, K versus dye concentration c_0 (using eq. 5-11).

An experiment was conducted to measure the partition coefficient of dye in the PEG-salt system. It was found that the dye partitioned to the top phase (PEG) and the bottom phase (salt) appeared colourless. This suggested that the dye partitioned very strongly to the top phase. The exact dye concentration in the salt phase is not known since it was lower than the concentration measurable by the spectrophotometer. The partition coefficient is thus much greater than 1, so that $c_d \rangle\rangle \frac{c_c}{m}$. Thus neglecting $\frac{c_c}{m}$ in equation (5-8) is justified.

5.4 Discussion of the results

All the results of the mass transfer experiments show that K increased with dye concentration in the dispersed phase (Figures 5.2 and 5.3). Theoretically, the partition coefficient m is a function of dye concentration in both phases. However, since the dye concentration in the continuous phase was very low ($c_c \cong 2.0 * 10^{-4}$ wt%) (see previous section), it is reasonable to assume that m is a constant over the experimental conditions (Coulson and Richardson, 1956). Therefore, the increase in K with dye concentration in the dispersed phase must be due to other reasons; these are discussed below.

1) *Reaction*

Olander (1960) derived an equation to predict the effect of various chemical reactions on the rate of liquid-phase mass transfer. The calculated mass transfer coefficients were found to be a function of the concentration driving force, the precise form of the dependence being controlled by the rate of reaction and equilibrium stoichiometry.

2) *Interfacial turbulence*

As discussed in Chapter 2, interfacial turbulence or spontaneous interfacial convection is known to substantially increase the mass transfer rates in the course of liquid-liquid extraction.

Sternling and Scriven (1959) discussed the conditions under which a small fluctuation in surface tension during mass transfer can build-up into a macroscopic eddy. This process can enhance the mass transfer process, by producing eddy transport in addition to molecular diffusion.

Sawistowski (1971) describes the formation of ordered convection cells which create movement at the interface. This movement enhances the mass transfer and can be shown to cause the mass transfer coefficient to increase as a function of the solute concentration.

Golovin (1984) also found that the mass transfer coefficient in the presence of interfacial turbulence greatly exceeds the value in the diffusion regime, and that it depends upon the concentration driving force and the interfacial tension between the phases.

3) *Solubility*

Application of the two-film model assumes that the dye is dissolved in the dispersed phase (salt phase). However, if this assumption is not correct, for example if the dye dissolves in the dispersed phase or is suspended as particulates, a new model may need to be derived.

4) *Non-equilibrium and convection effect*

Alternatively if the addition of solute shifts the equilibrium of the PEG/salt system, the mass transfer will then be affected.

In order to confirm or eliminate each possible reason listed as 1 to 4 above a number of further investigations were conducted.

1) *Reaction*

The first reason for the increase of mass transfer coefficient with the increase of solute concentration is a possible reaction between the dye (Cibacron Blue 3 GA) and the PEG solution.

Johansson (1984) describes the use of a Cibacron-PEG ligand complex to extract proteins selectively. The complex was prepared by reacting PEG and dye in alkaline solution (pH 10-11) at 80°C for two hours and the low yield of product was purified by column chromatography (Johansson, 1984).

Although these conditions did not occur in the experiments described here, it was considered necessary to confirm that there was no reaction between PEG and dye. Thus an aqueous mixture of PEG (Molecular Weight 6000) and dye was prepared under typical experimental conditions and a sample taken for mass spectrometric analysis. Mass spectra were obtained from a standard procedure with a VG Zabspec mass spectrometer using Liquid Secondary Ion Mass Spectrometry (LSIMS) as the ionisation technique. Use of this technique provides accuracy and high result resolution. Samples were dissolved in a small volume of m-nitrobenzyl alcohol which had been previously coated onto a stainless steel probe. Spectra were obtained by scanning in the positive-ion mode at a scan speed of 10 seconds per decade.

Samples of a pure PEG solution and pure dye solution were also run, for comparison. The results showed (Figure 5-4) that the PEG spectrum was observed in the mixed sample but that there were no peaks at wave length >1500 nm, which is where any reaction product, such as triazine dye-polyethylene glycol (Johannsson, 1984) should appear. Thus no reaction appeared to have taken place between the dye (Cibacron Blue 3 GA) and PEG.

Since a further possibility was that the reaction could be very slow, a further sample of the PEG-dye mixture was left over a week at normal ambient conditions prior to analysis. The results (Figure 5-5) also showed no sign of reaction between the dye and PEG.

The evidence from the Mass Spectrometry tests confirmed that the increase in mass transfer coefficient with dye concentration was not due to a reaction between the dye and PEG.

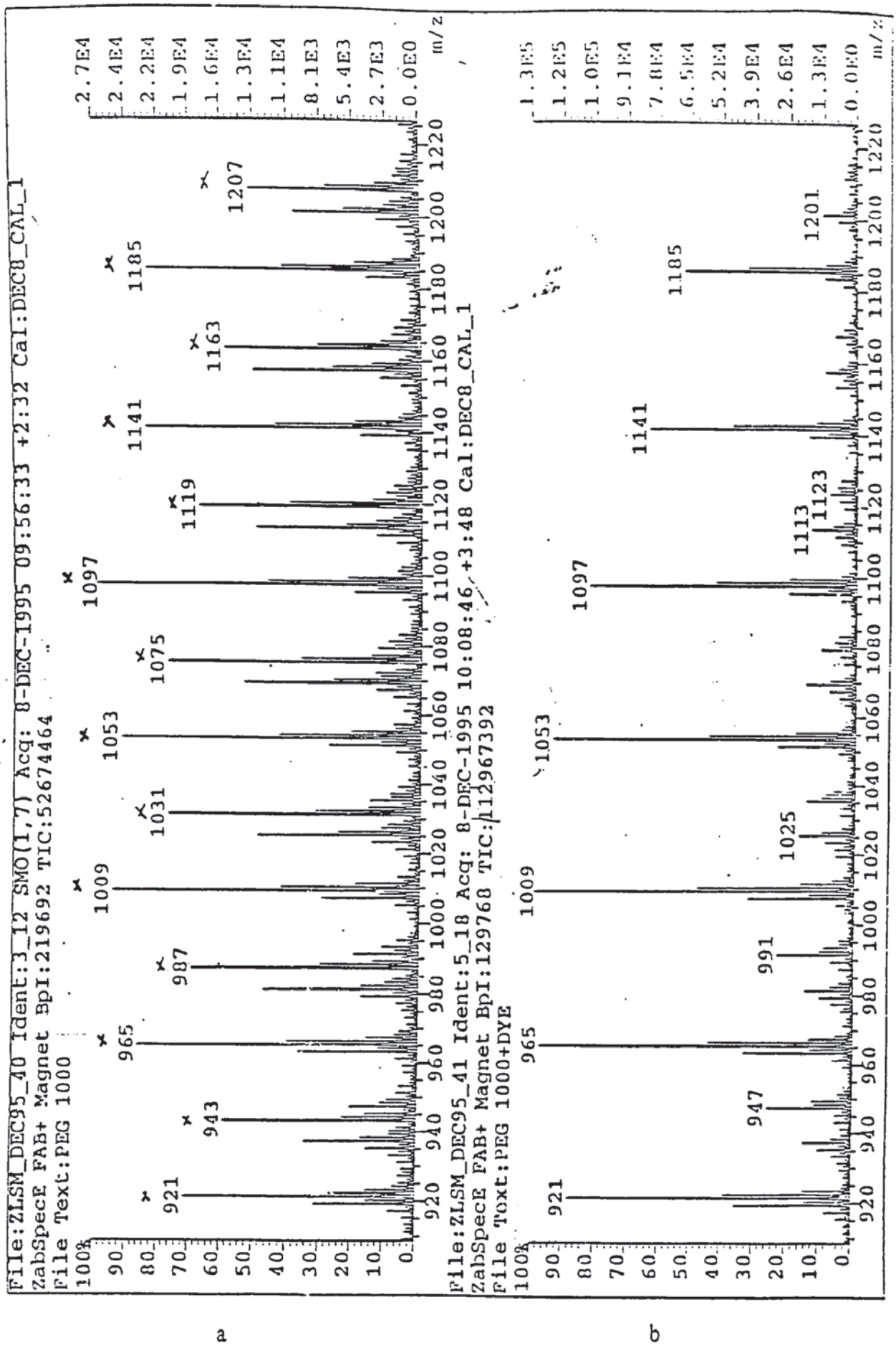

Figure 5-4 Spectrum for PEG and PEG + Dye

a) Spectrum for PEG b) Spectrum for PEG + Dye

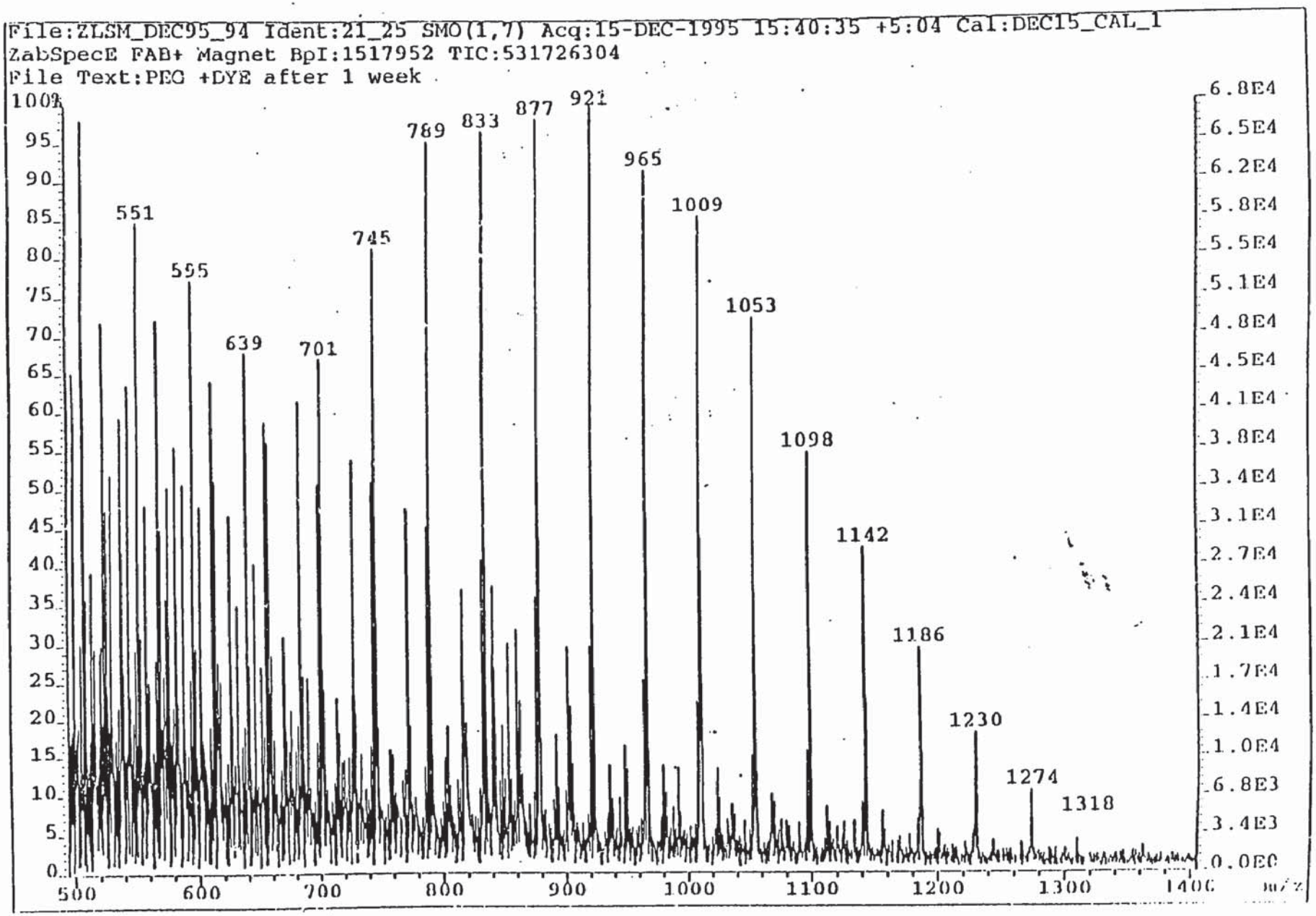

Figure 5-5 a Spectrum for PEG + Dye after one week

2) *Interfacial turbulence*

The second possibility is interfacial turbulence in the PEG/salt system. One criterion for the existence of interfacial turbulence is that the interfacial tension is a function of the solute concentration (Sawistowski, 1971).

Experiments were undertaken to measure the interfacial tension with different dye concentrations in the PEG phase. The solutions for these experiments were initially prepared as described in Chapter Three. The two phases were pre-equilibrated with different amounts of dye, before the PEG phase was separated and the interfacial tension measurements made.

The interfacial tension was then re-measured, as shown in Table 5-1, which gives interfacial tension values versus dye concentration in the drop.

Table 5-1 Interfacial tension versus dye concentration at 24°C.

20 wt % phase system	
c_0 (wt)%	σ (N/m)
0.01	1.43×10^{-4}
0.1	1.28×10^{-4}
0.2	1.07×10^{-4}

As can be seen, the interfacial tension decreased with the dye concentration in the drop. According to Slater (1994) the relationship between interfacial tension and mass transfer coefficient can be expressed by:

$$k \propto \sigma^{-1.25} \qquad (5\text{-}14)$$

Assuming that an analogous relationship exists between the interfacial tension and the dye concentration in the drops for 25%w/w and 30%w/w phase systems, the maximum

increase in mass transfer coefficient K due to the increase in the dye concentration in the drop (from 0.01 to 0.1 % w/w) can thus be estimated as less than 20%. This increase is not sufficient to explain the variation in K, as shown in Figures 5-2 and 5-3.

3) *Insolubility of the dye in the salt phase*

During storage, the dye was observed to be present in the salt phase as a very finely dispersed solid, rather than in solution. This behaviour suggested that the dye may not have been dissolved in the salt phase, but was simply well-dispersed as fine i.e. < 1 μm, solid particles. Alternatively, the separation might have resulted from precipitation of the dye due to temperature change.

An experiment was undertaken to investigate whether the dye precipitated because of temperature changes. Using a water bath to control the temperature of the dye-salt solution overnight at 24 °C , the dye was still observed to have settled to the bottom of the flask. This indicated that the settling of the dye in the salt phase was not due to temperature change.

The solubility of the dye in the salt solution was therefore investigated. An experiment was undertaken to check the solubility of the dye. A sample of the solution after the dye had settled under gravity was centrifuged for ten minutes at 19 000 RPM. Virtually all the blue colour was seen to have separated to the bottom of the test tube. This result indicates that the dye solubility in the salt solution was in fact very low, i.e. below the limit of detection by eye.

The solubility results suggest that the dye was essentially undissolved in the salt solution but formed particles of colloidal size, i.e. 10^{-1} to 10^{-3}μm, at the start of each experiment.

The apparently uniform blue colour on mixing could only be due to the very fine solid dye particles being evenly dispersed in the liquid.

The simple two-film model of mass transfer may not be used to describe the overall mass transfer process in this case, since the dye remains undissolved in the salt solution and does not diffuse to the drop surface. Therefore an alternative model was developed to describe the mass transfer process:

If the dye is in the form of uniformly-dispersed particles within the salt drop,

$$c_d' = \frac{N}{V} = \frac{N}{\frac{\pi}{6} d^3} \tag{5-15}$$

where c_d' is the concentration of particles in the drop, N is the total number of particles in the drop, and V is the drop volume assuming a spherical drop.

Mass transfer from the drops occurs by solid particles near the surface of the drop coming into contact with the continuous phase and dissolving into it. Only particles within a surface layer inside the drop are able to take part in this process. The thickness of this layer may be assumed to be equal to the diameter of the solid particles. The volume of this surface layer is thus approximately $\pi d^2 d_i$ where d_i is the particle diameter and πd^2 is the surface area of the drop.

Then, assuming that the particles are uniformly distributed throughout the droplet, the number of particles in the surface layer is n_i, given by

$$n_i \approx \pi d^2 d_i c_d' \tag{5-16}$$

The total surface area of the particles in the surface layer of the drop is

$$\begin{aligned} a = n_i \pi d_i^2 &= (\pi d^2 d_i c_d') \pi d_i^2 \\ &= \pi^2 d_i^3 d^2 c_d' \end{aligned} \tag{5-17}$$

Since $\frac{\pi}{6} d_i^3 \rho_s c_d' = \rho_d \frac{c_d}{100}$, then

and

$$c_d' = \frac{c_d \rho_d}{\frac{\pi}{6} d_i^3 \rho_s 100}, \qquad a = 6\pi d^2 \frac{c_d}{100} \frac{\rho_d}{\rho_s}$$

where ρ_s is the density of the solid particles, and ρ_d is the density of the dispersed phase.

In practice, not all the surface of the particles will be exposed to the continuous phase. However, given a large number of particles it may be assumed that the active surface area per particle is essentially constant. Thus the active surface area for mass transfer may be written as:

$$a = k' d^2 \frac{c_d}{100} \tag{5-18}$$

where $k' = 6\pi \frac{\rho_d}{\rho_s}$ for the case where the whole of the surface of each particle is active.

The mass transfer process away from the drop surface can still be described by a film model, so that

$$-\frac{\pi d^3}{6} \frac{dc_d}{dt} = ka\left(c^* - c_c\right) \tag{5-19}$$

In this case, c^* is the solubility of the dye in the continuous phase, since the mass transfer is occurring by dissolution of the solid dye particles at the surface of the drop. The concentration relative to the dissolving solid is the solubility, assuming equilibrium at the solid surface.

Thus

$$-\frac{dc_d}{dt} = \frac{kk' d^2 c_d \left(c^* - c_c\right)}{100 \frac{\pi}{6} d^3} \tag{5-20}$$

Equation (5-20) cannot be solved directly because it includes two variables: c_d and c_c.

Assuming as before that the concentration of the dye in the continuous phase $c_c \approx 0$, then equation (5-20) gives

$$\frac{dc_d}{dt} = -\frac{6kk'c_d c^*}{\pi d} = -\frac{k_0}{d}c_d \qquad (5\text{-}21)$$

where $k_0 = \frac{6kk'c^*}{\pi}$. Solving equation (5-21) gives

$$\int_{c_0}^{c_f} \frac{dc_d}{c_d} = -\frac{k_0}{d}\int_0^t dt$$

$$\ln\frac{c_d}{c_0} = -\frac{k_0}{d}t$$

$$k_0 = \frac{d}{t}\ln\frac{c_0}{c_f} \qquad (5\text{-}22)$$

This result is identical in form to the two-film model (equation 5-11) and predicts that the apparent mass transfer coefficient k_0 for the particle model should be independent of the dye concentration in the dispersed phase. Plots of k_0 are presented as a function of dye concentration in Figures 5.7 and 5.8.

4) *Non-equilibrium and Concentration Effects*

Experiments were undertaken to measure the interfacial tension with different dye concentrations in the PEG phase. The solutions for these experiments were initially prepared as described in Chapter Three. The PEG phase was first separated, and a known concentration of dye added before undertaking the interfacial tension measurements. In the experiments, mass transfer was observed as the PEG drop was

formed. Material from the continuous phase (salt phase) transferred to the drop which contained PEG/dye; microscopic drops of the salt phase then formed inside the PEG/dye drop. These small drops rapidly coalesced to form droplets visible to the naked eye. A circulation flow was observed inside the PEG/dye drop, although it was unclear whether this was a direct result of the transfer of salt, or was caused by the internal salt phase drops falling to the base of the drop (Figure 5-6).

The circular motion inside the PEG/dye drop might be expected to enhance the dye mass transfer by improving dye transport to the drop surface.

It was thought that the observed salt transfer might be caused by the presence of the dye affecting the salt-PEG phase equilibrium. To eliminate this, the interfacial tension experiments were repeated using PEG-dye and salt solutions which had previously been stirred together to allow the dye to equilibrate between the salt and PEG phases.

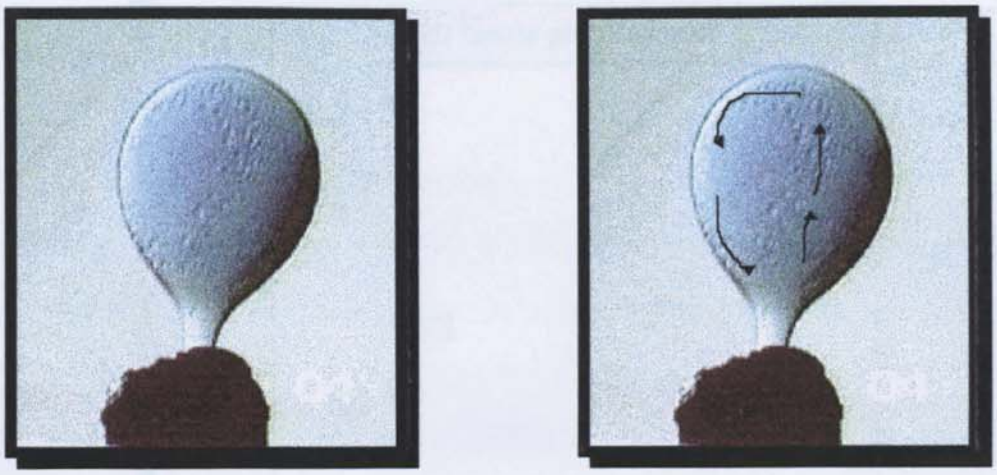

Figure 5-6 Salt drops circulating inside (Dye/ PEG) drop.

The interfacial tension was then re-measured, the data being presented in Table 5-1. No significant mass transfer was observed during the re-measurements. This observation suggests that equilibrating the dye within the system reduces the mass transfer from the bulk phase to the PEG/dye drop. It appears to confirm that the dye had shifted the equilibrium of the PEG system.

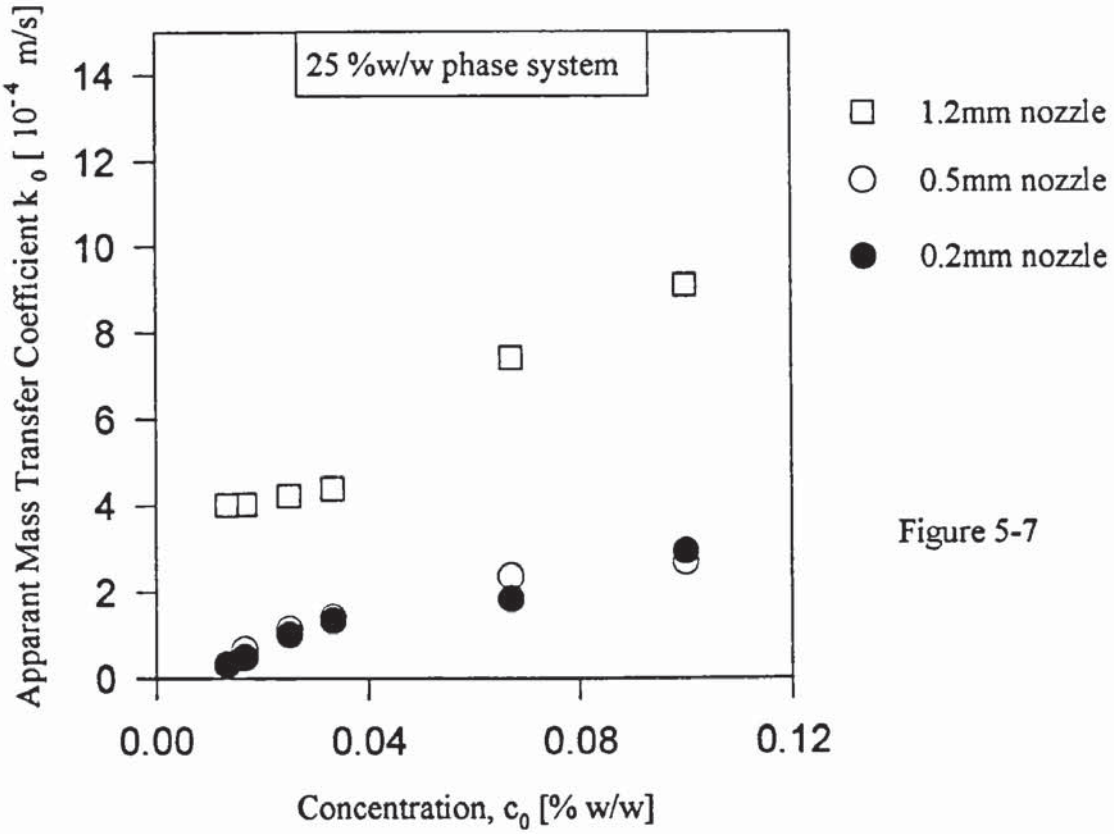

Figure 5-7

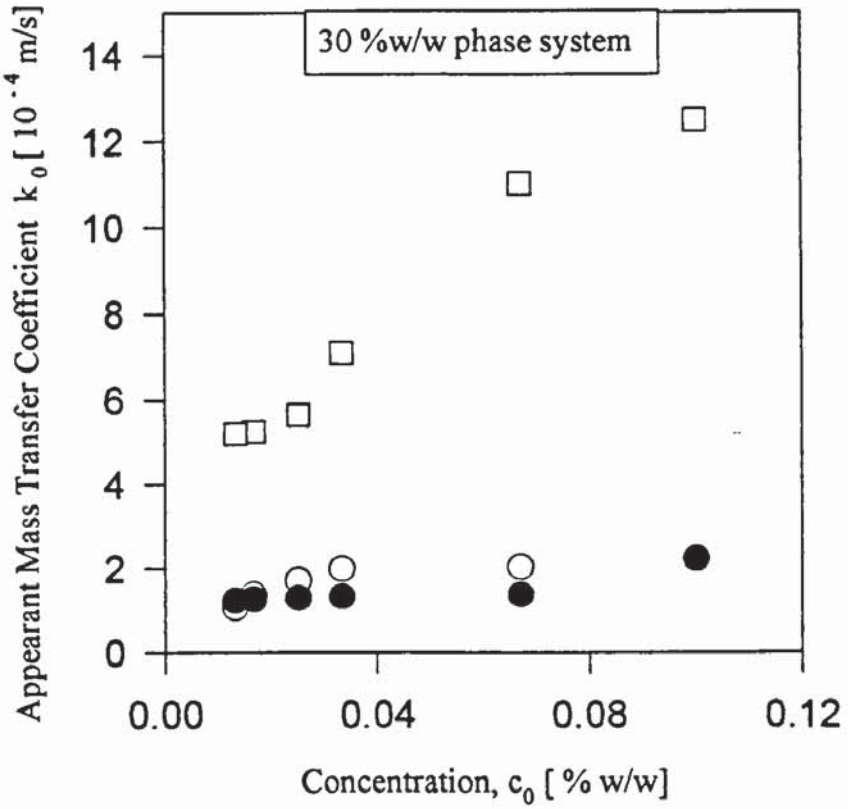

Figure 5-8

Figures 5-7 and 5-8 Apparent mass transfer coefficient k_0 versus dye concentration) c_0 calculated using equation 5-22.

Further observations

Figures 5-7 and 5-8 also show that the largest drops (using the 1.2mm diameter nozzle) resulted in a higher value for the apparent mass transfer coefficient than the smallest ones by a factor of about five. This may be due to the following reasons.

Deformability of the larger drop

According to the theory proposed by Grace, Wairegi and Nguyen (1976), the shape of drops can be predicted when they move freely under the action of gravity in liquids. An attempt has been made to predict the shape of the drops in this system, which shows that the largest drops (3.7mm in diameter) are in the ellipsoidal regime and the smaller drops (2.8mm, 3mm in diameter) are in the spherical regime. It was observed from the experimental work that the largest drops (3.7mm in diameter) were ellipsoidal and the smaller drops spherical. The visual observations thus support the prediction. When the large drops are deformed from the original spherical shape into an ellipsoidal shape there is an increase in surface area, which may enhance the mass transfer rate.

Large drop internal motion and breakage

During the measurement of the mass transfer, the nozzle on which the drop formed was placed about 3 mm above the surface of the continuous phase. On entering the continuous phase, the drop had significant kinetic energy, which will largely be converted to internal motion in the drop (Figure 5-9). Although the circulation may be damped by viscous forces at the interface, it will contribute to enhanced mass transfer from the drop as mentioned in Section 2.6.1.

It was also observed that some of the large drops broke into two. The two drops consisted of a large drop which left behind a smaller drop. The smaller drop either accelerated and coalesced with the large drop (Figure 5-10a), if the smaller drop was in the wake of the larger drop, or moved along with the large drop if they were outside the wake region of the large drop (Figure 5-10b). This breakage of the large drops

would increase the interfacial area and the interior of the resultant drops would initially be turbulent, which leads to an increase in the rate of mass transfer. This observed effect suggests that under the conditions of present study the mass transfer rate may be expected to be higher for large drops than for smaller rigid drops.

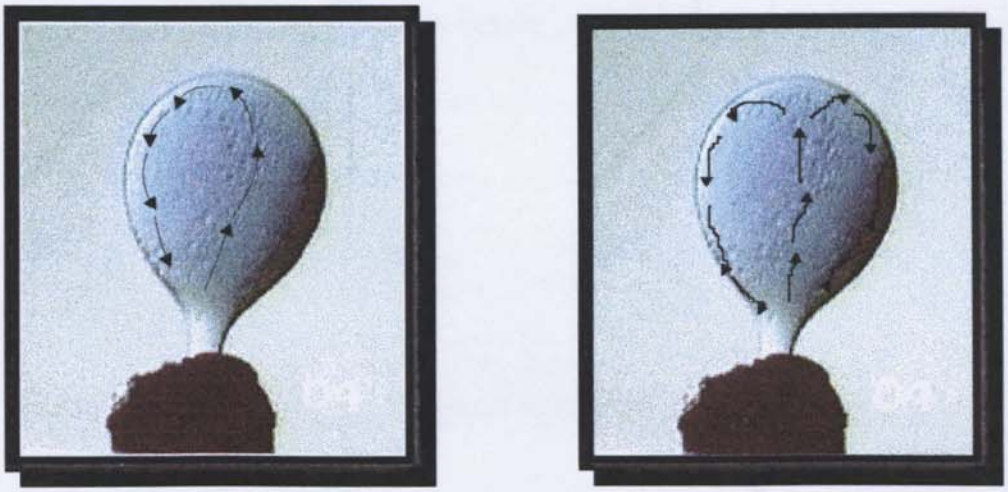

Figure 5-9 Drop internal motion

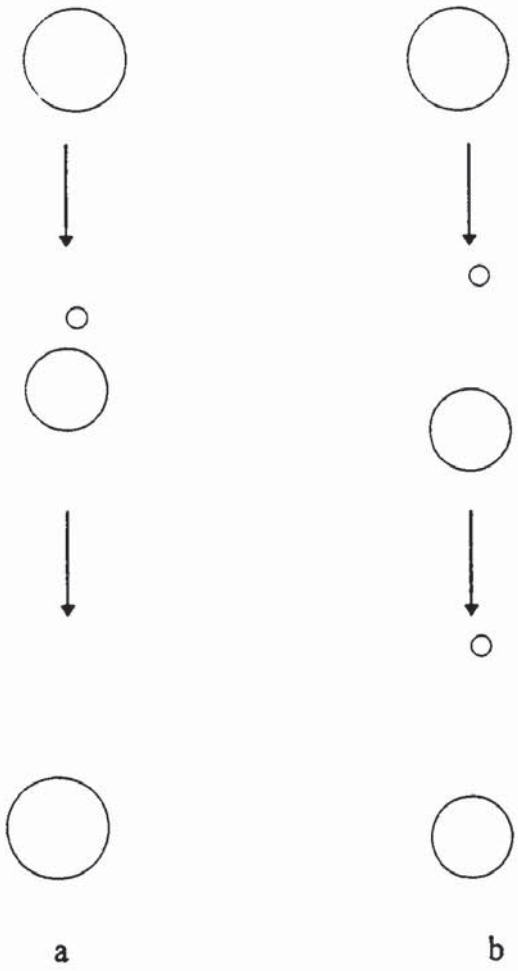

Figure 5-10 Droplet behaviour following break-up.

a) Smaller drop within influence of wake of remaining large drop

b) Smaller drop behaviour independent of remaining drop.

6 Drop Size Distribution in an Agitated Vessel

6.1 Introduction

The behaviour of liquid-liquid dispersions in stirred tanks is of special interest in chemical engineering practice. If two immiscible liquids are agitated, a dispersion is formed, in which continuous break-up and, if the hold-up is sufficient, coalescence of droplets occur simultaneously. If the agitation is continued over a sufficient period of time, a local dynamic balance is established between break-up and coalescence. The average size of the droplets at equilibrium will then depend on the conditions of agitation, physical properties of the system, temperature of the system and the dispersed phase hold-up.

Drop size distributions are an important characteristic of liquid-liquid dispersions, since the physical and chemical phenomena which occur in an agitated vessel depend largely on the size of the dispersed droplets. For processes such as mass transfer, it is essential that the size of the droplets can be estimated to enable the mass transfer area and hence the rate to be predicted.

Several methods have been used previously for the measurement of drop size distribution, e.g. the photographic technique, light transmission, conductivity (Coulter Electronic Counter) and light diffraction. The photographic technique is based on use of a microscopic camera to take a picture of the dispersion usually with back-illumination; the number of drops collected are generally around 100. The actual determination of drop

sizes by the photographic technique may, however, result in significant error, especially if small drops cannot be distinguished very clearly, as described by Chatzi et al., 1989 & 1991 and Mlyneck and Resnick, 1972. Clearly droplets below the limit of detection cannot be counted. Those which are partially-shielded, or out of the plane of focus, may also be ignored. The Coulter Counter is an instrument for determining both the number and size of the droplets as they pass through a small aperture between two electrodes. The resistance between the electrodes changes as a particle goes through the aperture and this change is converted to a voltage pulse in the instrument (Sprow, 1966). The technique is only applicable to dispersions in a filtered electrolyte. Light diffraction techniques offer a short measuring time and permit on-line analysis with minimal possible instrumental, sampling and dispersion errors (Chatzi et al., 1991). The latter method was employed in this research because of its accuracy, reproducibility, the ability of the instrument to measure very small drops (~ 1 μm) in the dispersion and the feasibility of on-line measurement.

A number of studies dealing with the experimental measurement of drop sizes in stirred liquid-liquid systems have been reported in the literature (Chatzi, 1991, Chen and Middleman, 1967, Shinnar and Church, 1960, Konno et, al., 1977, 1987, 1993).

However, most investigations refer to systems with a high interfacial tension, i.e. in the range of 0.015 - 0.05 N/m. and with a high density difference between the phases i.e. in the range of 116 - 300 kg/m^3.

In the present study, the dispersion process has been examined essentially in the absence of coalescence, by working at very small dispersed phase fractions, i.e. 0.03% v/v to 0.07%

v/v. Drop size distributions were measured as a function of agitator speed, the physical properties of the system and the dispersed phase hold-up. The temperature of the system studied was kept constant throughout the investigation. A theoretical treatment based on the theory of isotropic turbulence has been used to correlate the data.

6.2 Experimental investigation and equipment design

Two phase system

The two aqueous phase systems used possess a very low interfacial tension, i.e.$\leq 1.28 \times 10^{-4}$ N/m, a small density difference i.e. 27 kg/m^3 and a low continuous phase viscosity, i.e.1.7 Ns/m^2. All these factors tend to result in very small drop size distributions.

The design of the experimental apparatus to investigate drop size distribution with such systems is strongly dependent upon the method selected for measurement.

Particle size determination with the Malvern analyser

Laser diffraction is a relatively recent technique for particle or drop size determination and is based on the measurement and interpretation of the angular distribution of the light diffracted by the particles or droplets. It is an extremely flexible measurement technique that does not require calibration (because it is based on the theory of light diffraction of particles) and can be used equally well for liquid and solid dispersions. Light scattering

was chosen as the method of measurement because droplets formed in the system investigated can be very small, e.g. 7μm, and the Malvern Particle Size Analyser has a detection range going down to 1.2μm. A typical measurement is completed within seconds, thus making the technique suitable for on-line size analysis (Chatzi et al., 1991).

The instrument uses a low-power laser transmitter to produce a parallel, monochromatic beam of light that illuminates the droplets or particles flowing in the cell. The incident light is diffracted by the illuminated particles, resulting in a stationary diffraction pattern regardless of particle movement. As particles flow through the illuminated area, the evolving diffraction pattern reflects the instantaneous size distribution in this area. Thus, by using a continuous flux of particles through the illuminated area and by integrating over a suitable time period, the final measured diffraction pattern is representative of the bulk sample of the particles. A Fourier transform lens focuses the diffraction pattern onto a multi-element photoelectric detector, which produces an analogue signal proportional to the incident light intensity. The detector consists of a concentric array of 32 semicircular photodiodes, each representing a certain size band (Malvern Instrument Ltd., 1987).

Once the diffraction pattern of a sample has been obtained, the particle size data are extracted by iterative non-linear least-square calculations. An initial size distribution is assumed, either from raw data (model independent) or from some particular form of distribution, e.g., Rosin-Rammler. The software supplied by Malvern Instruments Ltd., (1987) allows the user to specify the type of size distribution, either as a Rosin-Rammler, normal or log-normal form. Alternatively a model-independent analysis can be selected; in

the latter case, multimodal particle size distribution can be identified with high resolution (Chatzi et al., 1991).

The on-line capability of the laser diffraction instrument is a very desirable feature in the measurement of drop sizes in a liquid-liquid dispersion since any technique based upon the withdrawal of a sample introduces inherent sampling errors, temperature changes, and the possibility of drop fragmentation or coalescence. Samples can be scanned as they flow in a cell, and a number of sweeps of the detector are used for data averaging (typically 1000) in order to obtain representative and statistically meaningful drop size distributions (Malvern Instruments Ltd., 1987).

Typical results generated by the instrument include cumulative size distribution, volume fraction within each size band, and a listing of the main parameters of the distribution including volume mean, median mean and Sauter mean diameters (Malvern Instruments Ltd., 1987). Detailed results and examples are discussed in the results section.
At low phase concentrations, poor signal level and large random errors may exist, while at high concentrations multiple scattering effects may introduce systematic errors (Malvern Instruments Ltd., 1987). Consequently, there are limitations on the range of hold-up that can be used.

A major difficulty in using the Malvern Particle Size Analyser is that it normally requires a 30 ml sample to be withdrawn from the mixing vessel and transferred to the measurement cell. Such a procedure could introduce coalescence and other problems noted earlier and

hence lead to inaccurate results. Another potential difficulty is that of air entrainment, which may limit system operation.

A special apparatus was designed to solve the above problems and to facilitate on-line drop measurement. This apparatus consisted of a one litre vessel designed with a special window to allow the laser beam to pass through the dispersion, enabling measurements whilst the droplets were in motion. Details are given in the following section.

6.3 Equipment

6.3.1 Mixing vessel

All the drop size experiments were carried out in one litre cylindrical glass vessels, of the type shown in Figure 6-1. The vessel diameter was 105 mm and the height to diameter ratio was one.

6.3.1.1 Mixing vessel design I

The apparatus, as shown in photograph 1 and in Figure 6-1, was based on a one litre glass vessel designed with a special window to allow passage of the laser beam. The design allowed continuous on-line measurement of the drop sizes in the vessel without any disturbance to the dispersion. However, some disadvantages were discovered during operation.

1. The windows were constructed from ordinary glass, which was not to the same specification as the glass (anti-reflection coated) designed for the Malvern Particle Size Analyser.
2. The special tube designed to accommodate the glass window obscured some of the scattered light. This led to inaccurate measurement of the drop size.

A new design was therefore developed to resolve these problems.

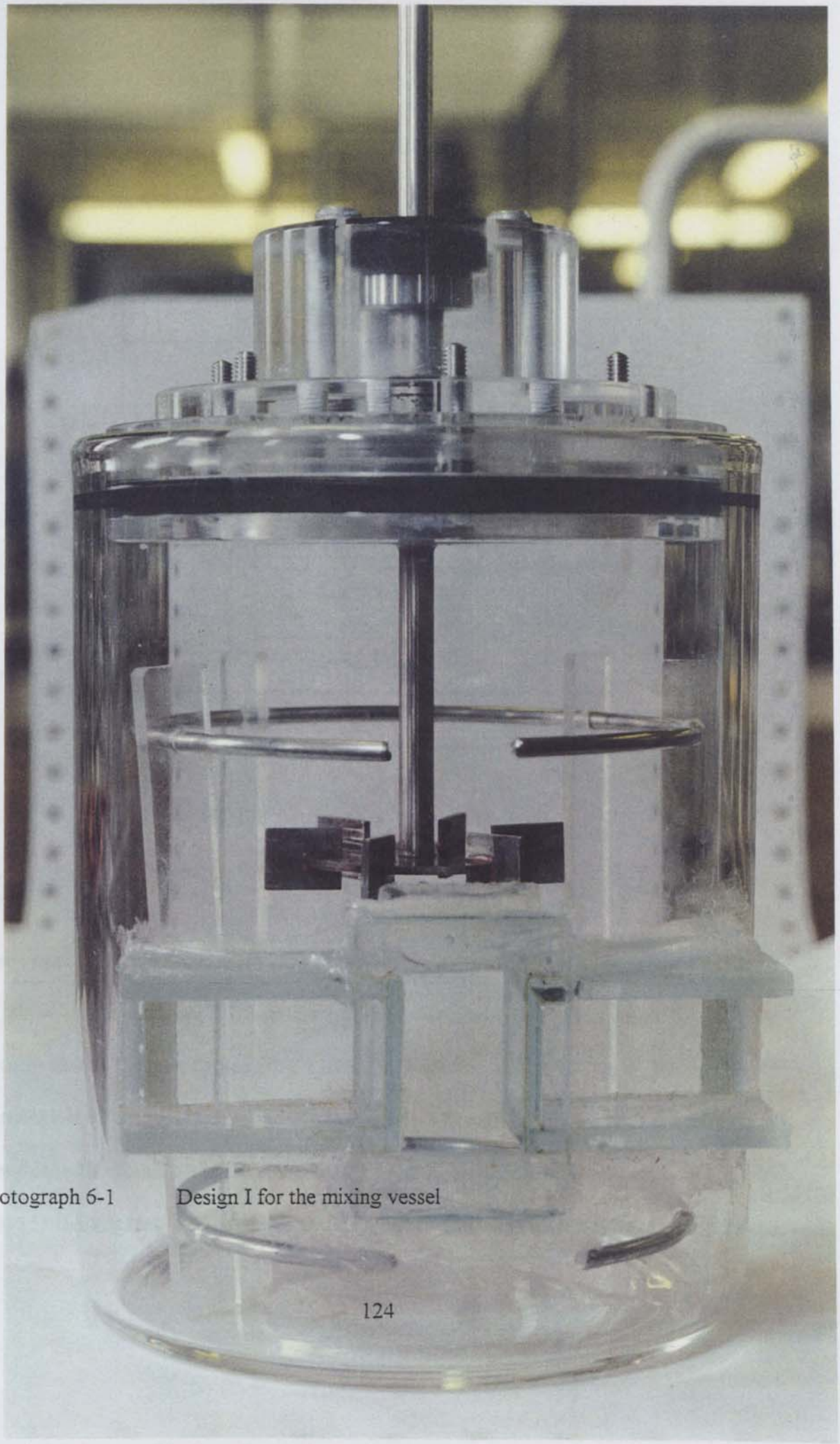

Photograph 6-1 Design I for the mixing vessel

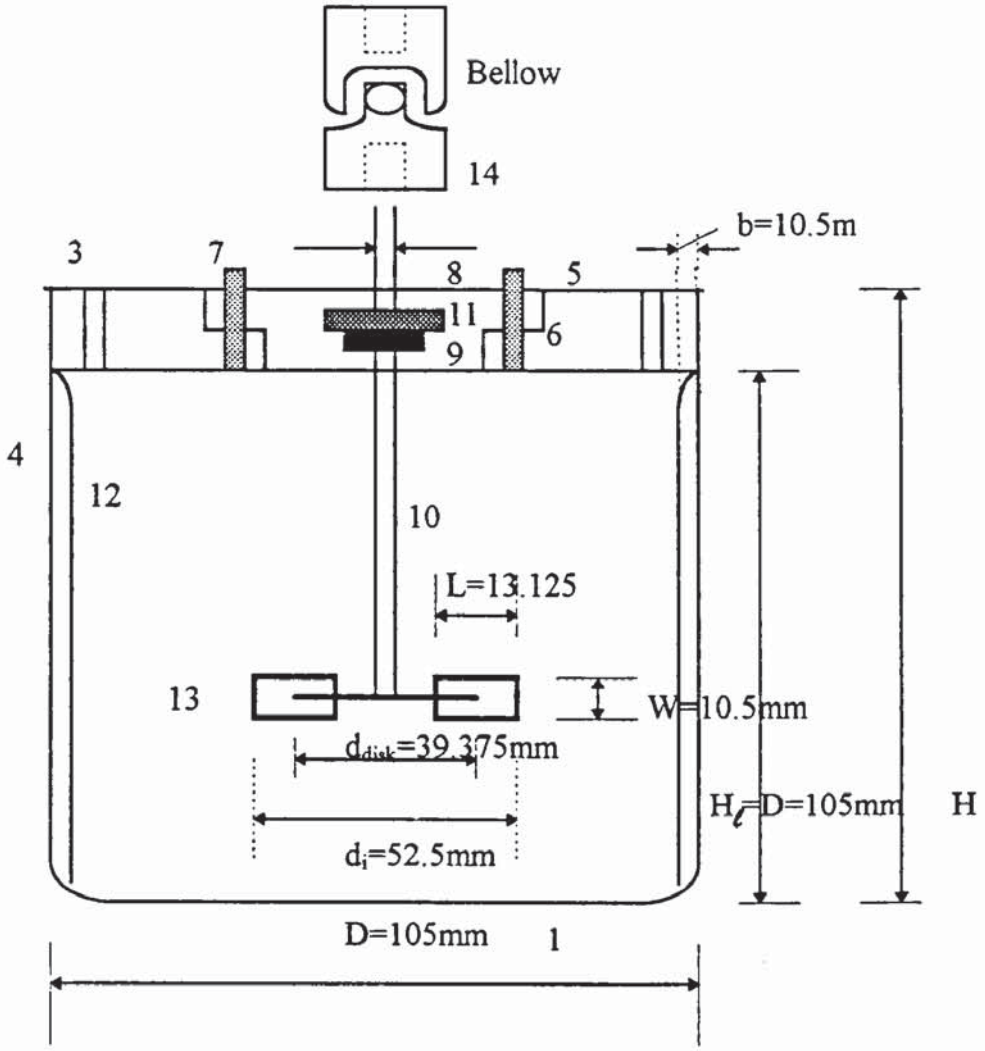

Figure 6-1 Mixing Vessel Design I

$$\frac{d_i}{D}=0.5,\ W=\frac{1}{5}d_i,\ L=\frac{1}{4}d_i,\ \frac{d_{disk}}{d_i}=0.75,\ \frac{b}{D}=0.08,\ \frac{h_1}{d_i}=0.5-1.5,\ \frac{H_l}{H}=0.75-0.85$$

The vessel (4) had a flat bottom with rounded corners. It had specially-designed windows to allow the laser beam to pass through the dispersion (see photograph 6-1). Four equally-spaced Perspex baffles (12), 1.05×10^{-2} wide and 10.5×10^{-2} long, were arranged vertically at 90 degrees intervals inside the vessel. The baffles (12) were placed as close as possible to the vessel wall. They were supported at the middle by a steel coil. A Perspex ring (5) (photograph 6-2) supplied by VT Plastics Ltd. was inserted into the top of the

vessel using an O-ring seal; this lid contained a port (8) for the agitator shaft (Photograph 6-3). There were two ports for addition of small quantities of the dispersed phase. The lid was air and dust-tight to avoid any extraneous contamination from the atmosphere.

6.3.1.2 Mixing vessel design II

The improved design consisted of a one litre Perspex vessel (photograph 6-4 and illustrated in Figure 6-2) with a stainless steel cell and glass window specified and supplied by Malvern. The specification covered the use of specially-coated glass, the size of the glass window (2cm in diameter) and the geometry of the cell. The cell was screwed into the middle of the vessel, at the same level as the impeller to ensure good drop dispersion throughout the cell.

Several important factors influenced design of the vessel.

1. The thickness of the vessel, the thickness of the jacket and the gap between the two walls created a substantial distance, i.e. 3 cm, which could have influenced the flow of the drops to the cell. Therefore, to minimise the distance, the mixing vessel was placed off-centre relative to the water jacket, as shown in photograph 6-5. This design did not significantly affect the performance of the water jacket, because of the large surface area around the vessel.
2. The apparatus had to be constructed of Perspex (i.e. polymethyl methacrylate) because of the complexity of the design.

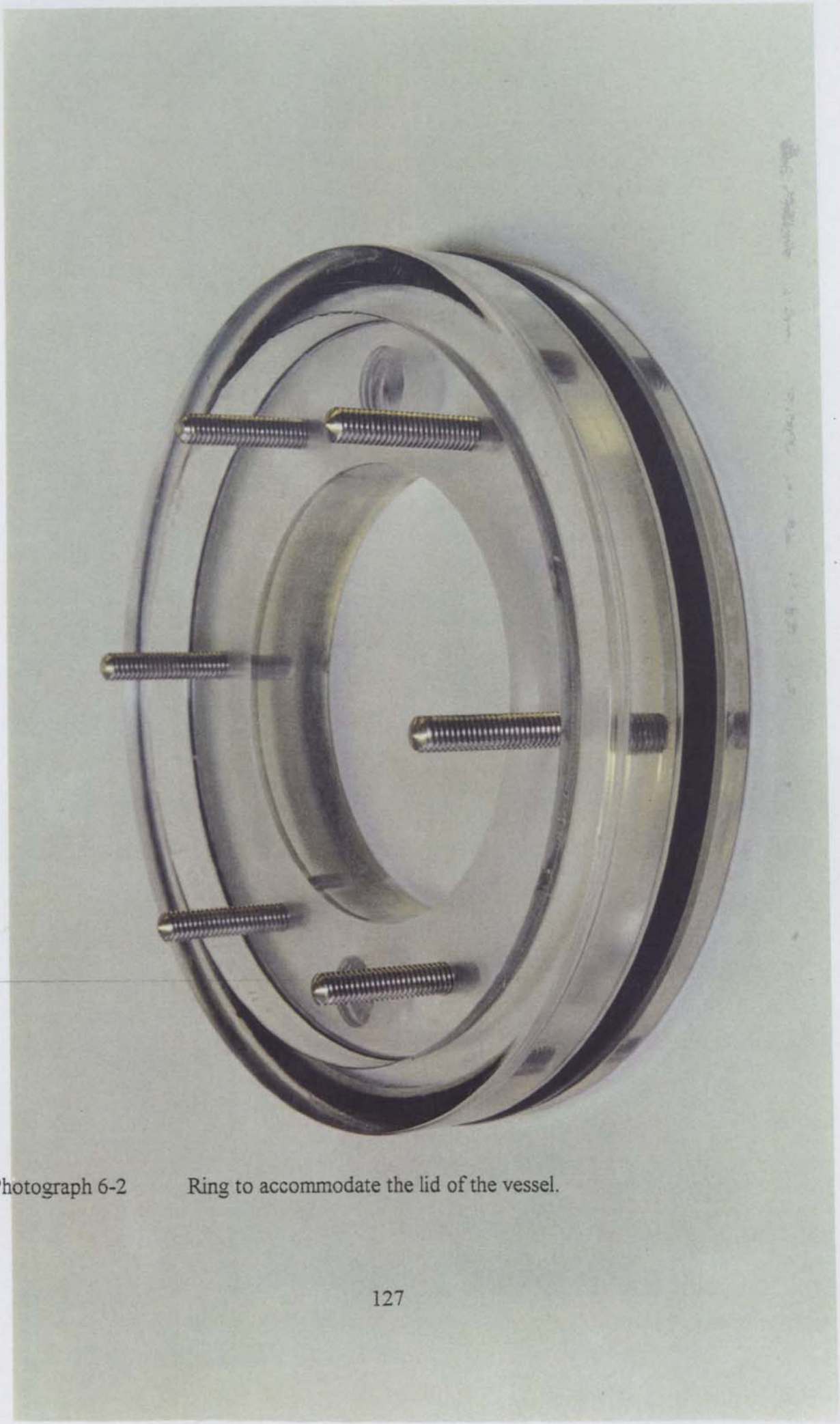

Photograph 6-2 Ring to accommodate the lid of the vessel.

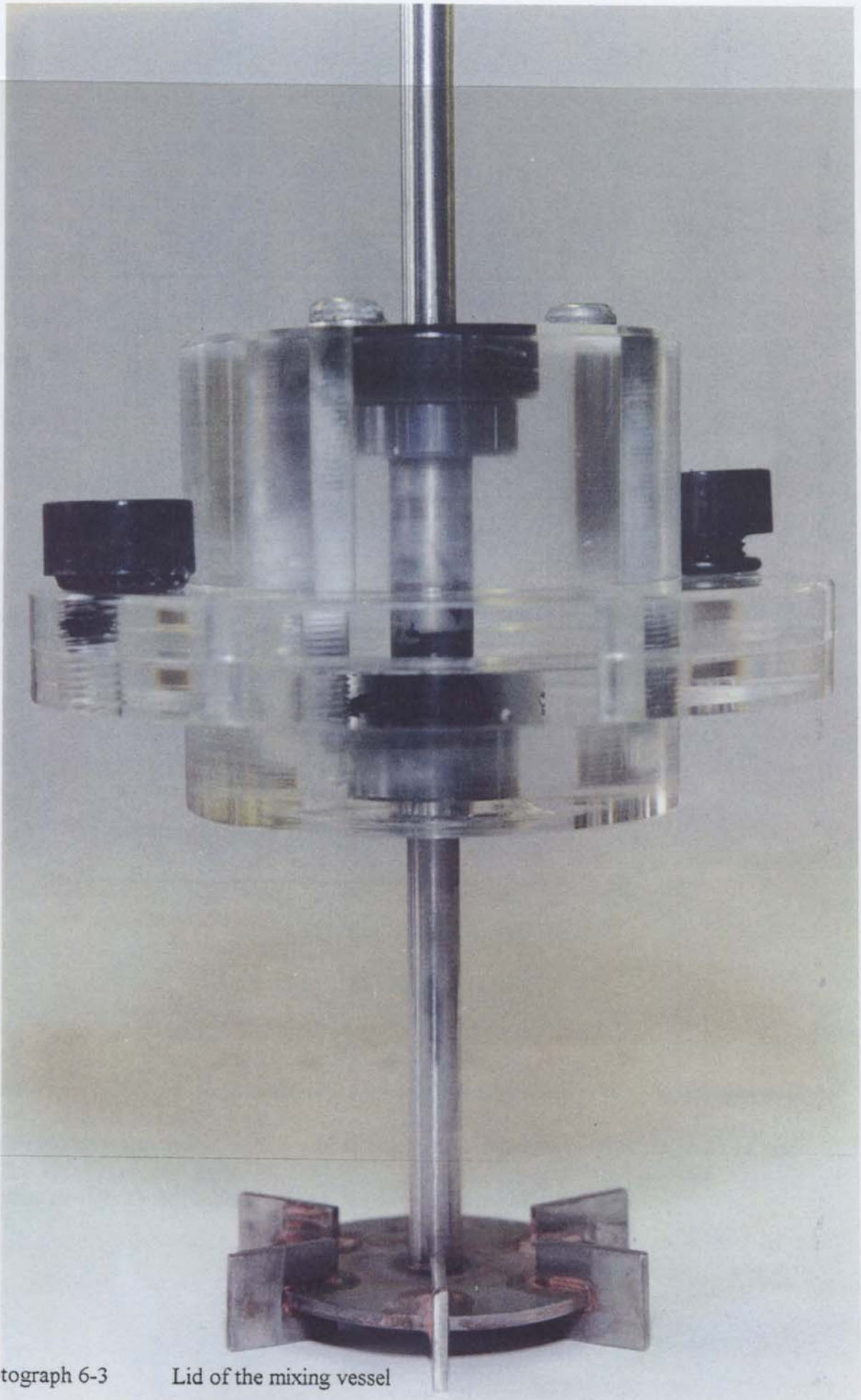

Photograph 6-3 Lid of the mixing vessel

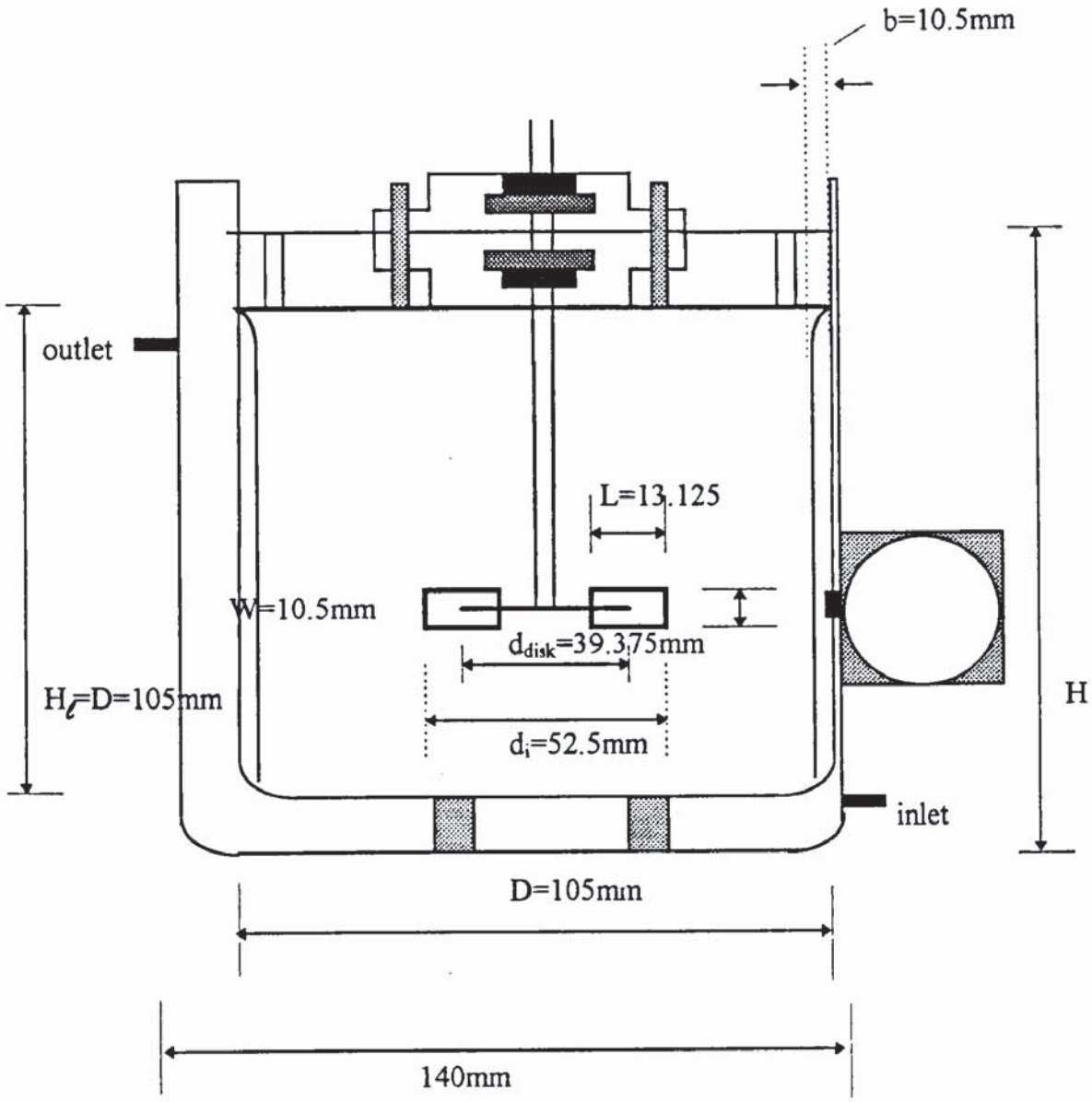

Figure 6-2 Mixing vessel Design II

The Perspex lid (8) was fixed to the ring with stainless steel screws (7). The stainless steel shaft (10) was also sealed with a rubber bearing (9) supplied by HPC Drives Ltd. and another air-tight O-ring rubber seal (11) supplied by Brunwell Ltd.

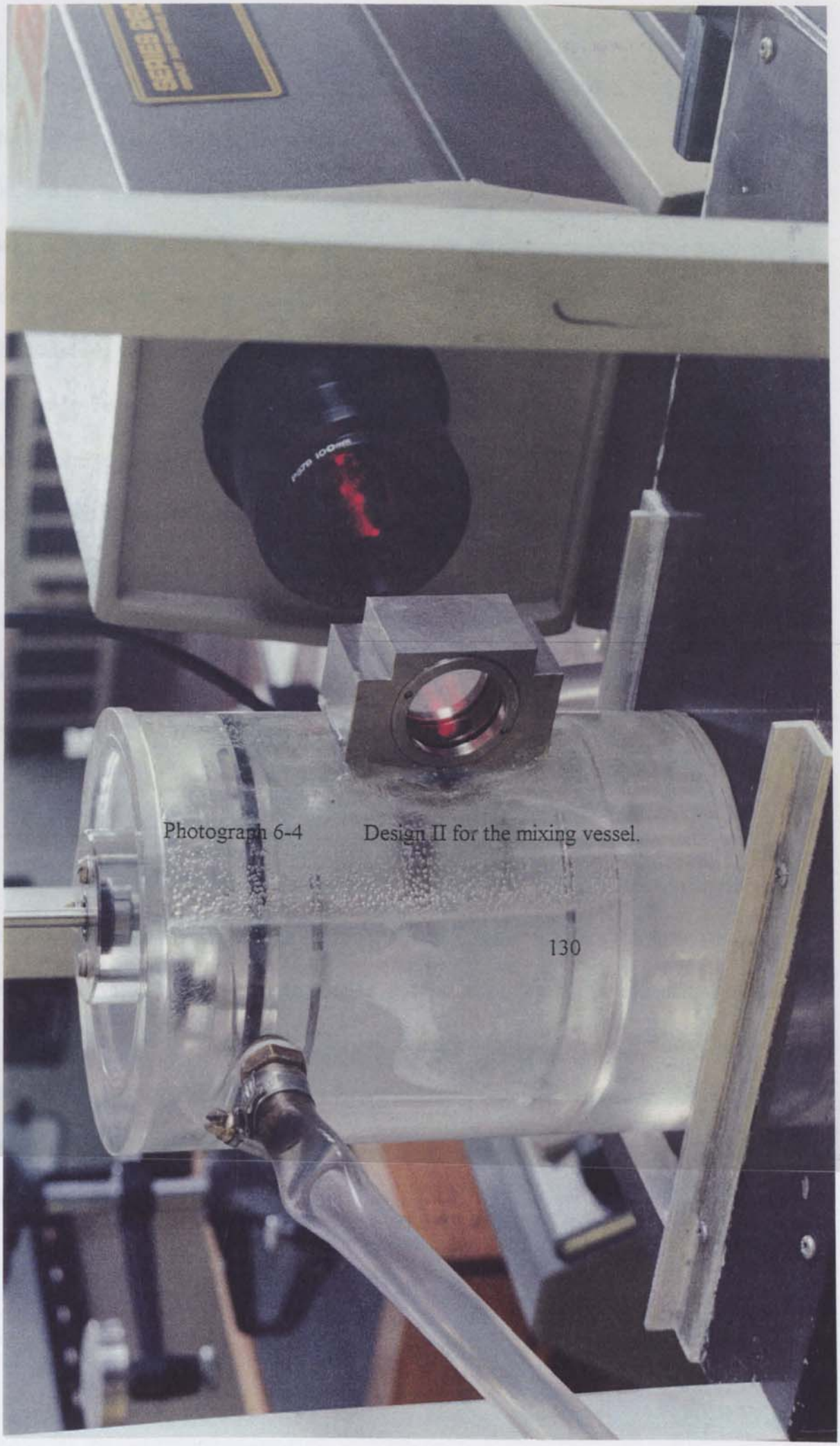

Photograph 6-4 Design II for the mixing vessel.

The impeller (13) used for all experiments was a standard, six-bladed Rushton turbine. The diameter of the impeller (13) was 2.25 x 10^{-2} m, the width of the blades was 1.05x10^{-2} m, and the length of the blades was 1.31 x 10^{-2} m. These dimensions were within the range determining standard tank configurations. The impeller was centred vertically and axially in the vessel.

The vessel (4) was jacketed as shown. The water jacket (1) was served by a water-bath supplied by Techne, Model C-400 (range -20°C - 80°C) photograph 6-6; this enabled the temperature to be controlled at T=20 ± 0.1 °C. The vessel (4) was placed on an in-house built rig with a variable speed motor (range 50-2000 rpm) controlled by a voltage regulator. The motor was supplied by Scientific Lab Supplies Ltd., model Eurostar, with a digital speed indicator, which was calibrated in revolutions per minute. The impeller was attached to a stainless steel shaft 6mm in diameter (10). A bellows (14), which acted as a universal joint, was attached to the shaft (10).

6.3.2 Light scattering equipment

A Malvern 2600C Particle Size Analyser was used to measure the drop size distribution of the dispersed phase. It was connected to a Personal Computer to run the software and a printer. The vessel was modified to install a glass window, 2 x 10^{-2} in diameter, supplied by Malvern Ltd. and designed to meet the measurement requirement, i.e. to allow the laser beam to pass through the dispersion as shown in Figure 6-3. The vessel was placed in the path of the laser beam, such that the beam travelled through the window of the vessel (photograph 6-7).

The vessel was supported by a stainless steel stand. The stirrer motor was mounted on top of the stand.

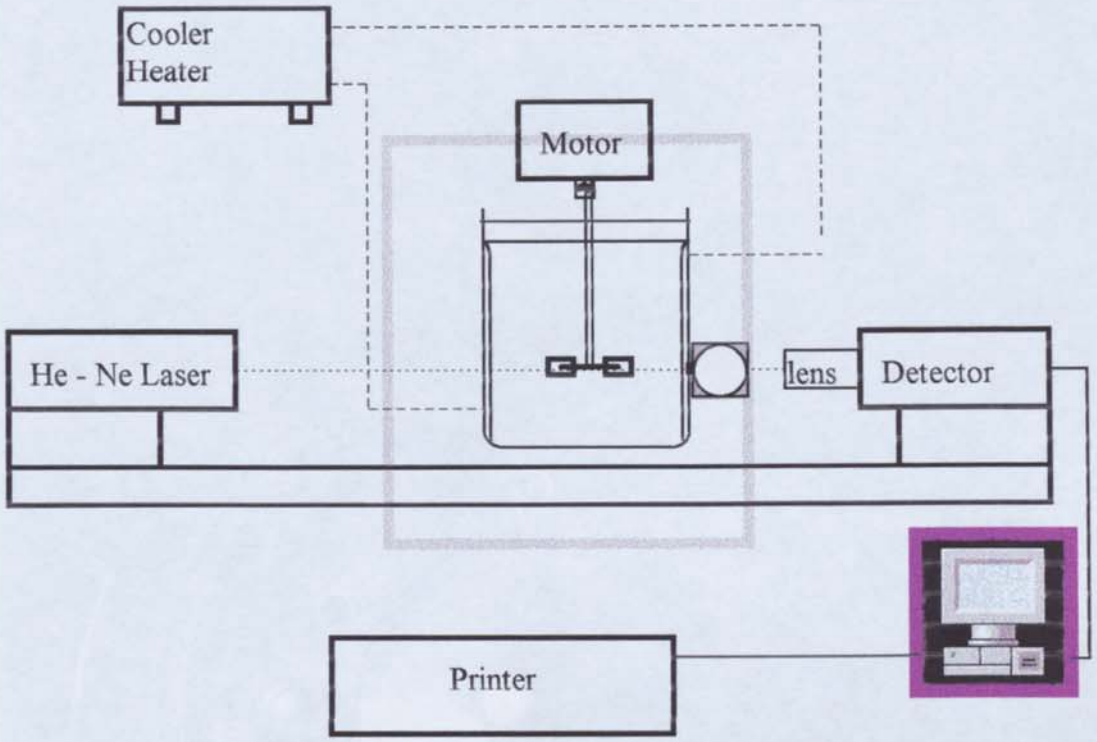

Figure 6-3 Equipment set-up.

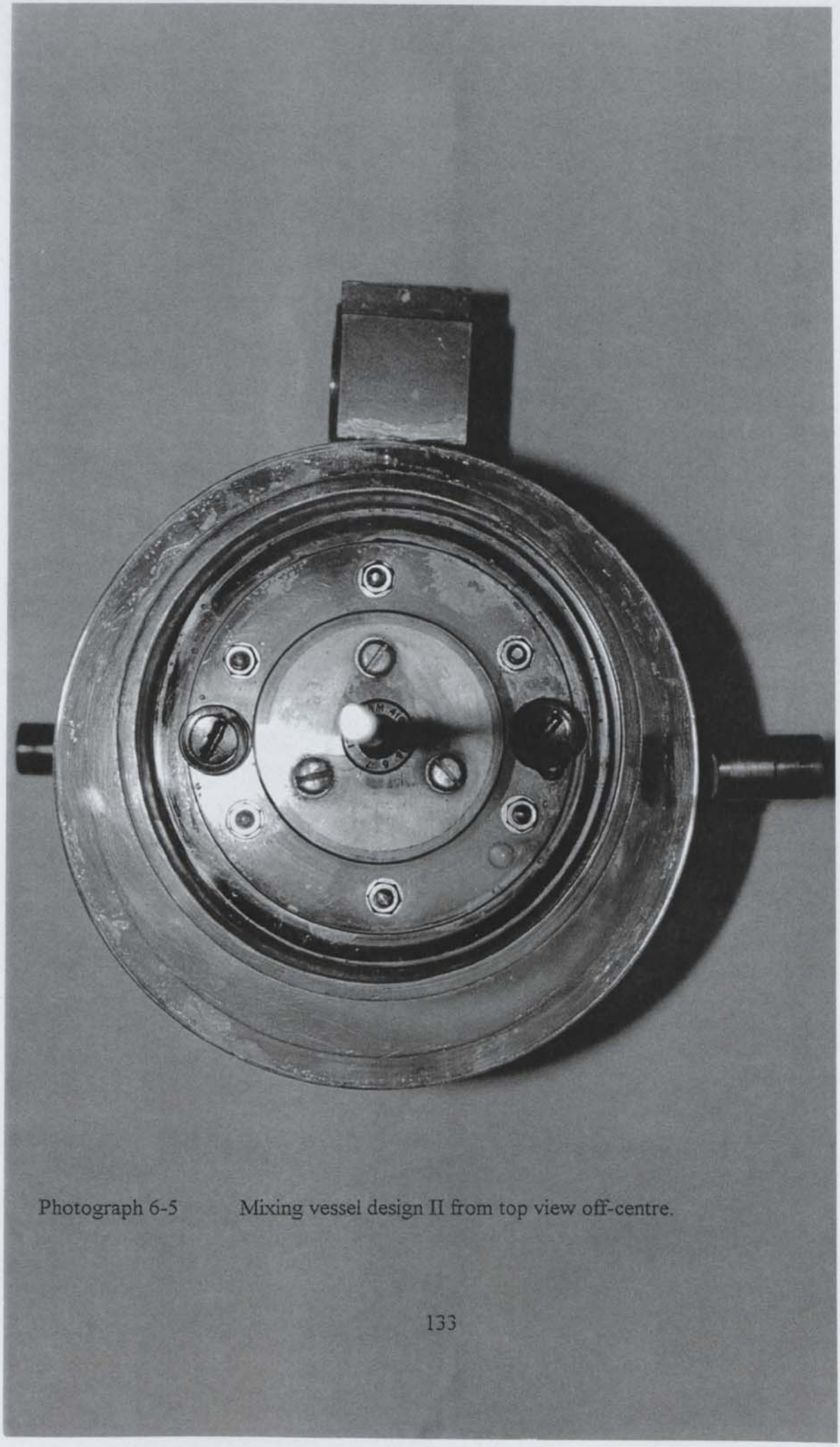

Photograph 6-5 Mixing vessel design II from top view off-centre.

Photograph 6-6 Cooling-heating unit (Malvern monitor displaying distribution in background.

Photograph 6-7 Experimental set-up for the Laser diffraction, rig and the vessel. (Emitter on left, mixing vessel, reciever on right; display on monitor)

6.4 General procedure

6.4.1 Vessel preparation

Periodically, the mixing vessel, the baffles and impeller were removed and washed in a 2% solution of 'Decon 90' detergent and then left overnight. Following this, they were washed under running tap water for an hour, after which each item was rinsed three times with deionised, distilled water. They were subsequently washed with a high purity certified water (HPLC Water), then dried in an oven at 80 °C.

6.4.2 Preparation of the phases

The phases were prepared as described in Chapter Three. They were equilibrated at 20 °C ±0.1 °C and then separated into clean sealed bottles. To ensure the phases were free of impurities, they were then filtered through a 0.1μm filter supplied by Gelmann Inc. This was considered necessary to ensure that the laser beam would not detect any particles below 0.15μm.

6.4.3 Filling the vessel

Due to the nature of the design and the potential for ingress of air bubbles associated with filling the vessel, extra care was taken to ensure no bubbles were present in the dispersion prior to any measurements being made. The filling of the vessel was undertaken through the inlet hole slowly and with extreme caution. The vessel was tilted several times during filling to expel all of the air from the system.

6.4.4 De-aeration

The presence of air in the system would have caused a major error in measuring drop size with the Malvern Particle Size Analyser since it cannot distinguish between drops and bubbles. The presence of cavitated air in the system was unavoidable. Therefore, the system was first filled with the continuous phase and then the impeller was started at a low stirrer speed, i.e.200 rpm, to expel any cavitated air bubbles. The impeller was next stopped and the air bubbles removed from the filling / draining holes. This procedure was then repeated with a high stirrer speed, i.e. 1500 rpm, to ensure the system was bubble free.

6.5 Experimental procedure

1 The volume of the vessel was determined by weighing the empty vessel, with the Perspex lid and Rushton turbine in position, and then filling the vessel completely with distilled water and reweighing.

2 The vessel was filled with the required volume of salt solution. A known 0.03% by volume of the dispersed phase (PEG) was then added. The vessel was tilted at an angle of about 45° to ensure that any air inside the vessel escaped through the two ports. The screws in the lid were tightened to seal the vessel from the air.

3 The vessel was placed on the rig. The water jacket of the vessel was connected to the cooler-heater unit, set to 20 °C, and circulation continued for one hour before start-up.

4 The Malvern was switched-on and the background reading measured using the laser beam.

5 The stirrer motor was switched on and the impeller speed set to the desired value; at the same time the stop-watch was activated.

6 Drop size distribution was measured at 15 minute intervals until a steady drop size was obtained. The results of each measurement were then printed out.

6.6 Experimental programme

6.6.1 Determination of time to steady state.

The vessel was filled with the salt phase at a concentration of 20 % w/w. Sufficient PEG phase from the 20 % w/w mixture was then added to give a 0.03% by volume dispersion of the PEG phase in the salt. The stirrer was then started and measurements taken at hourly intervals until a constant Sauter mean drop size (d_{32}) was obtained.

The time required to reach steady state was then used to set the sample time for parts 6.6.2 and 6.6.3 of the programme.

6.6.2 Determination of the effect of the stirrer speed.

The same mixture (20% w/w) was used in this part as in part 6.6.1. The stirrer was started at 300 rpm, and, after a start-up time as determined in part 6.6.1, measurements of the drop size distribution were taken and analysed as in part 6.6.1. The stirrer speed was

then increased by increments of 100 rpm and the process repeated, usually over the range from 300-1000 rpm.

6.6.3 Determination of the effect of dispersed phase concentration.

New dispersions were prepared as in part 6.6.1. Concentrations of 0.03% to 0.07% by volume of the PEG solution were used.

6.6.4 Determination of the effect of mixture composition

The above series of experiments was repeated using salt and PEG solutions of 25 % w/w and 30 % w/w concentrations.

6.7 Experimental results:

6.7.1 An overview

The experimental results are presented in Figure 6-4. These show the effect of stirrer speed, N, phase composition and dispersed phase hold-up upon drop size distribution, in terms of the Sauter mean drop diameter.

Stirrer speed clearly had a significant influence on Sauter mean drop diameter, d_{32}. For the 20 % w/w phase composition, d_{32} decreased linearly with N; the curve is steep. For the 25 and 30 % w/w phase compositions, the effect of N on d_{32} is still roughly linear within the range 600 rpm to 1000 rpm but the gradient is less steep. In the range of 400 rpm to 600 rpm the gradient of the curve matches that for the 20% w/w phase composition.

The effect of dispersed phase hold-up upon d_{32} was relatively small, i.e. only ± 10 %, over the range studied (0.03 - 0.07 % v/v). The effect of phase composition on mean drop size, d_{32}, was small in the case of the 25 % w/w and 30 % w/w dispersions, where the results are comparable and follow the same pattern. At 20 % w/w, phase composition had a marginally greater effect on the mean drop size d_{32} (see Figure 6-4).

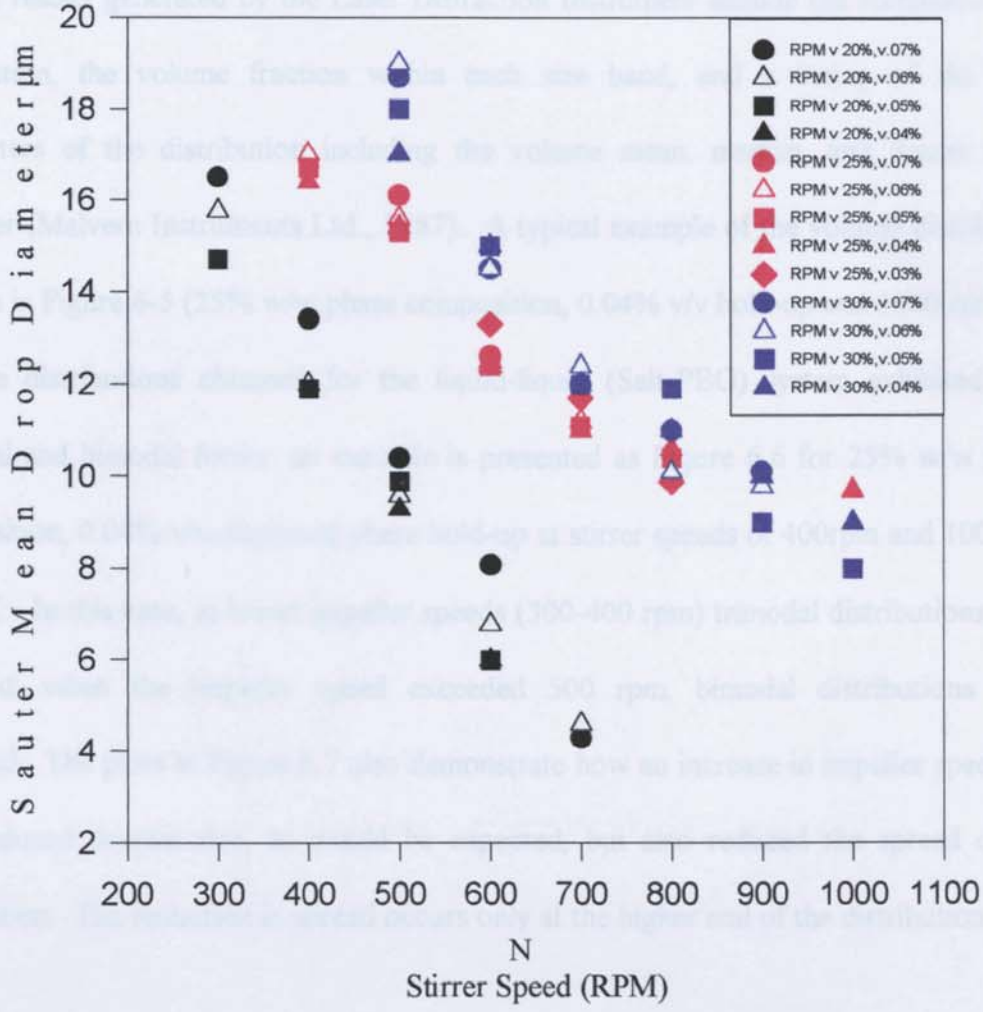

Figure 6-4 Effect of agitation speed, phase composition and hold-up on drop size, d_{32}.

6.7.2 Drop size distribution

Typical results generated by the Laser Diffraction Instrument include the cumulative size distribution, the volume fraction within each size band, and a listing of the main parameters of the distribution including the volume mean, median, and Sauter mean diameter (Malvern Instruments Ltd., 1987). A typical example of the volume distribution is given in Figure 6-5 (25% w/w phase composition, 0.04% v/v hold-up and 1000 rpm). Volume distributions obtained for the liquid-liquid (Salt-PEG) system exhibited both trimodal and bimodal forms: an example is presented as Figure 6.6 for 25% w/w phase composition, 0.04% v/v dispersed phase hold-up at stirrer speeds of 400rpm and 1000rpm at 20°C. In this case, at lower impeller speeds (300-400 rpm) trimodal distributions were obtained; when the impeller speed exceeded 500 rpm, bimodal distributions were recorded. The plots in Figure 6.7 also demonstrate how an increase in impeller speed not only reduced droplet size, as would be expected, but also reduced the spread of the distribution. The reduction in spread occurs only at the higher end of the distribution.

MALVERN Series 2600 SB.20 Master Mode 12 Feb 1998 4:37 pm

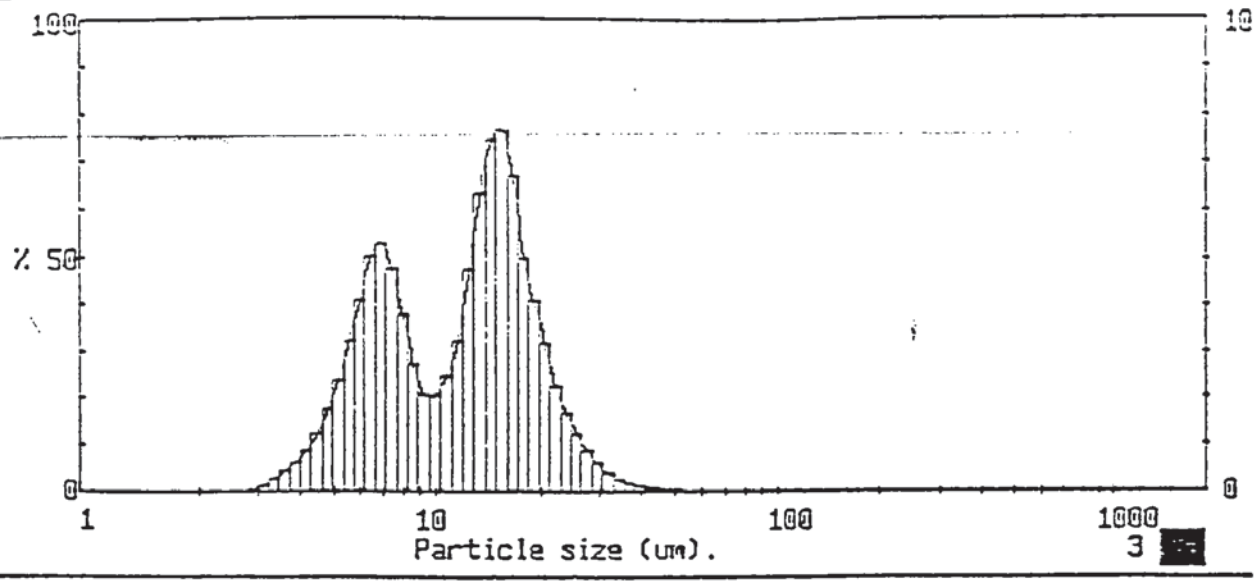

1598 pil IDR459 / 0/ 0/0.00/1.00/
25% w/w salt soln
1000 rpm
0000000000215

MALVERN Series 2600 SB.20 Master Mode 12 Feb 1998 4:37 pm

High Size	Under %	High Size	Under %	High Size	Under %	High Size	Under %	High Size	Under %	High Size	Under %	Span 1.16
188	100	84.5	100	38.0	99.6	17.1	79.8	7.69	10.3	3.46	0.4	D[4,3] 12.62µm
175	100	78.6	100	35.4	99.4	15.9	73.0	7.15	25.5	3.21	0.2	
163	100	73.1	100	32.9	99.2	14.8	65.4	6.65	20.2	2.99	0.0	
151	100	68.0	100	30.6	98.8	13.7	57.8	6.18	15.1	2.78	0.0	D[3,2] 9.76µm
141	100	63.2	100	28.4	98.2	12.8	51.5	5.75	11.0	2.59	0.0	
131	100	58.8	99.9	26.4	97.3	11.9	46.7	5.35	7.8	2.40	0.0	
122	100	54.7	99.9	24.6	96.0	11.1	43.5	4.97	5.4	2.24	0.0	D[7,0.9] 20.23µm
113	100	50.8	99.9	22.9	94.4	10.3	41.0	4.62	3.6	2.08	0.0	
105	100	47.3	99.9	21.3	92.1	9.56	38.9	4.30	2.4	1.93	0.0	
97.8	100	44.0	99.8	19.8	88.9	8.89	36.8	4.00	1.6			D[7,0.1] 5.61µm
90.9	100	40.9	99.7	18.4	84.8	8.27	34.1	3.72	0.9			

Source = Data:p25v004	Beam length = 2.2 mm	Model indp	D[7,0.5] 12.53µm
Record No. = 15	Log. Diff. = 4.661		
Focal length = 100 mm	Obscuration = 0.4788	Volume Conc. = 0.0963%	
Presentation = pil	Volume distribution	Sp.S.A 0.6145 m²/cc.	Shape C??

1598 pil IDR459 / 0/ 0/0.00/1.00/
25% w/w salt soln
1000 rpm
0000000000215

MALVERN Series 2600 SB.20 Master Mode 12 Feb 1998 4:37 pm

Particle diameters		Volume percentiles	
D(4,3)	12.62 µm	D(7,.10)	5.61
D(4,2)	11.10 µm	D(7,.20)	6.63
D(4,1)	9.79 µm	D(7,.30)	7.65
D(4,0)	8.75 µm	D(7,.40)	9.96
		D(7,.50)	12.53
D(3,2)	9.76 µm	D(7,.60)	14.05
D(3,1)	8.63 µm	D(7,.70)	15.44
D(3,0)	7.75 µm	D(7,.80)	17.14
		D(7,.90)	20.23
D(2,1)	7.62 µm	D(7,.99)	31.67
D(2,0)	6.90 µm		
		Span 1.17	
D(1,0)	6.24 µm	Unif. 0.40	

Distribution Moments.			
Distbn	Mean	Stan.Dev.	Skewness
Volume	12.62	6.41	1.43
Surface	9.76	5.28	1.42
Length	7.62	4.04	1.87
Number	6.24	2.93	2.39

Source =Data:p25v004
Record 15

1598 pil IDR459 / 0/ 0/0.00/1.00/
25% w/w salt soln
1000 rpm
0000000000215

Figure 6-5 Typical volume density distribution and drop diameter results

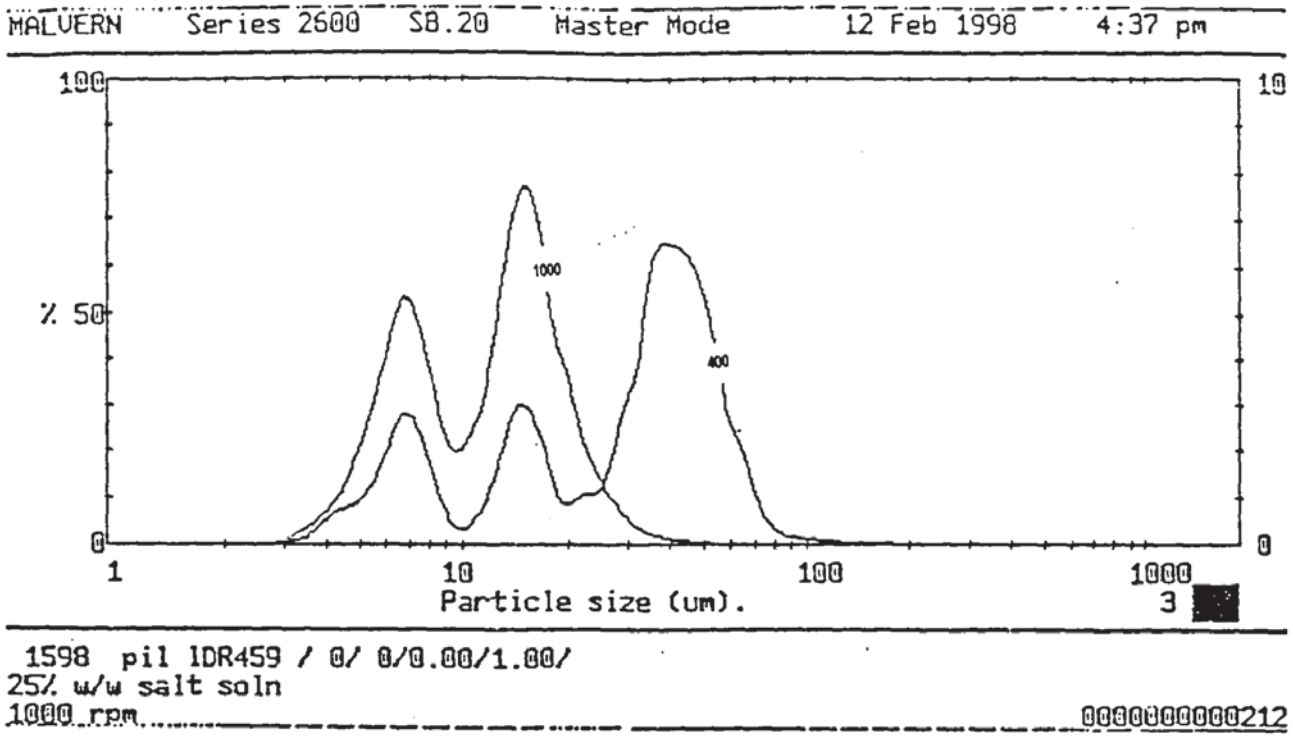

Figure 6-6 Distribution change from trimodal to bimodal as a result of the increase of the impeller speed

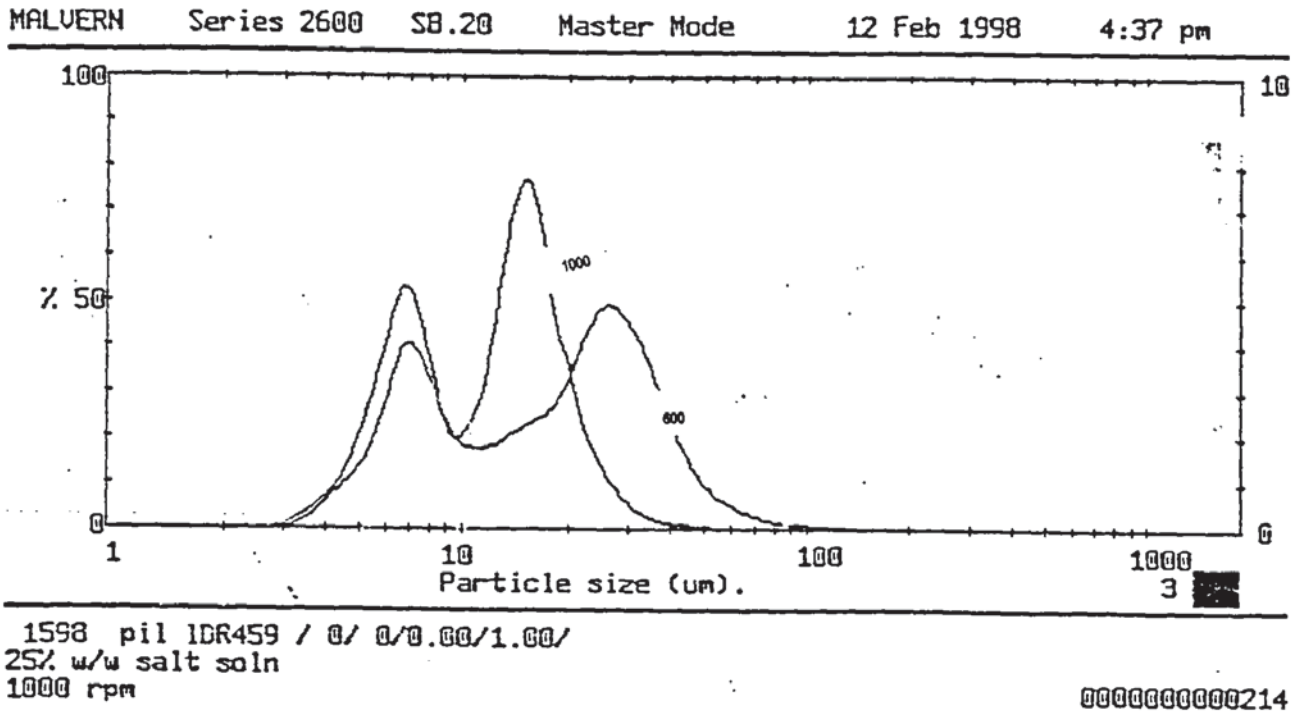

Figure 6-7 The spread of drop size distributions (demonstrating a reduction in size as well as sharper peaks as the impeller speed increases).

6.7.3 Time to steady state

The minimum time required for the system to reach dynamic equilibrium, i.e. a stable drop size distribution, was determined experimentally. This was done by measuring the drop size and the change in drop size distribution from the start of the experiment. The measurements were undertaken initially at 1 minute intervals over a period of 20 minutes and then at 15 minute intervals. This was extended to 8 hours, and in some cases up to 24 hours, to ensure no change in mean drop size or size distribution occurred. The stirrer speed had a major effect on this parameter: the time required with a phase concentration of 30%w/w at 300 rpm was about one hour; while at 1000 rpm the time required was about 15 minutes.

The time required was also dependent upon the physical properties of the system. The time required to reach steady state for a phase composition of 20% w/w, which had the lowest interfacial tension, was about 45 minutes at a speed of 300 rpm compared to 10 minutes at a stirrer speed of 1000 rpm..

The minimum time required to reach a steady state at different conditions was found, as might be expected, to depend on the Weber number N_{wc}. An increase in the rate of agitation or a decrease in the interfacial tension, caused a reduction in time to reach a dynamic equilibrium.

6.7.4 Reproducibility

The reproducibility of the laser diffraction method was tested by carrying out consecutive measurements as the sample was flowing in the stirred vessel; this procedure was repeated using new batches of the PEG-salt system of the same composition. The reproducibility was considered to be satisfactory as illustrated in Figure 6-8

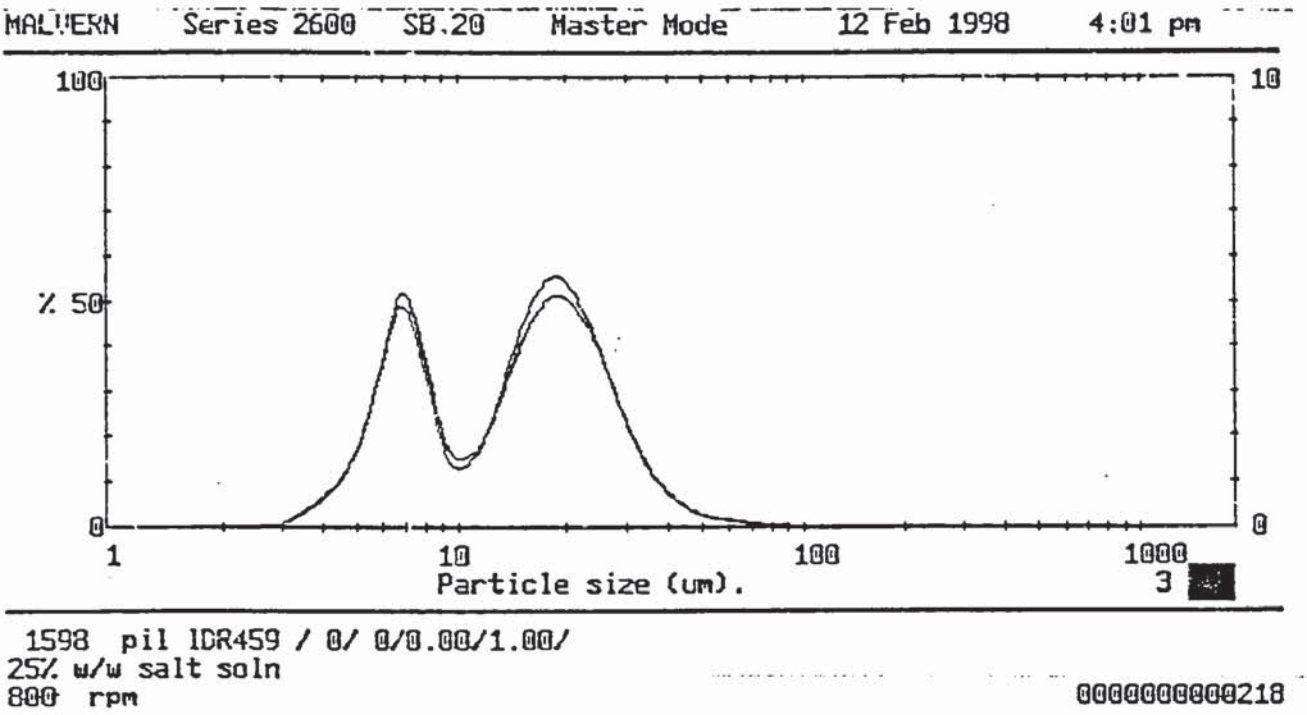

Figure 6-8 Reproducibility of a 25 % w/w phase composition at 800 rpm.

6.7.5 *Nature of the distributions*

The drop size distribution was mainly bimodal, with the large-size peak shifting from about 50 μm to 15 μm as the agitation speed was increased; simultaneously the smaller-size peak increased in height but with little change in the typical drop size of 7μm. The shape of the distribution was in some cases trimodal. At low agitation speeds (≤ 500 rpm) it was always multimodal. An increase in the agitation speed caused the spread of the distribution to shrink, and the bimodal distribution evolved as illustrated in Figure 6-9 (see also Figure 6-7).

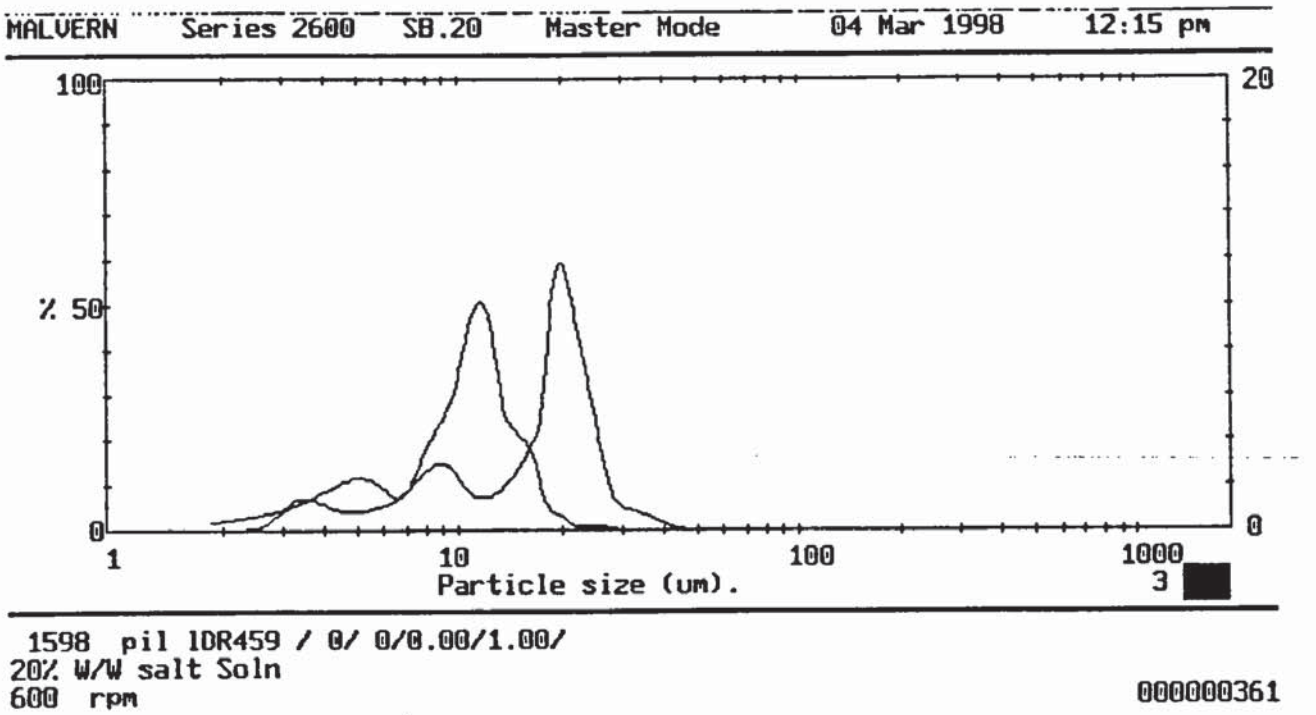

Figure 6-9 Reduction of distribution as a result of the increase in agitation speed.

6.7.6 Volume, surface and number density distribution:

Typical results generated by the software available with the Malvern instrument include volume ,surface, diameter and number density distributions. The raw data were obtained as a volume density distribution but could be transformed to any of the above density distributions as illustrated in Figure 6-10.

It will be observed that the peak associated with the smaller drops moves from right to left in a systematic manner as the basis for the distribution changes from a volume density to number density distribution. The same is true of the distribution associated with the large drops.

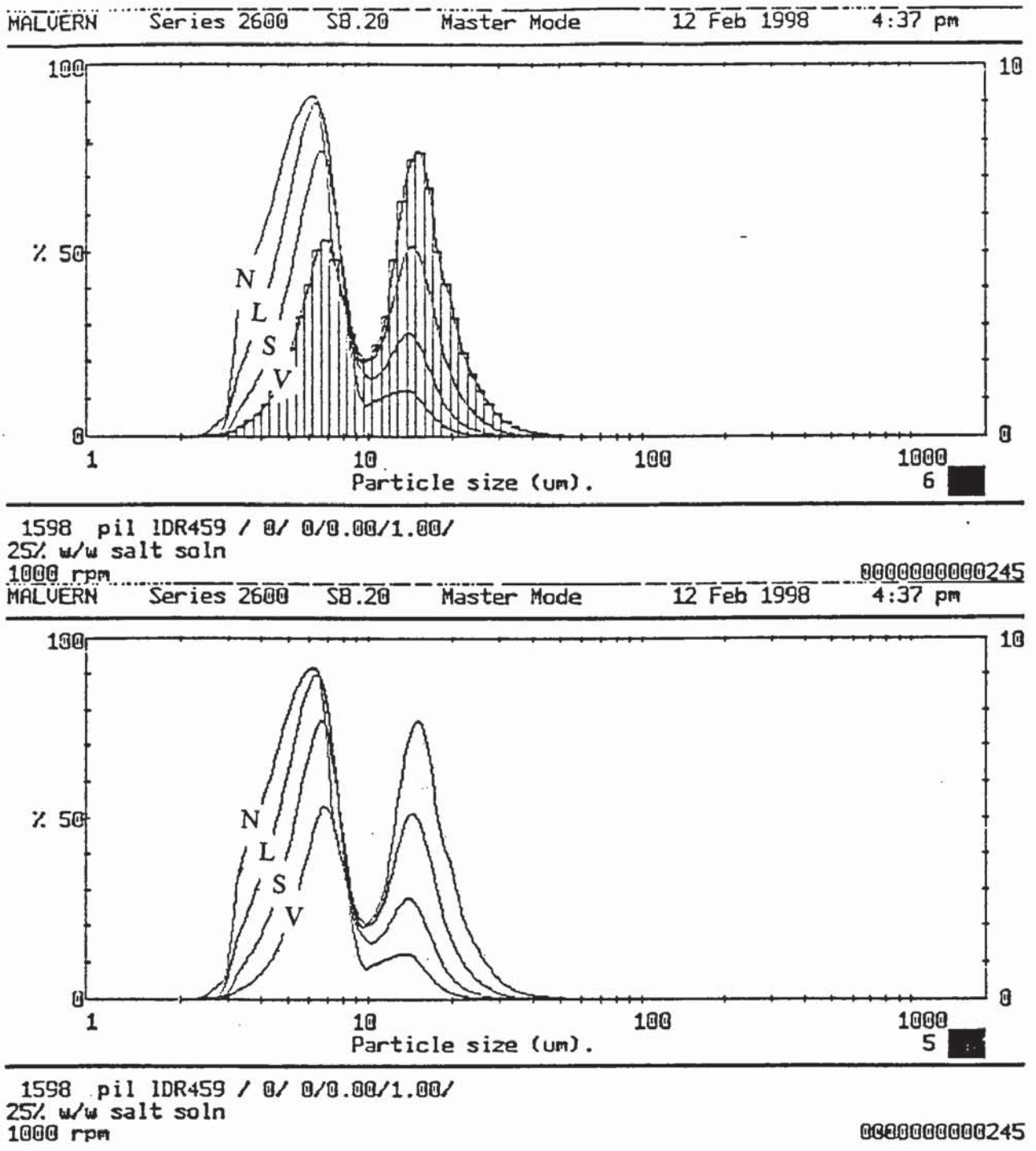

Figure 6-10 Volume, surface, diameter and number density distribution (See Malvern, 1987).

6.7.7 Limitations on the operating range

Limitations on the operating conditions were established at the time of the experimental work. It was found necessary to operate the system designated mixing vessel design II and discussed in Section 6.3 above a minimum speed to ensure representative sampling of the main vessel flow: based on visual observations and drop size measurements, it was found to be about 300 rpm. Previous upper limits for the impeller speed were overcome by designing the vessel to be air-tight. This new design provided considerable flexibility when measuring drop size and size distribution at high agitation speeds. By comparison other workers (e.g. Chatzi et. al, 1991) were limited by bubble entrainment when running their equipment at high impeller speeds, i.e. > 300 rpm.

The range of the dispersed phase hold-up studied (0.03 - 0.07% v/v) was limited. The upper limit for the dispersed phase hold-up was dictated by the measurement technique. Liquid drops under high agitation speed break into numerous small drops, which, if the fraction present is above a certain value, prevent the laser beam passing through the measuring cell. Consequently, the maximum dispersed phase hold-up had to be restricted to 0.07% v/v. The laser intensity (the beam passing through the cell and collected by the lens) must also exceed a certain minimum level to yield an accurate reading; this consideration limited the lower dispersed phase hold-up determined by the Laser Particle Size Analyser to 0.03% v/v.

6.8 Discussion of results

6.8.1 Sauter mean drop diameter

The results in Figure 6.4 show that the effect of stirrer speed, N, on Sauter mean diameter, d_{32}, was, as expected, very strong. The plot for the 20% w/w system shows that the steady state Sauter mean drop diameter, d_{32}, decreased approximately linearly with increase in agitation speed. The 20% w/w system did not follow the same pattern as the 25% w/w and 30% w/w systems due to the significant difference in physical properties, (see Table 3-1).

The bimodal distribution observed in the present work has previously been reported in the literature (Ward and Knudsen,1967; Austgen et. al., 1991; Laso et al., 1987).
This may be attributed to the method of measurement (i.e., light scattering), which permits an accurate measurement of the size distribution. The spread of the distribution shrank in size as the stirrer speed was increased. As illustrated in Figure 6-7, the two peaks represented a mean drop diameter d_{32} of 7μm for the 1st peak and 50 μm for the 2nd peak. As the stirrer speed was increased the 2nd peak shifted from 50μm to 15 μm; the 1st peak was unchanged in terms of the mean drop diameter but grew in size. The 2nd peak represents the larger drop sizes in the distribution, which naturally reduce in size as the agitation speed is increased. The smaller peak represents the smallest population in the dispersion and as the larger drops split into two or more drops, satellite drops derived

from the split accumulate to represent the 1st peak. As the breakage process continues, the number and volume of the satellite drops increased without their mean size changing significantly.

Figures 6-11 and 6-12 provide complete sets of steady-state drop size distributions for impeller speeds from 400-1000 rpm.

The effect of dispersed phase hold-up on the Sauter mean drop diameter is very small (± 10 %) within the range of concentration studied (0.03 - 0.07 % v/v). The majority of workers (Sprow, 1966, Chen and Middleman, 1967, Bouyatiotis and Thornton, 1967), who have studied the breakage process, have worked with 1 to 10% v/v dispersed phase hold-up. Unlike in the present study, therefore, interdrop coalescence was a factor and the mean drop size showed a significant increase with hold-up, obviously due to the increased frequency of droplet collisions.

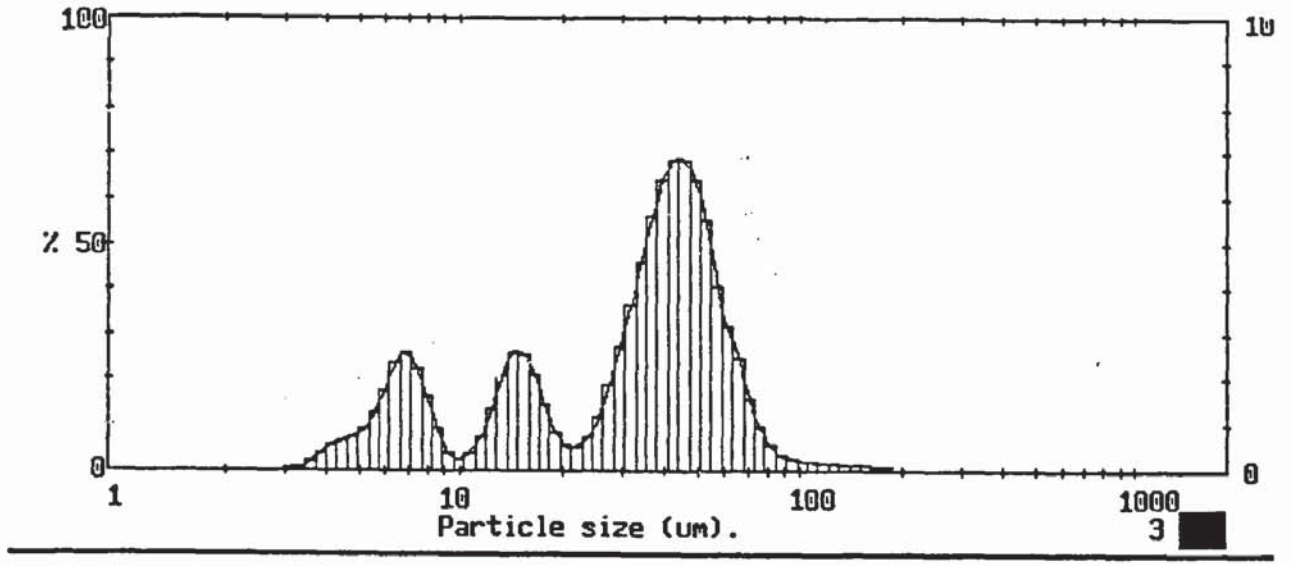

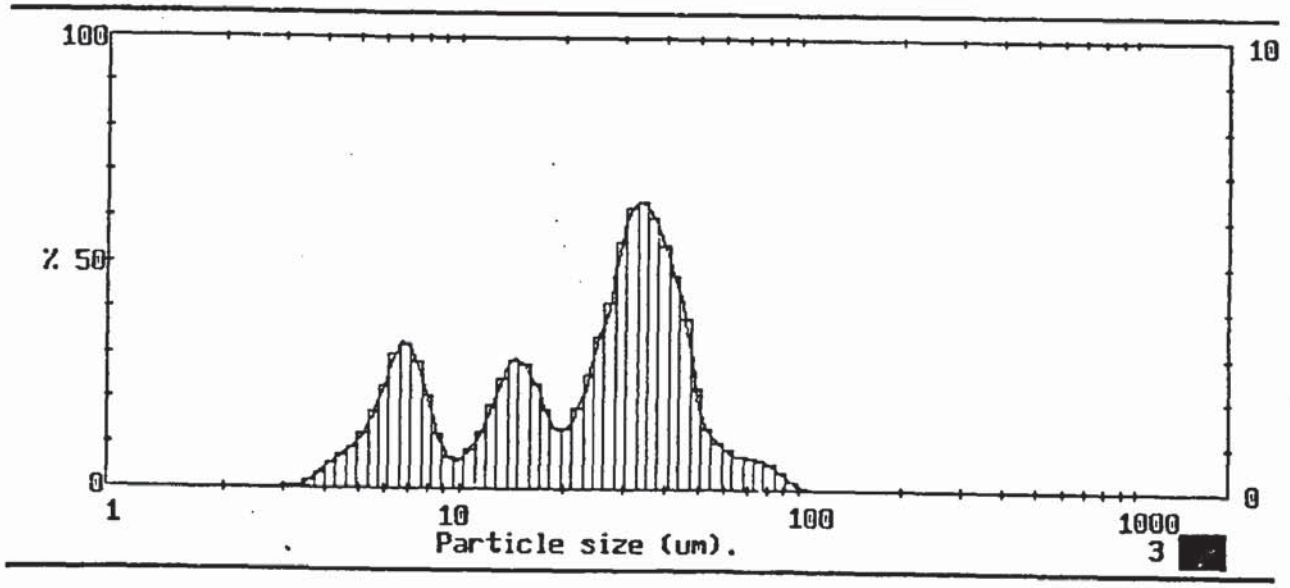

Figure 6-11A The effect of impeller speed on drop size distribution i) 400rpm, ii)500rpm

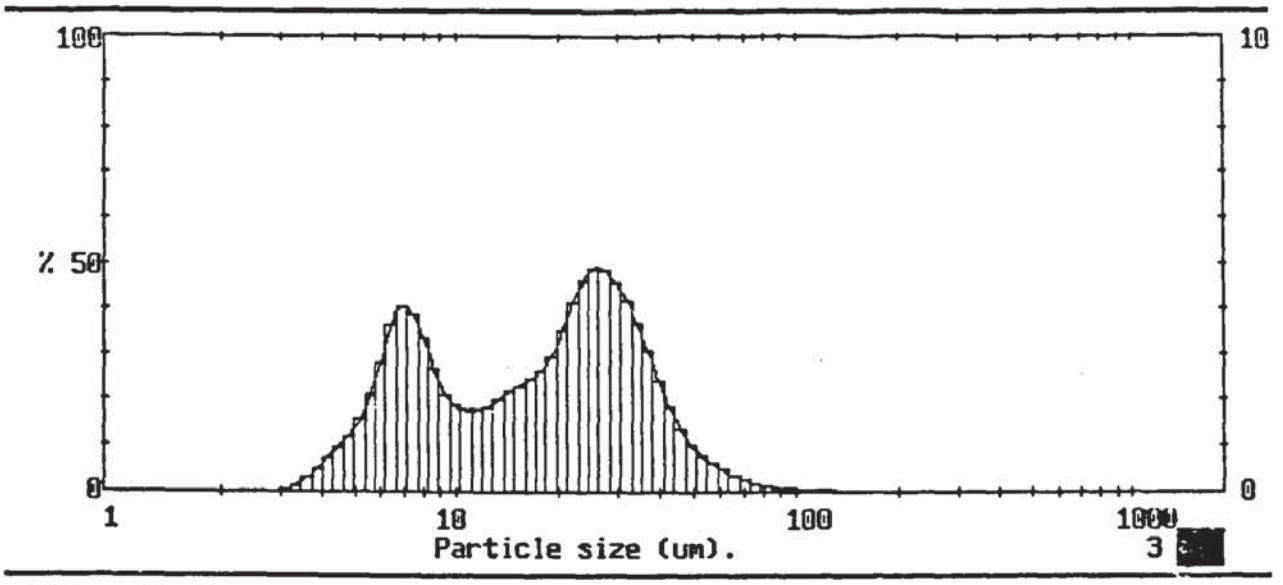

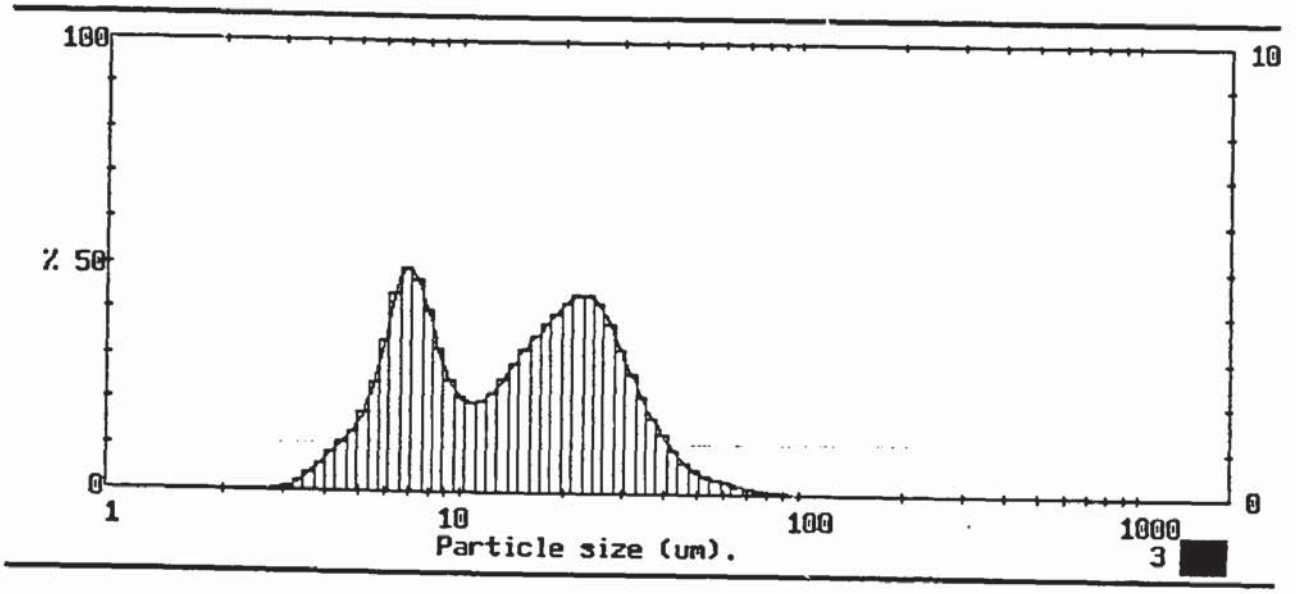

Figure 6-11B The effect of impeller speed on drop size distribution iii) 600rpm,iv)700rpm

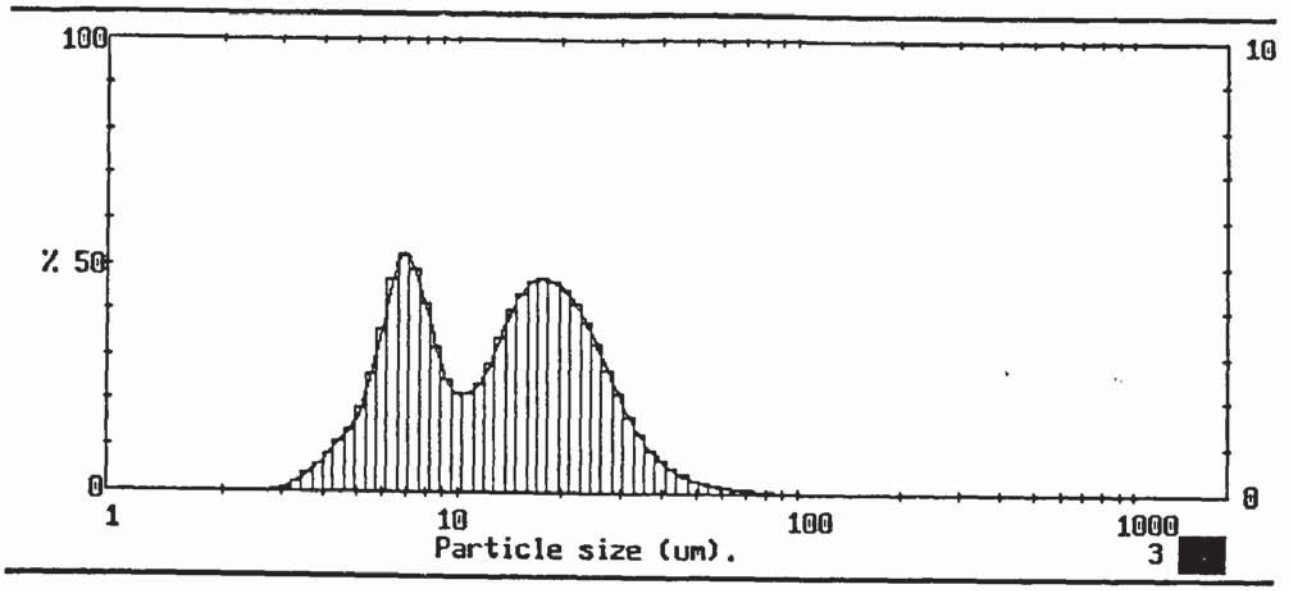

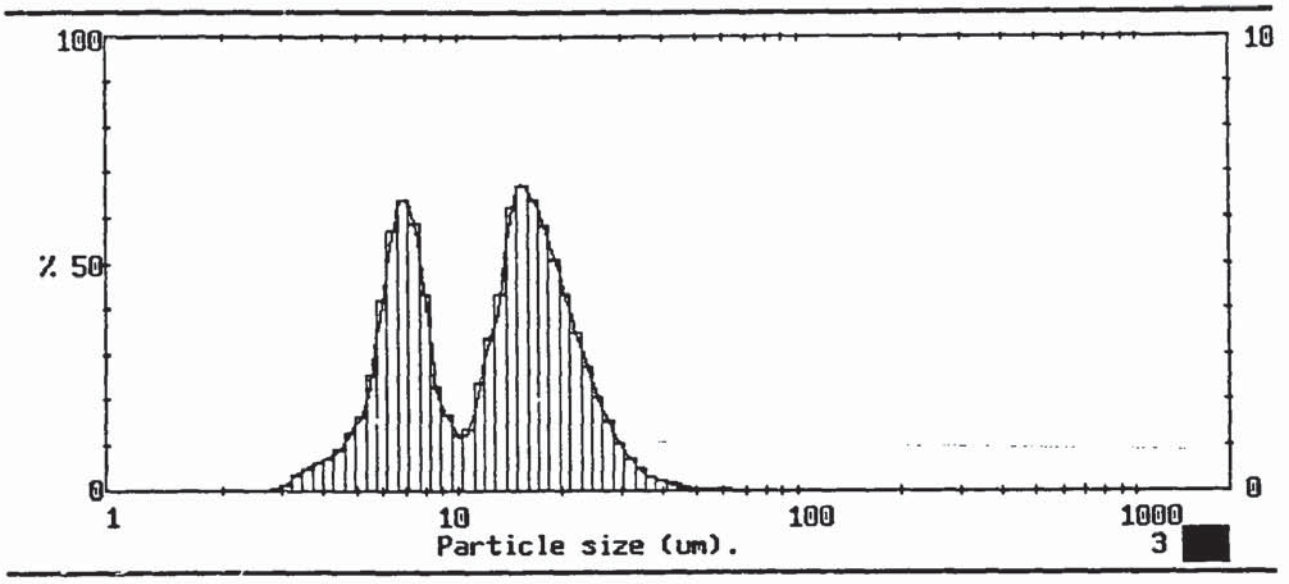

Figure 6-11C The effect of impeller speed on drop size distribution v) 800rpm, vi)900rpm

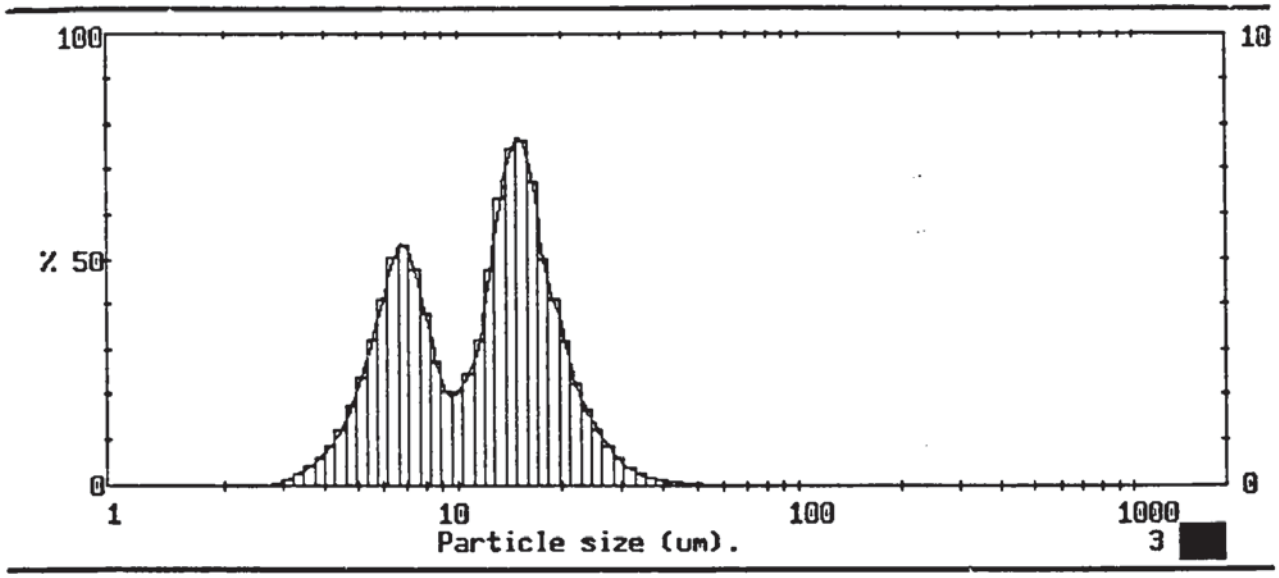

Figure 6-11D The effect of impeller speed on drop size distribution vii) 1000.

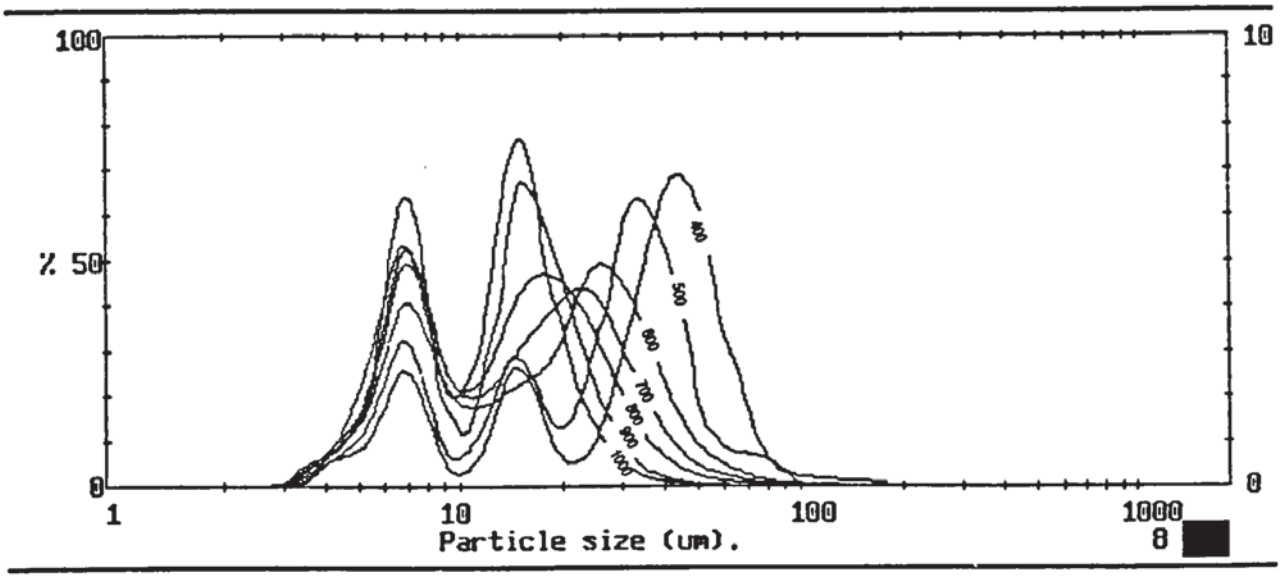

Figure 6-12 Speed spectrum from 400-1000 and the effect on the distribution

6.8.2 Data analysis

6.8.2.1 Correlations for the steady-state mean drop size

Shinnar and Church (1960) and Shinnar (1961) used Kolmogoroff's theory, as discussed in Chapter Two section 2.7, of universal equilibrium assuming local isotropy to derive the following equation for systems where the break-up process is the dominant mechanism:

$$\frac{\bar{d}_{vs}}{D} = K We_I^{-0.6} \qquad 6\text{-}1$$

The term $N^3 D^2$ is representative of power input per unit volume provided $Re > 10^4$. Hence, for equivalent dispersion on scale-up, a general rule is to apply equivalent power input per unit volume.

As was shown previously, the drop size in the system studied in the present work was mainly determined by the breakage process. Also, since the Reynolds number for the system studied was $\geq 10^4$, the power number N_p attained a constant value.

Plot of log $\frac{d_{32}}{D}$ vs. log N_{we} in Figure 6-13 shows that, despite there being no allowance for $\rho_d, \Delta\rho, \mu_c$ and μ_d, a reasonable fit of the data is obtained The regression line correlates the data in Figure 6-13 with a slope = -0.6 and intercept of K = 0.11.

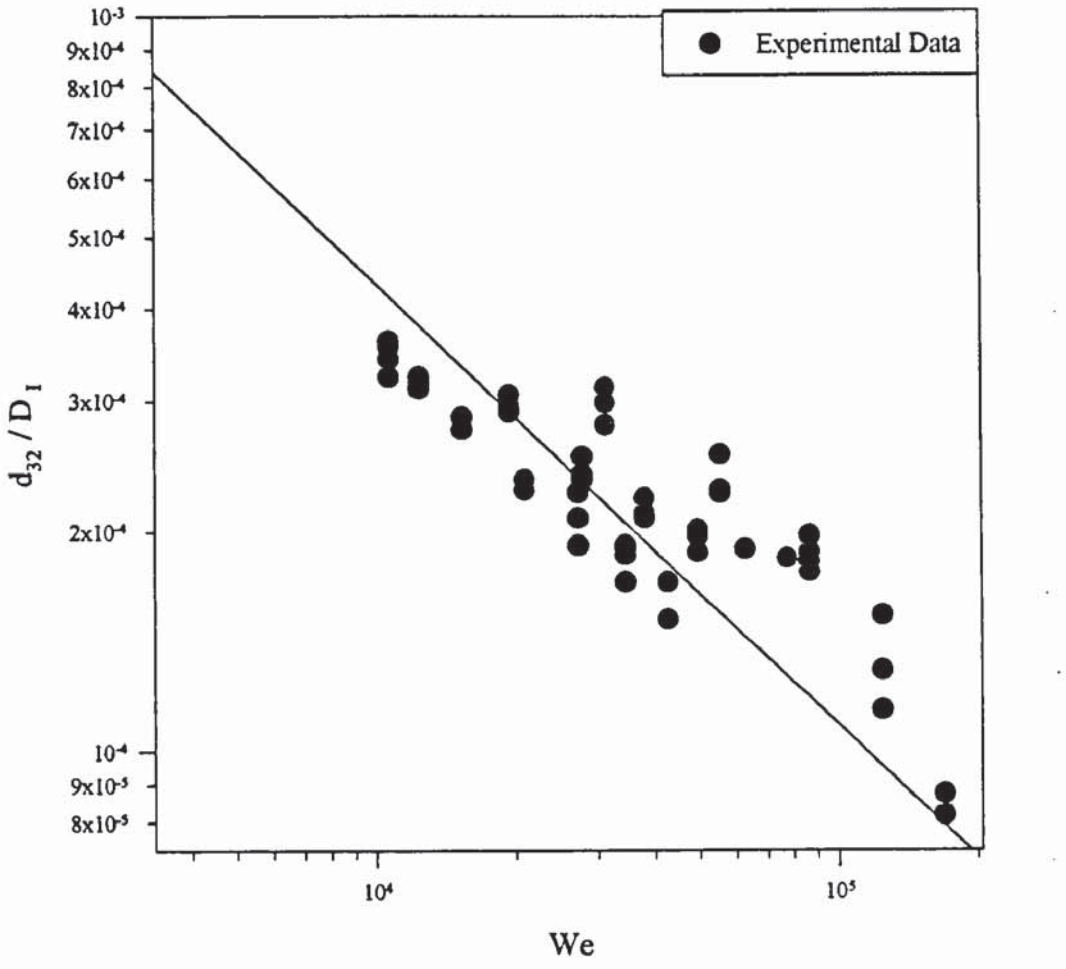

Figure 6-13 The effect of Weber number N_{we} on Sauter mean drop diameter d_{32}.

The empirical correlation for the system can be written as:

$$\frac{\bar{d}_{32}}{D_I} = 0.11\, We_I^{-0.6} \qquad 6\text{-}2$$

Equation 6-2 was tested by plotting the experimental values of the Sauter mean drop against the predicted values, as shown in Figure 6-14.

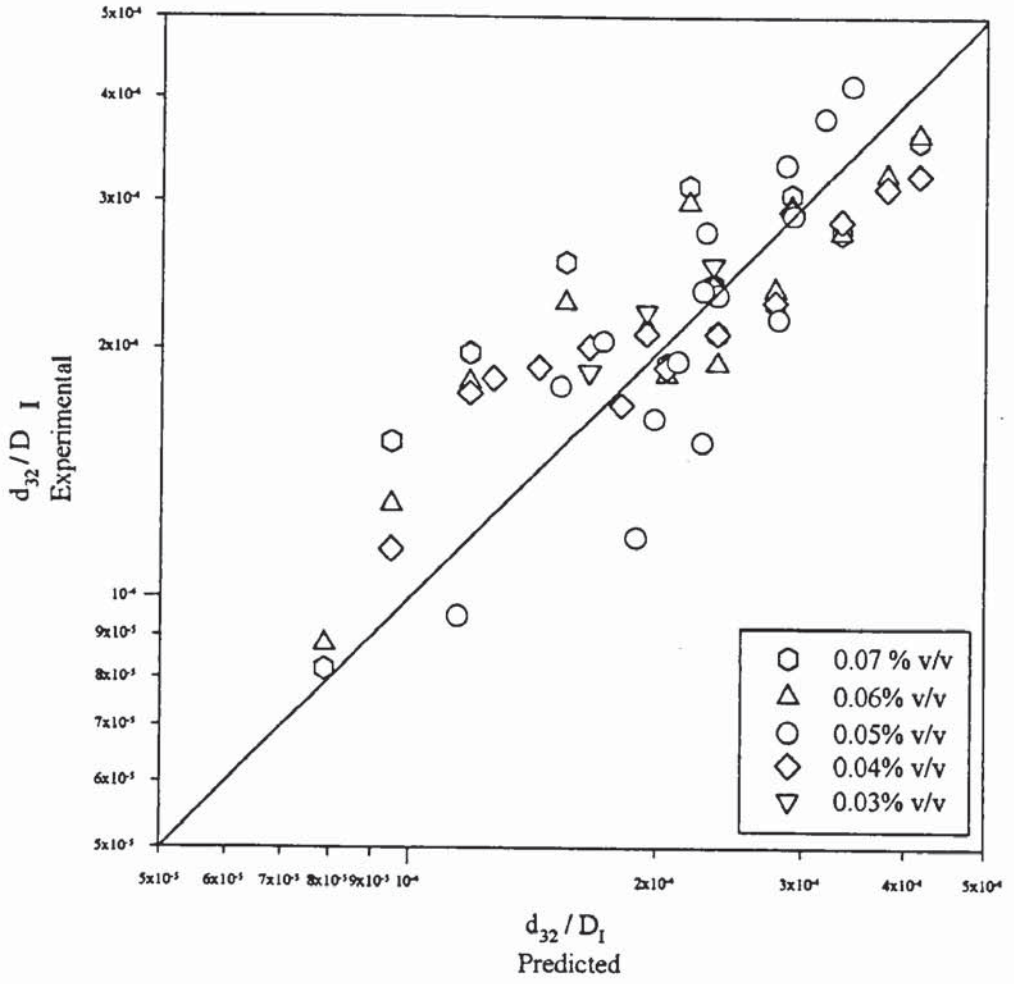

Figure 6-14 Comparison of experimentally determined d_{32} values with those predicted by Equation 6-2.

Figure 6-15 provides a comparison between the experimental values for d_{32}/D_I and those predicted from four correlations in the literature. The slopes are the same because of the choice of -0.6 for the exponent on the Weber number. It is differences in the value of K (see equation 6-1) that account for the higher values of d_{32} obtained in the present work.

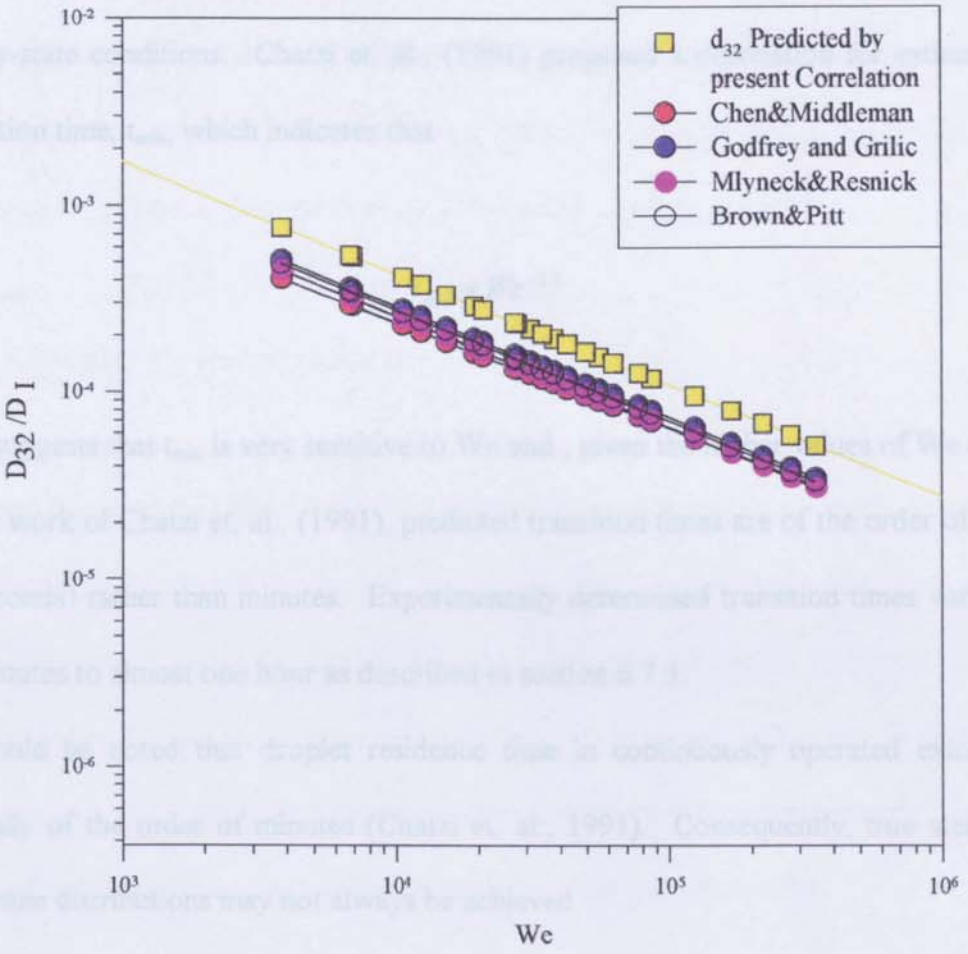

Figure 6-15 Comparison plot for the theoretical correlation and other workers correlations.

6.8.2.2 Time effects

Konno et. al., (1993) and Chatzi et. al., (1991) have both explored the effect of agitation time on drop size distribution following changes in operating parameters. With their systems (kerosene / water, *n*-butanol / water, *o*-xylene / 0.01% PVA in water, *o*-xylene / 0.1% PVA in water and styrene / 0.1 PVA in water) it took about an hour to approach steady-state conditions. Chatzi et. al., (1991) proposed a correlation for estimating the transition time, t_{min}, which indicates that

$$t_{min} \propto We^{-2.3} \qquad 6\text{-}3$$

This suggests that t_{min} is very sensitive to We and , given the higher values of We explored in the work of Chatzi et. al., (1991), predicted transition times are of the order of seconds (2 seconds) rather than minutes. Experimentally determined transition times varied from 15 minutes to almost one hour as described in section 6.7.3.

It should be noted that droplet residence time in continuously operated extractors is typically of the order of minutes (Chatzi et. al., 1991). Consequently, true steady-state drop-size distributions may not always be achieved.

6.8.2.3 d_{32} and d_{max}

Strictly speaking, theories of drop-break-up are concerned with the maximum stable drop size, d_{max}. Nevertheless, most of the reported data is in terms of d_{32}; this is usually justified on the grounds that d_{32} is linearly related to d_{max}. Brown and Pitt (1972) have quoted $d_{32} = 0.70\ d_{max}$, although lower values for the coefficient have also been reported. In the case of multi-modal distributions, the choice of characteristic drop diameter is more problematic. Because of the systematic trends in d_{32} values obtained in the present work and the strong correlation between peak values and d_{32}, it is the Sauter mean drop diameter, d_{32}, diameter that has been used for purposes of correlation.

6.8.2.4 Range of We and Re numbers

It should be noted that the range of We number covered in this study was in the range 10^4 to 10^5. This is several orders of magnitude greater than the range used by other researchers and is due to (a) the low interfacial tensions and (b) the relatively high values of agitation speed and hence large agitator Reynolds numbers. This point is illustrated by the plots in Figure 6-15; it should be noted that the published correlations have been extrapolated beyond the range of We numbers studied experimentally.

6.8.2.5 Drop size and scale of turbulence

As discussed in Chapter 2, correlations of the form

$$d_{max} \propto We_I^{-0.6} \qquad 6\text{-}4$$

are based on the assumption of isotropic turbulence coupled with the constraint that d is large with respect to the scale of energy dissipation eddies. The length of the primary eddy is given approximately by the width of the impeller (Shinnar and Church, 1960). The d_{max} values observed in the present work were of the order of 100μm; this is small relative to the scale of large primary eddies in the region close to the agitator which are of order 10mm. This shows that the drops are much smaller than the primary eddies and of a scale where the assumption of isotropic turbulence will be applicable. An estimate of the energy dissipation eddies can be made from the expression:

$$Eddy\,length = \left[\left(\frac{\mu_c}{\rho_c}\right)^3 / \varepsilon\right]^{\frac{1}{4}} \qquad 6\text{-}5$$

where ε, is the power input per unit mass of liquid (Appendix 7). For the range of agitator speeds from 300 rpm to 1000 rpm, the estimated eddy length is from about 70μm to 25 μm. The order of magnitude of this scale is close to that of the larger drop sizes and nearly ten times that of the smaller drop sizes encountered in the present work. This

suggests that viscous as well as inertial forces will affect drop break-up for the PEG-salt system. Konno et. al., (1993) have reached the same conclusion as a result of their research with different systems.

In principle, another way of assessing the relative importance of inertial and viscous effects is to examine the relationship between d_{32} and impeller speed N. Calbrese et. al., (1986) have suggested that

$$d_{32} \propto N^{-0.75} \qquad 6\text{-}6$$

when dispersed phase viscosity, μ_d, is the dominant property. An alternative relationship which assumes interfacial tension is the factor responsible for resulting drop break-up is the familiar form

$$d_{32} \propto N^{-1.2} \qquad 6\text{-}7$$

Consequently, the experimental data of the present work have been plotted as log d_{32} versus log N, as presented in Figure 6-16. Using linear regression, the values of the exponent for N have been computed and the results are given in Table 6-1. Figure 6-16 shows that the exponent on N is near to, or greater than, -1.0, the range being from -1.0 to -1.4; the latter figure is associated with the 20% w/w PEG-salt system and the value of -1.0 with the 30% PEG-salt system. These results suggest that both inertial and viscous forces can be expected to influence d_{32}.

Table 6-1 The effect of phase concentration on the slope of log d_{32} versus log N.

Phase Concentration (% w/w)	Average Slope	Accuracy (%)
20	-1.4	±7
25	-1.2	±4
30	-1.0	±7

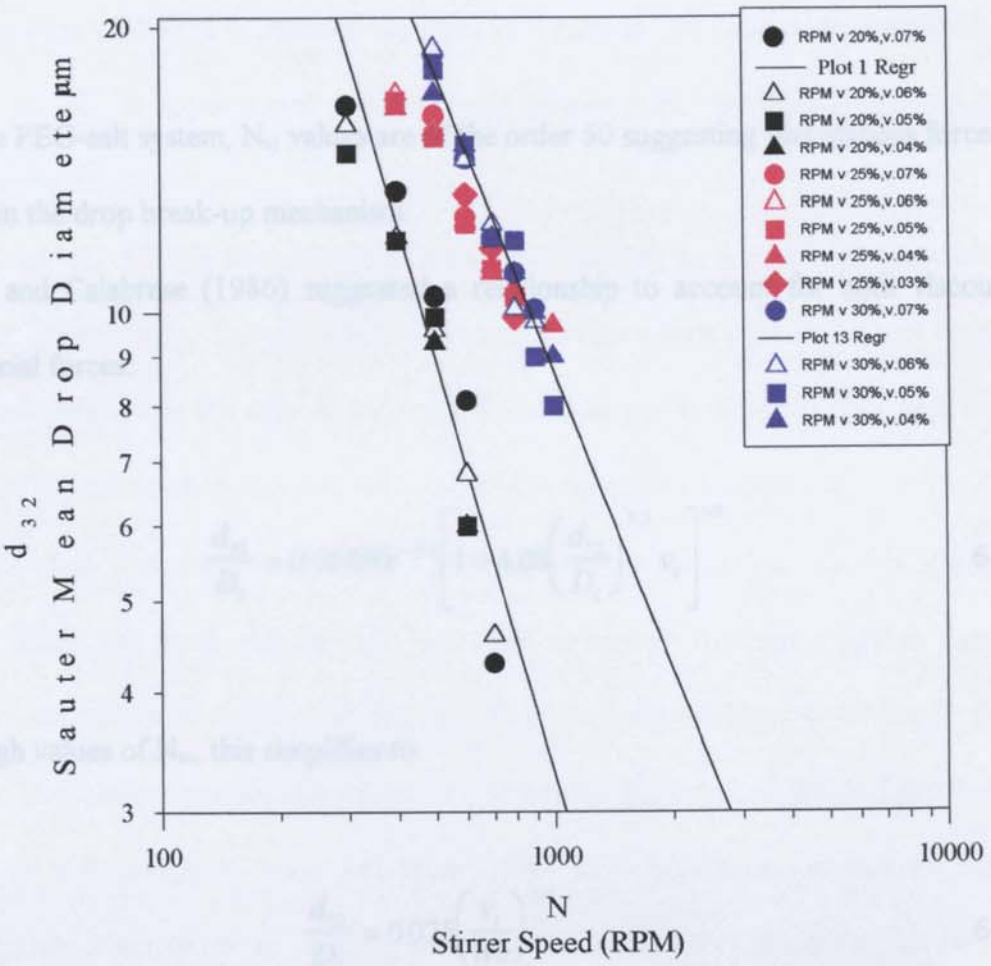

Figure 6-16 Plots of log d_{32} vs. Log N

6.8.2.6 Relative influence of viscosity and interfacial tension

The relative magnitude of the viscosity and interfacial tension forces is given by the tank viscosity group, N_{vi}. This has been defined by Wang and Calabrese (1986) as

$$N_{vi} = \frac{\mu_d ND}{\sigma}\left(\frac{\rho_c}{\rho_d}\right)^{\frac{1}{2}} \qquad 6\text{-}8$$

For the PEG-salt system, N_{vi} values are of the order 50 suggesting that viscous forces play a role in the drop break-up mechanism.

Wang and Calabrese (1986) suggested a relationship to account for both viscous and interfacial forces:

$$\frac{d_{32}}{D_I} = 0.054We^{-3/5}\left[1 + 4.08\left(\frac{d_{32}}{D_I}\right)^{1/3} v_i\right]^{3/5} \qquad 6\text{-}9$$

For high values of N_{vi}, this simplifies to

$$\frac{d_{32}}{D_I} = 0.075\left(\frac{v_i}{We}\right)^{3/4} \qquad 6\text{-}10$$

$\left(\frac{v_i}{We}\right)$ is in fact $\frac{\mu_d}{ND^2\rho_d}$; on inversion, this is seen to be an agitator Reynolds number based on dispersed phase physical properties. This predicts, as discussed earlier, that

$$d_{32} \propto N^{-0.75} \qquad 6\text{-}11$$

which is not the case for the present work.

The correlation of Wang and Calabrese (1986) also greatly over-predicts $\frac{d_{32}}{D_I}$ values and so cannot be used with confidence for PEG-salt systems. Consequently, despite the high values for N_{vi}, it appears that the interfacial tension (and the Weber number) have a dominating effect.

Konno et. al., (1993) have reached similar conclusions as a result of their extensive studies. Interestingly, Levich (1962) also suggests that a high viscosity cannot on its own serve to stabilise the droplets; if, however, the viscosity is sufficiently high, then the time required for deformation and fragmentation of the drop can be significant.

Finally, some comment is necessary about the smaller drops (~2-5μm) in the system. These drops are much smaller than the scale of energy dissipation eddies and, once formed, are not likely to break-up further. Their formation is likely to be due to primary droplet break-up, when because of the low interfacial tension, a number of small satellite drops as well daughter drops will arise. This hypothesis receives support from the experiments of Konno et. al., (1983) who found that three or more drops can be formed during break-up near the agitator.

7. Conclusions

7.1 Basic conclusions

The Physical Properties of the PEG-salt System

The physical properties of the two-aqueous phase liquid-liquid system used were determined for various PEG and salt concentrations. The viscosities of both phases were found to increase as the phase composition was increased. The interfacial tension between the phases was very low, i.e. 1.28×10^{-4} to 1.11×10^{-3} N/m. However, it increased with an increase of phase composition. Further experiments in which the system temperature was varied in the range of 15°C to 30°C indicated that the temperature effect on the viscosities of the PEG and salt phases was negligible for the salt phase. However, temperature change had a significant effect on the higher concentration PEG phase (30% w/w), resulting in a 40 % reduction in viscosity over a temperature range of 15°C to 30°C.

Dispersion Settling Times

The effect of phase composition and volume ratios on settling behaviour for two aqueous phase systems indicated that separation was slow, with break-times of several minutes. The rate of the separation process was limited by the recoalescence of drops at the interface.

The rate of sedimentation increased with an increase in phase composition. It was observed that, after reaching a clear interface, there was a haze (cloudiness) in both layers, with a particularly intense haze in the bottom phase (salt-rich). The final disappearance of this haze did not alter the height of the interface between the layers after the haze had cleared. In reality the height would not be expected to alter

because, despite their large numbers, the extremely small size drops will not constitute a significant volume fraction as mentioned in Section 4.3.1.

Mass Transfer from Single Drops

Mass transfer between the two phases was studied. Detailed investigation revealed that the solute (dye) used to study the mass transfer process was well dispersed, rather than dissolved, in the salt phase and the overall mass transfer coefficient was found to increase as a function of concentration. Interfacial tension between the phases was found to decrease as a function of the concentration of dye solute.

Tests showed that the increase in mass transfer coefficient was not due to reaction of the solute. However, the effect of the dye on interfacial tension (Marangoni effect) and on the equilibrium between phases could have caused the observed increase. The largest drops used in the tests (3.7mm in diameter) resulted in higher values for the apparent mass transfer coefficient than the smallest ones (2.8mm) by a factor of about five. This increase is believed to be due to the deformability and breakage of the large drops during the mass transfer process. Such phenomena are well-established, e.g. as summarised in Section 2.6.

Drop Size Distribution in an Agitated Vessel

Drop size distribution and the mean Sauter diameter are important characteristics of liquid-liquid dispersions. For processes such as mass transfer, it is essential that drop size can be estimated to enable mass transfer rate to be predicted. Drop size and size distribution were measured using a light diffraction technique. This technique proved very accurate, reproducible, easy to operate, and fast measuring (~15 seconds), which

makes it suitable for on-line measurement. A novel vessel was designed to facilitate on-line measurements of the dispersion. The design of the vessel is unique providing an air-tight system to avoid aeration, which allows high agitation speed, and the utilisation of on-line measurement.

The Sauter mean drop diameter, d_{32}, was used to express the drop size. As expected, Sauter mean drop size was found to be a function of stirrer speed, N, but the volume fraction had only a very small effect on drop size d_{32} within the limit studied. The effect of the phase composition on drop size d_{32} was notable and greater with the 20% w/w solutions than with the 25 and 30% w/w solutions.

The drop size distribution is a function of the stirrer speed N, and at the lowest stirrer speed, i.e. 300 rpm, there was a wide spread and trimodal distribution. At high stirrer speed, the drop size distribution became bimodal and the spread reduced.

The time to reach equilibrium drop size (steady state) depended upon the physical properties of the system and agitation speed. The accuracy and the reproducibility of the time for any one system was within ±2 %.

The empirical correlation $\frac{\bar{d}_{32}}{D_I} = 0.11\, We_I^{-0.6}$ satisfactorily represented the experimental data.

7.1.1 Development of experimental technique

Standard techniques were used for studying the physical properties, settling and mass transfer. However a new improved technique was developed for measuring interfacial tension.

A new method was also developed for measuring drop size and size distribution for liquid-liquid systems, containing small drops (< 2μm) at low hold-ups (0.03% to 0.07 % v/v)

7.1.2 Significance of the work

This work has revealed several significant features relating to break-time, the complexity involved in studying mass transfer and temperature effects.

A relatively short primary-break time, e.g. 10 minutes, was sufficient for the settling process. The secondary haze was ignored, since it is reported as insignificant in practical extractions because the fractional hold-up it represents is very small.

The various factors affecting mass transfer in a stirred vessel - for example the addition of a solute shifts the equilibrium of the system, both diffusional and convective mass transfer take place, and drop breakage and recoalescence may enhance the mass transfer process - render practical mixer-settler extraction studies complex. Hence given the wide range of liquid-liquid systems and operating variables, there is an important gap to be covered between single drop studies and commercial operation.

Reports in the literature indicate that a temperature variation of ±2°C would not affect system behaviour. On the contrary, the present work shows that the temperature is likely to have some effect on the physical properties, phase equilibrium, mass transfer, and drop size and therefore drop size distribution.

8. Application to Design

It follows from the above that in the future design of two aqueous phase liquid-liquid separation processes consideration needs to be given to the following.

1) The interfacial tension between the phases is likely to be very low and the density difference small. Therefore gravity settling will be slow and the rate of coalescence will also be slow. This may impose a limit on volumetric throughput. An improvement might be achieved by for example, increasing the density difference between the phases or the use of a centrifuge, selected to separate the two phases at a speed which will not damage the biologically active material. The settling process for the liquid-liquid system used here was primary settling (where almost 99 % of the phases were separated) which took about 10 minutes whereas secondary settling required 1-2 days. In the design of a practical process primary settling will probably be sufficient.

2) As discussed in Chapter 5, the addition of a solute to the system shifted its equilibrium. Mass transfer rate was by a combination of diffusional and convective mass transfer. Mass transfer rates for the specific solute and operating concentrations in the PEG/salt system therefore need to be determined.

3) Determination of drop size and drop size distribution in a specific dispersion is essential in order to estimate the interfacial area available for mass transfer. As summarised in Section 2.6 the mass transfer film coefficients are also drop-size dependent. Drop size

also controls the sedimentation and coalescence rates. In all cases the distribution may not be adequately characterised by the mean size; this is particularly relevant to situations where a bimodal distribution is generated. The experimental evidence shows that the dispersed phase hold-up did not have a significant effect on the Sauter mean drop size. The phase concentration also had only a small effect on the Sauter mean drop diameter. However the agitation speed had a significant effect on the Sauter mean drop diameter and would require careful selection, or provision of a variable drive, for a practical process.

9. Suggestion for Future Work

9.1 Additional Studies

Further work should include comparative tests with other two- aqueous phase systems e.g. PEG/dextran systems and other organic-aqueous systems with similar physical properties. Studies using model biochemical solutes, e.g. proteins, are also required since they strongly affect system physical properties, droplet behaviour and the settling of the dispersion.

More research is needed on the effect of different solutes on mass transfer rate. Consideration also needs to be given to how mass transfer models for swarms of drops in such systems will differ from those for single drops.

The phenomena involved in the formation of multi-modal drop size distributions in agitated vessels also need to be examined further. There is also scope for further analysis of the experimental data acquired by the author.

9.2 Application of Techniques

- *Interfacial tension measurement technique*

The development of the interfacial tension technique will facilitate the measurement of this property in virtually any liquid-liquid system. The technique could also be extended to the measurement of surface tension for gas-liquid systems.

- *Vessel design for the use with the laser diffractor*

The new vessel design facilitates the on-line measurement of drop size and size distribution in liquid-liquid systems with the Malvern particle size analyser. The vessel is of air-tight design which enables drop size to be studied at high agitation speed. The new design can be used with liquid-liquid systems or suspensions of particles in liquid.

REFERENCES

1. Albertsson, P-Å., *Sci. Tools*, **17**, No.3, 56, (1970).

2. Albertsson, P-Å., "*Partition of cell particles and macromolecules*" 2nd Ed., John Wiley and Sons, New York (1971).

3. Albertsson, P-Å., Andersson B., Larsson, C. and Akerlund, H.E., *Methods of Biochemical Analysis* Vol. 28 ed. Glick. D., John Wiley and sons, 115-150, (1982).

4. Andreas, J.M., Hauser, E.A. and Tucker, W.B., " Boundry Tension by Pendant Drops", *J. Phy. Chem.*, **42**, 1001, (1938).

5. Batchelor, G. K., " Pressure Flucuations in Isotropic Turbulence" *Proc. Cambridge Phil. Soc.* **47**, 359 (1950).

6. Backman, L. "*Partitioning in Aqueous Two Phase Systems, Theory, Methods, Uses and Applications to Biotechnology*" ed. Walter, H., Brooks, D.E. and Fisher, D. Academic Press Inc. pp. 267-314 (1985).

7. Bakker, C.A.P., Fentener Van Vlissingen, F.H. and Beek, W.J., " The Influence of Driving Force in Liquid-Liquid Extraction" *Chem. Eng. Sci.*, **22**, 1349-1355, (1967).

8. Berg, J. C. and Acrivos, A., *Chem. Eng. Sci.*, **20**, 737 (1965).

9. Bird, R., Stewart, W, Lightfoot, E., *Transport Phenomena* John Wiley and Sons, Inc.; New York (1960).

10. Bouyatiotis, B. A., Thornton, D., "Liquid-liquid Extraction in Stirred Tank. I", *Symp. Liquid-Liquid Extr.*, Prog., 43-51, (1967).

11. Brooks, D. E., " *Partitioning in Aqueous Two Phase Systems, Theory, Methods, Uses and Applications to Biotechnology*" ed. Walter, H., Brooks, D.E. and Fisher, D. Academic Press Inc., (1985).

12. Brown, D. E.; Pitt, K. "Drop Breakup in Stirred Liquid-Liquid Contactor": *Chem. Eng. Sci.*, **27**, 577, (1972).

13. Calabrese, R. V., Change T. P. K. and Dany, P., "Drop Breakup in a Turbulent Stirred-Tank Contactors": *AIChE J.*, **32**, 657, (1986).

14. Chatzi, E.G., Boutris, C. J., and Kiparissides, C.,"On-Line Monitoring of Drop Size Distribution in Agitated Vessels" *Ind. Eng. Chem. Res.*, **30**, 3, (1991).

15. Chatzi, E. G.; Gavrielides, A. D.;Kiparissides, C. " Generalized model for prediction of the steady-state drop size distributions in batch stirred vessels". *Ind. Eng. Chem. Res.*, **28**, 1704, (1989).

30. Hartland, S. "Coalescence in Dense-Packed Dispersions" in *Thin Liquid Films Fundamentals and Applications*; Ivanov, I.B., Ed; Surfactant Science Series 24; Marcel Dekker, Inc.: New York; Chapter 10, pp 668-766, (1988).

31. Hinze, J. O.," Fundamentals of the Hydrodynamic Mechanism of Splitting in Dispersion Processes" *AIChE* , **1**, No. 3, 289-295, (1955).

32. Hustedt, H.; *Biotechnol. Lett.*, **8**, No. 11, 791-796, (1986).

33. Hustedt, H., Kroner, K. H., Menge, U. and Kula, M-R., "*Trends in Biotechnol.*, **3**, No. 6, 139- 144, (1985).

34. Jeelani, S. A. K., and Hartland, S.; "Prediction of Dispersion Height in Liquid-Liquid Gravity Settlers from Settling Data", *Chem. Eng. Res. Des.*, **64**, 450-460 (1986).

35. Jeelani, S. A. K., Pandit, A. and Hartland, S., " Factors Affecting the Decay of Batch liquid-liquid Dispersions"; *Can J Chem Eng*, **68**, 924 (1990).

36. Johansson, G., *Methods Enzymol*, " Affinity Partitioning of enzymes", **104**, 356, (1984).

37. Johansson, G., "*Partitioning in Aqueous Two Phase Systems, Theory, Methods, Uses and Applications to Biotechnology*" ed. Walter, H., Brooks, D.E. and Fisher, D. Academic Press Inc. 161-226, (1985).

38. Konno, M. K., Kosaka, N., "Correlations of Transient Drop Sizes in Breakup Process in Liquid-Liquid Agitation": *J Chem. Eng. Japan*, **26**, No. 1, (1993).

39. Konno, M. K., Saitos, "Correlation of Drop Sizes in Liquid-Liquid Agitation At Low Dispersed Phase Volume Fractions": *J Chem. Eng. Japan*, **20**, No. 5, (1987).

40. Konno, M. K., Aoki, M. and Saitos, S. ." Scale Effect on Breakup Process in Liquid-Liquid Agitated Tanks": *J Chem. Eng. Japan*, **16**, No. 4, 312-319 (1983).

41. Konno, M. K., Arai, K. and Saitos, S." The effect of Viscous and Inertial Forces on Drop Breakup in Agitated Tank ":*J Chem. Eng. Japan*, **10**, No.6, 474-477 (1977).

42. Kroner, K .H. , Hustedt, H., Granda, S. and Kula, M-R., " Technical Aspects of Separation Using Aqueous Two-Phase Systems in Enzyme Isolation Processes" *Biotech. Bioeng.*, **20**, 1967-1988, (1978).

43. Kroner, K. H., Hustedt, H. and Kula, M-R.; *Process Biochem*. No. **19**, 170-179, (1984).

16. Chen, H. T; Middlemann, S." Drop Size Distribution in Agitated Liquid-Liquid Systems": *AIChE J.*, **13**, No. 5, 989-995, (1967).

17. Clift, R., Grace, J. P. and Weber, M.E., *Bubbles Drops and Particles*, Academic Press, Inc. New York, (1978).

18. Coulson, J. M. and Richardson, J. F., Chemical Engineering; Ed. Pergmon Press, Vol. **2**, (1956).

19. Dalingaros, W., Hartland, S., "Effect of Drop Size and Physical Properties on Dispersion Height in the Separating Section of a Liquid-Liquid Extraction Column". *Can. J. Chem. Eng.*, **64**, 925-930, (1986).

20. Dalingaros, W.,Jeelani, S. A. K., Hartland, S., Prediction of Steady State Dispersion Height in the Disengaging Section of an Extraction Column from Batch Settling Data. *Can. J. Chem. Eng.*, **65**, 210-213, (1987).

21. Davies, G. A., Mixing and Coalescing Phenomena in Liquid-Liquid Systems *in Science and Practice of Liquid-Liquid Extraction*; Thornton, J. D., Ed; Oxford University Press; Vol. **1**, Chapter 5, (1992).

22. Davies, J. T. *Turbulence Phenomena*, Academic Press, New York (1972).

23. Davies, J. T.,"Drop Sizes of Emulsions Related to Turbulent Energy Dissipation Rates"; *Chem. Eng. Sci.*, **40**, No. 5, 839-842, (1985).

24. Fordham, S., *Proc. Roy. Soc.* (London), " On the Calculation of Surface Tension From Measurements of Pendant Drops" **194**, No A1036, 1-16 (1948).

25. Gaggero. M, Arato, E . ,Costa, P. and Lodi , G. *"liquid-liquid mixing studies on the phase formation in stirred tanks* " 6th European Conference on Mixing, B.H.R.A, Cranfield, England (1988).

26. Garner, F. H. and Skelland, A. H. P.; " Some Factors Affecting Droplet behaviour in Liquid-Liquid Systems"; *Chem. Eng. Sci.*, **4**, 149-158 (1955).

27. Grace, J. R., Wairegi, T. and Nguyen, T. H.;" Shapes and Velocities of Single Drops and Bubbles Moving Freely Trough Immiscible Liquids"; *Trans. Instn. Chem. Engrs.*, **54**, 167-173 (1976).

28. Godfrey, J. C. and Grilie, V. European Conference on Mixing, BHRA, C1, Cambridge (1977).

29. Golovin, A. A., "Interfacial Turbulence and Mass Transfer at Liquid-Liquid Extraction" in Extraction 90, *I Chem. E. Symp Ser.*, No. 119; I Chem E 1990, 313-326, (1990).

44. Kula, M-R. "Applied Biochemistry and Bioengineering: in *Enzyme Technology*" ed. Wingard, L. B., Katchalski-Katzire, E. and Goldstein, L. Academic Press. Vol. **2**, 71-95, (1979).

45. Kula, M-R., Kroner, K. H., Husredt, H. and Schütte; "Technical aspects of extractive enzyme purification". Ann. N. Y. Acad. Sci., **369**, 341-354, (1981).

46. Kula, M-R. Kroner, K. H. and Hustedt, H. *Advances in Biochemical Engineering* ed. Fiechter, A.; **24**, 73-118, (1982).

47. Kula, M-R.; "*Comprehensive Biotechnology Vol. II: The Principles, Applications and Regulations of Biotechnology in Industry, Agriculture and Medicine*", ed. Murray Moo-Young; Pergamon Press 451-471, (1985).

48. Kumar, A. and Hartland, S.; " Gravity Settling in Liquid-Liquid Dispersions"; *Can J Chem Eng,*. **63**, 368-376 (1985).

49. Laso, M; Steiner, L.; Hartland, S. "Dynamic simulation of agitated liquid-liquid dispersions II. Experimental determination of breakage and coalescence rates in stirred tank". *Chem. Eng. Sci.*, **42**, (10), 2437-2445, (1987).

50. Levich, V. G.; *Physiochemical Hydrodynamics*, Prentice-Hall, Englewood Cliffs, New Jersey, (1962).

51. Lode, T., Heideger, W., *Chem Eng Sci*, " Single Drop Mass Transfer Augmented by Interfacial Stabilities", **25**, 1081-1090, (1970).

52. Malvern Instrument Ltd. "Particle Size Reference Manual", Malvern, Worcestershire, England, (1987).

53. Maroudas, N. S. and Sawistowski, H., "Simultaneous Transfer of Two Solutes Across Liquid-Liquid Interfaces"; *Chem, Eng. Sci*, **19**, pp 919-931, (1964).

54. Mills, O.S., *Brit. J. Appl. Phy.*, **4**, 274, (1953).

55. Nadiv, C., Semiat, R, *Ind. Chem Eng. Res.*, " Batch Settling of Liquid-Liquid Dispersion", **34**, No 7, 2427-2435, (1995).

56. Mlynek, Y. and Resnick, W.; "Drop sizes in an agitated Liquid-Liquid system" *AIChE.*, **18**, No. 1, 122-127 (1972).

57. Niederhauser, D. O. and Bartell, F. E., Report of Progress-Fundamental Research on Occurrence and Recovery of Petroleum, 1948-1949, American Petroleum Institute, Baltimore, p.114, (1950).

58. Olander, D. R.; *AIChE*; **6**, No. 2, 233-239, (1960).

59. Padday, J. F.," Surface Tension: Part I: The Theory of Surface Tension"in *Surface and Colloid Science*, Matijevic, E., Ed; John Wiley and Sons, Inc.,39, (1969).

60. Richardson, J. F. and Zaki, W. N., "Sedimentation and Fluidisation: Part I", *Tans. Instn. Chem. Engrs.*, **32**, 35-53, (1954).

61. Rodger, W. A., Trice, V. G., and Rushton, J. H., *Chem. Eng. Progr.*, **52**, 515, (1955).

62. Ryden, J. and Albertsson, P-Å.; *J. Colloid Interface Sci.*, **37**, 219-222, (1971).

63. Sawistowski, H., Goltz, G. " The Effect of Interface Phenomena on Mass Transfer Rates in Liquid-Liquid Extraction, *Trans. Instn. Chem. Engrs.*, **41**, 174-181, (1963).

64. Sawistowski, H.," Interfacial Phenomena" in *Recent Advances in Liquid-Liquid Extraction; Hanson*, C., Pergmon Press Ltd., New York, (1971).

65. Schügerl, K., *Solvent Extraction in Biotechnology: Recovery of Primary and Secondary Metabolites*, Springer-Verlag Berlin Heidelberg, (1994).

66. Shinnar, R. "On the behaviour of liquid dispersions in mixing vessels". *J.Fluid Mech.*, **10** ,259-275, (1961).

67. Shinnar, R. ; Church, J. M., "Predicting particle size in agitated dispersions". *Ind. Eng. Chem.*, **52** (3), 253, (1960).

68. Slater, M. J.,"Rate Coefficients in Liquid-Liquid Extraction Systems" in *Liquid-Liquid Extraction Equipment*, Godfrey, J. C. and Slater, M. J.; Ed; John Wiley and Sons, Inc; Chapter 4, pp 45-94, (1994).

69. Sprow, F. B., "Distribution of drop sizes produced in turbulent liquid-liquid dispersion". *Chem. Eng. Sci.*, **22**, 435-442, (1967).

70. Stauffer, C. E., " The Measurement of Surface Tension by Pendant Drop Technique " *J. Phy. Chem.*, **69**, 1933, (1965).

71. Sternling, C.V. and Scriven, L. E., *AIChE.*, **5**, 514, (1959).

72. Takeuchi, H., Numata, Y., *International Chemical Engineering* (Japan), **17**, No. 3, 468-474, (1977).

73. Treybal R. E. *Liquid Extraction*; 2nd ed. McGraw-Hill Book Company Inc., NewYork, pp 414-416, (1963).

74. Verrall, M. S., "Liquid-Liquid Partition in the Pharmaceutical Industry" *in Science and Practice of Liquid-Liquid Extraction*; Thornton, J. D., Ed; Oxford University Press; **2**, Chapter 3. p194, (1992).

75. Vermeulen, Theore, G. M. Williams, and G. E. Longlois "Interfacial Area in Liquid-Liquid and Gas Liquid Agitation", *Chem. Eng. Progr.*, **51**, (1955).

76. Wang, C. Y. and Calabrese, R. V., " Drop Breakup in Turbulent Stirred-Tank Contactors": *AIChE* , **32**, No. 4, 667, (1986).

77. Ward, J. P.; Knudsen, J. G.; "Turbulent flow of unstable liquid-liquid dispersion: Drop sizes and velocity distributions". *AIChE.*, **13** (2), 356, (1967).

78. West, F. B., Herrman, A. J., Chong, A. T., and Thomas, L. E. K., *Ind. Eng Chem.*, **44**, 1621, (1952).

Constants for the calculation of the viscosity for the contraves Double-Gap measuring system.

Mess-System/Measuring System MS-0 — rm 30

D-τ-η - Tabelle, repräsentative Werte

D-τ-η - table, representative values

$D_{rep} = n \cdot 4{,}889\ [s^{-1}]$

$\frac{\tau_{rep}}{K_{rep}} = Ti \quad \frac{D_{rep}}{K_{rep}} = Di$

System No. : 2041

τ_{rep} % 58,24 mPa

K_{rep} = 0,9792

Die τ_{rep}% und η_{rep}% Werte sind gültig für den Drehmomentbereich 0-4,91 · 10^{-3} Nm (50 cmp)

τ_{rep}% and η_{rep}% values apply to the torquerange of 0-4,91 · 10^{-3} Nm (50cmp)

RM 30 Stufe/step	1	2	3	4	5	6	7	8	9	10
D_{rep} [s^{-1}]	0,233	0,316	0,430	0,584	0,794	1,080	1,467	1,995	2,71	3,69
η_{rep}% [mPa·s]	250	184,3	135,4	99,7	73,4	53,9	39,7	29,2	21,5	15,78
RM 30 Stufe/step	11	12	13	14	15	16	17	18	19	20
D_{rep} [s^{-1}]	5,01	6,81	9,26	12,56	17,11	23,3	31,6	43,0	58,4	79,4
η_{rep}% [mPa·s]	11,62	8,55	6,29	4,64	3,40	2,50	1,843	1,354	0,997	0,734
RM 30 Stufe/step	21	22	23	24	25	26	27	28	29	30
D_{rep} [s^{-1}]	108,0	146,7	199,5	271	369	501	681	926	1256	1711
η_{rep}% [mPa·s]	0,539	0,397	0,292	0,215	0,1578	0,1162	0,0855	0,0629	0,0464	0,0341

Datum 19.10.84 Visum Schr

CM 301 284-Z

Appendix 3

Density of water at various temperatures.(from Perry, 1994)

Temperature T_2 ($^{\circ}C$)	Density of water $\rho_{H_2O\,T_2}$ (g/ml)	Temperature T_2 ($^{\circ}C$)	Density of water $\rho_{H_2O\,T_2}$ (g/ml)	Temperature T_2 ($^{\circ}C$)	Density of water (g/ml)
15	0.99805	35	0.99298	55	0.98465
16	0.99789	36	0.99264	56	0.98416
17	0.99772	37	0.99228	57	0.98367
18	0.99754	38	0.99192	58	0.98317
19	0.99735	39	0.99155	59	0.98267
20	0.99715	40	0.99117	60	0.98217
21	0.99694	41	0.99079	61	0.98165
22	0.99672	42	0.99039	62	0.98113
23	0.99649	43	0.98999	63	0.98060
24	0.99624	44	0.98958	64	0.98006
25	0.99599	45	0.98917	65	0.97952
26	0.99573	46	0.98874		
27	0.99546	47	0.98832		
28	0.99518	48	0.98788		
29	0.99490	49	0.98744		
30	0.99460	50	0.98699		
31	0.99429	51	0.98654		
32	0.99398	52	0.98607		
33	0.99365	53	0.98561		
34	0.99332	54	0.98513		

Appendix 4

Values of S = *1/H*, for the range of S from 0.33 to 0.66 (C. E. Stauffer, *J Phys. Chem.*, **69**, 1933, 1965)

S	0	1	2	3	4	5	6	7	8	9
0.30	7.09837	7.03966	6.98161	6.92421	6.86746	6.81135	6.75586	6.70099	6.64672	6.59306
0.31	6.53998	6.48748	6.43556	6.38421	6.33341	6.28317	6.23347	6.18431	6.13567	6.08756
0.32	6.03997	5.99288	5.94629	5.90019	5.85459	5.80946	5.76481	5.72063	5.67690	5.22474
0.33	5.59082	5.54845	5.50651	5.46501	5.42393	5.38327	5.34303	5.30320	5.26377	5.22474
0.34	5.18611	5.14786	5.11000	5.07252	5.03542	4.99868	4.96231	4.92629	4.89061	4.85527
0.35	4.82029	4.78564	4.75134	4.71737	4.68374	4.65043	4.61745	4.58479	4.55245	4.52042
0.36	4.48870	4.45729	4.42617	4.39536	4.36484	4.33461	4.30467	4.27501	4.24564	4.21654
0.37	4.18771	4.15916	4.13087	4.1028.5	4.07509	4.04759	4.02034	3.99334	3.96660	3.94010
0.38	3.91384	3.88786	3.86212	3.83661	3.81133	3.78627	3.76143	3.73682	3.71242	3.69824
0.39	3.66427	3.64051	3.61696	3.59362	3.57047	3.54752	3.52478	3.50223	3.47987	3.45770
0.40	3.43572	3.41393	3.39232	3.37089	3.34965	3.328.58	3.30769	3.28698	3.26643	3.24606
0.41	3.22582	3.20576	3.18587	3.16614	3.14657	3.12717	3.10794	3.09886	3.06994	3.05118
0.42	3.03258	3.01413	2.99583	2.97769	2.95969	2.94184	2.92415	2.90659	2.88918	2.87192
0.43	2.85479	2.83781	2.82097	2.80426	2.78769	2,77125	2.75496	2.73880	2.72277	2.70687
0.44	2.69110	2.67545	2.65992	2.64452	2.62924	2.61408	2.59904	2.58412	2.56932	2.55463
0.45	2.54005	2.52559	2.51124	2.49700	2.48287	2.46885	2.45494	2.44114	2.42743	2.41384
0.46	2.40034	2.38695	2.37366	2.36047	2.34738	2.33439	2.32150	2.30870	2.29600	2.28339
0.47	2.27088	2.25846	2.24613	2.23390	2.22176	2.20970	2.19773	2.18586	2.17407	2.16236
0.48	2.15074	2.13921	2.12276	2.11640	2.10511	2.09391	2.08279	2.07175.	2.06079	2.04991
0.49	2.03910	2.02838	2.01473	2.00715	1.99666	1.98623	1.97588	1.96561	1.95540	1.94527
0.50	1.93521	1.92522	1.91530	1.90545	1.89567	1.88596	1.87632	1.86674	1.85723	1.84778
0.51	1.83840	1.82909	1.81984	1.81065	1.80153	1.79247	1.78347	1.77453	1.76565	1.75683
0.52	1.74808	1.73938	1.73074	1.72216	1.71364	1.70517	1.69676	1.68841	1.68012	1.67188
0.53	1.66369	1.65556	1.64748	1.63946	1.63149	1.62357	1.61571	1.60790	1.60014	1.59242
0.54	1.58477	1.57716	1.56960	1.56209	1.55462	1.54721	1.53985	1.53253	1.52526	1.51804
0.55	1.51086	1.50373	1.49665	1.48961	1.48262	1.47567	1.46876	1.46190	1.45509	1.44831
0.56	1.44158	1.43489	1.42825	1.42164	1.41508	1.40856	1.40208	1.39564	1.38924	1.38288
0.57	1.37656	1.37028	1.36404	1.35784	1.35168	1.34555	1.33946	1.33341	1.32740	1.32142
0.58	1.31549	1.30958	1.30372	1.29788	1.29209	1.28633	1.28060	1.27491	1.26926	1.26364
0.59	1.25805	1.25250	1.24698	1.24149	1.23603	1.23061	1.22522	1.21987	1.21454	1.20925
0.60	1.20399	1.19875	1.19356	1.18839	1.18325	1.17814	1.17306	1.16801	1.16300	1.15801
0.61	1.15305	1.14812	1.14322	1.13834	1.13350	1.12868	1.23389	1.11913	1.11440	1.10969
0.62	1.10501	1.10036	1.09574	1.09114	1.08656	1.08202	1.07750	1.07300	1.06853	1.06409
0.63	1.05967	1.05528	1.05091	1.04657	1.04225	1.03796	1.03368	1.02944	1.02522	1.02102
0.64	1.01684	1.01269	1.00856	1.00446	1.00037	0.99631	0.99227	0.98826	0.98427	0.98029
0.65	0.97635	0.97242	0.96851	0.96463	0.96077	0.95692	0.95310	0.94930	0.94552	0.94176
0.66	0.93803	0.93431	0.93061	0.92693	0.92327	0.91964	0.91602	0.91242	0.90884	0.90528

Appendix 5

Value of S = *1/H*, for the range of S from 0.66 to 1 (S. Fordham, *Proc. Roy. Soc.* (London), **194**, **1**, 1948)

S	0	1	2	3	4	5	6	7	8	9
0.66	0.93828	0.93454	0.93082	0.92712	0.92345	0.91979	0.91616	0.91255	0.90895	0.90538
0.67	0.90183	0.89830	0.89478	0.89129	0.88782	0.88436	0.88092	0.87751	0.87411	0.87073
0.68	0.86737	0.86403	0.86070	0.85739	0.85410	0.85083	0.84758	0.84434	0.84112	0.83792
0.69	0.83473	0.83156	0.82841	0.82527	0.82215	0.81905	0.81596	0.81289	0.80983	0.80679
0.70	0.80376	0.80075	0.79776	0.79478	0.79182	0.78887	0.78594	0.78302	0.78011	0.77722
0.71	0.77435	0.77149	0.76864	0.76581	0.76300	0.76019	0.75741	0.75463	0.75187	0.74912
0.72	0.74639	0.74367	0.74097	0.73828	0.73560	0.73293	0.73028	0.72764	0.72502	0.72240
0.73	0.71980	0.71722	0.71464	0.71208	0.70953	0.70700	0.70447	0.70196	0.69946	0.69697
0.74	0.69449	0.69202	0.68957	0.68713	0.68470	0.68228	0.67988	0.67748	0.67510	0.67273
0.75	0.67037	0.66803	0.66569	0.66337	0.66105	0.65875	0.65646	0.65418	0.65191	0.64965
0.76	0.64740	0.64516	0.64294	0.64072	0.63851	0.63632	0.63413	0.63195	0.62979	0.62763
0.77	0.62549	0.62335	0.62122	0.61911	0.61700	0.61490	0.61281	0.61074	0.60867	0.60661
0.78	0.60457	0.60253	0.60050	0.59848	0.59647	0.59447	0.59248	0.59049	0.58852	0.58656
0.79	0.58460	0.58265	0.58072	0.57879	0.57687	0.57496	0.57305	0.57116	0.56927	0.56739
0.80	0.56553	0.56366	0.56181	0.55997	0.55813	0.55630	0.55448	0.55266	0.55086	0.54906
0.81	0.54727	0.54549	0.54371	0.54195	0.54019	0.53844	0.53669	0.53496	0.53323	0.53151
0.82	0.52979	0.52808	0.52638	0.52469	0.52300	0.52132	0.51965	0.51799	0.51634	0.51469
0.83	0.51305	0.51142	0.50979	0.50817	0.50656	0.50496	0.50336	0.50176	0.50018	0.49860
0.84	0.49703	0.49546	0.49390	0.49234	0.49090	0.48926	0.48772	0.48619	0.48467	0.48316
0.85	0.48165	0.48015	0.47865	0.47716	0.47567	0.47420	0.47272	0.47126	0.46980	0.46834
0.86	0.46690	0.46545	0.46402	0.46259	0.46116	0.45974	0.45833	0.45692	0.45552	0.45412
0.87	0.45273	0.45134	0.44996	0.44858	0.44721	0.44584	0.44448	0.44313	0.44178	0.44044
0.88	0.43910	0.43777	0.43644	0.43512	0.43380	0.43249	0.43118	0.42988	0.42858	0.42729
0.89	0.42600	0.42471	0.42344	0.42216	0.42089	0.41963	0.41837	0.41712	0.41587	0.41462
0.90	0.41338	0.41214	0.41091	0.40968	0.40846	0.40724	0.40602	0.40481	0.40360	0.40240
0.91	0.40121	0.40001	0.39882	0.39764	0.39646	0.39528	0.39411	0.39294	0.39177	0.39061
0.92	0.38946	0.38831	0.38716	0.38601	0.38487	0.38374	0.38260	0.38147	0.38035	0.37922
0.93	0.37810	0.37699	0.37588	0.37477	0.37366	0.37256	0.37146	0.37037	0.36928	0.36819
0.94	0.36711	0.36602	0.36494	0.36387	0.36280	0.36173	0.36066	0.35960	0.35854	0.35748
0.95	0.35643	0.35538	0.35433	0.35328	0.35224	0.35120	0.35016	0.34913	0.34809	0.34700
0.96	0.34604	0.34501	0.34399	0.34297	0.34195	0.34093	0.33992	0.33890	0.33789	0.33688
0.97	0.33588	0.33487	0.33387	0.33287	0.33186	0.33086	0.32987	0.32887	0.32787	0.32688
0.98	0.32588	0.32489	0.32389	0.32290	0.32191	0.32092	0.31992	0.31893	0.31794	0.31695
0.99	0.21595	0.31496	0.31396	0.31296	0.31196	0.31095	0.30994	0.30893	0.30792	0.30690
1.00	0.30580	0.30484	0.30381	0.30276	-	-	-	-	-	-

Appendix 6

Drop size distributions for various phase compositions, volume fractions and agitation speed.

20% w/w and 0.03% v/v

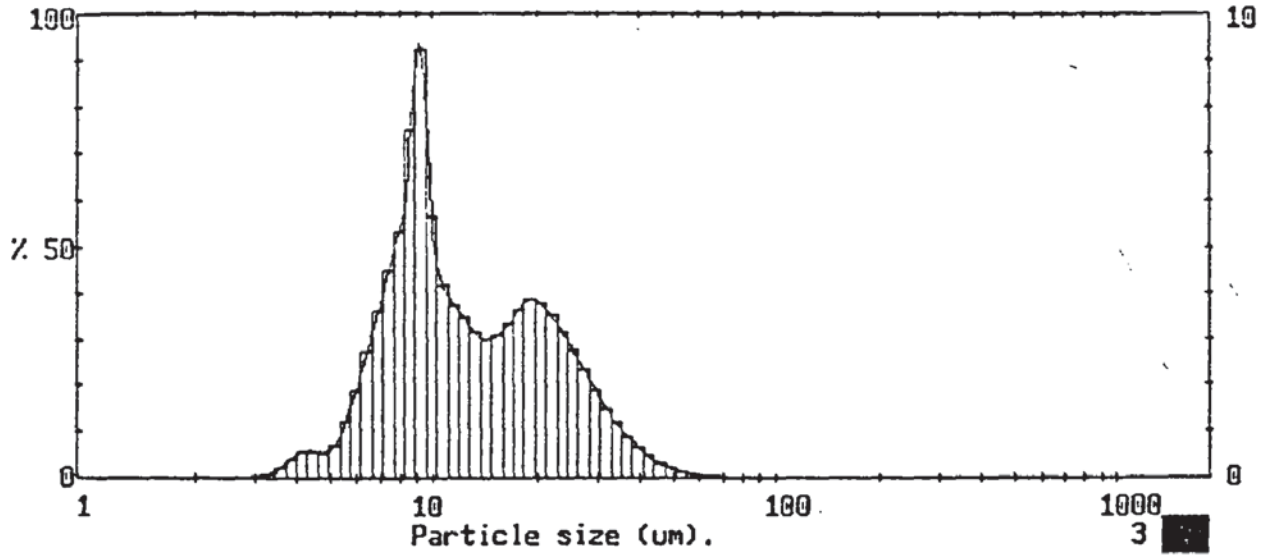

1598 pil 1DR459 / 0/ 0/0.00/1.00/
20% W/W salt Soln
500 rpm

000000396

MALVERN Series 2600 SB.20 Master Mode 02 Mar 1998 6:31 pm

High Size	Under %	High Size	Under %	High Size	Under %	High Size	Under %	High Size	Under %	High Size	Under %	Span 1.76
188	100	84.5	99.9	38.0	97.8	17.1	69.1	7.69	17.3	3.46	0.2	D[4,3] 14.72µm
175	100	78.6	99.8	35.4	96.9	15.9	65.7	7.15	12.7	3.21	0.1	
163	100	73.1	99.8	32.9	95.7	14.8	62.7	6.65	9.1	2.99	0.0	D[3,2] 10.94µm
151	100	68.0	99.8	30.6	94.2	13.7	59.6	6.18	6.4	2.78	0.0	
141	100	63.2	99.8	28.4	92.3	12.8	56.5	5.75	4.5	2.59	0.0	
131	99.9	58.8	99.7	26.4	89.9	11.9	53.0	5.35	3.2	2.40	0.0	D[v,0.9] 26.48µm
122	99.9	54.7	99.6	24.6	87.2	11.1	49.2	4.97	2.5	2.24	0.0	
113	99.9	50.8	99.5	22.9	84.0	10.3	45.0	4.62	2.0	2.08	0.0	
105	99.9	47.3	99.3	21.3	80.5	9.56	39.4	4.30	1.4	1.93	0.0	D[v,0.1] 6.78µm
97.8	99.9	44.0	98.9	19.8	76.7	8.89	30.1	4.00	0.8			
90.9	99.9	40.9	98.5	18.4	72.8	8.27	22.6	3.72	0.4			

Source = Data:p20v003	Beam length = 14.3 mm	Model indp	D[v,0.5] 11.22µm
Record No. = 8	Log. Diff. = 4.978		
Focal length = 100 mm	Obscuration = 0.0168	Volume Conc. = 0.0004%	Shape OFF
Presentation = pil	Volume distribution	Sp.S.A 0.5486 m²/cc.	

1598 pil 1DR459 / 0/ 0/0.00/1.00/
20% W/W salt Soln
500 rpm

000000396

MALVERN Series 2600 SB.20 Master Mode 02 Mar 1998 6:31 pm

Particle diameters		Volume percentiles	
D(4,3)	14.72 µm	D[v,.10]	6.78
D(4,2)	12.69 µm	D[v,.20]	7.99
D(4,1)	11.17 µm	D[v,.30]	8.88
D(4,0)	10.00 µm	D[v,.40]	9.62
		D[v,.50]	11.22
D(3,2)	10.94 µm	D[v,.60]	13.87
D(3,1)	9.73 µm	D[v,.70]	17.41
D(3,0)	8.80 µm	D[v,.80]	21.07
		D[v,.90]	26.48
D(2,1)	8.66 µm	D[v,.99]	44.42
D(2,0)	7.89 µm		
		Span	1.76
D(1,0)	7.19 µm	Unif.	0.58

Distribution Moments.			
Distbn	Mean	Stan.Dev.	Skewness
Volume	14.72	9.76	3.79
Surface	10.94	6.43	2.81
Length	8.66	4.44	2.65
Number	7.19	3.26	2.35

Source =Data:p20v003
Record 8

1598 pil 1DR459 / 0/ 0/0.00/1.00/
20% W/W salt Soln
500 rpm

000000396

20% w/w and 0.04% v/v

MALVERN Series 2600 SB.20 Master Mode 02 Mar 1998 7:21 pm

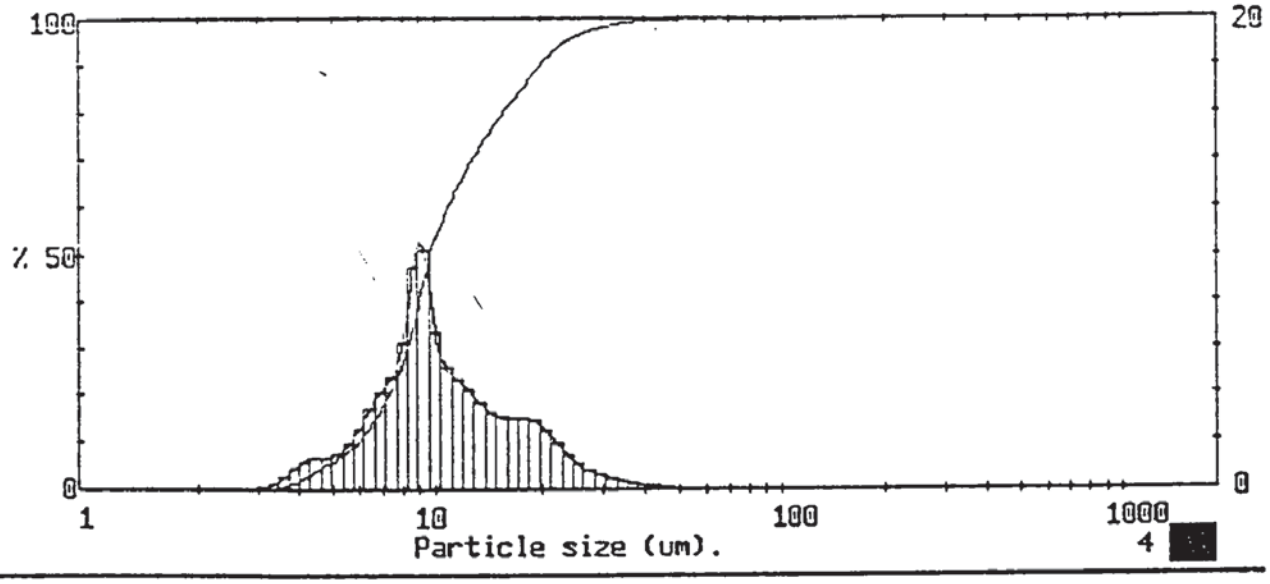

1598 pil 1DR459 / 0/ 0/0.00/1.00/
20% W/W salt Soln
500 rpm

000000256

MALVERN Series 2600 SB.20 Master Mode 02 Mar 1998 7:21 pm

High Size	Under %	High Size	Under %	High Size	Under %	High Size	Under %	High Size	Under %	High Size	Under %	Span 1.45
188	100	84.5	100	38.0	99.4	17.1	84.1	7.69	24.0	3.46	0.3	D[4,3] 11.58µm
175	100	78.6	100	35.4	99.2	15.9	81.1	7.15	19.3	3.21	0.1	
163	100	73.1	100	32.9	98.8	14:8	78.0	6.65	15.1	2.99	0.1	
151	100	68.0	100	30.6	98.3	13.7	74.8	6.18	11.7	2.78	0.0	D[3,2] 9.28µm
141	100	63.2	100	28.4	97.7	12.8	71.0	5.75	9.1	2.59	0.0	
131	100	58.8	99.9	26.4	97.0	11.9	66.8	5.35	7.1	2.40	0.0	
122	100	54.7	99.9	24.6	95.9	11.1	62.1	4.97	5.6	2.24	0.0	D[v,0.9] 19.76µm
113	100	50.8	99.9	22.9	94.5	10.3	56.9	4.62	4.3	2.08	0.0	
105	100	47.3	99.9	21.3	92.5	9.56	50.2	4.30	2.9	1.93	0.0	
97.8	100	44.0	99.8	19.8	90.0	8.89	39.9	4.00	1.7			D[v,0.1] 5.92µm
90.9	100	40.9	99.6	18.4	87.1	8.27	30.3	3.72	0.9			

Source = Data:p20v004	Beam length = 14.3 mm	Model indp	D[v,0.5] 9.54µm
Record No. = 8	Log. Diff. = 4.906		
Focal length = 100 mm	Obscuration = 0.0380	Volume Conc. = 0.0008%	
Presentation = pil	Volume distribution	Sp.S.A 0.6468 m²/cc.	Shape OFF

1598 pil 1DR459 / 0/ 0/0.00/1.00/
20% W/W salt Soln
500 rpm

000000256

MALVERN Series 2600 SB.20 Master Mode 02 Mar 1998 7:21 pm

Particle diameters		Volume percentiles	
D(4,3)	11.58 µm	D[v,.10]	5.92
D(4,2)	10.36 µm	D[v,.20]	7.23
D(4,1)	9.37 µm	D[v,.30]	8.24
D(4,0)	8.53 µm	D[v,.40]	8.90
		D[v,.50]	9.54
D(3,2)	9.28 µm	D[v,.60]	10.72
D(3,1)	8.43 µm	D[v,.70]	12.55
D(3,0)	7.71 µm	D[v,.80]	15.48
		D[v,.90]	19.76
D(2,1)	7.66 µm	D[v,.99]	34.06
D(2,0)	7.03 µm		
		Span	1.45
D(1,0)	6.45 µm	Unif.	0.44

Distribution Moments.

Distbn	Mean	Stan.Dev.	Skewness
Volume	11.58	6.31	2.24
Surface	9.28	4.62	2.22
Length	7.66	3.52	2.04
Number	6.45	2.79	1.80

Source =Data:p20v004
Record 8

1598 pil 1DR459 / 0/ 0/0.00/1.00/
20% W/W salt Soln
500 rpm

000000256

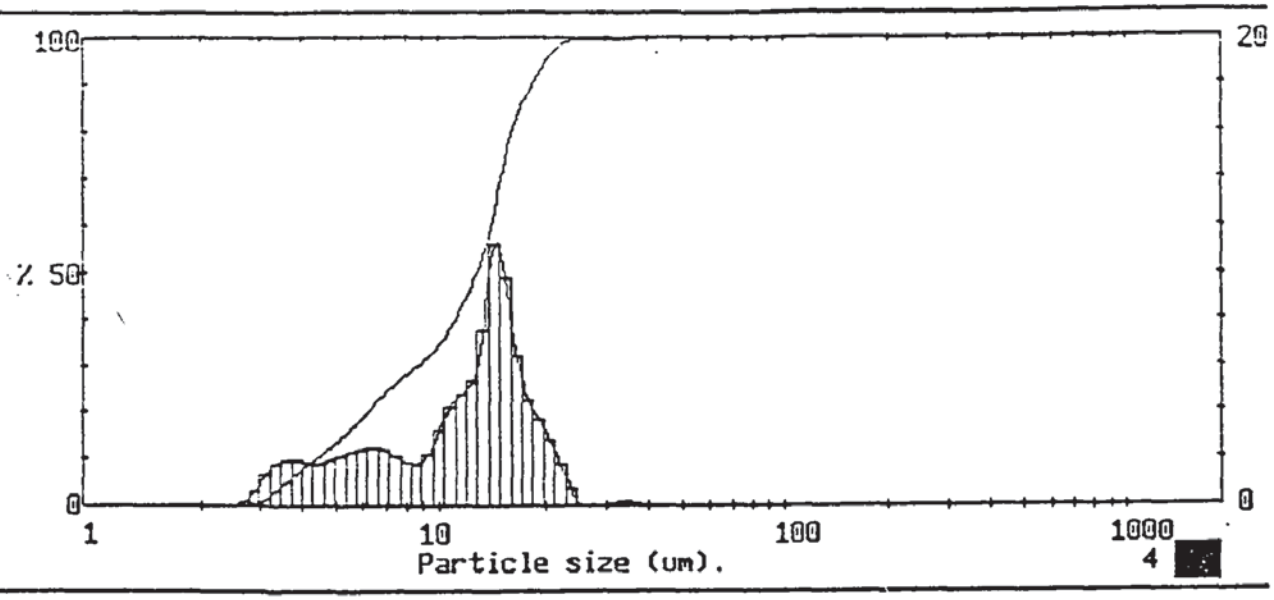

1598 pil 1DR459 / 0/ 0/0.00/1.00/
20% W/W salt Soln
600 rpm

000000257

MALVERN Series 2600 SB.20 Master Mode 02 Mar 1998 7:48 pm

High Size	Under %	High Size	Under %	High Size	Under %	High Size	Under %	High Size	Under %	High Size	Under %	Span 1.09
188	100	84.5	100	38.0	99.9	17.1	86.0	7.69	27.3	3.46	3.9	D[4,3] 11.88µm
175	100	78.6	100	35.4	99.8	15.9	79.6	7.15	25.1	3.21	2.1	
163	100	73.1	100	32.9	99.7	14.8	69.7	6.65	22.7	2.99	0.8	
151	100	68.0	100	30.6	99.6	13.7	58.5	6.18	20.2	2.78	0.2	D[3,2] 8.94µm
141	100	63.2	100	28.4	99.6	12.8	50.8	5.75	17.8	2.59	0.0	
131	100	58.8	100	26.4	99.6	11.9	45.4	5.35	15.5	2.40	0.0	
122	100	54.7	100	24.6	99.6	11.1	40.6	4.97	13.4	2.24	0.0	D[v,0.9] 18.20µm
113	100	50.8	100	22.9	98.9	10.3	36.4	4.62	11.4	2.08	0.0	
105	100	47.3	100	21.3	97.1	9.56	33.1	4.30	9.6	1.93	0.0	
97.8	100	44.0	99.9	19.8	94.3	8.89	30.9	4.00	7.8			D[v,0.1] 4.37µm
90.9	100	40.9	99.9	18.4	90.6	8.27	29.2	3.72	5.9			

Source = Data:p20v004	Beam length = 14.3 mm	Model indp	D[v,0.5] 12.65µm
Record No. = 10	Log. Diff. = 4.891		
Focal length = 100 mm	Obscuration = 0.6745	Volume Conc. = 0.0234%	Shape OFF
Presentation = pil	Volume distribution	Sp.S.A 0.6712 m²/cc.	

1598 pil 1DR459 / 0/ 0/0.00/1.00/
20% W/W salt Soln
600 rpm

000000257

MALVERN Series 2600 SB.20 Master Mode 02 Mar 1998 7:48 pm

Particle diameters		Volume percentiles	
D(4,3)	11.88 µm	D[v,.10]	4.37
D(4,2)	10.30 µm	D[v,.20]	6.14
D(4,1)	8.76 µm	D[v,.30]	8.56
D(4,0)	7.53 µm	D[v,.40]	10.94
		D[v,.50]	12.65
D(3,2)	8.94 µm	D[v,.60]	13.89
D(3,1)	7.53 µm	D[v,.70]	14.81
D(3,0)	6.47 µm	D[v,.80]	15.97
		D[v,.90]	18.20
D(2,1)	6.34 µm	D[v,.99]	22.98
D(2,0)	5.50 µm		
		Span	1.09
D(1,0)	4.77 µm	Unif.	0.34

Distribution Moments.

Distbn	Mean	Stan.Dev.	Skewness
Volume	11.88	5.36	0.61
Surface	8.94	5.13	0.74
Length	6.34	4.06	1.57
Number	4.77	2.73	2.67

Source =Data:p20v004
Record 10

1598 pil 1DR459 / 0/ 0/0.00/1.00/
20% W/W salt Soln
600 rpm

000000257

20% w/w and 0.05% v/v

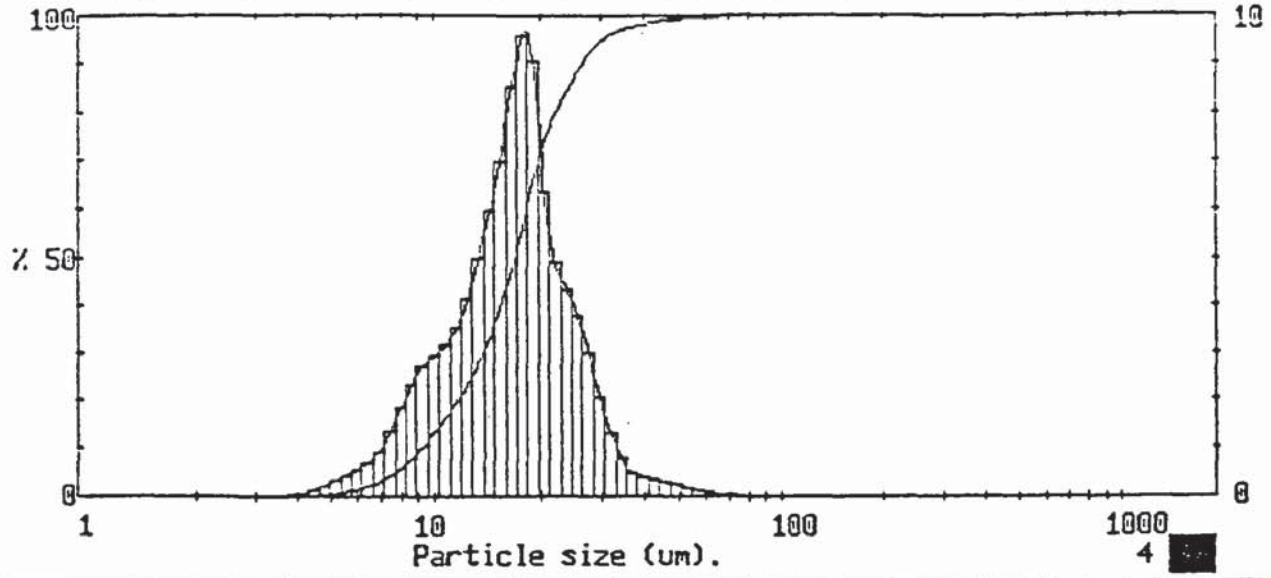

1598 pil 1DR459 / 0/ 0/0.00/1.00/
20% W/W salt Soln
300 rpm

000000258

MALVERN Series 2600 SB.20 Master Mode 03 Mar 1998 12:15 pm

High Size	Under %	High Size	Under %	High Size	Under %	High Size	Under %	High Size	Under %	High Size	Under %	Span 1.02
188	100	84.5	100	38.0	98.1	17.1	52.2	7.69	4.9	3.46	0.0	D[4,3] 17.55µm
175	100	78.6	100	35.4	97.6	15.9	43.7	7.15	3.5	3.21	0.0	
163	100	73.1	99.9	32.9	96.8	14.8	36.7	6.65	2.5	2.99	0.0	
151	100	68.0	99.9	30.6	95.5	13.7	30.7	6.18	1.8	2.78	0.0	D[3,2] 14.71µm
141	100	63.2	99.9	28.4	93.4	12.8	25.7	5.75	1.3	2.59	0.0	
131	100	58.8	99.8	26.4	90.4	11.9	21.5	5.35	0.8	2.40	0.0	
122	100	54.7	99.6	24.6	86.6	11.1	18.0	4.97	0.5	2.24	0.0	D[v,0.9] 26.22µm
113	100	50.8	99.5	22.9	82.2	10.3	14.8	4.62	0.3	2.08	0.0	
105	100	47.3	99.2	21.3	77.3	9.56	11.9	4.30	0.1	1.93	0.0	
97.8	100	44.0	98.9	19.8	70.9	8.89	9.1	4.00	0.1			D[v,0.1] 9.11µm
90.9	100	40.9	98.5	18.4	61.8	8.27	6.7	3.72	0.0			

Source = Data:p20v005	Beam length = 14.3 mm	Model indp	D[v,0.5] 16.79µm
Record No. = 1	Log. Diff. = 4.992		
Focal length = 100 mm	Obscuration = 0.1130	Volume Conc. = 0.0041%	Shape OFF
Presentation = pil	Volume distribution	Sp.S.A 0.4079 m²/cc.	

1598 pil 1DR459 / 0/ 0/0.00/1.00/
20% W/W salt Soln
300 rpm

000000258

MALVERN Series 2600 SB.20 Master Mode 03 Mar 1998 12:15 pm

Particle diameters		Volume percentiles	
D(4,3)	17.55 µm	D[v,.10]	9.11
D(4,2)	16.07 µm	D[v,.20]	11.53
D(4,1)	14.62 µm	D[v,.30]	13.62
D(4,0)	13.23 µm	D[v,.40]	15.33
		D[v,.50]	16.79
D(3,2)	14.71 µm	D[v,.60]	18.14
D(3,1)	13.35 µm	D[v,.70]	19.61
D(3,0)	12.04 µm	D[v,.80]	22.09
		D[v,.90]	26.22
D(2,1)	12.11 µm	D[v,.99]	44.92
D(2,0)	10.89 µm		
		Span	1.02
D(1,0)	9.80 µm	Unif.	0.32

Distribution Moments.			
Distbn	Mean	Stan.Dev.	Skewness
Volume	17.55	7.76	2.47
Surface	14.71	6.46	1.45
Length	12.11	5.61	1.17
Number	9.80	4.75	1.30

Source =Data:p20v005
Record 1

1598 pil 1DR459 / 0/ 0/0.00/1.00/
20% W/W salt Soln
300 rpm

000000258

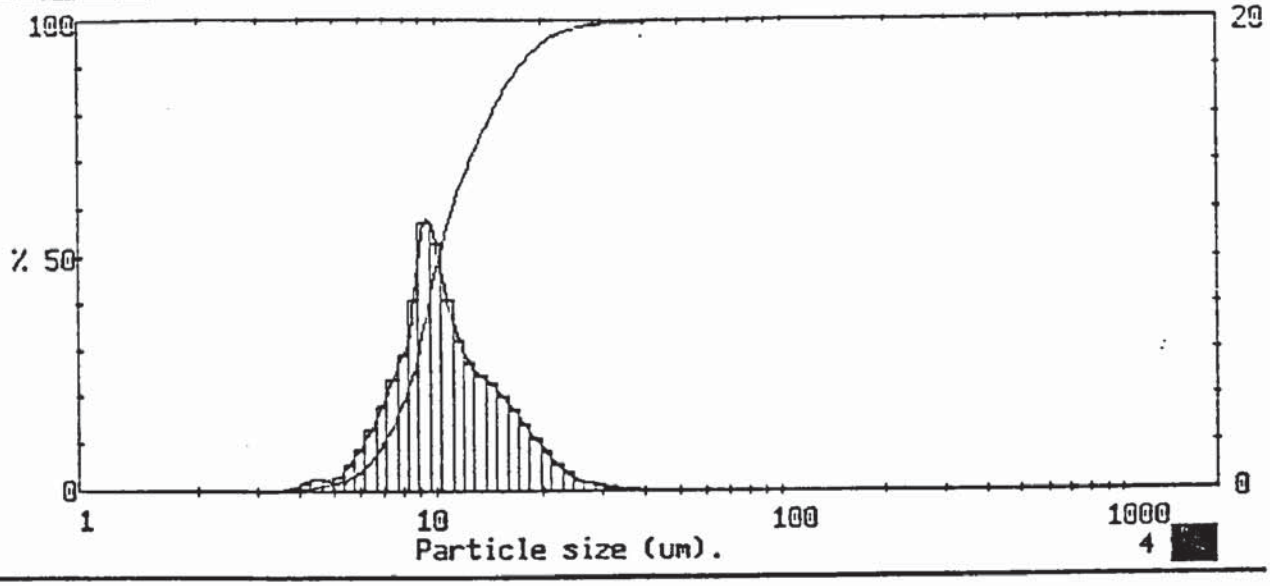

1598 pil 1DR459 / 0/ 0/0.00/1.00/
20% W/W salt Soln
500 rpm

000000259

MALVERN Series 2600 SB.20 Master Mode 03 Mar 1998 2:07 pm

High Size	Under %	High Size	Under %	High Size	Under %	High Size	Under %	High Size	Under %	High Size	Under %	Span 1.01
188	100	84.5	100	38.0	99.9	17.1	89.8	7.69	16.2	3.46	0.0	D[4,3] 11.33µm
175	100	78.6	100	35.4	99.8	15.9	86.3	7.15	11.4	3.21	0.0	
163	100	73.1	100	32.9	99.7	14.8	82.2	6.65	7.8	2.99	0.0	
151	100	68 0	100	30.6	99.5	13.7	77.7	6.18	5.2	2.78	0.0	D[3,2] 9.94µm
141	100	63.2	100	28.4	99.3	12.8	72.7	5.75	3.4	2.59	0.0	
131	100	58.8	100	26.4	98.9	11.9	67.2	5.35	2.3	2.40	0.0	
122	100	54.7	100	24.6	98.5	11.1	60.7	4.97	1.6	2.24	0.0	D[v,0.9] 17.17µm
113	100	50.8	100	22.9	97.7	10.3	52.5	4.62	1.1	2.08	0.0	
105	100	47.3	99.9	21.3	96.5	9.56	41.9	4.30	0.6	1.93	0.0	
97.8	100	44.0	99.9	19.8	94.9	8.89	30.3	4.00	0.2			D[v,0.1] 6.96µm
90.9	100	40.9	99.9	18.4	92.7	8.27	22.1	3.72	0.1			

Source = Data:p20v005	Beam length = 14.3 mm	Model indp	D[v,0.5] 10.09µm
Record No. = 4	Log. Diff. = 5.230		
Focal length = 100 mm	Obscuration = 0.4010	Volume Conc. = 0.0119%	Shape OFF
Presentation = pil	Volume distribution	Sp.S.A 0.6035 m²/cc.	

1598 pil 1DR459 / 0/ 0/0.00/1.00/
20% W/W salt Soln
500 rpm

000000259

MALVERN Series 2600 SB.20 Master Mode 03 Mar 1998 2:07 pm

Particle diameters		Volume percentiles	
D(4,3)	11.33 µm	D[v,.10]	6.96
D(4,2)	10.61 µm	D[v,.20]	8.07
D(4,1)	9.98 µm	D[v,.30]	8.87
D(4,0)	9.41 µm	D[v,.40]	9.45
		D[v,.50]	10.09
D(3,2)	9.94 µm	D[v,.60]	10.97
D(3,1)	9.37 µm	D[v,.70]	12.32
D(3,0)	8.85 µm	D[v,.80]	14.25
		D[v,.90]	17.17
D(2,1)	8.83 µm	D[v,.99]	26.71
D(2,0)	8.35 µm		
		Span	1.01
D(1,0)	7.88 µm	Unif.	0.32

Distbn	Mean	Stan.Dev.	Skewness
Volume	11.33	4.59	2.18
Surface	9.94	3.71	1.80
Length	8.83	3.13	1.50
Number	7.88	2.74	1.23

Source =Data:p20v005
Record 4

1598 pil 1DR459 / 0/ 0/0.00/1.00/
20% W/W salt Soln
500 rpm

000000259

20% w/w and 0.06% v/v

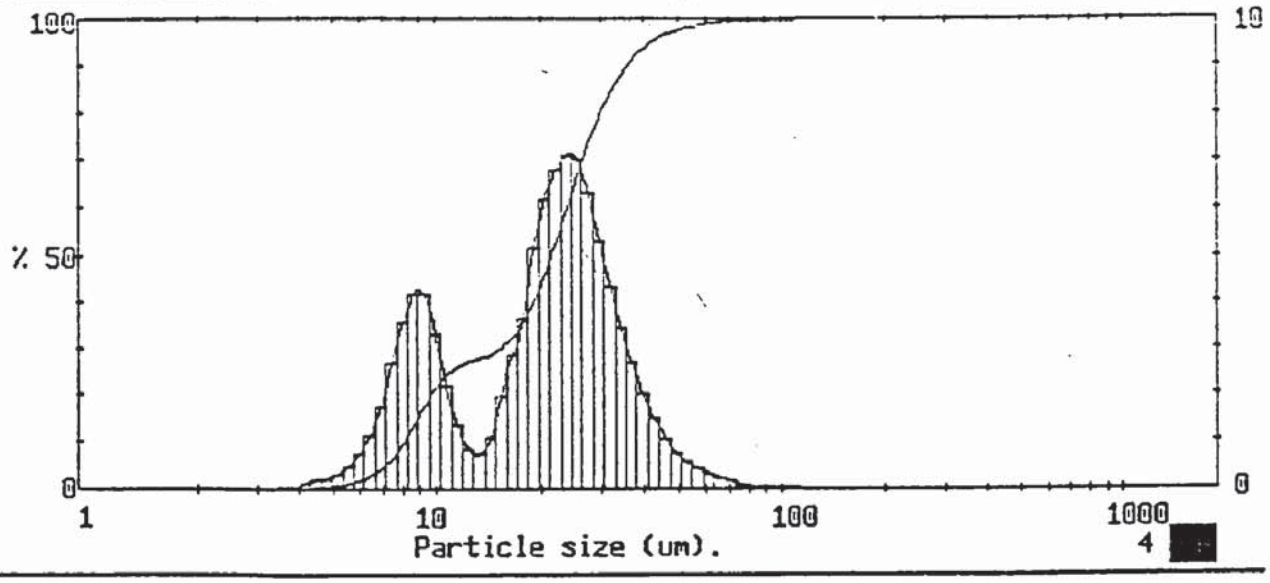

1598 pil 1DR459 / 0/ 0/0.00/1.00/
20% W/W salt Soln
300 rpm

000000260

MALVERN Series 2600 SB.20 Master Mode 05 Mar 1998 12:32 pm

High Size	Under %	High Size	Under %	High Size	Under %	High Size	Under %	High Size	Under %	High Size	Under %	Span 1.28
188	100	84.5	99.8	38.0	92.5	17.1	34.3	7.69	7.9	3.46	0.0	D[4,3] 21.88µm
175	100	78.6	99.7	35.4	89.8	15.9	31.4	7.15	5.2	3.21	0.0	
163	100	73.1	99.6	32.9	86.4	14.8	29.4	6.65	3.4	2.99	0.0	D[3,2] 15.75µm
151	100	68.0	99.4	30.6	82.0	13.7	28.3	6.18	2.2	2.78	0.0	
141	100	63.2	99.2	28.4	76.7	12.8	27.6	5.75	1.5	2.59	0.0	
131	99.9	58.8	98.9	26.4	70.3	11.9	26.7	5.35	1.0	2.40	0.0	D[v,0.9] 35.51µm
122	99.9	54.7	98.5	24.6	63.3	11.1	25.4	4.97	0.7	2.24	0.0	
113	99.9	50.8	97.9	22.9	56.2	10.3	23.1	4.62	0.4	2.08	0.0	
105	99.9	47.3	97.1	21.3	49.4	9.56	19.8	4.30	0.2	1.93	0.0	D[v,0.1] 8.05µm
97.8	99.9	44.0	96.0	19.8	43.2	8.89	15.6	4.00	0.1			
90.9	99.8	40.9	94.5	18.4	38.0	8.27	11.4	3.72	0.0			

Source = Data:p20v006	Beam length = 14.3 mm	Model indp	D[v,0.5] 21.41µm
Record No. = 16	Log. Diff. = 5.618		
Focal length = 100 mm	Obscuration = 0.4387	Volume Conc. = 0.0212%	
Presentation = pil	Volume distribution	Sp.S.A 0.3803 m²/cc.	Shape OFF

1598 pil 1DR459 / 0/ 0/0.00/1.00/
20% W/W salt Soln
300 rpm

000000260

MALVERN Series 2600 SB.20 Master Mode 05 Mar 1998 12:32 pm

Particle diameters		Volume percentiles	
D(4,3)	21.88 µm	D[v,.10]	8.05
D(4,2)	18.57 µm	D[v,.20]	9.59
D(4,1)	15.69 µm	D[v,.30]	15.17
D(4,0)	13.50 µm	D[v,.40]	18.96
		D[v,.50]	21.41
D(3,2)	15.75 µm	D[v,.60]	23.77
D(3,1)	13.29 µm	D[v,.70]	26.34
D(3,0)	11.50 µm	D[v,.80]	29.70
		D[v,.90]	35.51
D(2,1)	11.21 µm	D[v,.99]	60.30
D(2,0)	9.82 µm		
		Span	1.28
D(1,0)	8.61 µm	Unif.	0.42

Distribution Moments.

Distbn	Mean	Stan.Dev.	Skewness
Volume	21.88	12.28	2.01
Surface	15.75	9.83	1.53
Length	11.21	7.14	2.04
Number	8.61	4.73	2.87

Source =Data:p20v006
Record 16

1598 pil 1DR459 / 0/ 0/0.00/1.00/
20% W/W salt Soln
300 rpm

000000260

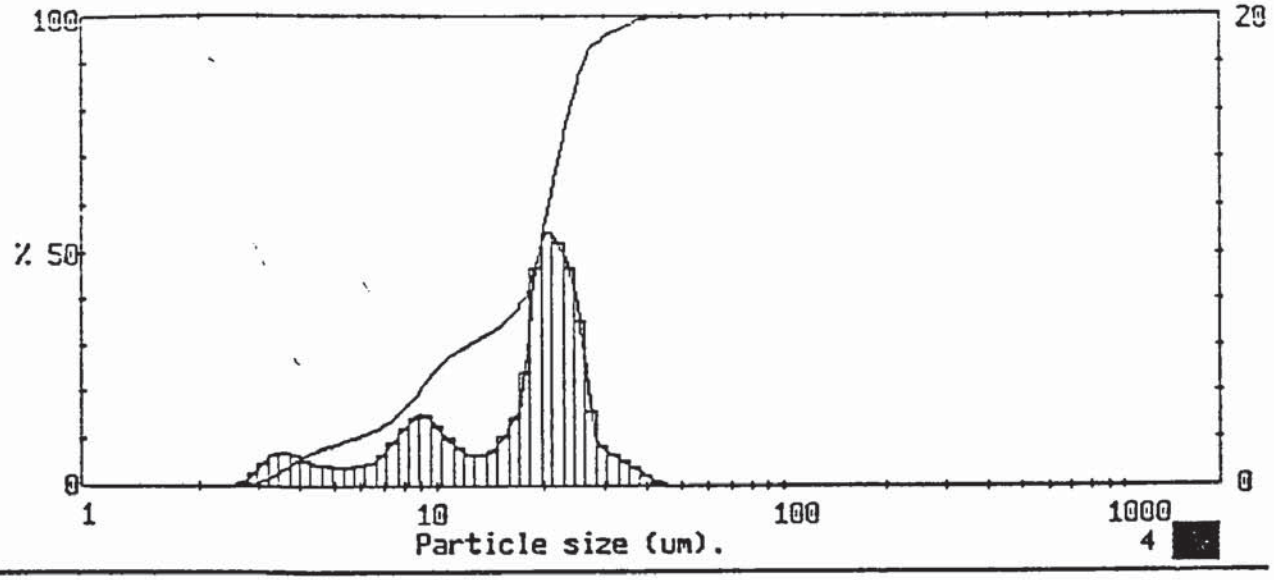

1598 pil 1DR459 / 0/ 0/0.00/1.00/
20% W/W salt Soln
400 rpm

000000261

MALVERN Series 2600 SB.20 Master Mode 04 Mar 1998 11:23 am

High Size	Under %	High Size	Under %	High Size	Under %	High Size	Under %	High Size	Under %	High Size	Under %	Span 1.06
188	100	84.5	100	38.0	99.2	17.1	39.1	7.69	15.3	3.46	3.0	D[4,3] 17.52µm
175	100	78.6	100	35.4	98.4	15.9	36.2	7.15	13.4	3.21	1.7	
163	100	73.1	100	32.9	97.3	14.8	34.1	6.65	12.1	2.99	0.6	
151	100	68.0	99.9	30.6	96.0	13.7	32.6	6.18	11.1	2.78	0.2	D[3,2] 12.00µm
141	100	63.2	99.9	28.4	94.3	12.8	31.3	5.75	10.3	2.59	0.0	
131	100	58.8	99.9	26.4	91.2	11.9	29.9	5.35	9.4	2.40	0.0	
122	100	54.7	99.9	24.6	84.1	11.1	28.3	4.97	8.6	2.24	0.0	D[v,0.9] 26.04µm
113	100	50.8	99.9	22.9	74.7	10.3	26.3	4.62	7.8	2.08	0.0	
105	100	47.3	99.9	21.3	64.3	9.56	23.7	4.30	6.9	1.93	0.0	
97.8	100	44.0	99.8	19.8	53.4	8.89	20.7	4.00	5.8			D[v,0.1] 5.62µm
90.9	100	40.9	99.6	18.4	44.0	8.27	17.7	3.72	4.4			

Source = Data:p20v006	Beam length = 14.3 mm	Model indp	D[v,0.5] 19.30µm
Record No. = 2	Log. Diff. = 5.286		
Focal length = 100 mm	Obscuration = 0.8456	Volume Conc. = 0.0523%	Shape OFF
Presentation = pil	Volume distribution	Sp.S.A 0.4998 m²/cc.	

1598 pil 1DR459 / 0/ 0/0.00/1.00/
20% W/W salt Soln
400 rpm

000000261

MALVERN Series 2600 SB.20 Master Mode 04 Mar 1998 11:23 am

Particle diameters		Volume percentiles	
D(4,3)	17.52 µm	D[v,.10]	5.62
D(4,2)	14.50 µm	D[v,.20]	8.75
D(4,1)	11.46 µm	D[v,.30]	11.94
D(4,0)	9.20 µm	D[v,.40]	17.43
		D[v,.50]	19.30
D(3,2)	12.00 µm	D[v,.60]	20.66
D(3,1)	9.26 µm	D[v,.70]	22.10
D(3,0)	7.43 µm	D[v,.80]	23.78
		D[v,.90]	26.04
D(2,1)	7.15 µm	D[v,.99]	37.32
D(2,0)	5.84 µm		
		Span	1.06
D(1,0)	4.77 µm	Unif.	0.34

Distribution Moments.			
Distbn	Mean	Stan.Dev.	Skewness
Volume	17.52	8.26	0.30
Surface	12.00	8.14	0.72
Length	7.15	5.89	1.93
Number	4.77	3.37	3.63

Source =Data:p20v006
Record 2

1598 pil 1DR459 / 0/ 0/0.00/1.00/
20% W/W salt Soln
400 rpm

000000261

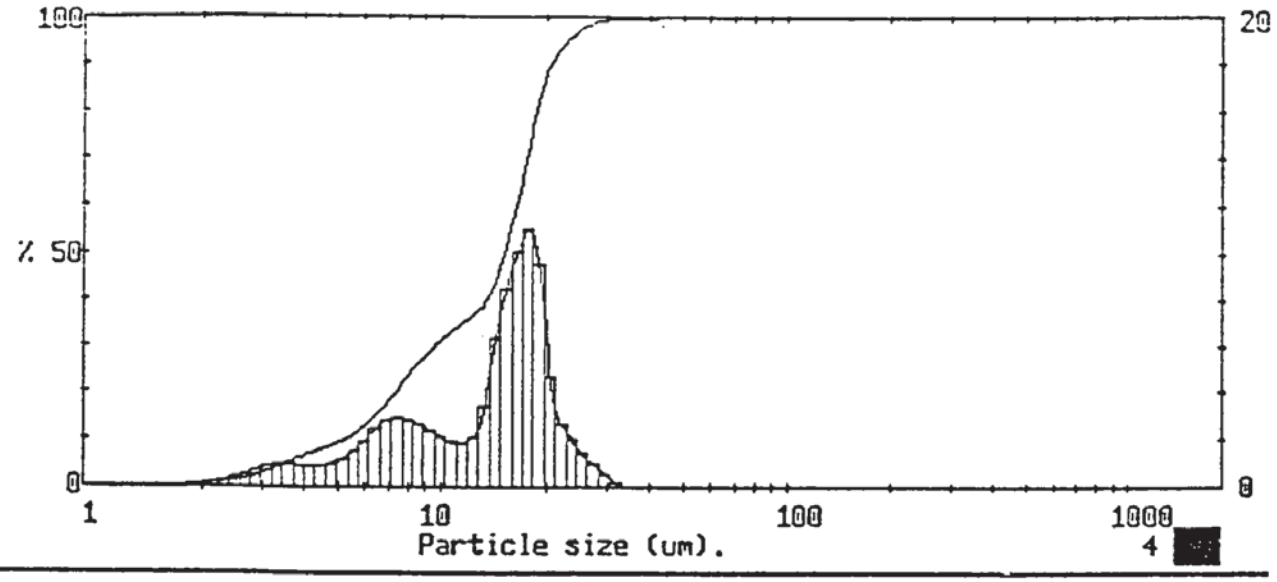

1598 pil 1DR459 / 0/ 0/0.00/1.00/
20% W/W salt Soln
500 rpm

000000262

MALVERN Series 2600 SB.20 Master Mode 04 Mar 1998 11:50 am

High Size	Under %	High Size	Under %	High Size	Under %	High Size	Under %	High Size	Under %	High Size	Under %	Span 1.01
188	100	84.5	100	38.0	99.8	17.1	66.6	7.69	22.1	3.46	4.7	D[4,3] 13.83µm
175	100	78.6	100	35.4	99.8	15.9	56.5	7.15	19.2	3.21	3.7	
163	100	73.1	100	32.9	99.8	14.8	48.0	6.65	16.4	2.99	2.9	D[3,2] 9.59µm
151	100	68.0	100	30.6	99.6	13.7	41.6	6.18	14.0	2.78	2.2	
141	100	63.2	100	28.4	99.0	12.8	38.2	5.75	12.0	2.59	1.6	
131	100	58.8	100	26.4	98.1	11.9	36.0	5.35	10.5	2.40	1.2	D[v,0.9] 20.41µm
122	100	54.7	100	24.6	96.7	11.1	34.1	4.97	9.3	2.24	0.9	
113	100	50.8	100	22.9	94.7	10.3	32.2	4.62	8.3	2.08	0.7	
105	100	47.3	99.9	21.3	92.0	9.56	30.1	4.30	7.5	1.93	0.6	D[v,0.1] 5.19µm
97.8	100	44.0	99.9	19.8	87.3	8.89	27.7	4.00	6.6			
90.9	100	40.9	99.9	18.4	77.7	8.27	25.0	3.72	5.7			

Source = Data:p20v006	Beam length = 14.3 mm	Model indp	D[v,0.5] 15.06µm
Record No. = 3	Log. Diff. = 4.893		
Focal length = 100 mm	Obscuration = 0.9251	Volume Conc. = 0.0579%	
Presentation = pil	Volume distribution	Sp.S.A 0.6254 m²/cc.	Shape OFF

1598 pil 1DR459 / 0/ 0/0.00/1.00/
20% W/W salt Soln
500 rpm

000000262

MALVERN Series 2600 SB.20 Master Mode 04 Mar 1998 11:50 am

Particle diameters		Volume percentiles	
D(4,3)	13.83 µm	D[v,.10]	5.19
D(4,2)	11.52 µm	D[v,.20]	7.29
D(4,1)	8.67 µm	D[v,.30]	9.53
D(4,0)	6.15 µm	D[v,.40]	13.38
		D[v,.50]	15.06
D(3,2)	9.59 µm	D[v,.60]	16.32
D(3,1)	6.86 µm	D[v,.70]	17.49
D(3,0)	4.69 µm	D[v,.80]	18.67
		D[v,.90]	20.41
D(2,1)	4.91 µm	D[v,.99]	28.34
D(2,0)	3.28 µm		
		Span	1.01
D(1,0)	2.20 µm	Unif.	0.34

Distribution Moments.

Distbn	Mean	Stan.Dev.	Skewness
Volume	13.83	6.30	0.41
Surface	9.59	6.38	0.63
Length	4.91	4.80	1.76
Number	2.20	2.44	3.69

Source =Data:p20v006
Record 3

1598 pil 1DR459 / 0/ 0/0.00/1.00/
20% W/W salt Soln
500 rpm

000000262

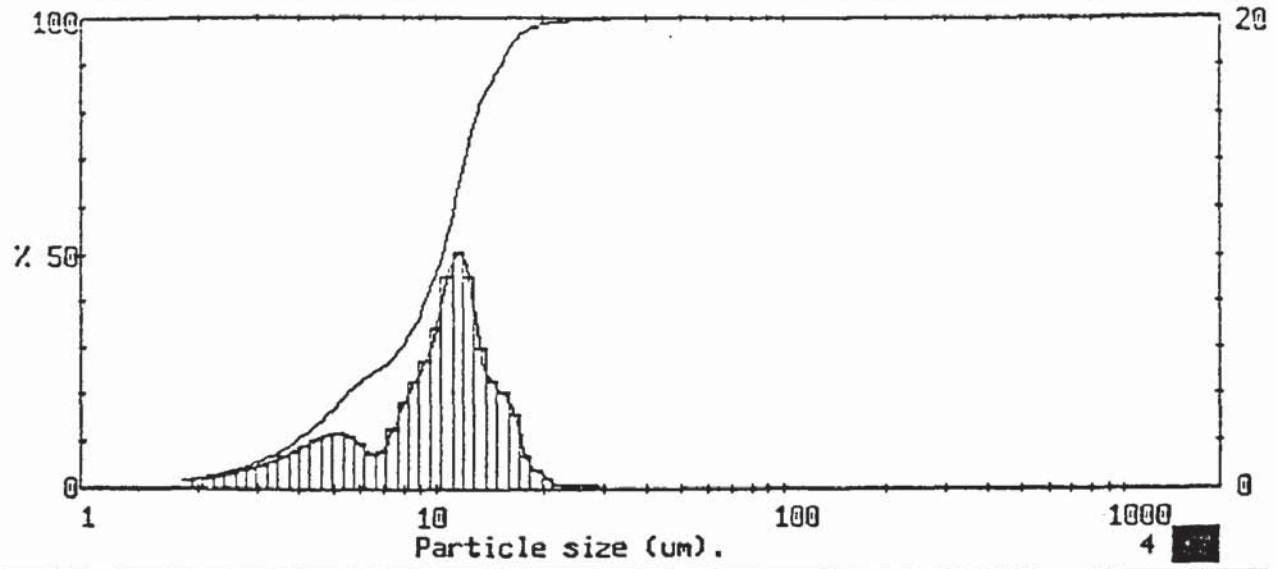

1598 pil lDR459 / 8/ 0/0.00/1.00/
20% W/W salt Soln
600 rpm

000000263

MALVERN Series 2600 SB.20 Master Mode 04 Mar 1998 12:15 pm

High Size	Under %	High Size	Under %	High Size	Under %	High Size	Under %	High Size	Under %	High Size	Under %	Span 1.09
188	100	84.5	100	38.0	100	17.1	96.4	7.69	29.3	3.46	7.8	D[4,3] 9.84µm
175	100	78.6	100	35.4	99.9	15.9	93.2	7.15	26.8	3.21	6.6	
163	100	73.1	100	32.9	99.9	14.8	89.1	6.65	25.2	2.99	5.6	D[3,2] 6.88µm
151	100	68.0	100	30.6	99.9	13.7	84.4	6.18	23.7	2.78	4.7	
141	100	63.2	100	28.4	99.8	12.8	78.4	5.75	21.7	2.59	4.0	
131	100	58.8	100	26.4	99.7	11.9	69.3	5.35	19.5	2.40	3.3	D[v,0.9] 15.02µm
122	100	54.7	100	24.6	99.5	11.1	59.1	4.97	17.1	2.24	2.8	
113	100	50.8	100	22.9	99.3	10.3	50.0	4.62	14.8	2.08	2.3	
105	100	47.3	100	21.3	99.2	9.56	43.1	4.30	12.7	1.93	1.9	D[v,0.1] 3.86µm
97.8	100	44.0	100	19.8	98.7	8.89	37.6	4.00	10.8			
90.9	100	40.9	100	18.4	97.8	8.27	33.0	3.72	9.2			

Source = Data:p20v006	Beam length = 14.3 mm	Model indp	D[v,0.5] 10.28µm
Record No. = 7	Log. Diff. = 4.817		
Focal length = 100 mm	Obscuration = 0.9794	Volume Conc. = 0.0622%	Shape OFF
Presentation = pil	Volume distribution	Sp.S.A 0.8717 m²/cc.	

1598 pil lDR459 / 0/ 0/0.00/1.00/
20% W/W salt Soln
600 rpm

000000263

MALVERN Series 2600 SB.20 Master Mode 04 Mar 1998 12:15 pm

Particle diameters		Volume percentiles	
D(4,3)	9.84 µm	D[v,.10]	3.86
D(4,2)	8.23 µm	D[v,.20]	5.43
D(4,1)	6.15 µm	D[v,.30]	7.80
D(4,0)	4.43 µm	D[v,.40]	9.19
		D[v,.50]	10.28
D(3,2)	6.88 µm	D[v,.60]	11.13
D(3,1)	4.87 µm	D[v,.70]	11.95
D(3,0)	3.40 µm	D[v,.80]	12.99
		D[v,.90]	15.02
D(2,1)	3.44 µm	D[v,.99]	20.61
D(2,0)	2.39 µm		
		Span	1.09
D(1,0)	1.66 µm	Unif.	0.33

Distribution Moments.			
Distbn	Mean	Stan.Dev.	Skewness
Volume	9.84	4.40	0.53
Surface	6.88	4.51	0.58
Length	3.44	3.44	1.72
Number	1.66	1.72	3.93

Source =Data:p20v006
Record 7

1598 pil lDR459 / 0/ 0/0.00/1.00/
20% W/W salt Soln
600 rpm

000000263

20% w/w and 0.07% v/v

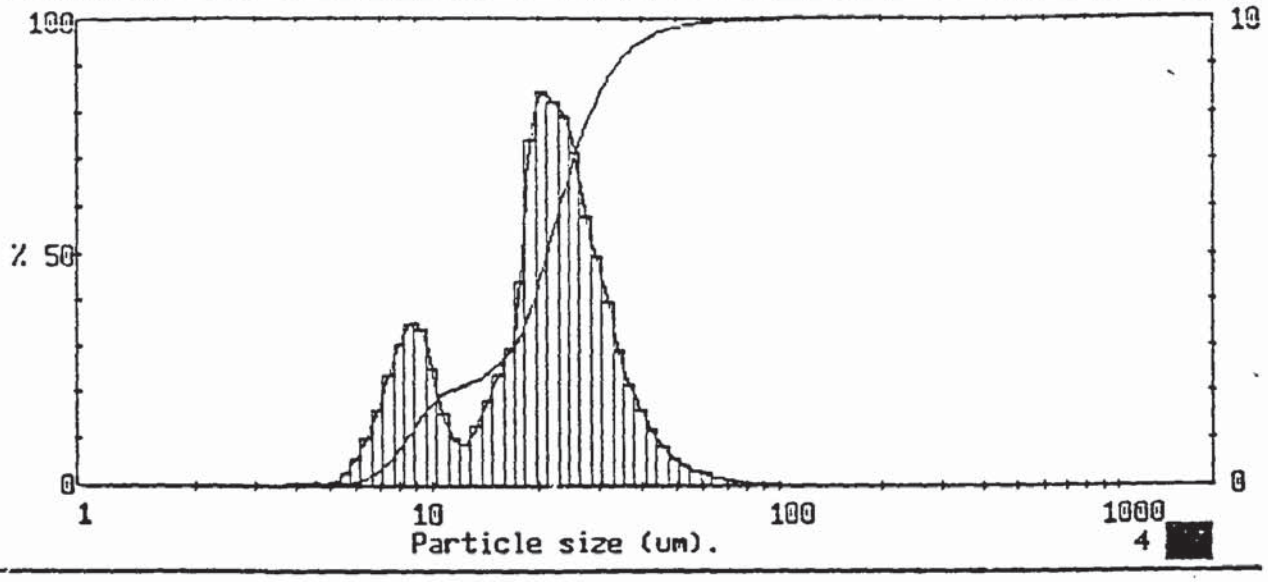

1598 pil 1DR459 / 0/ 0/0.00/1.00/
20% W/W salt Soln
300 rpm

000000264

MALVERN Series 2600 SB.20 Master Mode 05 Mar 1998 1:52 pm

High Size	Under %	High Size	Under %	High Size	Under %	High Size	Under %	High Size	Under %	High Size	Under %	Span 1.20
188	100	84.5	99.8	38.0	94.1	17.1	30.6	7.69	6.3	3.46	0.0	D[4,3] 21.68µm
175	100	78.6	99.8	35.4	91.9	15.9	27.6	7.15	3.9	3.21	0.0	
163	100	73.1	99.7	32.9	89.0	14.8	25.3	6.65	2.2	2.99	0.0	D[3,2] 16.56µm
151	100	68.0	99.6	30.6	85.0	13.7	23.4	6.18	1.2	2.78	0.0	
141	100	63.2	99.4	28.4	80.1	12.8	22.2	5.75	0.6	2.59	0.0	
131	100	58.8	99.1	26.4	74.3	11.9	21.3	5.35	0.3	2.40	0.0	D[v,0.9] 33.61µm
122	99.9	54.7	98.8	24.6	67.1	11.1	20.3	4.97	0.2	2.24	0.0	
113	99.9	50.8	98.4	22.9	59.2	10.3	18.7	4.62	0.1	2.08	0.0	
105	99.9	47.3	97.8	21.3	50.9	9.56	16.2	4.30	0.1	1.93	0.0	D[v,0.1] 8.39µm
97.8	99.9	44.0	97.0	19.8	42.5	8.89	12 8	4.00	0.0			
90.9	99.9	40.9	95.8	18.4	35.0	8.27	9.3	3.72	0.0			

Source = Data:p20v007	Beam length = 14.3 mm	Model indp	D[v,0.5] 21.09µm
Record No. = 3	Log. Diff. = 5.567		
Focal length = 100 mm	Obscuration = 0.2875	Volume Conc. = 0.0131%	
Presentation = pil	Volume distribution	Sp.S.A 0.1624 m²/cc.	Shape OFF

1598 pil 1DR459 / 0/ 0/0.00/1.00/
20% W/W salt Soln
300 rpm

000000264

MALVERN Series 2600 SB.20 Master Mode 05 Mar 1998 1:52 pm

Particle diameters		Volume percentiles	
D(4,3)	21.68 µm	D(v,.10)	8.39
D(4,2)	18.94 µm	D(v,.20)	10.90
D(4,1)	16.40 µm	D(v,.30)	16.86
D(4,0)	14.31 µm	D(v,.40)	19.33
		D(v,.50)	21.09
D(3,2)	16.56 µm	D(v,.60)	23.03
D(3,1)	14.26 µm	D(v,.70)	25.28
D(3,0)	12.46 µm	D(v,.80)	28.40
		D(v,.90)	33.61
D(2,1)	12.28 µm	D(v,.99)	56.75
D(2,0)	10.81 µm		
		Span	1.20
D(1,0)	9.51 µm	Unif.	0.37

Distribution Moments.

Distbn	Mean	Stan.Dev.	Skewness
Volume	21.68	11.04	2.13
Surface	16.56	9.21	1.34
Length	12.28	7.25	1.63
Number	9.51	5.13	2.38

Source =Data:p20v007
Record 3

1598 pil 1DR459 / 0/ 0/0.00/1.00/
20% W/W salt Soln
300 rpm

000000264

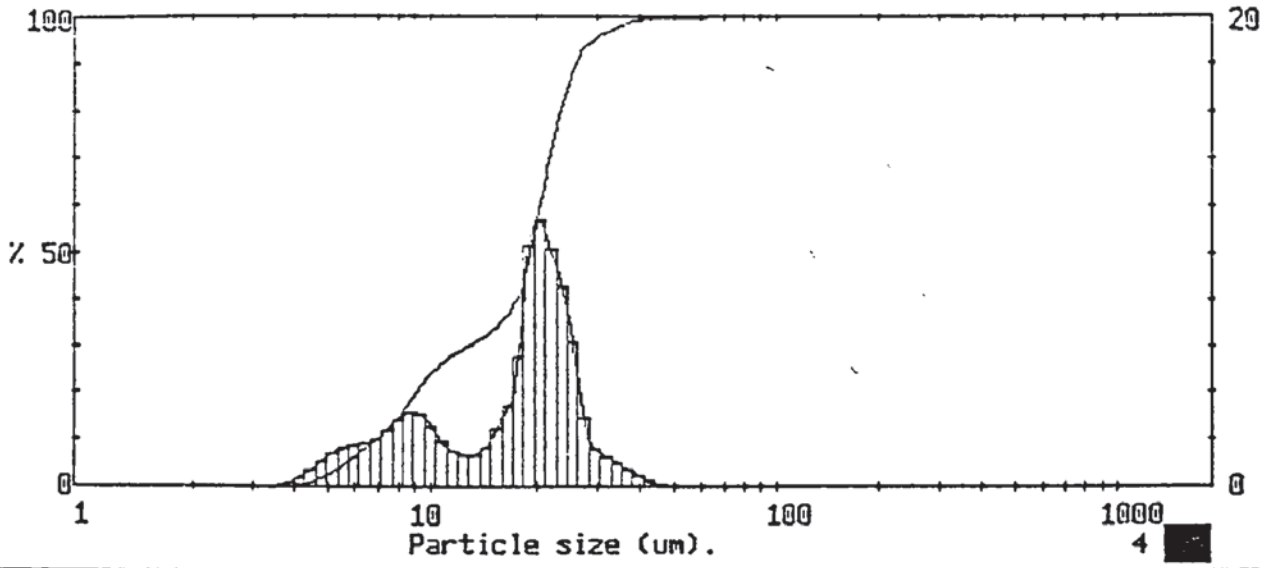

1598 pil lDR459 / 0/ 0/0.00/1.00/
20% W/W salt Soln
400 rpm
000000265

MALVERN Series 2600 SB.20 Master Mode 05 Mar 1998 2:55 pm

High Size	Under %	High Size	Under %	High Size	Under %	High Size	Under %	High Size	Under %	High Size	Under %	Span 0.99
188	100	84.5	100	38.0	99.0	17.1	39.1	7.69	13.5	3.46	0.0	D[4,3] 17.72µm
175	100	78.6	100	35.4	98.3	15.9	35.6	7.15	11.1	3.21	0.0	
163	100	73.1	99.9	32.9	97.3	14.8	33.2	6.65	9.0	2.99	0.0	
151	100	68.0	99.9	30.6	96.0	13.7	31.5	6.18	7.2	2.78	0.0	D[3,2] 13.48µm
141	100	63.2	99.9	28.4	94.4	12.8	30.1	5.75	5.4	2.59	0.0	
131	100	58.8	99.9	26.4	91.4	11.9	28.8	5.35	3.8	2.40	0.0	
122	100	54.7	99.8	24.6	85.2	11.1	27.2	4.97	2.4	2.24	0.0	D[v,0.9] 25.90µm
113	100	50.8	99.8	22.9	76.7	10.3	25.3	4.62	1.3	2.08	0.0	
105	100	47.3	99.8	21.3	66.5	9.56	22.7	4.30	0.6	1.93	0.0	
97.8	100	44.0	99.7	19.8	55.1	8.89	19.5	4.00	0.2			D[v,0.1] 6.89µm
90.9	100	40.9	99.5	18.4	44.7	8.27	16.4	3.72	0.1			

Source = Data:p20v007	Beam length = 14.3 mm	Model indp	D[v,0.5] 19.13µm
Record No. = 5	Log. Diff. = 5.477		
Focal length = 100 mm	Obscuration = 0.6151	Volume Conc. = 0.0300%	
Presentation = pil	Volume distribution	Sp.S.A 0.4452 m²/cc.	Shape OFF

1598 pil lDR459 / 0/ 0/0.00/1.00/
20% W/W salt Soln
400 rpm
000000265

MALVERN Series 2600 SB.20 Master Mode 05 Mar 1998 2:55 pm

Particle diameters		Volume percentiles		Distribution Moments.			
D(4,3)	17.72 µm	D[v,.10]	6.89	Distbn	Mean	Stan.Dev.	Skewness
D(4,2)	15.46 µm	D[v,.20]	8.98				
D(4,1)	13.22 µm	D[v,.30]	12.71	Volume	17.72	7.95	0.67
D(4,0)	11.41 µm	D[v,.40]	17.39	Surface	13.48	7.56	0.75
		D[v,.50]	19.13	Length	9.68	6.06	1.51
D(3,2)	13.48 µm	D[v,.60]	20.39	Number	7.32	4.16	2.56
D(3,1)	11.42 µm	D[v,.70]	21.78				
D(3,0)	9.85 µm	D[v,.80]	23.48				
		D[v,.90]	25.90				
D(2,1)	9.68 µm	D[v,.99]	38.00	Source =Data:p20v007			
D(2,0)	8.42 µm			Record 5			
		Span	0.99				
D(1,0)	7.32 µm	Unif.	0.32				

1598 pil lDR459 / 0/ 0/0.00/1.00/
20% W/W salt Soln
400 rpm
000000265

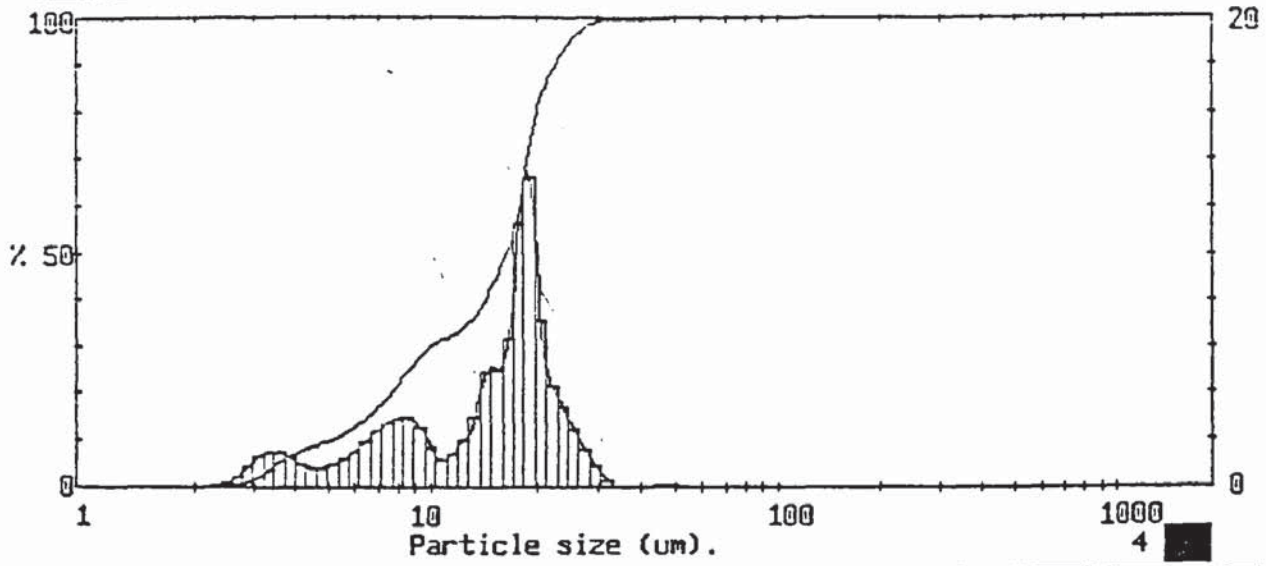

1598 pil IDR459 / 0/ 0/0.00/1.00/
20% W/W salt Soln
500 rpm

000000266

MALVERN Series 2600 SB.20 Master Mode 05 Mar 1998 3:10 pm

High Size	Under %	High Size	Under %	High Size	Under %	High Size	Under %	High Size	Under %	High Size	Under %	Span 1.07
188	100	84.5	100	38.0	99.7	17.1	54.9	7.69	20.6	3.46	4.4	D[4,3] 14.78µm
175	100	78.6	100	35.4	99.7	15.9	48.5	7.15	17.9	3.21	2.9	
163	100	73.1	100	32.9	99.7	14.8	43.5	6.65	15.5	2.99	1.6	D[3,2] 10.42µm
151	100	68.0	100	30.6	99.4	13.7	38.5	6.18	13.6	2.78	0.7	
141	100	63.2	100	28.4	98.5	12.8	35.5	5.75	12.0	2.59	0.3	
131	100	58.8	100	26.4	96.9	11.9	33.5	5.35	10.8	2.40	0.1	D[v,0.9] 22.45µm
122	100	54.7	99.9	24.6	94.4	11.1	32.0	4.97	9.9	2.24	0.0	
113	100	50.8	99.9	22.9	91.0	10.3	30.9	4.62	9.1	2.08	0.0	
105	100	47.3	99.9	21.3	86.7	9.56	29.2	4.30	8.2	1.93	0.0	D[v,0.1] 5.02µm
97.8	100	44.0	99.8	19.8	79.5	8.89	26.6	4.00	7.2			
90.9	100	40.9	99.7	18.4	66.2	8.27	23.6	3.72	5.9			

Source = Data:p20v007	Beam length = 14.3 mm	Model indp	D[v,0.5] 16.23µm
Record No. = 8	Log. Diff. = 5.060		
Focal length = 100 mm	Obscuration = 0.8129	Volume Conc. = 0.0407%	Shape OFF
Presentation = pil	Volume distribution	Sp.S.A 0.5758 m²/cc.	

1598 pil IDR459 / 0/ 0/0.00/1.00/
20% W/W salt Soln
500 rpm

000000266

MALVERN Series 2600 SB.20 Master Mode 05 Mar 1998 3:10 pm

Particle diameters		Volume percentiles	
D(4,3)	14.78 µm	D[v,.10]	5.02
D(4,2)	12.41 µm	D[v,.20]	7.56
D(4,1)	10.01 µm	D[v,.30]	9.85
D(4,0)	8.14 µm	D[v,.40]	14.08
		D[v,.50]	16.23
D(3,2)	10.42 µm	D[v,.60]	17.75
D(3,1)	8.24 µm	D[v,.70]	18.75
D(3,0)	6.67 µm	D[v,.80]	19.84
		D[v,.90]	22.45
D(2,1)	6.51 µm	D[v,.99]	29.31
D(2,0)	5.34 µm		
		Span	1.07
D(1,0)	4.38 µm	Unif.	0.34

Distribution Moments.

Distbn	Mean	Stan.Dev.	Skewness
Volume	14.78	6.87	0.34
Surface	10.42	6.74	0.71
Length	6.51	5.05	1.79
Number	4.38	3.05	3.17

Source =Data:p20v007
Record 8

1598 pil IDR459 / 0/ 0/0.00/1.00/
20% W/W salt Soln
500 rpm

000000266

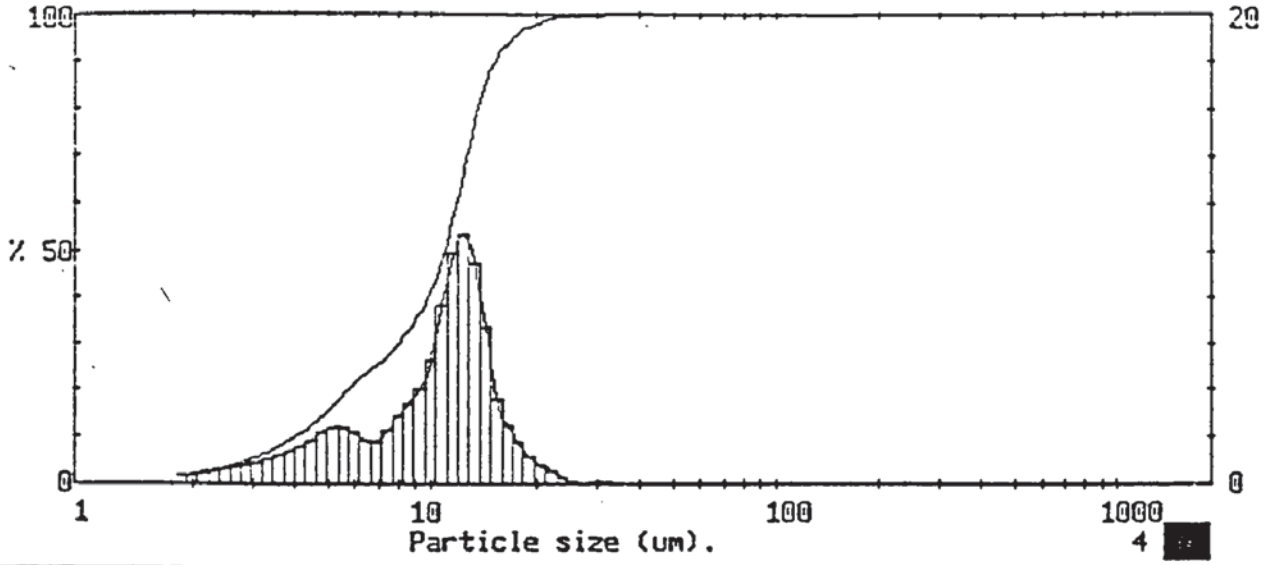

1598 pil 1DR459 / 0/ 0/0.00/1.00/
20% W/W salt Soln
600 rpm

000000267

MALVERN Series 2600 SB.20 Master Mode 05 Mar 1998 3:38 pm

High Size	Under %	High Size	Under %	High Size	Under %	High Size	Under %	High Size	Under %	High Size	Under %	Span 1.01
188	100	84.5	100	38.0	100	17.1	95.1	7.69	28.6	3.46	7.3	D[4,3] 10.22µm
175	100	78.6	100	35.4	99.9	15.9	92.6	7.15	26.3	3.21	6.3	
163	100	73.1	100	32.9	99.9	14.8	88.9	6.65	24.5	2.99	5.4	D[3,2] 7.12µm
151	100	68.0	100	30.6	99.9	13.7	82.2	6.18	22.7	2.78	4.6	
141	100	63.2	100	28.4	99.8	12.8	72.8	5.75	20.5	2.59	3.9	
131	100	58.8	100	26.4	99.8	11.9	62.0	5.35	18.1	2.40	3.2	
122	100	54.7	100	24.6	99.7	11.1	52.2	4.97	15.6	2.24	2.7	D[v,0.9] 15.03µm
113	100	50.8	100	22.9	99.4	10.3	44.5	4.62	13.4	2.08	2.2	
105	100	47.3	100	21.3	98.8	9.56	39.1	4.30	11.5	1.93	1.8	
97.8	100	44.0	100	19.8	98.0	8.89	35.0	4.00	9.9			D[v,0.1] 4.01µm
90.9	100	40.9	100	18.4	96.9	8.27	31.6	3.72	8.5			

Source = Data:p20v007	Beam length = 14.3 mm	Model indp	D[v,0.5] 10.86µm
Record No. = 13	Log. Diff. = 4.768		
Focal length = 100 mm	Obscuration = 0.9719	Volume Conc. = 0.0592%	Shape OFF
Presentation = pil	Volume distribution	Sp.S.A 0.8431 m²/cc.	

1598 pil 1DR459 / 0/ 0/0.00/1.00/
20% W/W salt Soln
600 rpm

000000267

MALVERN Series 2600 SB.20 Master Mode 05 Mar 1998 3:38 pm

Particle diameters		Volume percentiles	
D(4,3)	10.22 µm	D[v,.10]	4.01
D(4,2)	8.53 µm	D[v,.20]	5.66
D(4,1)	6.32 µm	D[v,.30]	7.97
D(4,0)	4.52 µm	D[v,.40]	9.70
		D[v,.50]	10.86
D(3,2)	7.12 µm	D[v,.60]	11.72
D(3,1)	4.98 µm	D[v,.70]	12.54
D(3,0)	3.44 µm	D[v,.80]	13.49
		D[v,.90]	15.03
D(2,1)	3.48 µm	D[v,.99]	21.68
D(2,0)	2.39 µm		
		Span	1.01
D(1,0)	1.65 µm	Unif.	0.33

Distribution Moments.

Distbn	Mean	Stan.Dev.	Skewness
Volume	10.22	4.52	0.42
Surface	7.12	4.70	0.55
Length	3.48	3.56	1.75
Number	1.65	1.74	4.08

Source =Data:p20v007
Record 13

1598 pil 1DR459 / 0/ 0/0.00/1.00/
20% W/W salt Soln
600 rpm

000000267

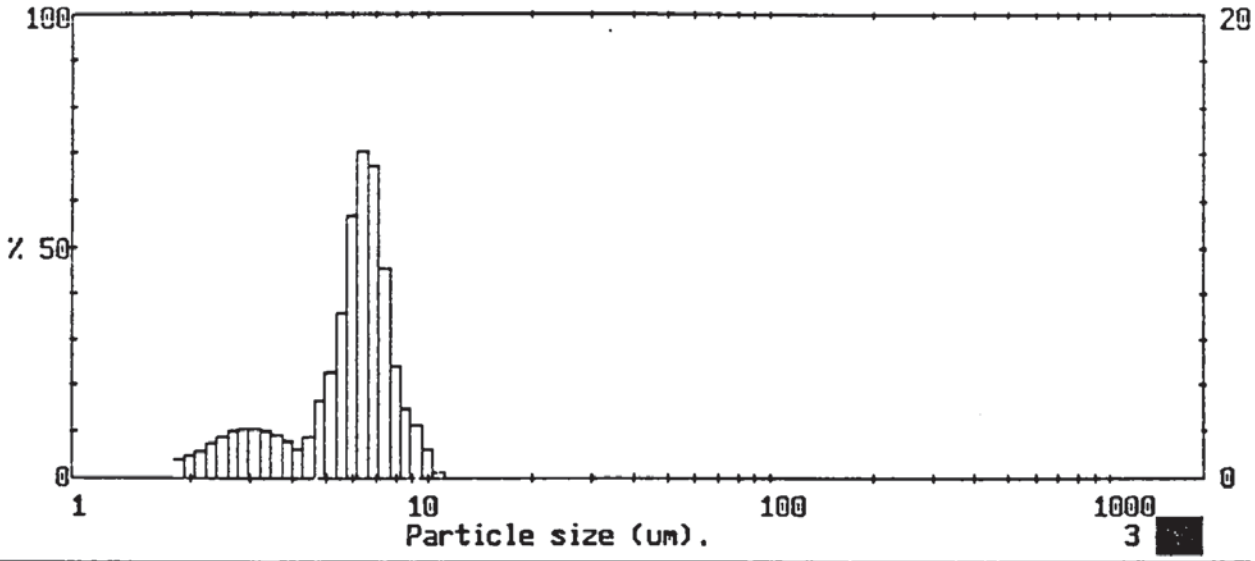

1598 pil lDR459 / 0/ 0/0.00/1.00/
20% W/W salt Soln
700 rpm

000000365

MALVERN Series 2600 SB.20 Master Mode 05 Mar 1998 4:32 pm

High Size	Under %	High Size	Under %	High Size	Under %	High Size	Under %	High Size	Under %	High Size	Under %	Span 0.86
188	100	84.5	100	38.0	100	17.1	99.9	7.69	88.1	3.46	18.3	D[4,3] 5.71µm
175	100	78.6	100	35.4	100	15.9	99.9	7.15	79.0	3.21	16.3	
163	100	73.1	100	32.9	100	14.8	99.9	6.65	65.4	2.99	14.1	
151	100	68.0	100	30.6	100	13.7	99.9	6.18	51.2	2.78	11.9	D[3,2] 4.35µm
141	100	63.2	100	28.4	100	12.8	99.9	5.75	39.8	2.59	9.9	
131	100	58.8	100	26.4	100	11.9	99.9	5.35	32.7	2.40	8.1	
122	100	54.7	100	24.6	100	11.1	99.9	4.97	28.1	2.24	6.7	D[v,0.9] 7.86µm
113	100	50.8	100	22.9	100	10.3	99.6	4.62	24.7	2.08	5.5	
105	100	47.3	100	21.3	100	9.56	98.4	4.30	23.0	1.93	4.5	
97.8	100	44.0	100	19.8	100	8.89	96.0	4.00	21.7			D[v,0.1] 2.60µm
90.9	100	40.9	100	18.4	100	8.27	93.0	3.72	20.2			

Source = Data:p20v007	Beam length = 14.3 mm	Model indp	D[v,0.5] 6.14µm
Record No. = 15	Log. Diff. = 5.133		
Focal length = 100 mm	Obscuration = 0.9900	Volume Conc. = 0.0467%	Shape OFF
Presentation = pil	Volume distribution	Sp.S.A 1.3791 m²/cc.	

1598 pil lDR459 / 0/ 0/0.00/1.00/
20% W/W salt Soln
700 rpm

000000365

MALVERN Series 2600 SB.20 Master Mode 05 Mar 1998 4:32 pm

Particle diameters		Volume percentiles	
D(4,3)	5.71 µm	D[v,.10]	2.60
D(4,2)	4.99 µm	D[v,.20]	3.69
D(4,1)	4.00 µm	D[v,.30]	5.13
D(4,0)	3.13 µm	D[v,.40]	5.76
		D[v,.50]	6.14
D(3,2)	4.35 µm	D[v,.60]	6.47
D(3,1)	3.35 µm	D[v,.70]	6.80
D(3,0)	2.56 µm	D[v,.80]	7.20
		D[v,.90]	7.86
D(2,1)	2.58 µm	D[v,.99]	9.84
D(2,0)	1.97 µm		
		Span	0.86
D(1,0)	1.50 µm	Unif.	0.26

Distribution Moments.			
Distbn	Mean	Stan.Dev.	Skewness
Volume	5.71	2.08	-0.26
Surface	4.35	2.44	0.08
Length	2.58	2.14	1.19
Number	1.50	1.27	3.00

Source =Data:p20v007
Record 15

1598 pil lDR459 / 0/ 0/0.00/1.00/
20% W/W salt Soln
700 rpm

000000365

25% w/w and 0.04% v/v

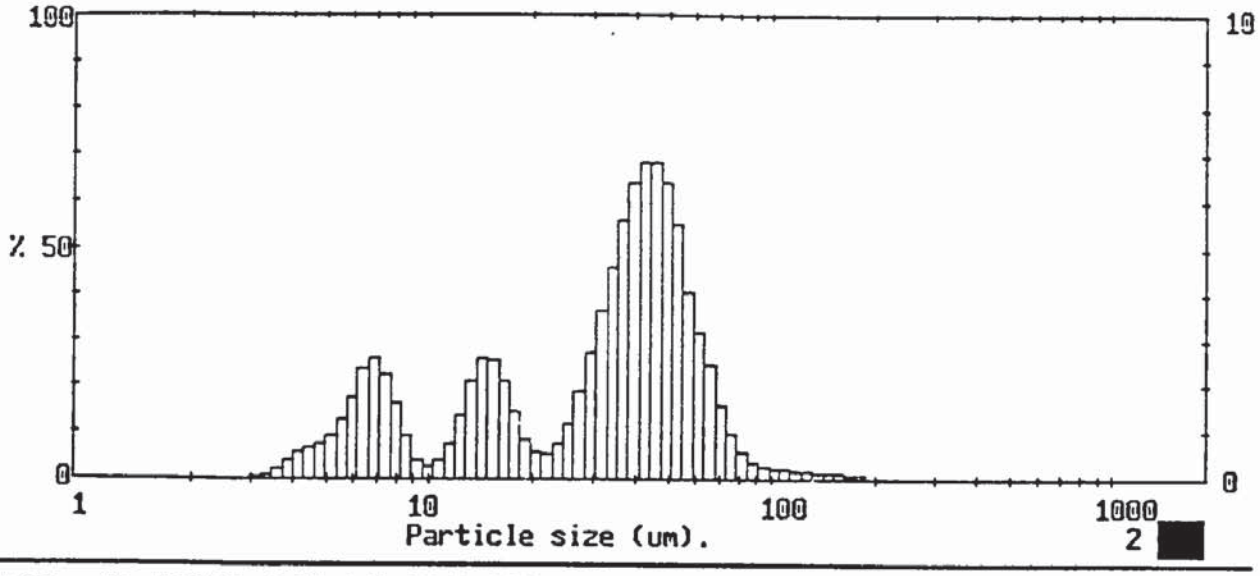

1598 pil lDR459 / 0/ 0/0.00/1.00/
25% w/w salt soln
400 rpm

0000000000366

MALVERN Series 2600 SB.20 Master Mode 11 Feb 1998 6:52 pm

High Size	Under %	High Size	Under %	High Size	Under %	High Size	Under %	High Size	Under %	High Size	Under %	Span 1.45
188	100	84.5	98.0	38.0	53.0	17.1	29.1	7.69	13.9	3.46	0.2	D[4,3] 35.28µm
175	99.9	78.6	97.5	35.4	47.4	15.9	27.0	7.15	11.7	3.21	0.1	
163	99.8	73.1	96.5	32.9	42.8	14.8	24.4	6.65	9.1	2.99	0.0	
151	99.7	68.0	94.9	30.6	39.1	13.7	21.8	6.18	6.7	2.78	0.0	D[3,2] 18.51µm
141	99.6	63.2	92.4	28.4	36.3	12.8	19.6	5.75	4.9	2.59	0.0	
131	99.4	58.8	89.2	26.4	34.5	11.9	18.3	5.35	3.6	2.40	0.0	
122	99.3	54.7	85.1	24.6	33.3	11.1	17.5	4.97	2.7	2.24	0.0	D[v,0.9] 59.79µm
113	99.1	50.8	79.6	22.9	32.5	10.3	17.1	4.62	2.0	2.08	0.0	
105	98.9	47.3	73.2	21.3	32.0	9.56	16.8	4.30	1.3	1.93	0.0	
97.8	98.7	44.0	66.3	19.8	31.4	8.89	16.4	4.00	0.8			D[v,0.1] 6.82µm
90.9	98.4	40.9	59.5	18.4	30.6	8.27	15.5	3.72	0.4			

Source = Data:p25v004	Beam length = 2.2 mm	Model indp
Record No. = 1	Log. Diff. = 5.026	
Focal length = 100 mm	Obscuration = 0.1629	Volume Conc. = 0.0500%
Presentation = pil	Volume distribution	Sp.S.A 0.3241 m²/cc.

D[v,0.5] 36.61µm

Shape OFF

1598 pil lDR459 / 0/ 0/0.00/1.00/
25% w/w salt soln
400 rpm

0000000000366

MALVERN Series 2600 SB.20 Master Mode 11 Feb 1998 6:52 pm

Particle diameters		Volume percentiles	
D(4,3)	35.28 µm	D[v,.10]	6.82
D(4,2)	25.56 µm	D[v,.20]	12.97
D(4,1)	18.12 µm	D[v,.30]	17.81
D(4,0)	13.88 µm	D[v,.40]	31.17
		D[v,.50]	36.61
D(3,2)	18.51 µm	D[v,.60]	41.11
D(3,1)	12.98 µm	D[v,.70]	45.69
D(3,0)	10.17 µm	D[v,.80]	51.08
		D[v,.90]	59.79
D(2,1)	9.10 µm	D[v,.99]	109.86
D(2,0)	7.53 µm		
		Span	1.45
D(1,0)	6.24 µm	Unif.	0.48

Distribution Moments.

Distbn	Mean	Stan.Dev.	Skewness
Volume	35.28	22.68	1.22
Surface	18.51	17.62	1.64
Length	9.10	9.26	3.60
Number	6.24	4.23	6.27

Source =Data:p25v004
Record 1

1598 pil lDR459 / 0/ 0/0.00/1.00/
25% w/w salt soln
400 rpm

0000000000366

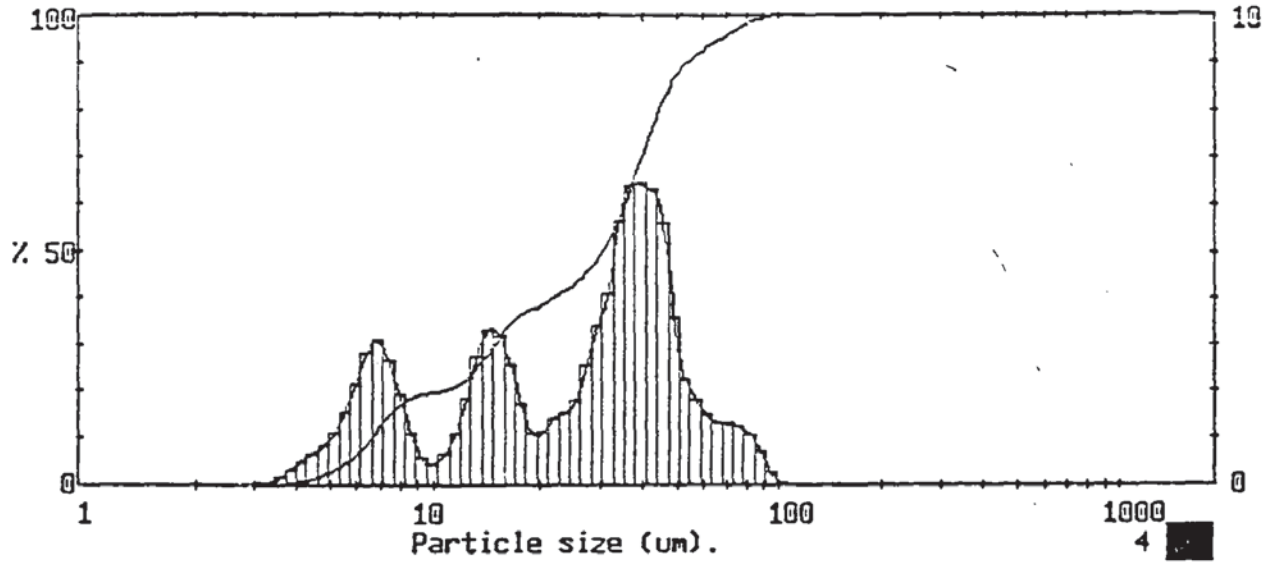

1598 pil IDR459 / 0/ 0/0.00/1.00/
25% w/w salt soln
450 rpm

0000000000269

MALVERN Series 2600 SB.20 Master Mode 11 Feb 1998 7:40 pm

High Size	Under %	High Size	Under %	High Size	Under %	High Size	Under %	High Size	Under %	High Size	Under %	Span 1.54
188	100	84.5	99.0	38.0	66.4	17.1	35.5	7.69	16.0	3.46	0.1	D[4,3] 29.94µm
175	100	78.6	97.9	35.4	60.0	15.9	32.9	7.15	13.3	3.21	0.0	
163	100	73.1	96.7	32.9	54.3	14.8	29.7	6.65	10.2	2.99	0.0	
151	100	68.0	95.4	30.6	50.2	13.7	26.4	6.18	7.4	2.78	0.0	D[3,2] 16.43µm
141	100	63.2	94.0	28.4	46.8	12.8	23.6	5.75	5.2	2.59	0.0	
131	100	58.8	92.5	26.4	44.2	11.9	21.8	5.35	3.7	2.40	0.0	
122	100	54.7	90.7	24.6	42.4	11.1	20.7	4.97	2.6	2.24	0.0	D[v,0.9] 53.40µm
113	100	50.8	88.4	22.9	40.9	10.3	20.0	4.62	1.8	2.08	0.0	
105	100	47.3	84.8	21.3	39.5	9.56	19.6	4.30	1.1	1.93	0.0	
97.8	100	44.0	79.2	19.8	38.4	8.89	19.0	4.00	0.6			D[v,0.1] 6.61µm
90.9	99.7	40.9	72.9	18.4	37.2	8.27	17.9	3.72	0.3			

Source = Data:p25v004	Beam length = 2.2 mm	Model indp	D[v,0.5] 30.45µm
Record No. = 5	Log. Diff. = 5.115		
Focal length = 100 mm	Obscuration = 0.1744	Volume Conc. = 0.0477%	
Presentation = pil	Volume distribution	Sp.S.A 0.3651 m²/cc.	Shape OFF

1598 pil IDR459 / 0/ 0/0.00/1.00/
25% w/w salt soln
450 rpm

0000000000269

MALVERN Series 2600 SB.20 Master Mode 11 Feb 1998 7:40 pm

Particle diameters		Volume percentiles		Distribution Moments.			
				Distbn	Mean	Stan.Dev.	Skewness
D(4,3)	29.94 µm	D[v,.10]	6.61				
D(4,2)	22.18 µm	D[v,.20]	10.23				
D(4,1)	16.45 µm	D[v,.30]	14.88	Volume	29.94	19.32	0.68
D(4,0)	13.04 µm	D[v,.40]	21.84	Surface	16.43	14.90	1.66
		D[v,.50]	30.45	Length	9.04	8.18	3.47
D(3,2)	16.43 µm	D[v,.60]	35.35	Number	6.50	4.06	5.50
D(3,1)	12.19 µm	D[v,.70]	39.57				
D(3,0)	9.89 µm	D[v,.80]	44.38				
		D[v,.90]	53.40				
D(2,1)	9.04 µm	D[v,.99]	84.58	Source =Data:p25v004			
D(2,0)	7.67 µm			Record 5			
		Span	1.54				
D(1,0)	6.50 µm	Unif.	0.52				

1598 pil IDR459 / 0/ 0/0.00/1.00/
25% w/w salt soln
450 rpm

0000000000269

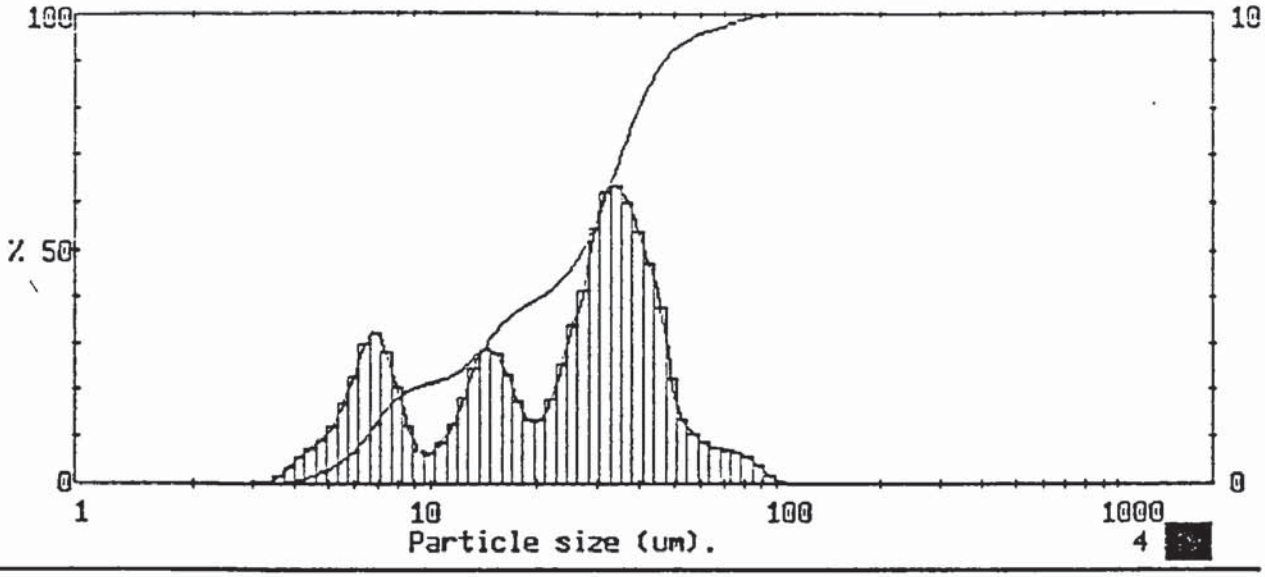

1598 pil 1DR459 / 0/ 0/0.00/1.00/
25% w/w salt soln
500 rpm

0000000000270

MALVERN Series 2600 SB.20 Master Mode 11 Feb 1998 8:47 pm

High Size	Under %	High Size	Under %	High Size	Under %	High Size	Under %	High Size	Under %	High Size	Under %	Span 1.47
188	100	84.5	99.4	38.0	77.1	17.1	36.5	7.69	17.2	3.46	0.1	D[4,3] 26.77µm
175	100	78.6	98.8	35.4	71.1	15.9	34.1	7.15	14.4	3.21	0.0	
163	100	73.1	98.1	32.9	64.7	14.8	31.3	6.65	11.2	2.99	0.0	D[3,2] 15.44µm
151	100	68.0	97.4	30.6	58.4	13.7	28.4	6.18	8.2	2.78	0.0	
141	100	63.2	96.6	28.4	52.9	12.8	25.9	5.75	5.8	2.59	0.0	
131	100	58.8	95.8	26.4	48.8	11.9	24.1	5.35	4.1	2.40	0.0	D[v,0.9] 46.22µm
122	100	54.7	94.7	24.6	45.4	11.1	22.8	4.97	2.9	2.24	0.0	
113	100	50.8	93.3	22.9	42.8	10.3	21.9	4.62	1.9	2.08	0.0	
105	100	47.3	91.0	21.3	41.0	9.56	21.2	4.30	1.2	1.93	0.0	D[v,0.1] 6.47µm
97.8	100	44.0	87.2	19.8	39.6	8.89	20.5	4.00	0.6			
90.9	99.8	40.9	82.5	18.4	38.2	8.27	19.3	3.72	0.2			

Source = Data:p25v004	Beam length = 2.2 mm	Model indp	D[v,0.5] 27.07µm
Record No. = 6	Log. Diff. = 5.063		
Focal length = 100 mm	Obscuration = 0.1817	Volume Conc. = 0.0469%	
Presentation = pil	Volume distribution	Sp.S.A 0.3886 m²/cc.	Shape OFF

1598 pil 1DR459 / 0/ 0/0.00/1.00/
25% w/w salt soln
500 rpm

0000000000270

MALVERN Series 2600 SB.20 Master Mode 11 Feb 1998 8:47 pm

Particle diameters		Volume percentiles	
D(4,3)	26.77 µm	D(v,.10)	6.47
D(4,2)	20.33 µm	D(v,.20)	8.56
D(4,1)	15.44 µm	D(v,.30)	14.30
D(4,0)	12.42 µm	D(v,.40)	20.22
		D(v,.50)	27.07
D(3,2)	15.44 µm	D(v,.60)	31.15
D(3,1)	11.72 µm	D(v,.70)	34.93
D(3,0)	9.62 µm	D(v,.80)	39.48
		D(v,.90)	46.22
D(2,1)	8.90 µm	D(v,.99)	80.48
D(2,0)	7.59 µm		
		Span	1.47
D(1,0)	6.48 µm	Unif.	0.51

Distribution Moments.			
Distbn	Mean	Stan.Dev.	Skewness
Volume	26.77	16.98	0.84
Surface	15.44	13.23	1.61
Length	8.90	7.63	3.19
Number	6.48	3.96	5.06

Source =Data:p25v004
Record 6

1598 pil 1DR459 / 0/ 0/0.00/1.00/
25% w/w salt soln
500 rpm

0000000000270

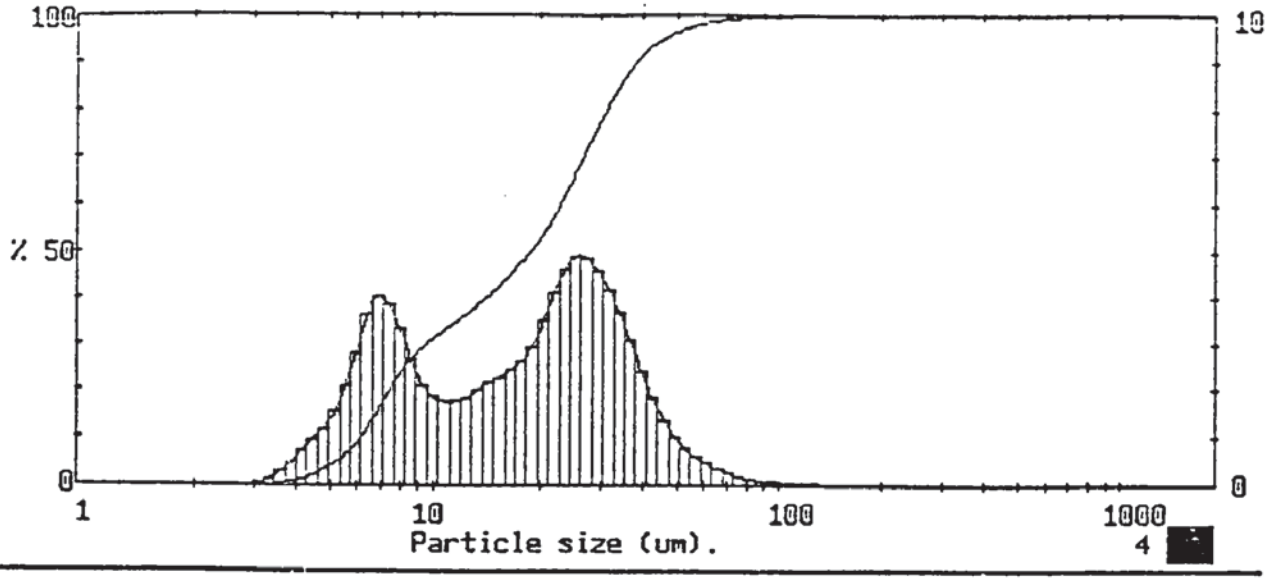

1598 pil 1DR459 / 0/ 0/0.00/1.00/
25% w/w salt soln
600 rpm

0000000000271

MALVERN Series 2600 SB.20 Master Mode 11 Feb 1998 9:20 pm

High Size	Under %	High Size	Under %	High Size	Under %	High Size	Under %	High Size	Under %	High Size	Under %	Span 1.70
188	100	84.5	99.6	38.0	90.1	17.1	46.7	7.69	22.2	3.46	0.2	D[4,3] 20.66µm
175	100	78.6	99.5	35.4	87.1	15.9	44.2	7.15	18.3	3.21	0.1	
163	100	73.1	99.3	32.9	83.4	14.8	41.9	6.65	14.2	2.99	0.0	
151	100	68.0	99.0	30.6	79.1	13.7	39.7	6.18	10.5	2.78	0.0	D[3,2] 12.56µm
141	100	63.2	98.7	28.4	74.5	12.8	37.7	5.75	7.7	2.59	0.0	
131	100	58.8	98.2	26.4	69.6	11.9	35.8	5.35	5.5	2.40	0.0	
122	99.9	54.7	97.6	24.6	64.7	11.1	34.0	4.97	3.9	2.24	0.0	D[v,0.9] 37.87µm
113	99.9	50.8	96.8	22.9	60.1	10.3	32.2	4.62	2.7	2.08	0.0	
105	99.9	47.3	95.8	21.3	55.9	9.56	30.3	4.30	1.7	1.93	0.0	
97.8	99.8	44.0	94.4	19.8	52.3	8.89	28.2	4.00	1.0			D[v,0.1] 6.11µm
90.9	99.7	40.9	92.6	18.4	49.4	8.27	25.5	3.72	0.5			

Source = Data:p25v004	Beam length = 2.2 mm	Model indp	D[v,0.5] 18.69µm
Record No. = 7	Log. Diff. = 4.955		
Focal length = 100 mm	Obscuration = 0.2350	Volume Conc. = 0.0510%	Shape OFF
Presentation = pil	Volume distribution	Sp.S.A 0.4776 m²/cc.	

1598 pil 1DR459 / 0/ 0/0.00/1.00/
25% w/w salt soln
600 rpm

0000000000271

MALVERN Series 2600 SB.20 Master Mode 11 Feb 1998 9:20 pm

Particle diameters		Volume percentiles	
D(4,3)	20.66 µm	D[v,.10]	6.11
D(4,2)	16.11 µm	D[v,.20]	7.38
D(4,1)	12.86 µm	D[v,.30]	9.44
D(4,0)	10.77 µm	D[v,.40]	13.88
		D[v,.50]	18.69
D(3,2)	12.56 µm	D[v,.60]	22.84
D(3,1)	10.14 µm	D[v,.70]	26.58
D(3,0)	8.67 µm	D[v,.80]	31.01
		D[v,.90]	37.87
D(2,1)	8.19 µm	D[v,.99]	67.20
D(2,0)	7.20 µm		
		Span	1.70
D(1,0)	6.34 µm	Unif.	0.59

Distribution Moments.			
Distbn	Mean	Stan.Dev.	Skewness
Volume	20.66	14.39	1.61
Surface	12.56	10.09	2.09
Length	8.19	5.98	3.25
Number	6.34	3.43	4.32

Source =Data:p25v004
Record 7

1598 pil 1DR459 / 0/ 0/0.00/1.00/
25% w/w salt soln
600 rpm

0000000000271

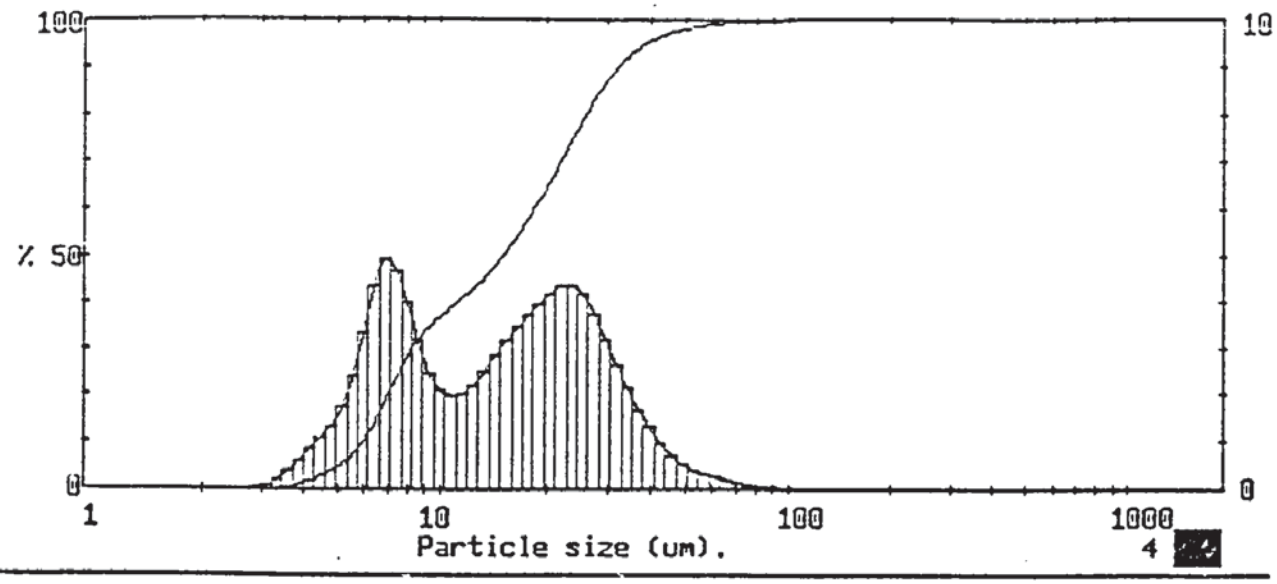

1598 pil 1DR459 / 0/ 0/0.00/1.00/
25% w/w salt soln
700 rpm

0000000000272

MALVERN Series 2600 SB.20 Master Mode 11 Feb 1998 9:33 pm

High Size	Under %	High Size	Under %	High Size	Under %	High Size	Under %	High Size	Under %	High Size	Under %	Span 1.75
188	100	84.5	99.8	38.0	94.9	17.1	56.5	7.69	26.3	3.46	0.3	D[4,3] 17.29µm
175	100	78.6	99.8	35.4	93.2	15.9	53.0	7.15	21.6	3.21	0.1	
163	100	73.1	99.7	32.9	91.0	14.8	49.8	6.65	16.6	2.99	0.0	
151	100	68.0	99.6	30.6	88.4	13.7	46.9	6.18	12.2	2.78	0.0	D[3,2] 11.18µm
141	100	63.2	99.4	28.4	85.1	12.8	44.4	5.75	8.9	2.59	0.0	
131	100	58.8	99.1	26.4	81.4	11.9	42.1	5.35	6.4	2.40	0.0	
122	99.9	54.7	98.8	24.6	77.2	11.1	40.1	4.97	4.7	2.24	0.0	D[v,0.9] 31.92µm
113	99.9	50.8	98.4	22.9	72.8	10.3	38.1	4.62	3.3	2.08	0.0	
105	99.9	47.3	97.9	21.3	68.4	9.56	36.0	4.30	2.2	1.93	0.0	
97.8	99.9	44.0	97.2	19.8	64.2	8.89	33.5	4.00	1.3			D[v,0.1] 5.91µm
90.9	99.9	40.9	96.2	18.4	60.2	8.27	30.3	3.72	0.7			

Source = Data:p25v004	Beam length = 2.2 mm	Model indp	D[v,0.5] 14.86µm
Record No. = 8	Log. Diff. = 4.866		
Focal length = 100 mm	Obscuration = 0.2762	Volume Conc. = 0.0547%	
Presentation = pil	Volume distribution	Sp.S.A 0.5367 m²/cc.	Shape OFF

1598 pil 1DR459 / 0/ 0/0.00/1.00/
25% w/w salt soln
700 rpm

0000000000272

MALVERN Series 2600 SB.20 Master Mode 11 Feb 1998 9:33 pm

Particle diameters		Volume percentiles	
D(4,3)	17.29 µm	D[v,.10]	5.91
D(4,2)	13.90 µm	D[v,.20]	6.99
D(4,1)	11.48 µm	D[v,.30]	8.22
D(4,0)	9.85 µm	D[v,.40]	11.02
		D[v,.50]	14.86
D(3,2)	11.18 µm	D[v,.60]	18.32
D(3,1)	9.35 µm	D[v,.70]	21.83
D(3,0)	8.16 µm	D[v,.80]	25.80
		D[v,.90]	31.92
D(2,1)	7.82 µm	D[v,.99]	56.85
D(2,0)	6.98 µm		
		Span	1.75
D(1,0)	6.22 µm	Unif.	0.61

Distribution Moments.			
Distbn	Mean	Stan.Dev.	Skewness
Volume	17.29	12.13	2.20
Surface	11.18	8.27	2.30
Length	7.82	5.12	3.10
Number	6.22	3.16	3.72

Source =Data:p25v004
Record 8

1598 pil 1DR459 / 0/ 0/0.00/1.00/
25% w/w salt soln
700 rpm

0000000000272

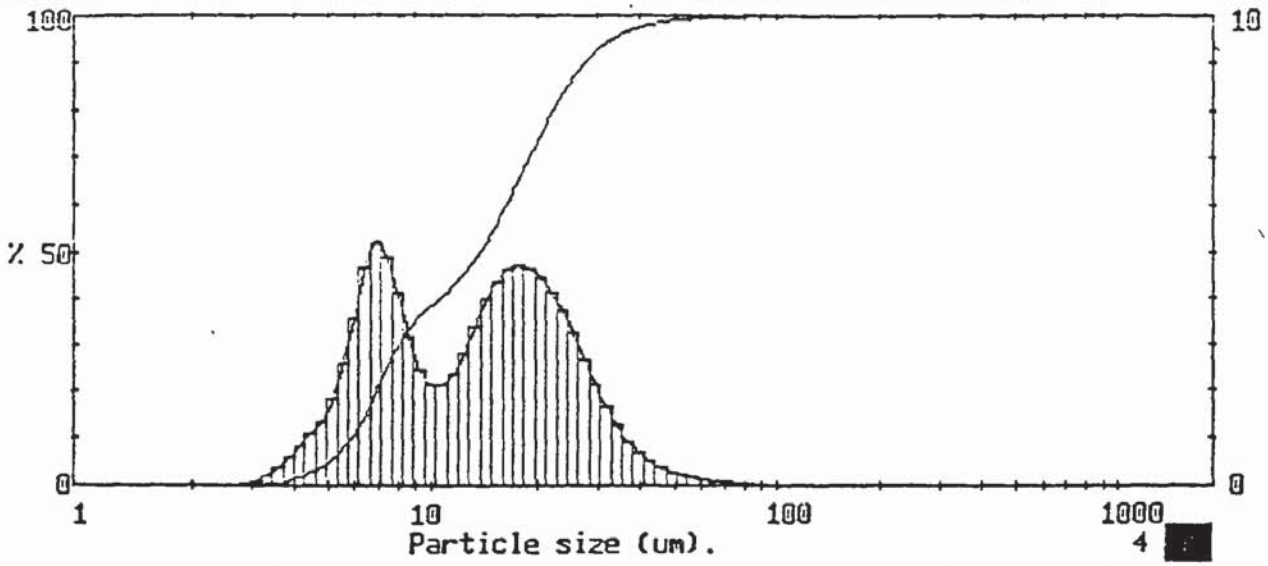

1598 pil 1DR459 / 0/ 0/0.00/1.00/
25% w/w salt soln
800 rpm

0000000000273

MALVERN Series 2600 SB.20 Master Mode 11 Feb 1998 9:45 pm

High Size	Under %	High Size	Under %	High Size	Under %	High Size	Under %	High Size	Under %	High Size	Under %	Span 1.59
188	100	84.5	99.9	38.0	97.3	17.1	63.5	7.69	27.7	3.46	0.4	D[4,3] 15.39µm
175	100	78.6	99.9	35.4	96.3	15.9	58.9	7.15	22.7	3.21	0.1	
163	100	73.1	99.8	32.9	95.1	14.8	54.5	6.65	17.5	2.99	0.1	
151	100	68.0	99.8	30.6	93.4	13.7	50.5	6.18	12.8	2.78	0.0	D[3,2] 10.63µm
141	100	63.2	99.7	28.4	91.2	12.8	47.0	5.75	9.2	2.59	0.0	
131	100	58.8	99.6	26.4	88.5	11.9	44.2	5.35	6.5	2.40	0.0	
122	100	54.7	99.4	24.6	85.3	11.1	41.8	4.97	4.7	2.24	0.0	D[v,0.9] 27.45µm
113	100	50.8	99.2	22.9	81.5	10.3	39.6	4.62	3.3	2.08	0.0	
105	100	47.3	98.9	21.3	77.4	9.56	37.5	4.30	2.2	1.93	0.0	
97.8	99.9	44.0	98.5	19.8	72.9	8.89	35.0	4.00	1.4			D[v,0.1] 5.85µm
90.9	99.9	40.9	98.0	18.4	68.2	8.27	31.8	3.72	0.7			

Source = Data:p25v004	Beam length = 2.2 mm	Model indp	D[v,0.5] 13.62µm
Record No. = 9	Log. Diff. = 4.879		
Focal length = 100 mm	Obscuration = 0.3337	Volume Conc. = 0.0654%	Shape OFF
Presentation = pil	Volume distribution	Sp.S.A 0.5643 m²/cc.	

1598 pil 1DR459 / 0/ 0/0.00/1.00/
25% w/w salt soln
800 rpm

0000000000273

MALVERN Series 2600 SB.20 Master Mode 11 Feb 1998 9:45 pm

Particle diameters		Volume percentiles	
D(4,3)	15.39 µm	D[v,.10]	5.85
D(4,2)	12.79 µm	D[v,.20]	6.88
D(4,1)	10.84 µm	D[v,.30]	7.99
D(4,0)	9.45 µm	D[v,.40]	10.41
		D[v,.50]	13.62
D(3,2)	10.63 µm	D[v,.60]	16.18
D(3,1)	9.10 µm	D[v,.70]	18.89
D(3,0)	8.03 µm	D[v,.80]	22.25
		D[v,.90]	27.45
D(2,1)	7.79 µm	D[v,.99]	48.29
D(2,0)	6.98 µm		
		Span	1.59
D(1,0)	6.26 µm	Unif.	0.55

Distribution Moments.

Distbn	Mean	Stan.Dev.	Skewness
Volume	15.39	10.11	2.36
Surface	10.63	7.11	2.20
Length	7.79	4.71	2.72
Number	6.26	3.09	3.17

Source =Data:p25v004
Record 9

1598 pil 1DR459 / 0/ 0/0.00/1.00/
25% w/w salt soln
800 rpm

0000000000273

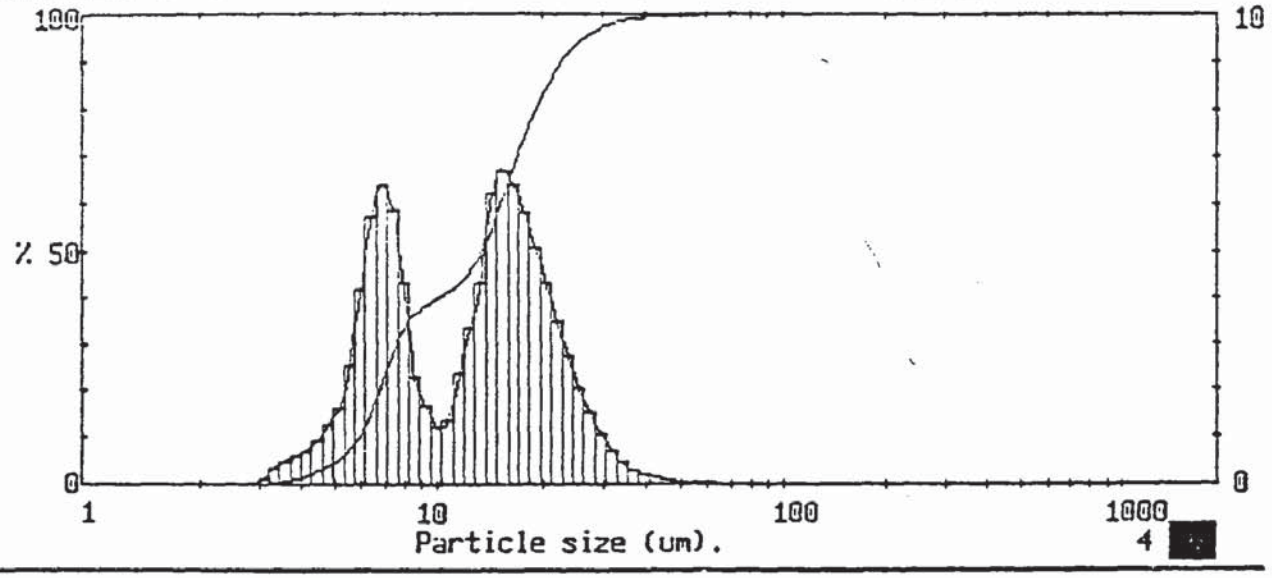

1598 pil 1DR459 / 0/ 0/0.00/1.00/
25% w/w salt soln
900 rpm

0000000000274

MALVERN Series 2600 SB.20 Master Mode 12 Feb 1998 4:14 pm

High Size	Under %	High Size	Under %	High Size	Under %	High Size	Under %	High Size	Under %	High Size	Under %	Span 1.25
188	100	84.5	100	38.0	99.3	17.1	71.5	7.69	31.1	3.46	0.5	D[4,3] 13.59µm
175	100	78.6	100	35.4	99.0	15.9	65.1	7.15	25.2	3.21	0.2	
163	100	73.1	100	32.9	98.5	14.8	58.3	6.65	18.8	2.99	0.0	D[3,2] 10.13µm
151	100	68.0	99.9	30.6	97.8	13.7	52.1	6.18	13.0	2.78	0.0	
141	100	63.2	99.9	28.4	96.7	12.8	47.7	5.75	8.8	2.59	0.0	
131	100	58.8	99.9	26.4	95.2	11.9	44.4	5.35	6.2	2.40	0.0	D[v,0.9] 22.70µm
122	100	54.7	99.9	24.6	93.1	11.1	42.0	4.97	4.6	2.24	0.0	
113	100	50.8	99.8	22.9	90.3	10.3	40.6	4.62	3.3	2.08	0.0	
105	100	47.3	99.8	21.3	86.8	9.56	39.4	4.30	2.4	1.93	0.0	D[v,0.1] 5.89µm
97.8	100	44.0	99.7	19.8	82.5	8.89	37.7	4.00	1.6			
90.9	100	40.9	99.5	18.4	77.4	8.27	35.4	3.72	1.0			

Source = Data:p25v004	Beam length = 2.2 mm	Model indp	D[v,0.5] 13.33µm
Record No. = 13	Log. Diff. = 4.799		
Focal length = 100 mm	Obscuration = 0.4263	Volume Conc. = 0.0852%	
Presentation = pil	Volume distribution	Sp.S.A 0.5925 m²/cc.	Shape C??

1598 pil 1DR459 / 0/ 0/0.00/1.00/
25% w/w salt soln
900 rpm

0000000000274

MALVERN Series 2600 SB.20 Master Mode 12 Feb 1998 4:14 pm

Particle diameters		Volume percentiles	
D(4,3)	13.59 µm	D[v,.10]	5.89
D(4,2)	11.73 µm	D[v,.20]	6.74
D(4,1)	10.20 µm	D[v,.30]	7.58
D(4,0)	9.03 µm	D[v,.40]	9.88
		D[v,.50]	13.33
D(3,2)	10.13 µm	D[v,.60]	15.05
D(3,1)	8.84 µm	D[v,.70]	16.80
D(3,0)	7.88 µm	D[v,.80]	19.06
		D[v,.90]	22.70
D(2,1)	7.71 µm	D[v,.99]	35.55
D(2,0)	6.96 µm		
		Span	1.26
D(1,0)	6.27 µm	Unif.	0.44

Distribution Moments.

Distbn	Mean	Stan.Dev.	Skewness
Volume	13.59	7.44	1.44
Surface	10.13	5.92	1.57
Length	7.71	4.31	2.14
Number	6.27	3.01	2.68

Source =Data:p25v004
Record 13

1598 pil 1DR459 / 0/ 0/0.00/1.00/
25% w/w salt soln
900 rpm

0000000000274

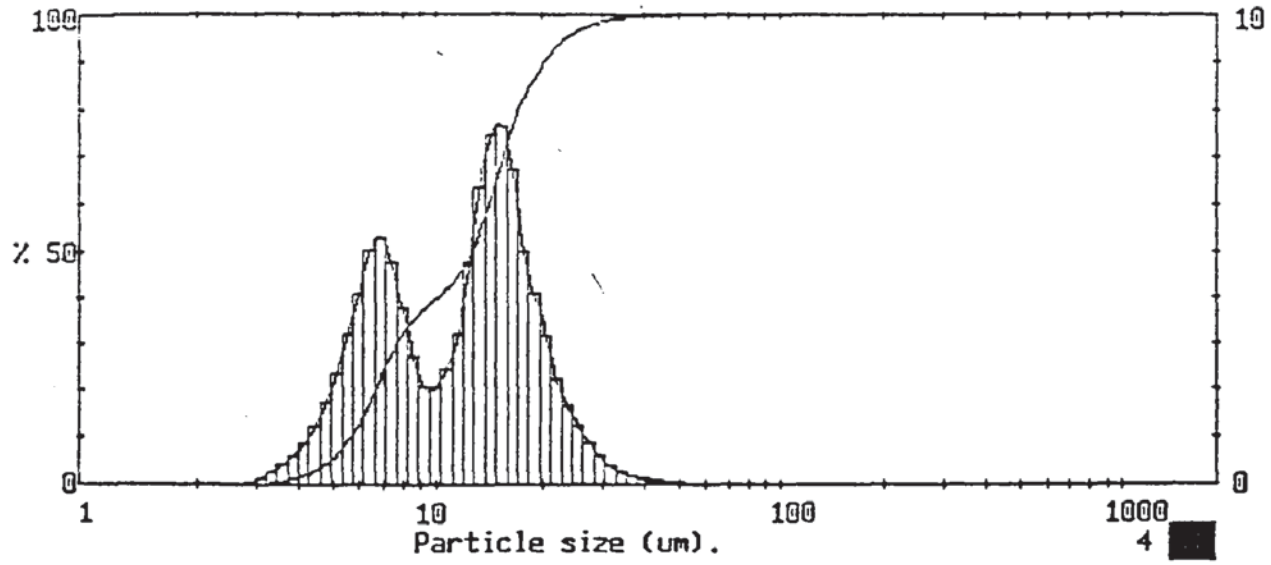

1598 pil IDR459 / 0/ 0/0.00/1.00/
25% w/w salt soln
1000 rpm

0000000000275

MALVERN Series 2600 SB.20 Master Mode 12 Feb 1998 4:37 pm

High Size	Under %	High Size	Under %	High Size	Under %	High Size	Under %	High Size	Under %	High Size	Under %	Span 1.16
188	100	84.5	100	38.0	99.6	17.1	79.8	7.69	30.3	3.46	0.4	D[4,3] 12.62µm
175	100	78.6	100	35.4	99.4	15.9	73.0	7.15	25.5	3.21	0.2	
163	100	73.1	100	32.9	99.2	14.8	65.4	6.65	20.2	2.99	0.0	D[3,2] 9.76µm
151	100	68.0	100	30.6	98.8	13.7	57.8	6.18	15.1	2.78	0.0	
141	100	63.2	100	28.4	98.2	12.8	51.5	5.75	11.0	2.59	0.0	D[v,0.9] 20.23µm
131	100	58.8	99.9	26.4	97.3	11.9	46.7	5.35	7.8	2.40	0.0	
122	100	54.7	99.9	24.6	96.0	11.1	43.5	4.97	5.4	2.24	0.0	
113	100	50.8	99.9	22.9	94.4	10.3	41.0	4.62	3.6	2.08	0.0	D[v,0.1] 5.63µm
105	100	47.3	99.9	21.3	92.1	9.56	38.9	4.30	2.4	1.93	0.0	
97.8	100	44.0	99.8	19.8	88.9	8.89	36.8	4.00	1.5			
90.9	100	40.9	99.7	18.4	84.8	8.27	34.1	3.72	0.9			

Source = Data:p25v004	Beam length = 2.2 mm	Model indp	D[v,0.5] 12.53µm
Record No. = 15	Log. Diff. = 4.661		
Focal length = 100 mm	Obscuration = 0.4788	Volume Conc. = 0.0963%	
Presentation = pil	Volume distribution	Sp.S.A 0.6145 m²/cc.	Shape OFF

1598 pil IDR459 / 0/ 0/0.00/1.00/
25% w/w salt soln
1000 rpm

0000000000275

MALVERN Series 2600 SB.20 Master Mode 12 Feb 1998 4:37 pm

Particle diameters		Volume percentiles		Distribution Moments.			
				Distbn	Mean	Stan.Dev.	Skewness
D(4,3)	12.62 µm	D[v,.10]	5.63				
D(4,2)	11.10 µm	D[v,.20]	6.63				
D(4,1)	9.79 µm	D[v,.30]	7.65	Volume	12.62	6.41	1.43
D(4,0)	8.75 µm	D[v,.40]	9.96	Surface	9.76	5.28	1.42
		D[v,.50]	12.53	Length	7.62	4.04	1.87
D(3,2)	9.76 µm	D[v,.60]	14.05	Number	6.24	2.93	2.39
D(3,1)	8.63 µm	D[v,.70]	15.44				
D(3,0)	7.75 µm	D[v,.80]	17.14				
		D[v,.90]	20.23				
D(2,1)	7.62 µm	D[v,.99]	31.67	Source =Data:p25v004			
D(2,0)	6.90 µm			Record 15			
		Span	1.17				
D(1,0)	6.24 µm	Unif.	0.40				

25% w/w and 0.05% v/v

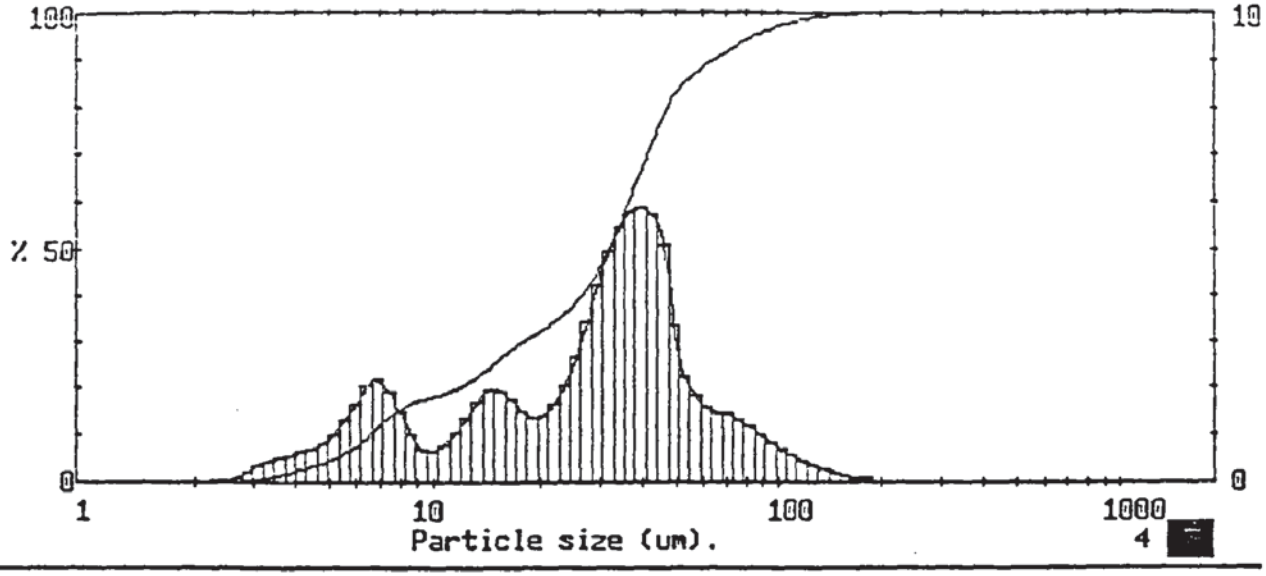

1598 pil 1DR459 / C/ 0/0.00/1.00/
25% w/w salt soln
400 rpm

0000000000276

MALVERN Series 2600 SB.20 Master Mode 13 Feb 1998 4:49 pm

High Size	Under %	High Size	Under %	High Size	Under %	High Size	Under %	High Size	Under %	High Size	Under %	Span 1.81
188	100	84.5	95.3	38.0	63.9	17.1	29.3	7.69	14.7	3.46	1.2	D[4,3] 33.94µm
175	99.9	78.6	94.1	35.4	58.1	15.9	27.5	7.15	12.8	3.21	0.8	
163	99.8	73.1	92.7	32.9	52.7	14.8	25.5	6.65	10.6	2.99	0.4	
151	99.7	68.0	91.3	30.6	47.7	13.7	23.6	6.18	8.5	2.78	0.2	D[3,2] 16.73µm
141	99.5	63.2	89.8	28.4	43.5	12.8	21.8	5.75	6.9	2.59	0.1	
131	99.2	58.8	88.2	26.4	40.0	11.9	20.5	5.35	5.5	2.40	0.0	
122	98.9	54.7	86.3	24.6	37.4	11.1	19.4	4.97	4.5	2.24	0.0	D[v,0.9] 63.89µm
113	98.4	50.8	84.1	22.9	35.3	10.3	18.6	4.62	3.7	2.08	0.0	
105	97.8	47.3	80.7	21.3	33.6	9.56	17.9	4.30	3.0	1.93	0.0	
97.8	97.1	44.0	75.6	19.8	32.2	8.89	17.2	4.00	2.3			D[v,0.1] 6.51µm
90.9	96.3	40.9	69.8	18.4	30.8	8.27	16.2	3.72	1.7			

Source = Data:p25v005	Beam length = 2.2 mm	Model indp	D[v,0.5] 31.65µm
Record No. = 2	Log. Diff. = 4.667		
Focal length = 100 mm	Obscuration = 0.1095	Volume Conc. = 0.0294%	
Presentation = pil	Volume distribution	Sp.S.A 0.3586 m²/cc.	Shape OFF

1598 pil 1DR459 / 0/ 0/0.00/1.00/
25% w/w salt soln
400 rpm

0000000000276

MALVERN Series 2600 SB.20 Master Mode 13 Feb 1998 4:49 pm

Particle diameters		Volume percentiles		Distribution Moments.			
				Distbn	Mean	Stan.Dev.	Skewness
D(4,3)	33.94 µm	D(v,.10)	6.51	Volume	33.94	25.26	1.63
D(4,2)	23.83 µm	D(v,.20)	11.55	Surface	16.73	15.97	2.21
D(4,1)	16.44 µm	D(v,.30)	17.68	Length	7.82	8.35	4.00
D(4,0)	12.17 µm	D(v,.40)	26.41	Number	4.94	3.77	5.86
		D(v,.50)	31.65				
D(3,2)	16.73 µm	D(v,.60)	36.20				
D(3,1)	11.44 µm	D(v,.70)	40.97				
D(3,0)	8.65 µm	D(v,.80)	46.77				
		D(v,.90)	63.89				
D(2,1)	7.82 µm	D(v,.99)	124.73	Source =Data:p25v005			
D(2,0)	6.22 µm			Record 2			
		Span	1.81				
D(1,0)	4.94 µm	Unif.	0.57				

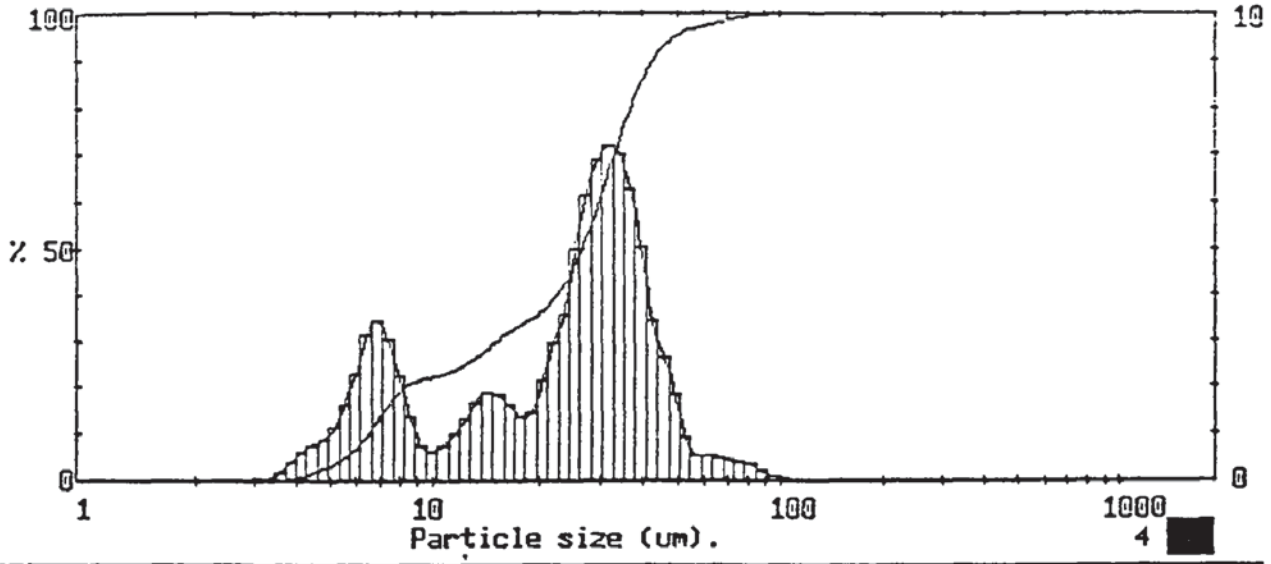

1598 pil IDR459 / 0/ 0/0.00/1.00/
25% w/w salt soln
500 rpm

0000000000277

MALVERN Series 2600 SB.20 Master Mode 13 Feb 1998 7:01 pm

High Size	Under %	High Size	Under %	High Size	Under %	High Size	Under %	High Size	Under %	High Size	Under %	Span 1.35
188	100	84.5	99.6	38.0	83.0	17.1	32.8	7.69	17.7	3.46	0.1	D[4,3] 25.61µm
175	100	78.6	99.3	35.4	76.7	15.9	31.2	7.15	14.6	3.21	0.0	
163	100	73.1	98.9	32.9	69.6	14.8	29.4	6.65	11.2	2.99	0.0	
151	100	68.0	98.5	30.6	62.4	13.7	27.5	6.18	8.1	2.78	0.0	D[3,2] 15.37µm
141	100	63.2	98.0	28.4	55.5	12.8	25.8	5.75	5.7	2.59	0.0	
131	100	58.8	97.4	26.4	49.4	11.9	24.5	5.35	4.1	2.40	0.0	
122	100	54.7	96.9	24.6	44.4	11.1	23.4	4.97	2.9	2.24	0.0	D[v,0.9] 42.45µm
113	100	50.8	96.0	22.9	40.8	10.3	22.7	4.62	2.1	2.08	0.0	
105	100	47.3	94.1	21.3	37.8	9.56	22.1	4.30	1.3	1.93	0.0	
97.8	99.9	44.0	91.5	19.8	35.7	8.89	21.3	4.00	0.7			D[v,0.1] 6.48µm
90.9	99.8	40.9	88.0	18.4	34.2	8.27	19.9	3.72	0.3			

Source = Data:p25v005	Beam length = 2.2 mm	Model indp	D[v,0.5] 26.64µm
Record No. = 4	Log. Diff. = 5.002		
Focal length = 100 mm	Obscuration = 0.1451	Volume Conc. = 0.0365%	Shape OFF
Presentation = pil	Volume distribution	Sp.S.A 0.3904 m²/cc.	

1598 pil IDR459 / 0/ 0/0.00/1.00/
25% w/w salt soln
500 rpm

0000000000277

MALVERN Series 2600 SB.20 Master Mode 13 Feb 1998 7:01 pm

Particle diameters		Volume percentiles	
D(4,3)	25.61 µm	D[v,.10]	6.48
D(4,2)	19.84 µm	D[v,.20]	8.29
D(4,1)	15.19 µm	D[v,.30]	15.15
D(4,0)	12.25 µm	D[v,.40]	22.44
		D[v,.50]	26.64
D(3,2)	15.37 µm	D[v,.60]	29.81
D(3,1)	11.69 µm	D[v,.70]	32.99
D(3,0)	9.58 µm	D[v,.80]	36.69
		D[v,.90]	42.45
D(2,1)	8.90 µm	D[v,.99]	74.47
D(2,0)	7.57 µm		
		Span	1.35
D(1,0)	6.44 µm	Unif.	0.45

Distribution Moments.			
Distbn	Mean	Stan.Dev.	Skewness
Volume	25.61	15.12	0.76
Surface	15.37	12.55	1.37
Length	8.90	7.59	2.89
Number	6.44	3.98	4.89

Source =Data:p25v005
Record 4

1598 pil IDR459 / 0/ 0/0.00/1.00/
25% w/w salt soln
500 rpm

0000000000277

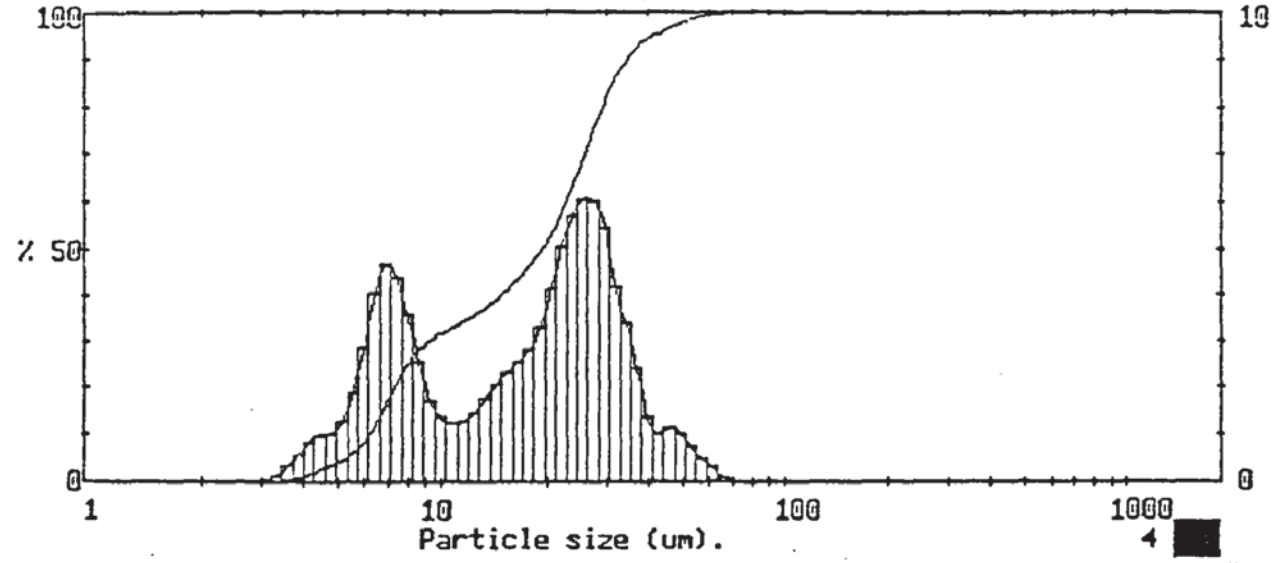

1598 pil 1DR459 / 0/ 0/0.00/1.00/
25% w/w salt soln
600 rpm
0000000000278

High Size	Under %	High Size	Under %	High Size	Under %	High Size	Under %	High Size	Under %	High Size	Under %	Span 1.46
188	100	84.5	99.9	38.0	93.7	17.1	45.1	7.69	23.2	3.46	0.2	D[4,3] 19.64µm
175	100	78.6	99.9	35.4	91.3	15.9	42.6	7.15	13.8	3.21	0.0	
163	100	73.1	99.9	32.9	87.9	14.8	40.2	6.65	14.1	2.99	0.0	
151	100	68.0	99.9	30.6	83.7	13.7	38.1	6.18	13.0	2.78	0.0	D[3,2] 12.48µm
141	100	63.2	99.8	28.4	78.2	12.8	36.4	5.75	7.2	2.59	0.0	
131	100	58.8	99.5	26.4	72.2	11.9	34.9	5.35	5.3	2.40	0.0	
122	100	54.7	99.0	24.6	66.2	11.1	33.6	4.97	4.0	2.24	0.0	D[v,0.9] 34.32µm
113	100	50.8	98.3	22.9	60.5	10.3	32.4	4.62	3.0	2.08	0.0	
105	100	47.3	97.3	21.3	55.4	9.56	31.1	4.30	2.0	1.93	0.0	
97.8	99.9	44.0	96.1	19.8	51.2	8.89	29.3	4.00	1.1			D[v,0.1] 6.18µm
90.9	99.9	40.9	95.1	18.4	47.9	8.27	26.8	3.72	0.5			

Source = Data:p25v005	Beam length = 2.2 mm	Model indy	D[v,0.5] 19.27µm
Record No. = 6	Log. Diff. = 4.927		
Focal length = 100 mm	Obscuration = 0.2966	Volume Conc. = 0.0665%	Shape OFF
Presentation = pil	Volume distribution	Sp.S.A 0.4309 m²/cc.	

1598 pil 1DR459 / 0/ 0/0.00/1.00/
25% w/w salt soln
600 rpm
0000000000278

Particle diameters		Volume percentiles	
D(4,3)	19.64 µm	D[v,.10]	6.18
D(4,2)	15.65 µm	D[v,.20]	7.29
D(4,1)	12.62 µm	D[v,.30]	9.12
D(4,0)	10.62 µm	D[v,.40]	14.68
		D[v,.50]	19.27
D(3,2)	12.48 µm	D[v,.60]	22.72
D(3,1)	10.12 µm	D[v,.70]	25.75
D(3,0)	8.65 µm	D[v,.80]	29.07
		D[v,.90]	34.32
D(2,1)	8.20 µm	D[v,.99]	54.53
D(2,0)	7.20 µm		
		Span	1.46
D(1,0)	6.33 µm	Unif.	0.51

Distribution Moments.

Distbn	Mean	Stan.Dev.	Skewness
Volume	19.64	12.21	1.11
Surface	12.43	9.46	1.64
Length	8.20	5.92	2.87
Number	6.33	3.44	4.13

Source =Data:p25v005
Record 6

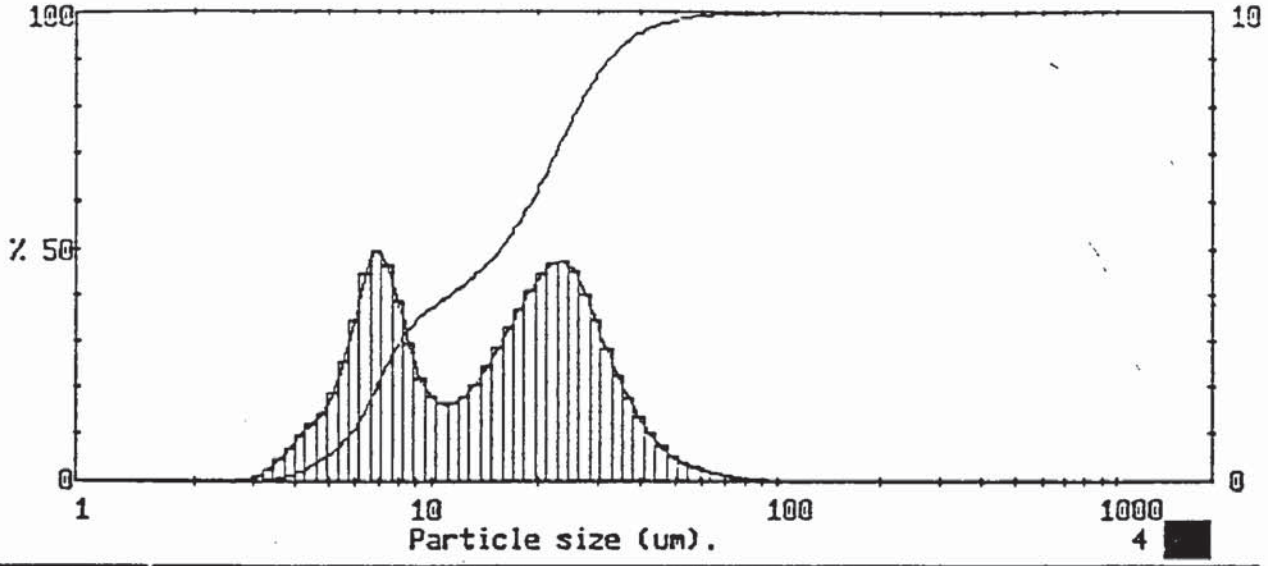

1598 pil 1DR459 / 0/ 0/0.00/1.00/
25% w/w salt soln
700 rpm
0000000000279

MALVERN Series 2600 SB.20 Master Mode 13 Feb 1998 8:01 pm

High Size	Under %	High Size	Under %	High Size	Under %	High Size	Under %	High Size	Under %	High Size	Under %	Span 1.70
188	100	84.5	99.8	38.0	94.8	17.1	54.2	7.69	27.3	3.46	0.5	D[4,3] 17.52µm
175	100	78.6	99.8	35.4	93.0	15.9	50.9	7.15	22.7	3.21	0.2	
163	100	73.1	99.7	32.9	90.8	14.8	48.0	6.65	17.7	2.99	0.1	D[3,2] 11.12µm
151	100	68.0	99.6	30.6	87.9	13.7	45.5	6.18	13.3	2.78	0.0	
141	100	63.2	99.4	28.4	84.5	12.8	43.5	5.75	9.8	2.59	0.0	
131	100	58.8	99.2	26.4	80.4	11.9	41.6	5.35	7.2	2.40	0.0	
122	99.9	54.7	98.9	24.6	75.9	11.1	40.0	4.97	5.4	2.24	0.0	D[v,0.9] 32.19µm
113	99.9	50.8	98.5	22.9	71.2	10.3	38.3	4.62	3.9	2.08	0.0	
105	99.9	47.3	97.9	21.3	66.5	9.56	36.5	4.30	2.6	1.93	0.0	
97.8	99.9	44.0	97.2	19.8	62.0	8.89	34.2	4.00	1.7			D[v,0.1] 5.78µm
90.9	99.9	40.9	96.2	18.4	57.9	8.27	31.3	3.72	0.9			

Source = Data:p25v005	Beam length = 2.2 mm	Model indp	D[v,0.5] 15.57µm
Record No. = 7	Log. Diff. = 4.764		
Focal length = 100 mm	Obscuration = 0.3683	Volume Conc. = 0.0774%	
Presentation = pil	Volume distribution	Sp.S.A 0.5395 m²/cc.	Shape 0??

1598 pil 1DR459 / 0/ 0/0.00/1.00/
25% w/w salt soln
700 rpm
0000000000279

MALVERN Series 2600 SB.20 Master Mode 13 Feb 1998 8:01 pm

Particle diameters		Volume percentiles		Distribution Moments.			
D(4,3)	17.52 µm	D[v,.10]	5.78	Distbn	Mean	Stan.Dev.	Skewness
D(4,2)	13.96 µm	D[v,.20]	6.87				
D(4,1)	11.41 µm	D[v,.30]	8.06	Volume	17.52	12.21	2.07
D(4,0)	9.72 µm	D[v,.40]	11.08	Surface	11.12	8.44	2.20
		D[v,.50]	15.57	Length	7.62	5.16	3.14
D(3,2)	11.12 µm	D[v,.60]	19.09	Number	6.00	3.12	3.88
D(3,1)	9.21 µm	D[v,.70]	22.45				
D(3,0)	7.98 µm	D[v,.80]	26.24				
		D[v,.90]	32.19				
D(2,1)	7.62 µm	D[v,.99]	56.26	Source =Data:p25v005			
D(2,0)	6.76 µm			Record 7			
		Span	1.70				
D(1,0)	6.00 µm	Unif.	0.60				

1598 pil 1DR459 / 0/ 0/0.00/1.00/
25% w/w salt soln
700 rpm
0000000000279

MALVERN Series 2600 SB.20 Master Mode 13 Feb 1998 8:15 pm

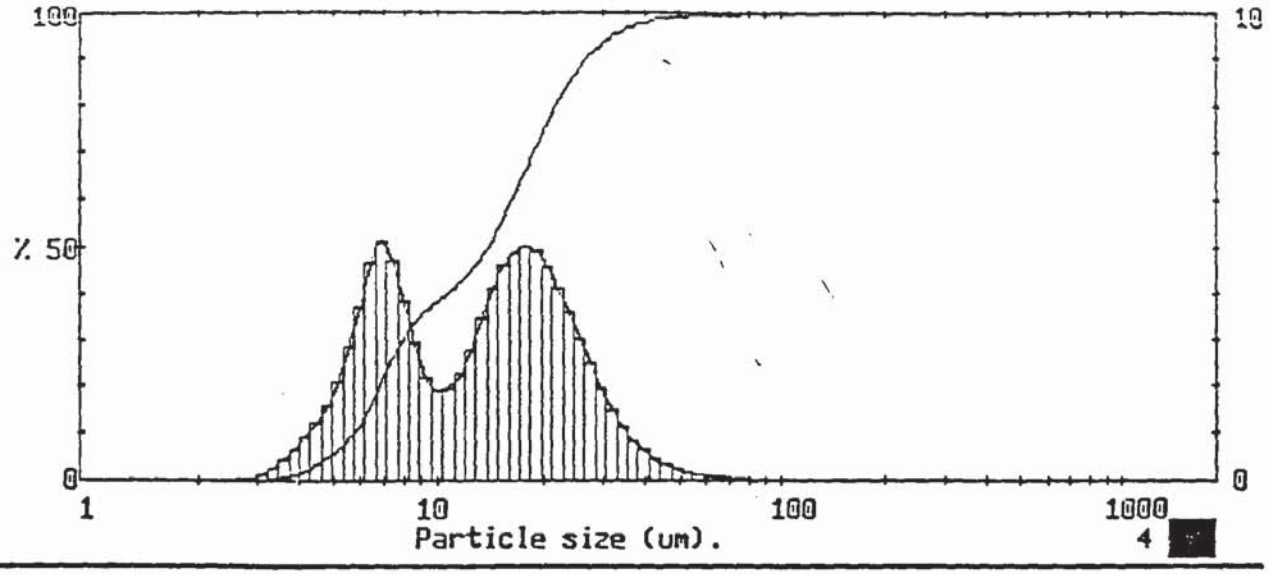

1598 pil IDR459 / 0/ 0/0.00/1.00/
25% w/w salt soln
800 rpm
0000000000280

MALVERN Series 2600 SB.20 Master Mode 13 Feb 1998 8:15 pm

High Size	Under %	High Size	Under %	High Size	Under %	High Size	Under %	High Size	Under %	High Size	Under %	Span 1.54
188	100	84.5	99.9	38.0	97.6	17.1	64.1	7.69	28.7	3.46	0.5	D[4,3] 15.12µm
175	100	78.6	99.9	35.4	96.7	15.9	59.2	7.15	24.0	3.21	0.2	
163	100	73.1	99.9	32.9	95.6	14.8	54.5	6.65	18.8	2.99	0.1	
151	100	68.0	99.8	30.6	94.1	13.7	50.3	6.18	14.1	2.78	0.0	D[3,2] 10.45µm
141	100	63.2	99.7	28.4	92.1	12.8	46.8	5.75	10.4	2.59	0.0	
131	100	58.8	99.6	26.4	89.6	11.9	44.0	5.35	7.5	2.40	0.0	
122	100	54.7	99.5	24.6	86.5	11.1	41.7	4.97	5.4	2.24	0.0	D[v,0.9] 26.73µm
113	100	50.8	99.3	22.9	82.9	10.3	39.7	4.62	3.8	2.08	0.0	
105	100	47.3	99.0	21.3	78.7	9.56	37.8	4.30	2.6	1.93	0.0	
97.8	100	44.0	98.7	19.8	74.1	8.89	35.6	4.00	1.6			D[v,0.1] 5.70µm
90.9	99.9	40.9	98.2	18.4	69.1	8.27	32.6	3.72	1.0			

Source = Data:p25v005	Beam length = 2.2 mm	Model indp	D[v,0.5] 13.66µm
Record No. = 8	Log. Diff. = 4.815		
Focal length = 100 mm	Obscuration = 0.4707	Volume Conc. = 0.1007%	
Presentation = pil	Volume distribution	Sp.S.A 0.5741 m²/cc.	Shape OFF

1598 pil IDR459 / 0/ 0/0.00/1.00/
25% w/w salt soln
800 rpm
0000000000280

MALVERN Series 2600 SB.20 Master Mode 13 Feb 1998 8:15 pm

Particle diameters		Volume percentiles	
D(4,3)	15.12 µm	D[v,.10]	5.70
D(4,2)	12.57 µm	D[v,.20]	6.76
D(4,1)	10.63 µm	D[v,.30]	7.86
D(4,0)	9.25 µm	D[v,.40]	10.39
		D[v,.50]	13.66
D(3,2)	10.45 µm	D[v,.60]	16.10
D(3,1)	8.92 µm	D[v,.70]	18.62
D(3,0)	7.85 µm	D[v,.80]	21.73
		D[v,.90]	26.73
D(2,1)	7.61 µm	D[v,.99]	46.71
D(2,0)	6.80 µm		
		Span	1.54
D(1,0)	6.08 µm	Unif.	0.53

Distribution Moments.

Distbn	Mean	Stan.Dev.	Skewness
Volume	15.12	9.81	2.35
Surface	10.45	6.98	2.13
Length	7.61	4.65	2.66
Number	6.08	3.05	3.15

Source =Data:p25v005
Record 8

1598 pil IDR459 / 0/ 0/0.00/1.00/
25% w/w salt soln
800 rpm
0000000000280

25% w/w and 0.06% v/v

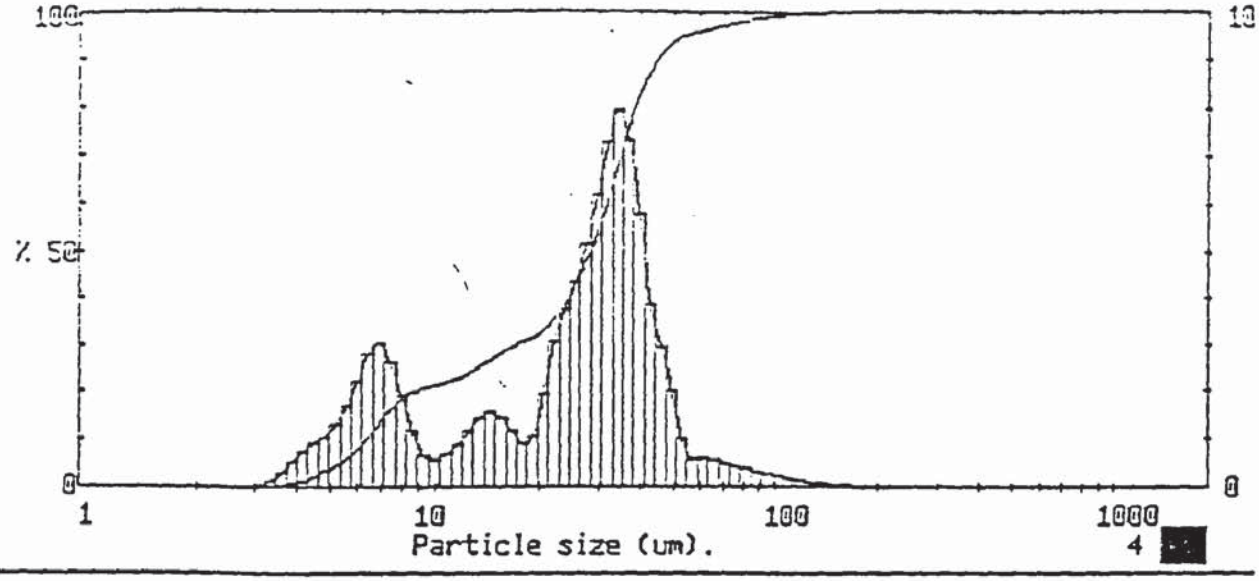

1598 pil IDR459 / 0/ 0/0.00/1.00/
25% w/w salt soln
500 rpm

0000000000282

MALVERN Series 2600 SB.20 Master Mode 16 Feb 1998 7:25 pm

High Size	Under %	High Size	Under %	High Size	Under %	High Size	Under %	High Size	Under %	High Size	Under %	Span 1.36
188	100	84.5	98.6	38.0	79.8	17.1	30.5	7.69	17.6	3.46	0.2	D(4,3) 27.46µm
175	100	78.6	98.2	35.4	72.5	15.9	29.3	7.15	15.0	3.21	0.1	
163	100	73.1	97.8	32.9	64.5	14.8	27.8	6.65	11.9	2.99	0.0	D(3,2) 15.63µm
151	99.9	68.0	97.3	30.6	57.2	13.7	26.2	6.18	9.1	2.78	0.0	
141	99.9	63.2	96.7	28.4	51.0	12.8	24.7	5.75	6.8	2.59	0.0	
131	99.8	58.8	96.1	26.4	45.8	11.9	23.6	5.35	5.1	2.40	0.0	D(v,0.9) 44.46µm
122	99.7	54.7	95.5	24.6	41.4	11.1	22.7	4.97	3.8	2.24	0.0	
113	99.6	50.8	94.5	22.9	37.6	10.3	22.0	4.62	2.7	2.08	0.0	
105	99.4	47.3	92.5	21.3	34.5	9.56	21.4	4.30	1.8	1.93	0.0	D(v,0.1) 6.34µm
97.8	99.2	44.0	89.5	19.8	32.5	8.89	20.7	4.00	1.0			
90.9	98.9	40.9	85.6	18.4	31.4	8.27	19.5	3.72	0.5			

Source = Data:p25v006	Beam length = 2.2 mm	Model indp	D(v,0.5) 28.06µm
Record No. = 5	Log. Diff. = 4.852		
Focal length = 100 mm	Obscuration = 0.2803	Volume Conc. = 0.0730%	Shape 079
Presentation = pil	Volume distribution	Sp.S.A 0.3838 m²/cc.	

1598 pil IDR459 / 0/ 0/0.00/1.00/
25% w/w salt soln
500 rpm

0000000000282

MALVERN Series 2600 SB.20 Master Mode 16 Feb 1998 7:25 pm

Particle diameters		Volume percentiles		Distribution Moments.			
				Distbn	Mean	Stan.Dev.	Skewness
D(4,3)	27.46 µm	D(v,.10)	6.34	Volume	27.46	17.84	1.66
D(4,2)	20.72 µm	D(v,.20)	8.46	Surface	15.63	13.60	1.70
D(4,1)	15.42 µm	D(v,.30)	16.59	Length	8.54	7.78	3.17
D(4,0)	12.21 µm	D(v,.40)	23.97	Number	6.07	3.88	5.38
		D(v,.50)	28.06				
D(3,2)	15.63 µm	D(v,.60)	31.48				
D(3,1)	11.56 µm	D(v,.70)	34.57				
D(3,0)	9.32 µm	D(v,.80)	38.10				
		D(v,.90)	44.46				
D(2,1)	8.54 µm	D(v,.99)	92.44	Source =Data:p25v006			
D(2,0)	7.20 µm			Record 5			
		Span	1.36				
D(1,0)	6.07 µm	Unif.	0.46				

1598 pil IDR459 / 0/ 0/0.00/1.00/
25% w/w salt soln
500 rpm

0000000000282

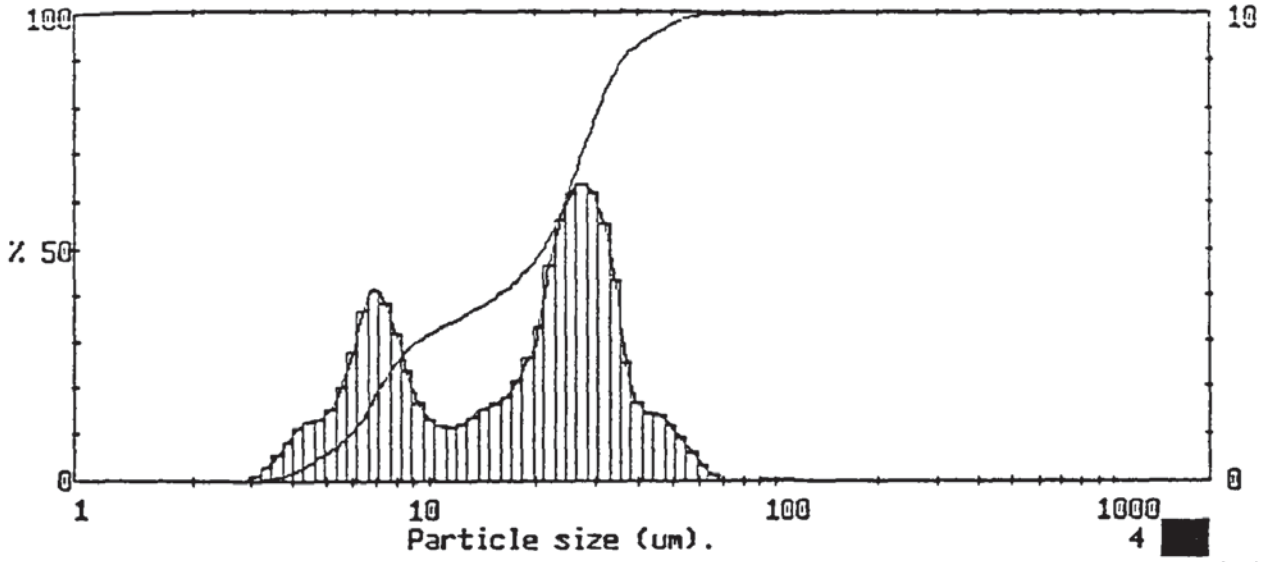

1598 pil lDR459 / 0/ 0/0.00/1.00/
25% w/w salt soln
600 rpm
0000000000283

MALVERN Series 2600 SB.20 Master Mode 16 Feb 1998 7:55 pm

High Size	Under %	High Size	Under %	High Size	Under %	High Size	Under %	High Size	Under %	High Size	Under %	Span 1.42
188	100	84.5	99.8	38.0	92.0	17.1	42.4	7.69	23.8	3.46	0.5	D[4,3] 20.69µm
175	100	78.6	99.8	35.4	89.4	15.9	40.6	7.15	19.9	3.21	0.1	
163	100	73.1	99.8	32.9	85.1	14.8	38.9	6.65	15.7	2.99	0.0	D[3,2] 12.41µm
151	100	68.0	99.8	30.6	79.6	13.7	37.3	6.18	12.1	2.78	0.0	
141	100	63.2	99.7	28.4	73.4	12.8	35.9	5.75	9.3	2.59	0.0	D[v,0.9] 35.79µm
131	99.9	58.8	99.3	26.4	67.0	11.9	34.7	5.35	7.2	2.40	0.0	
122	99.9	54.7	98.7	24.6	60.8	11.1	33.6	4.97	5.7	2.24	0.0	D[v,0.1] 5.87µm
113	99.9	50.8	97.8	22.9	55.2	10.3	32.4	4.62	4.3	2.08	0.0	
105	99.9	47.3	96.6	21.3	50.5	9.56	31.0	4.30	3.0	1.93	0.0	D[v,0.5] 21.05µm
97.8	99.9	44.0	95.2	19.8	47.2	8.89	29.3	4.00	1.9			
90.9	99.8	40.9	93.7	18.4	44.6	8.27	27.0	3.72	1.0			Shape OFF

Source = Data:p25v006	Beam length = 2.2 mm	Model indp
Record No. = 8	Log. Diff. = 4.696	
Focal length = 100 mm	Obscuration = 0.4168	Volume Conc. = 0.1014%
Presentation = pil	Volume distribution	Sp.S.A 0.4834 m²/cc.

1598 pil lDR459 / 0/ 0/0.00/1.00/
25% w/w salt soln
600 rpm
0000000000283

MALVERN Series 2600 SB.20 Master Mode 16 Feb 1998 7:55 pm

Particle diameters		Volume percentiles	
D(4,3)	20.69 µm	D[v,.10]	5.87
D(4,2)	16.02 µm	D[v,.20]	7.16
D(4,1)	12.56 µm	D[v,.30]	9.12
D(4,0)	10.37 µm	D[v,.40]	15.53
		D[v,.50]	21.05
D(3,2)	12.41 µm	D[v,.60]	24.34
D(3,1)	9.78 µm	D[v,.70]	27.36
D(3,0)	8.23 µm	D[v,.80]	30.73
		D[v,.90]	35.79
D(2,1)	7.71 µm	D[v,.99]	56.33
D(2,0)	6.71 µm		
		Span	1.42
D(1,0)	5.83 µm	Unif.	0.51

Distribution Moments.

Distbn	Mean	Stan.Dev.	Skewness
Volume	20.69	13.37	1.41
Surface	12.41	10.13	1.72
Length	7.71	6.02	3.13
Number	5.83	3.31	4.65

Source =Data:p25v006
Record 8

1598 pil lDR459 / 0/ 0/0.00/1.00/
25% w/w salt soln
600 rpm
0000000000283

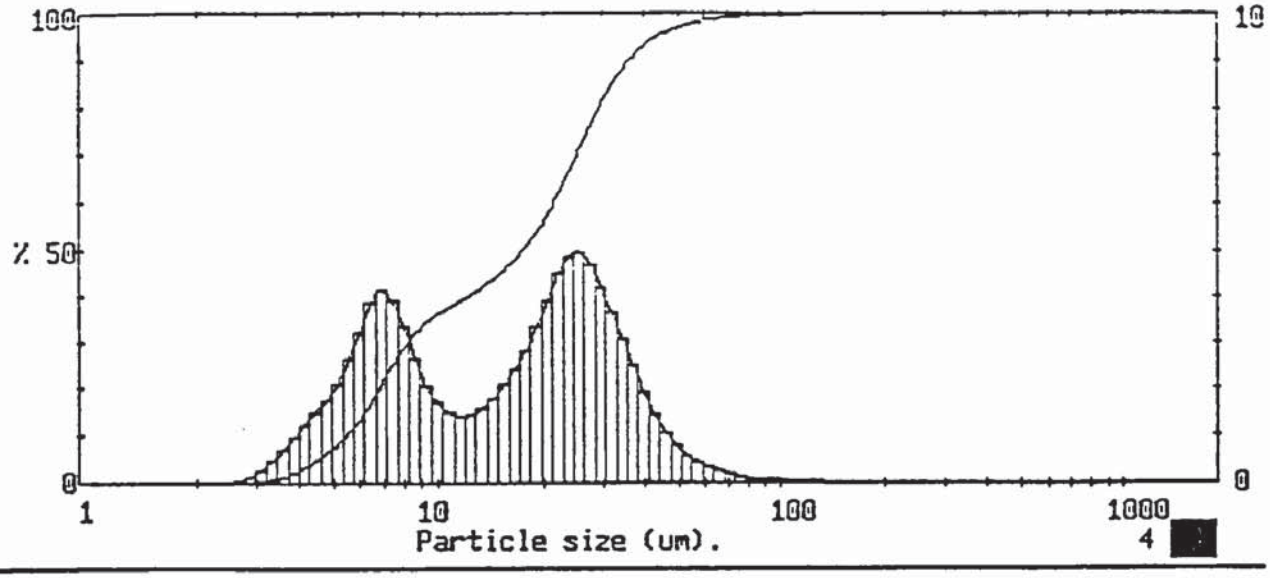

1598 pil IDR459 / 0/ 0/0.00/1.00/
25% w/w salt soln
700 rpm

0000000000284

MALVERN Series 2600 S8.20 Master Mode 16 Feb 1998 8:01 pm

High Size	Under %	High Size	Under %	High Size	Under %	High Size	Under %	High Size	Under %	High Size	Under %	Span 1.74
188	100	84.5	99.6	38.0	92.2	17.1	49.4	7.69	27.3	3.46	1.0	D[4,3] 19.23µm
175	100	78.6	99.5	35.4	89.7	15.9	47.0	7.15	23.3	3.21	0.5	
163	100	73.1	99.3	32.9	86.6	14.8	44.9	6.65	19.2	2.99	0.2	
151	100	68.0	99.1	30.6	82.9	13.7	43.0	6.18	15.3	2.78	0.1	D[3,2] 11.23µm
141	100	63.2	98.9	28.4	78.7	12.8	41.4	5.75	12.0	2.59	0.0	
131	99.9	58.8	98.5	26.4	74.0	11.9	40.0	5.35	9.4	2.40	0.0	
122	99.9	54.7	98.0	24.6	69.0	11.1	38.6	4.97	7.2	2.24	0.0	D[v,0.9] 35.66µm
113	99.9	50.8	97.5	22.9	64.1	10.3	37.1	4.62	5.4	2.08	0.0	
105	99.8	47.3	96.7	21.3	59.6	9.56	35.4	4.30	3.9	1.93	0.0	
97.8	99.8	44.0	95.6	19.8	55.6	8.89	33.3	4.00	2.7			D[v,0.1] 5.45µm
90.9	99.7	40.9	94.1	18.4	52.3	8.27	30.6	3.72	1.7			

Source = Data:p25v006	Beam length = 2.2 mm	Model indp	D[v,0.5] 17.37µm
Record No. = 9	Log. Diff. = 4.486		
Focal length = 100 mm	Obscuration = 0.4645	Volume Conc. = 0.1062%	Shape OFF
Presentation = pil	Volume distribution	Sp.S.A 0.5344 m²/cc.	

1598 pil IDR459 / 0/ 0/0.00/1.00/
25% w/w salt soln
700 rpm

0000000000284

MALVERN Series 2600 S8.20 Master Mode 16 Feb 1998 8:01 pm

Particle diameters		Volume percentiles	
D(4,3)	19.23 µm	D[v,.10]	5.45
D(4,2)	14.69 µm	D[v,.20]	6.75
D(4,1)	11.56 µm	D[v,.30]	8.15
D(4,0)	9.59 µm	D[v,.40]	11.89
		D[v,.50]	17.37
D(3,2)	11.23 µm	D[v,.60]	21.41
D(3,1)	8.97 µm	D[v,.70]	24.95
D(3,0)	7.61 µm	D[v,.80]	29.06
		D[v,.90]	35.66
D(2,1)	7.16 µm	D[v,.99]	65.36
D(2,0)	6.26 µm		
		Span	1.74
D(1,0)	5.48 µm	Unif.	0.62

Distribution Moments.

Distbn	Mean	Stan.Dev.	Skewness
Volume	19.23	14.20	2.02
Surface	11.23	9.48	2.32
Length	7.16	5.40	3.52
Number	5.48	3.04	4.45

Source =Data:p25v006
Record 9

1598 pil IDR459 / 0/ 0/0.00/1.00/
25% w/w salt soln
700 rpm

0000000000284

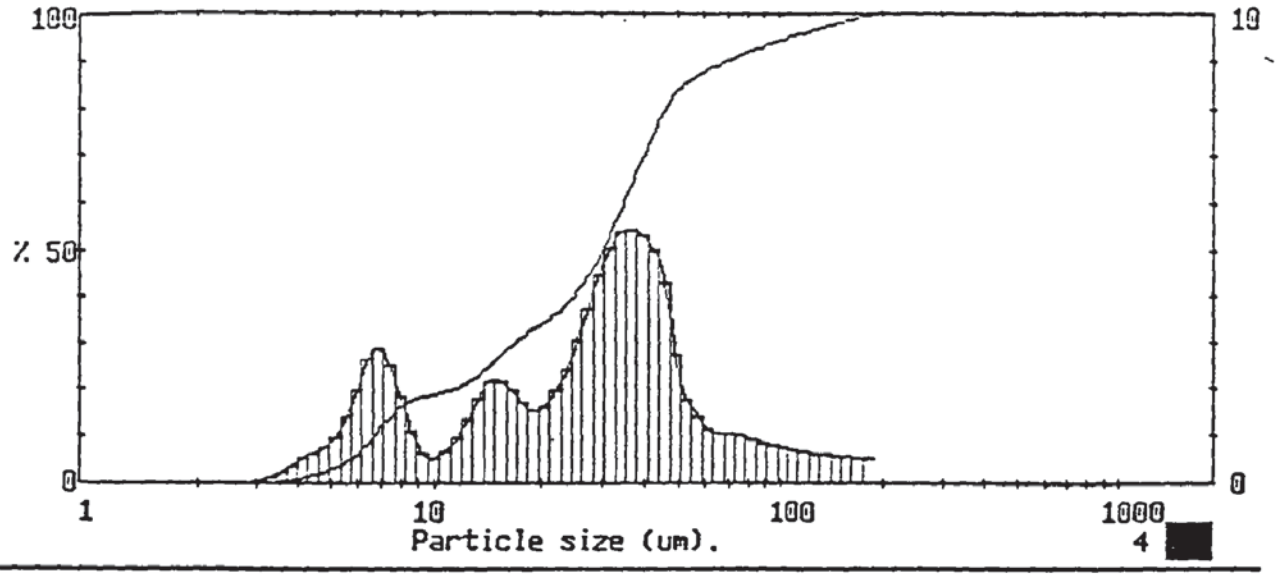

1598 pil lDR459 / 0/ 0/0.00/1.00/
25% w/w salt soln
800 rpm

0000000000281

MALVERN Series 2600 SB.20 Master Mode 16 Feb 1998 5:50 pm

High Size	Under %	High Size	Under %	High Size	Under %	High Size	Under %	High Size	Under %	High Size	Under %	Span 2.07
188	100	84.5	92.8	38.0	66.9	17.1	30.4	7.69	15.2	3.46	0.2	D[4,3] 35.35µm
175	99.5	78.6	91.8	35.4	61.5	15.9	28.5	7.15	12.7	3.21	0.1	
163	98.9	73.1	90.8	32.9	56.1	14.8	26.3	6.65	9.8	2.99	0.0	
151	98.4	68.0	89.8	30.6	51.1	13.7	24.1	6.18	7.1	2.78	0.0	D[3,2] 17.16µm
141	97.8	63.2	88.7	28.4	46.6	12.8	22.3	5.75	5.1	2.59	0.0	
131	97.2	58.8	87.6	26.4	42.8	11.9	20.9	5.35	3.7	2.40	0.0	
122	96.6	54.7	86.1	24.6	39.8	11.1	19.9	4.97	2.7	2.24	0.0	D[v,0.9] 69.00µm
113	95.9	50.8	84.3	22.9	37.3	10.3	19.3	4.62	2.0	2.08	0.0	
105	95.2	47.3	81.6	21.3	35.3	9.56	18.8	4.30	1.4	1.93	0.0	
97.8	94.4	44.0	77.3	19.8	33.7	8.89	18.2	4.00	0.8			D[v,0.1] 6.69µm
90.9	93.6	40.9	72.3	18.4	32.2	8.27	17.0	3.72	0.5			

Source = Data:p25v006	Beam length = 2.2 mm	Model indp	D[v,0.5] 30.09µm
Record No. = 1	Log. Diff. = 5.197		
Focal length = 100 mm	Obscuration = 0.1609	Volume Conc. = 0.0456%	
Presentation = pil	Volume distribution	Sp.S.A 0.3497 m²/cc.	Shape OFF

1598 pil lDR459 / 0/ 0/0.00/1.00/
25% w/w salt soln
800 rpm

0000000000281

MALVERN Series 2600 SB.20 Master Mode 16 Feb 1998 5:50 pm

Particle diameters		Volume percentiles		Distribution Moments.			
D(4,3)	35.35 µm	D[v,.10]	6.69	Distbn	Mean	Stan.Dev.	Skewness
D(4,2)	24.63 µm	D[v,.20]	11.12				
D(4,1)	17.56 µm	D[v,.30]	16.80	Volume	35.35	31.17	2.17
D(4,0)	13.56 µm	D[v,.40]	24.74	Surface	17.16	17.67	3.08
		D[v,.50]	30.09	Length	8.94	8.57	4.35
D(3,2)	17.16 µm	D[v,.60]	34.66	Number	6.24	4.10	5.78
D(3,1)	12.38 µm	D[v,.70]	39.63				
D(3,0)	9.85 µm	D[v,.80]	45.93				
		D[v,.90]	69.00				
D(2,1)	8.94 µm	D[v,.99]	164.36	Source =Data:p25v006			
D(2,0)	7.47 µm			Record 1			
		Span	2.07				
D(1,0)	6.24 µm	Unif.	0.67				

1598 pil lDR459 / 0/ 0/0.00/1.00/
25% w/w salt soln
800 rpm

0000000000281

25% w/w and 0.07% v/v

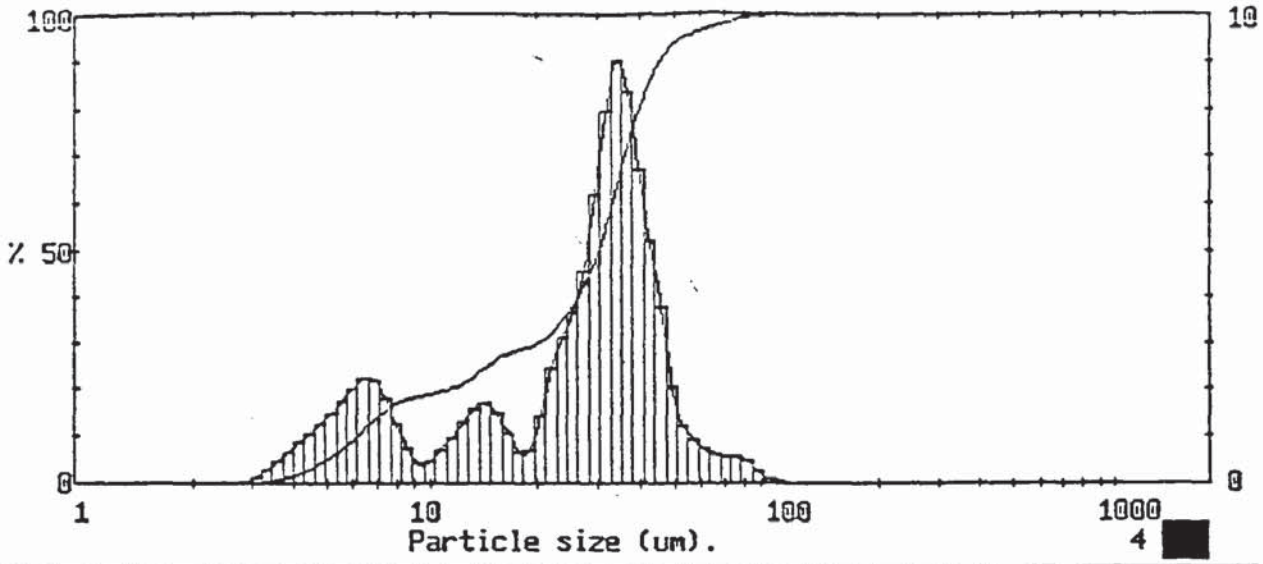

1598 pil 1DR459 / 0/ 0/0.00/1.00/
25% w/w salt soln
500 rpm

0000000000285

MALVERN Series 2600 SB.20 Master Mode 17 Feb 1998 5:28 pm

High Size	Under %	High Size	Under %	High Size	Under %	High Size	Under %	High Size	Under %	High Size	Under %	Span 1.29
188	100	84.5	99.6	38.0	76.6	17.1	28.2	7.69	15.4	3.46	0.5	D[4,3] 28.25µm
175	100	78.6	99.1	35.4	68.2	15.9	27.2	7.15	14.6	3.21	0.2	
163	100	73.1	98.5	32.9	59.1	14.8	25.7	6.65	12.4	2.99	0.1	D[3,2] 16.09µm
151	100	68.0	98.0	30.6	51.2	13.7	23.9	6.18	10.1	2.78	0.0	
141	100	63.2	97.3	28.4	45.0	12.8	22.3	5.75	8.1	2.59	0.0	
131	100	58.8	96.6	26.4	40.4	11.9	21.0	5.35	6.4	2.40	0.0	D[v,0.9] 45.08µm
122	100	54.7	95.6	24.6	36.7	11.1	20.0	4.97	4.8	2.24	0.0	
113	100	50.8	94.4	22.9	33.6	10.3	19.3	4.62	3.6	2.08	0.0	
105	100	47.3	92.3	21.3	31.1	9.56	18.8	4.30	2.5	1.93	0.0	D[v,0.1] 6.16µm
97.8	100	44.0	88.5	19.8	29.6	8.89	18.4	4.00	1.6			
90.9	99.9	40.9	83.3	18.4	28.9	8.27	17.7	3.72	1.0			

Source = Data:p25v007	Beam length = 2.2 mm	Model indp	D[v,0.5] 30.20µm
Record No. = 2	Log. Diff. = 4.513		
Focal length = 100 mm	Obscuration = 0.3433	Volume Conc. = 0.1027%	Shape OFF
Presentation = pil	Volume distribution	Sp.S.A 0.3729 m²/cc.	

1598 pil 1DR459 / 0/ 0/0.00/1.00/
25% w/w salt soln
500 rpm

0000000000285

MALVERN Series 2600 SB.20 Master Mode 17 Feb 1998 5:28 pm

Particle diameters		Volume percentiles	
D(4,3)	28.25 µm	D[v,.10]	6.16
D(4,2)	21.32 µm	D[v,.20]	11.03
D(4,1)	15.50 µm	D[v,.30]	20.25
D(4,0)	12.01 µm	D[v,.40]	26.25
		D[v,.50]	30.20
D(3,2)	16.09 µm	D[v,.60]	33.11
D(3,1)	11.49 µm	D[v,.70]	35.88
D(3,0)	9.03 µm	D[v,.80]	39.36
		D[v,.90]	45.08
D(2,1)	8.20 µm	D[v,.99]	77.52
D(2,0)	6.77 µm		
		Span	1.29
D(1,0)	5.58 µm	Unif.	0.41

Distribution Moments.

Distbn	Mean	Stan.Dev.	Skewness
Volume	23.25	15.94	0.52
Surface	15.09	13.99	1.21
Length	8.20	8.04	3.04
Number	5.58	3.82	5.70

Source =Data:p25v007
Record 2

1598 pil 1DR459 / 0/ 0/0.00/1.00/
25% w/w salt soln
500 rpm

0000000000285

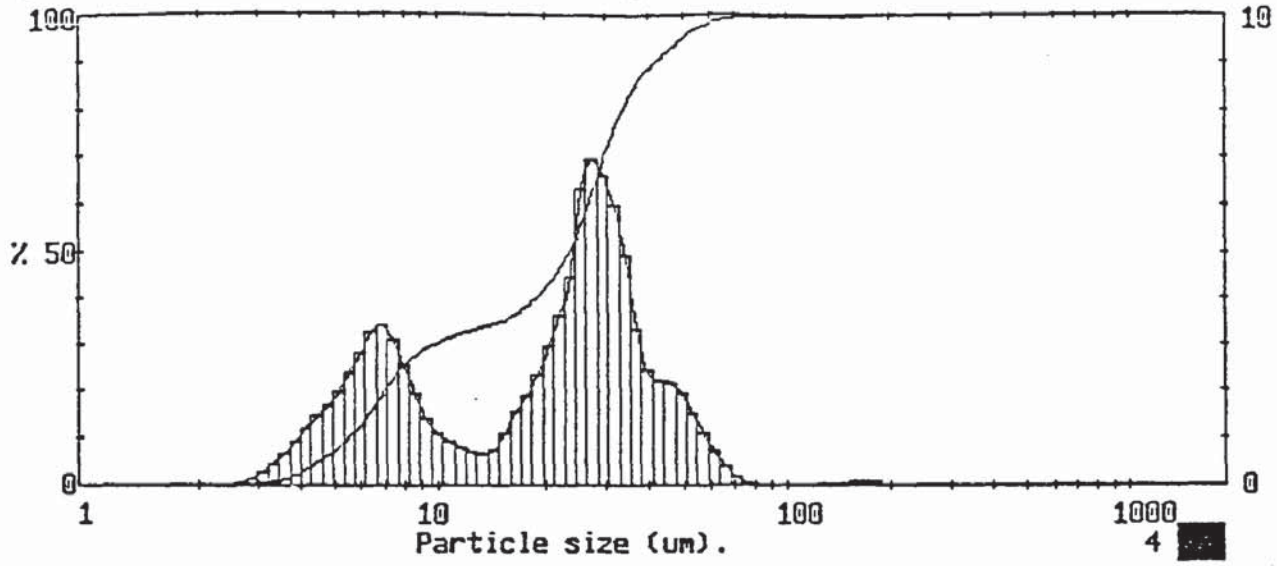

1598 pil lDR459 / 0/ 0/0.00/1.00/
25% w/w salt soln
600 rpm

0000000000286

MALVERN Series 2600 SB.20 Master Mode 17 Feb 1998 6:15 pm

High Size	Under %	High Size	Under %	High Size	Under %	High Size	Under %	High Size	Under %	High Size	Under %	Span 1.54
188	100	84.5	99.6	38.0	86.8	17.1	37.4	7.69	23.9	3.46	1.0	D[4,3] 23.17µm
175	99.9	78.6	99.6	35.4	83.5	15.9	35.9	7.15	20.8	3.21	0.5	
163	99.8	73.1	99.5	32.9	78.6	14.8	34.8	6.65	17.4	2.99	0.2	
151	99.8	68.0	99.4	30.6	72.6	13.7	34.0	6.18	14.1	2.78	0.1	D[3,2] 12.69µm
141	99.7	63.2	98.9	28.4	66.0	12.8	33.3	5.75	11.3	2.59	0.0	
131	99.6	58.8	98.2	26.4	59.1	11.9	32.6	5.35	8.9	2.40	0.0	
122	99.6	54.7	97.1	24.6	52.7	11.1	31.8	4.97	6.9	2.24	0.0	D[v,0.9] 41.87µm
113	99.6	50.8	95.6	22.9	48.3	10.3	30.9	4.62	5.2	2.08	0.0	
105	99.6	47.3	93.7	21.3	44.6	9.56	29.8	4.30	3.8	1.93	0.0	
97.8	99.6	44.0	91.5	19.8	41.7	8.89	28.4	4.00	2.6			D[v,0.1] 5.53µm
90.9	99.6	40.9	89.3	18.4	39.3	8.27	26.5	3.72	1.7			

Source = Data:p25v007	Beam length = 2.2 mm	Model indp	D[v,0.5] 23.59µm
Record No. = 4	Log. Diff. = 4.430		
Focal length = 100 mm	Obscuration = 0.4566	Volume Conc. = 0.1172%	Shape OFF
Presentation = pil	Volume distribution	Sp.S.A 0.4726 m²/cc.	

1598 pil lDR459 / 0/ 0/0.00/1.00/
25% w/w salt soln
600 rpm

0000000000286

MALVERN Series 2600 SB.20 Master Mode 17 Feb 1998 6:15 pm

Particle diameters		Volume percentiles	
D(4,3)	23.17 µm	D[v,.10]	5.53
D(4,2)	17.15 µm	D[v,.20]	7.03
D(4,1)	12.86 µm	D[v,.30]	9.67
D(4,0)	10.31 µm	D[v,.40]	18.80
		D[v,.50]	23.59
D(3,2)	12.69 µm	D[v,.60]	26.70
D(3,1)	9.58 µm	D[v,.70]	29.69
D(3,0)	7.87 µm	D[v,.80]	33.50
		D[v,.90]	41.87
D(2,1)	7.23 µm	D[v,.99]	63.68
D(2,0)	6.20 µm		
		Span	1.54
D(1,0)	5.32 µm	Unif.	0.52

Distribution Moments.

Distbn	Mean	Stan.Dev.	Skewness
Volume	23.17	16.59	2.40
Surface	12.69	11.53	2.09
Length	7.23	6.29	3.59
Number	5.32	3.19	5.40

Source =Data:p25v007
Record 4

1598 pil lDR459 / 0/ 0/0.00/1.00/
25% w/w salt soln
600 rpm

0000000000286

30% w/w and 0.04% v/v

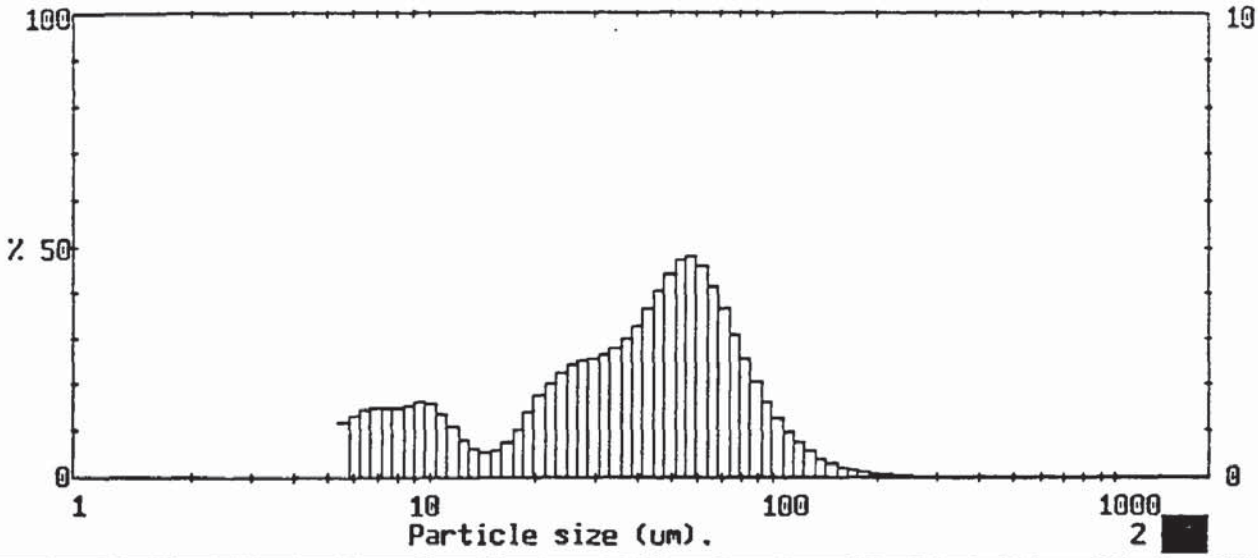

1598 pil 1DR459 / 0/ 0/0.00/1.00/
30% W/W salt Soln
500 rpm
000000368

MALVERN Series 2600 SB.20 Master Mode 24 Feb 1998 1:02 pm

High Size	Under %	High Size	Under %	High Size	Under %	High Size	Under %	High Size	Under %	High Size	Under %	Span 1.88
564	100	254	99.9	114	97.2	51.3	63.4	23.1	29.8	10.4	17.8	D[4,3] 43.70µm
524	100	236	99.9	106	96.2	47.7	59.0	21.4	27.7	9.64	16.2	
488	100	219	99.9	98.6	94.9	44.4	54.9	19.9	26.0	8.97	14.5	
454	100	204	99.8	91.7	93.2	41.2	51.3	18.5	24.6	8.34	13.0	D[3,2] 17.47µm
422	100	190	99.7	85.3	91.1	38.4	48.0	17.2	23.5	7.76	11.5	
392	100	176	99.6	79.3	88.5	35.7	45.0	16.0	22.8	7.21	9.9	
365	100	164	99.4	73.8	85.4	33.2	42.2	14.9	22.2	6.71	8.5	D[v,0.9] 82.50µm
339	100	153	99.2	68.6	81.8	30.8	39.6	13.9	21.7	6.24	7.0	
315	100	142	98.9	63.8	77.6	28.7	37.0	12.9	21.1	5.80	5.7	
293	99.9	132	98.5	59.3	73.0	26.7	34.5	12.0	20.3			D[v,0.1] 7.23µm
273	99.9	123	97.9	55.2	68.2	24.8	32.1	11.2	19.2			

Source = Data:p30v004r	Beam length = 2.2 mm	Model indp	D[v,0.5] 40.14µm
Record No. = 1	Log. Diff. = 4.082		
Focal length = 300 mm	Obscuration = 0.2677	Volume Conc. = 0.0825%	Shape OFF
Presentation = pil	Volume distribution	Sp.S.A 0.3434 m²/cc.	

1598 pil 1DR459 / 0/ 0/0.00/1.00/
30% W/W salt Soln
500 rpm
000000368

MALVERN Series 2600 SB.20 Master Mode 24 Feb 1998 1:02 pm

Particle diameters		Volume percentiles	
D(4,3)	43.70 µm	D[v,.10]	7.23
D(4,2)	27.63 µm	D[v,.20]	11.75
D(4,1)	16.65 µm	D[v,.30]	23.22
D(4,0)	11.46 µm	D[v,.40]	31.22
		D[v,.50]	40.14
D(3,2)	17.47 µm	D[v,.60]	48.50
D(3,1)	10.28 µm	D[v,.70]	56.68
D(3,0)	7.33 µm	D[v,.80]	66.44
		D[v,.90]	82.50
D(2,1)	6.04 µm	D[v,.99]	145.94
D(2,0)	4.75 µm		
		Span	1.88
D(1,0)	3.73 µm	Unif.	0.62

Distribution Moments.

Distbn	Mean	Stan.Dev.	Skewness
Volume	43.70	32.84	1.85
Surface	17.47	21.41	2.33
Length	6.04	8.31	5.47
Number	3.73	2.94	9.69

Source =Data:p30v004r
Record 1

1598 pil 1DR459 / 0/ 0/0.00/1.00/
30% W/W salt Soln
500 rpm

000000368

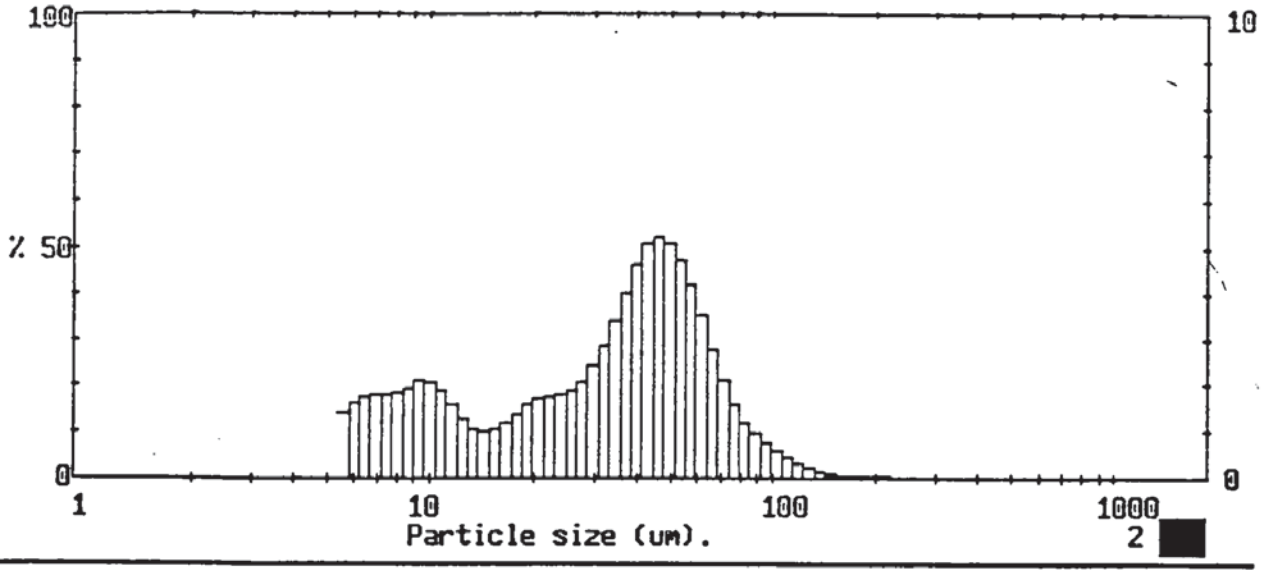

1598 pil 1DR459 / 0/ 0/0.00/1.00/
30% W/W salt Soln
600 rpm

000000369

MALVERN Series 2600 SB.20 Master Mode 24 Feb 1998 1:35 pm

High Size	Under %	High Size	Under %	High Size	Under %	High Size	Under %	High Size	Under %	High Size	Under %	Span 1.73
564	100	254	100	114	99.0	51.3	76.0	23.1	37.3	10.4	21.7	D[4,3] 35.48µm
524	100	236	100	106	98.6	47.7	70.9	21.4	35.5	9.64	19.6	
488	100	219	99.9	98.6	98.0	44.4	65.7	19.9	33.8	8.97	17.5	
454	100	204	99.9	91.7	97.2	41.2	60.6	18.5	32.2	8.34	15.5	D[3,2] 15.04µm
422	100	190	99.9	85.3	96.3	38.4	55.9	17.2	30.9	7.76	13.6	
392	100	176	99.9	79.3	95.1	35.7	51.9	16.0	29.7	7.21	11.8	
365	100	164	99.8	73.8	93.5	33.2	48.5	14.9	28.6	6.71	10.0	D[v,0.9] 66.10µm
339	100	153	99.8	68.6	91.3	30.8	45.6	13.9	27.6	6.24	8.3	
315	100	142	99.7	63.8	88.5	28.7	43.1	12.9	26.5	5.80	6.6	
293	100	132	99.5	59.3	85.0	26.7	41.1	12.0	25.2			D[v,0.1] 6.71µm
273	100	123	99.3	55.2	80.8	24.8	39.2	11.2	23.6			

Source = Data:p30v004r	Beam length = 2.2 mm	Model indp	D[v,0.5] 34.31µm
Record No. = 6	Log. Diff. = 3.788		
Focal length = 300 mm	Obscuration = 0.3132	Volume Conc. = 0.0857%	Shape OFF
Presentation = pil	Volume distribution	Sp.S.A 0.3388 m²/cc.	

1598 pil 1DR459 / 0/ 0/0.00/1.00/
30% W/W salt Soln
600 rpm

000000369

MALVERN Series 2600 SB.20 Master Mode 24 Feb 1998 1:35 pm

Particle diameters		Volume percentiles		Distribution Moments.			
				Distbn	Mean	Stan.Dev.	Skewness
D(4,3)	35.48 µm	D[v,.10]	6.71				
D(4,2)	23.10 µm	D[v,.20]	9.78				
D(4,1)	14.65 µm	D[v,.30]	16.38	Volume	35.48	25.86	1.27
D(4,0)	10.43 µm	D[v,.40]	25.63	Surface	15.04	17.54	2.17
		D[v,.50]	34.31	Length	5.89	7.34	5.02
D(3,2)	15.04 µm	D[v,.60]	40.90	Number	3.76	2.83	8.36
D(3,1)	9.42 µm	D[v,.70]	47.10				
D(3,0)	6.94 µm	D[v,.80]	54.49				
		D[v,.90]	66.10				
D(2,1)	5.89 µm	D[v,.99]	114.22	Source =Data:p30v004r			
D(2,0)	4.71 µm			Record 6			
		Span	1.73				
D(1,0)	3.76 µm	Unif.	0.59				

1598 pil 1DR459 / 0/ 0/0.00/1.00/
30% W/W salt Soln
600 rpm

000000369

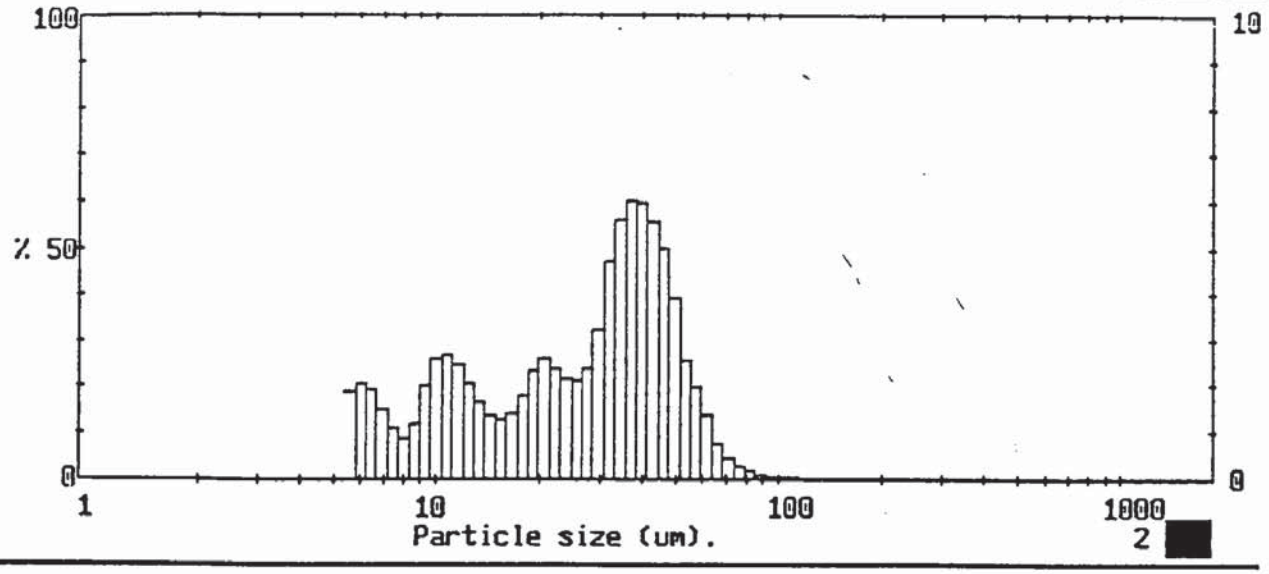

1598 pil 1DR459 / 0/ 0/0.00/1.00/
30% W/W salt Soln
700 rpm

000000370

MALVERN Series 2600 SB.20 Master Mode 24 Feb 1998 2:04 pm

High Size	Under %	High Size	Under %	High Size	Under %	High Size	Under %	High Size	Under %	High Size	Under %	Span 1.61
564	100	254	100	114	100	51.3	92.2	23.1	45.5	10.4	23.3	D[4,3] 26.99µm
524	100	236	100	106	100	47.7	88.3	21.4	43.1	9.64	20.7	
488	100	219	100	98.6	99.9	44.4	83.3	19.9	40.5	8.97	18.7	
454	100	204	100	91.7	99.9	41.2	77.7	18.5	38.1	8.34	17.5	D[3,2] 12.45µm
422	100	190	100	85.3	99.8	38.4	71.8	17.2	36.3	7.76	16.6	
392	100	176	100	79.3	99.6	35.7	65.7	16.0	34.9	7.21	15.5	
365	100	164	100	73.8	99.3	33.2	60.1	14.9	33.6	6.71	14.0	D[v,0.9] 49.09µm
339	100	153	100	68.6	98.9	30.8	55.4	13.9	32.2	6.24	12.0	
315	100	142	100	63.8	98.2	28.7	52.1	12.9	30.5	5.80	10.0	
293	100	132	100	59.3	96.8	26.7	49.7	12.0	28.5			D[v,0.1] 5.81µm
273	100	123	100	55.2	94.8	24.8	47.6	11.2	26.0			

Source = Data:p30v004r	Beam length = 2.2 mm	Model indp	D[v,0.5] 26.89µm
Record No. = 7	Log. Diff. = 3.313		
Focal length = 300 mm	Obscuration = 0.3633	Volume Conc. = 0.0852%	Shape OFF
Presentation = pil	Volume distribution	Sp.S.A 0.4818 m²/cc.	

1598 pil 1DR459 / 0/ 0/0.00/1.00/
30% W/W salt Soln
700 rpm

000000370

MALVERN Series 2600 SB.20 Master Mode 24 Feb 1998 2:04 pm

Particle diameters		Volume percentiles	
D(4,3)	26.99 µm	D[v,.10]	5.81
D(4,2)	18.33 µm	D[v,.20]	9.43
D(4,1)	12.10 µm	D[v,.30]	12.63
D(4,0)	8.90 µm	D[v,.40]	19.67
		D[v,.50]	26.89
D(3,2)	12.45 µm	D[v,.60]	33.12
D(3,1)	8.10 µm	D[v,.70]	37.56
D(3,0)	6.15 µm	D[v,.80]	42.46
		D[v,.90]	49.09
D(2,1)	5.27 µm	D[v,.99]	69.28
D(2,0)	4.33 µm		
		Span	1.61
D(1,0)	3.55 µm	Unif.	0.55

Distribution Moments.

Distbn	Mean	Stan.Dev.	Skewness
Volume	26.99	17.47	0.45
Surface	12.45	13.45	1.72
Length	5.27	6.15	4.41
Number	3.55	2.47	8.13

Source =Data:p30v004r
Record 7

1598 pil 1DR459 / 0/ 0/0.00/1.00/
30% W/W salt Soln
700 rpm

000000370

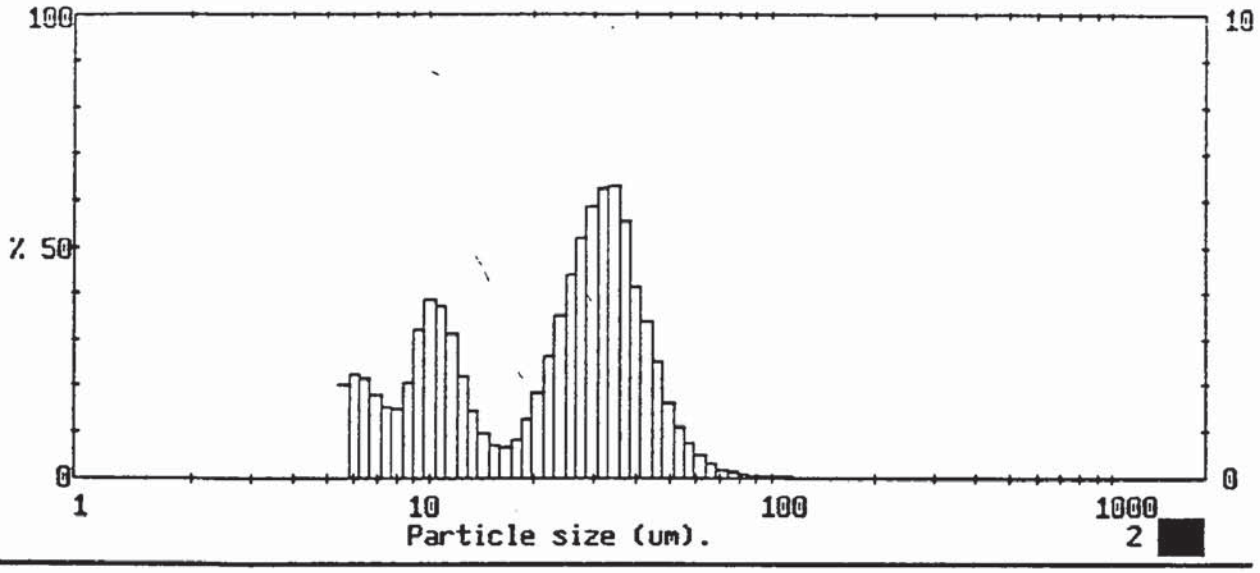

1598 pil 1DR459 / 0/ 0/0.00/1.00/
30% W/W salt Soln
800 rpm

000000371

MALVERN Series 2600 SB.20 Master Mode 24 Feb 1998 2:38 pm

High Size	Under %	High Size	Under %	High Size	Under %	High Size	Under %	High Size	Under %	High Size	Under %	Span 1.49
564	100	254	100	114	100	51.3	96.8	23.1	47.7	10.4	28.1	D[4,3] 23.32µm
524	100	236	100	106	100	47.7	95.1	21.4	45.0	9.64	24.2	
488	100	219	100	98.6	99.9	44.4	92.6	19.9	43.2	8.97	21.0	
454	100	204	100	91.7	99.9	41.2	89.2	18.5	41.9	8.34	18.9	D[3,2] 11.72µm
422	100	190	100	85.3	99.8	38.4	85.0	17.2	41.0	7.76	17.4	
392	100	176	100	79.3	99.8	35.7	79.4	16.0	40.4	7.21	15.8	
365	100	164	100	73.8	99.7	33.2	73.1	14.9	39.6	6.71	14.0	D[v,0.9] 41.93µm
339	100	153	100	68.6	99.5	30.8	66.8	13.9	38.7	6.24	11.8	
315	100	142	100	63.8	99.2	28.7	60.9	12.9	37.2	5.80	9.5	
293	100	132	100	59.3	98.6	26.7	55.6	12.0	35.0			D[v,0.1] 5.89µm
273	100	123	100	55.2	97.9	24.8	51.2	11.2	31.8			

Source = Data:p30v004r	Beam length = 2.2 mm	Model indp	D[v,0.5] 24.23µm
Record No. = 9	Log. Diff. = 3.716		
Focal length = 300 mm	Obscuration = 0.4138	Volume Conc. = 0.0948%	Shape OFF
Presentation = pil	Volume distribution	Sp.S.A 0.5120 m²/cc.	

1598 pil 1DR459 / 0/ 0/0.00/1.00/
30% W/W salt Soln
800 rpm

000000371

MALVERN Series 2600 SB.20 Master Mode 24 Feb 1998 2:38 pm

Particle diameters		Volume percentiles	
D(4,3)	23.32 µm	D[v,.10]	5.89
D(4,2)	16.53 µm	D[v,.20]	8.70
D(4,1)	11.44 µm	D[v,.30]	10.75
D(4,0)	8.62 µm	D[v,.40]	15.44
		D[v,.50]	24.23
D(3,2)	11.72 µm	D[v,.60]	28.35
D(3,1)	8.02 µm	D[v,.70]	32.02
D(3,0)	6.18 µm	D[v,.80]	35.92
		D[v,.90]	41.93
D(2,1)	5.48 µm	D[v,.99]	62.18
D(2,0)	4.49 µm		
		Span	1.49
D(1,0)	3.68 µm	Unif.	0.52

Distribution Moments.			
Distbn	Mean	Stan.Dev.	Skewness
Volume	23.32	15.06	0.63
Surface	11.72	11.66	1.67
Length	5.48	5.85	3.86
Number	3.68	2.58	6.64

Source =Data:p30v004r
Record 9

1598 pil 1DR459 / 0/ 0/0.00/1.00/
30% W/W salt Soln
800 rpm

000000371

MALVERN Series 2600 SB.20 Master Mode 24 Feb 1998 2:57 pm

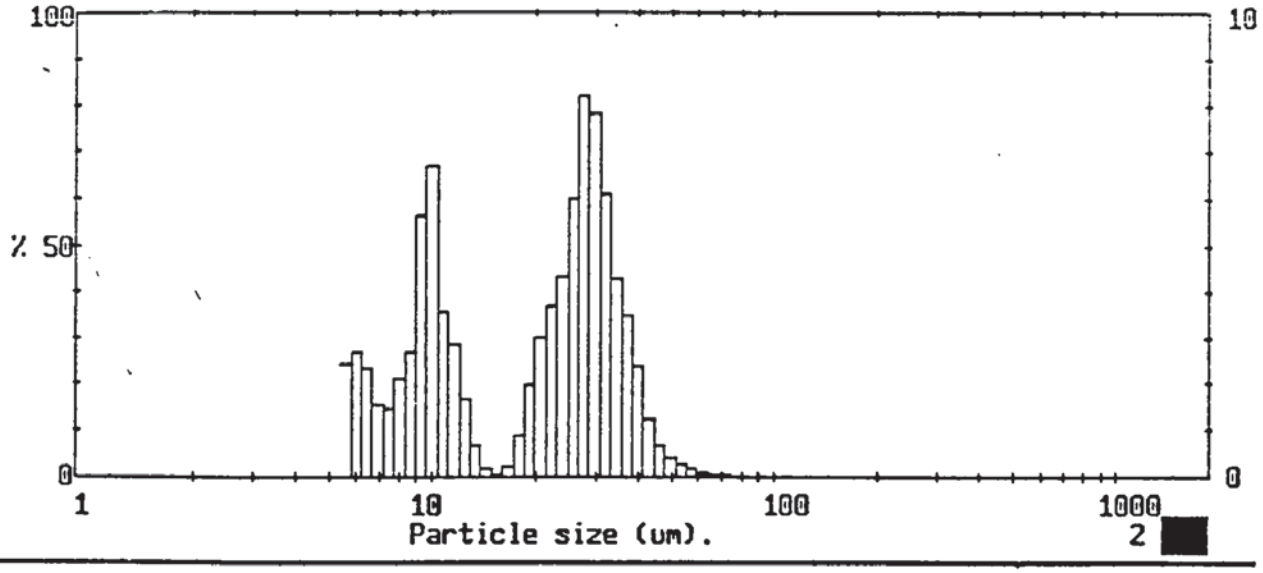

1598 pil 1DR459 / 0/ 0/0.00/1.00/
30% W/W salt Soln
900 rpm

000000372

MALVERN Series 2600 SB.20 Master Mode 24 Feb 1998 2:57 pm

High Size	Under %	High Size	Under %	High Size	Under %	High Size	Under %	High Size	Under %	High Size	Under %	Span 1.37
564	100	254	100	114	100	51.3	99.4	23.1	54.3	10.4	35.4	D[4,3] 19.82µm
524	100	236	100	106	100	47.7	99.0	21.4	50.6	9.64	28.7	
488	100	219	100	98.6	100	44.4	98.3	19.9	47.6	8.97	23.0	
454	100	204	100	91.7	100	41.2	97.1	18.5	45.5	8.34	20.3	D[3,2] 10.75µm
422	100	190	100	85.3	100	38.4	94.7	17.2	44.7	7.76	18.2	
392	100	176	100	79.3	100	35.7	91.2	16.0	44.4	7.21	16.8	
365	100	164	100	73.8	100	33.2	86.9	14.9	44.4	6.71	15.2	D[v,0.9] 34.88µm
339	100	153	100	68.6	99.9	30.8	80.8	13.9	44.2	6.24	12.9	
315	100	142	100	63.8	99.9	28.7	72.9	12.9	43.5	5.80	10.2	
293	100	132	100	59.2	99.8	26.7	64.7	12.0	41.9			D[v,0.1] 5.77µm
273	100	123	100	55.2	99.6	24.8	58.7	11.2	39.0			

Source = Data:p30v004r	Beam length = 2.2 mm	Model indp	D[v,0.5] 21.18µm
Record No. = 11	Log. Diff. = 3.747		
Focal length = 300 mm	Obscuration = 0.4629	Volume Conc. = 0.1013%	Shape OFF
Presentation = pil	Volume distribution	Sp.S.A 0.5579 m²/cc.	

1598 pil 1DR459 / 0/ 0/0.00/1.00/
30% W/W salt Soln
900 rpm

000000372

MALVERN Series 2600 SB.20 Master Mode 24 Feb 1998 2:57 pm

Particle diameters		Volume percentiles		Distribution Moments.			
				Distbn	Mean	Stan.Dev.	Skewness
D(4,3)	19.82 µm	D[v,.10]	5.77				
D(4,2)	14.60 µm	D[v,.20]	8.26				
D(4,1)	10.52 µm	D[v,.30]	9.77	Volume	19.82	12.14	0.37
D(4,0)	8.12 µm	D[v,.40]	11.42	Surface	10.75	9.87	1.48
		D[v,.50]	21.18	Length	5.47	5.38	3.40
D(3,2)	10.75 µm	D[v,.60]	25.29	Number	3.73	2.55	5.73
D(3,1)	7.67 µm	D[v,.70]	27.97				
D(3,0)	6.03 µm	D[v,.80]	30.59				
		D[v,.90]	34.88				
D(2,1)	5.47 µm	D[v,.99]	47.84	Source =Data:p30v004r			
D(2,0)	4.52 µm			Record 11			
		Span	1.37				
D(1,0)	3.73 µm	Unif.	0.50				

1598 pil 1DR459 / 0/ 0/0.00/1.00/
30% W/W salt Soln
900 rpm

000000372

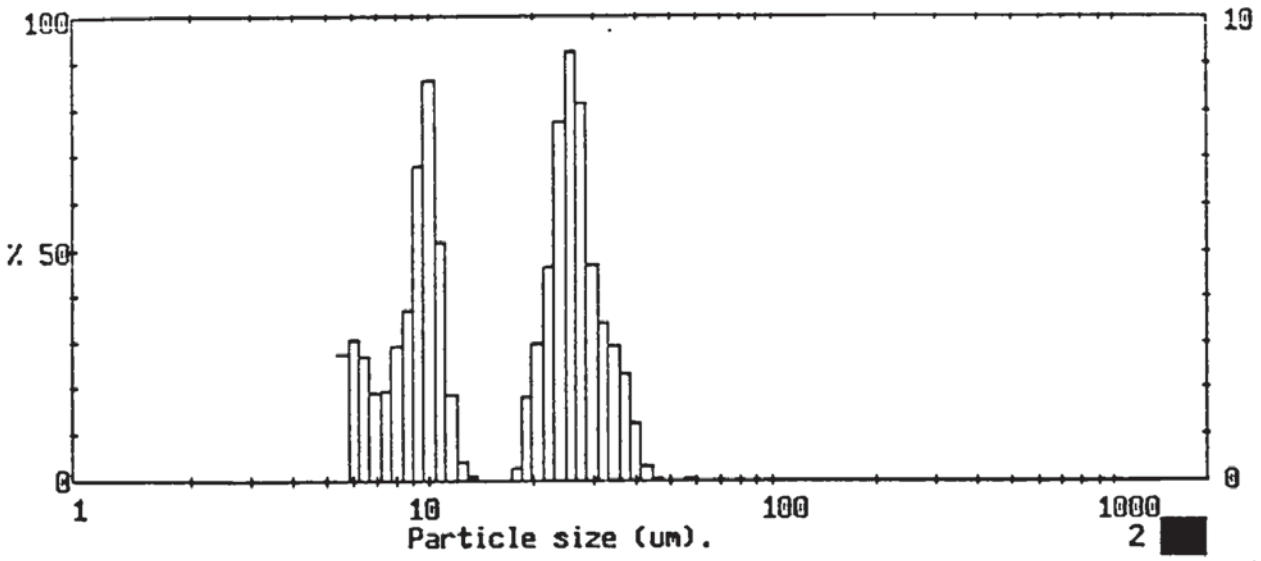

1598 pil 1DR459 / 0/ 0/0.00/1.00/
30% W/W salt Soln
1000 rpm

000000373

MALVERN Series 2600 SB.20 Master Mode 24 Feb 1998 3:52 pm

High Size	Under %	High Size	Under %	High Size	Under %	High Size	Under %	High Size	Under %	High Size	Under %	Span 2.02
564	100	254	100	114	100	51.3	100	23.1	59.9	10.4	42.7	D[4,3] 17.40µm
524	100	236	100	106	100	47.7	100	21.4	55.3	9.64	34.0	
488	100	219	100	98.6	100	44.4	99.9	19.9	52.3	8.97	27.2	D[3,2] 9.86µm
454	100	204	100	91.7	100	41.2	99.6	18.5	50.5	8.34	23.5	
422	100	190	100	85.3	100	38.4	98.4	17.2	50.2	7.76	20.6	
392	100	176	100	79.3	100	35.7	96.1	16.0	50.2	7.21	18.6	D[v,0.9] 31.00µm
365	100	164	100	73.8	100	33.2	93.2	14.9	50.2	6.71	16.7	
339	100	153	100	68.6	100	30.8	89.7	13.9	50.2	6.24	14.0	
315	100	142	100	63.8	100	28.7	85.0	12.9	50.1	5.80	11.0	
293	100	132	100	59.3	100	26.7	76.9	12.0	49.7			D[v,0.1] 5.65µm
273	100	123	100	55.2	100	24.8	67.7	11.2	47.8			

Source = Data:p30v004r	Beam length = 2.2 mm	Model indp	D[v,0.5] 12.53µm
Record No. = 14	Log. Diff. = 3.683		
Focal length = 300 mm	Obscuration = 0.5021	Volume Conc. = 0.1041%	Shape OFF
Presentation = pil	Volume distribution	Sp.S.A 0.6083 m²/cc.	

1598 pil 1DR459 / 0/ 0/0.00/1.00/
30% W/W salt Soln
1000 rpm

000000373

MALVERN Series 2600 SB.20 Master Mode 24 Feb 1998 3:52 pm

Particle diameters		Volume percentiles	
D(4,3)	17.40 µm	D[v,.10]	5.65
D(4,2)	13.10 µm	D[v,.20]	7.62
D(4,1)	9.74 µm	D[v,.30]	9.30
D(4,0)	7.68 µm	D[v,.40]	10.13
		D[v,.50]	12.53
D(3,2)	9.86 µm	D[v,.60]	23.09
D(3,1)	7.29 µm	D[v,.70]	25.28
D(3,0)	5.85 µm	D[v,.80]	27.35
		D[v,.90]	31.00
D(2,1)	5.39 µm	D[v,.99]	39.44
D(2,0)	4.50 µm		
		Span	2.02
D(1,0)	3.76 µm	Unif.	0.78

Distribution Moments.

Distbn	Mean	Stan.Dev.	Skewness
Volume	17.40	10.62	0.28
Surface	9.86	8.62	1.47
Length	5.39	4.91	3.20
Number	3.76	2.47	5.13

Source =Data:p30v004r
Record 14

1598 pil 1DR459 / 0/ 0/0.00/1.00/
30% W/W salt Soln
1000 rpm

000000373

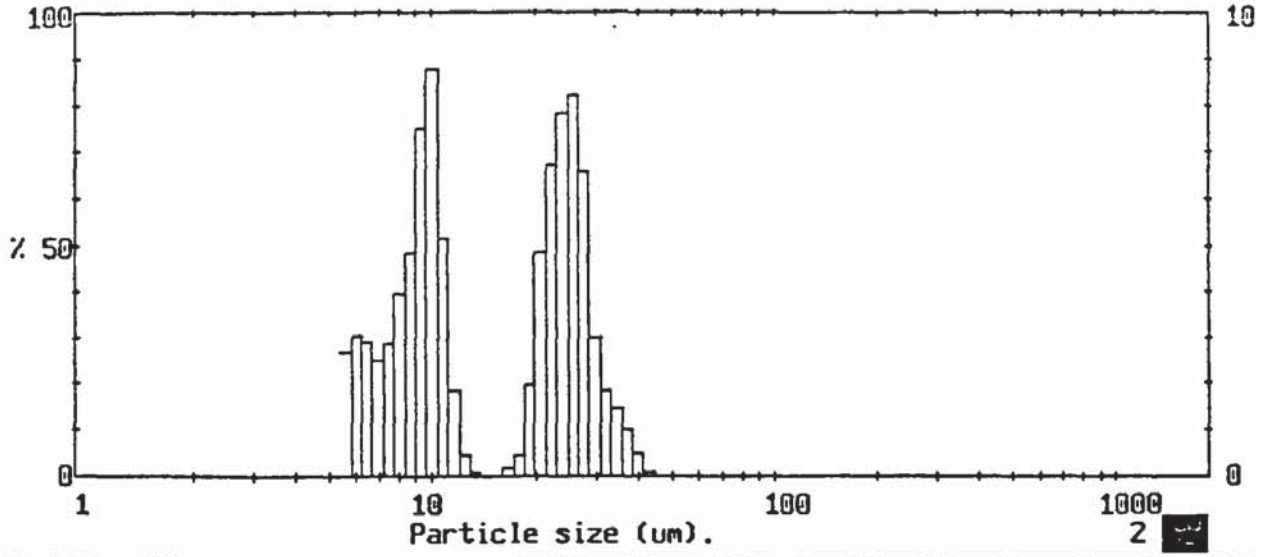

1598 pil lDR459 / 0/ 0/0.00/1.00/
30% W/W salt Soln
1100 rpm

000000374

MALVERN Series 2600 SB.20 Master Mode 24 Feb 1998 3:57 pm

High Size	Under %	High Size	Under %	High Size	Under %	High Size	Under %	High Size	Under %	High Size	Under %	Span 2.09
564	100	254	100	114	100	51.3	100	23.1	69.4	10.4	47.5	D[4,3] 15.70µm
524	100	236	100	106	100	47.7	100	21.4	62.6	9.64	38.7	
488	100	219	100	98.6	100	44.4	100	19.9	57.8	8.97	31.2	
454	100	204	100	91.7	100	41.2	99.9	18.5	55.8	8.34	26.3	D[3,2] 9.38µm
422	100	190	100	85.3	100	38.4	99.4	17.2	55.3	7.76	22.4	
392	100	176	100	79.3	100	35.7	98.4	16.0	55.1	7.21	19.5	
365	100	164	100	73.8	100	33.2	96.9	14.9	55.1	6.71	16.9	D[v,0.9] 27.92µm
339	100	153	100	68.6	100	30.8	95.1	13.9	55.1	6.24	14.0	
315	100	142	100	63.8	100	28.7	92.0	12.9	55.0	5.80	11.0	
293	100	132	100	59.3	100	26.7	85.4	12.0	54.6			D[v,0.1] 5.66µm
273	100	123	100	55.2	100	24.8	77.2	11.2	52.7			

Source = Data:p30v004r	Beam length = 2.2 mm	Model indp	D[v,0.5] 10.66µm
Record No. = 15	Log. Diff. = 3.653		
Focal length = 300 mm	Obscuration = 0.5261	Volume Conc. = 0.1061%	
Presentation = pil	Volume distribution	Sp.S.A 0.6396 m²/cc.	Shape OFF

1598 pil lDR459 / 0/ 0/0.00/1.00/
30% W/W salt Soln
1100 rpm

000000374

MALVERN Series 2600 SB.20 Master Mode 24 Feb 1998 3:57 pm

Particle diameters		Volume percentiles	
D(4,3)	15.70 µm	D[v,.10]	5.66
D(4,2)	12.13 µm	D[v,.20]	7.32
D(4,1)	9.30 µm	D[v,.30]	8.82
D(4,0)	7.46 µm	D[v,.40]	9.74
		D[v,.50]	10.66
D(3,2)	9.38 µm	D[v,.60]	20.71
D(3,1)	7.15 µm	D[v,.70]	23.21
D(3,0)	5.82 µm	D[v,.80]	25.42
		D[v,.90]	27.92
D(2,1)	5.46 µm	D[v,.99]	37.06
D(2,0)	4.58 µm		
		Span	2.09
D(1,0)	3.85 µm	Unif.	0.79

Distribution Moments.			
Distbn	Mean	Stan.Dev.	Skewness
Volume	15.70	9.56	0.39
Surface	9.38	7.70	1.48
Length	5.46	4.63	2.93
Number	3.85	2.49	4.45

Source =Data:p30v004r
Record 15

1598 pil lDR459 / 0/ 0/0.00/1.00/
30% W/W salt Soln
1100 rpm

000000374

30% w/w and 0.05% v/v

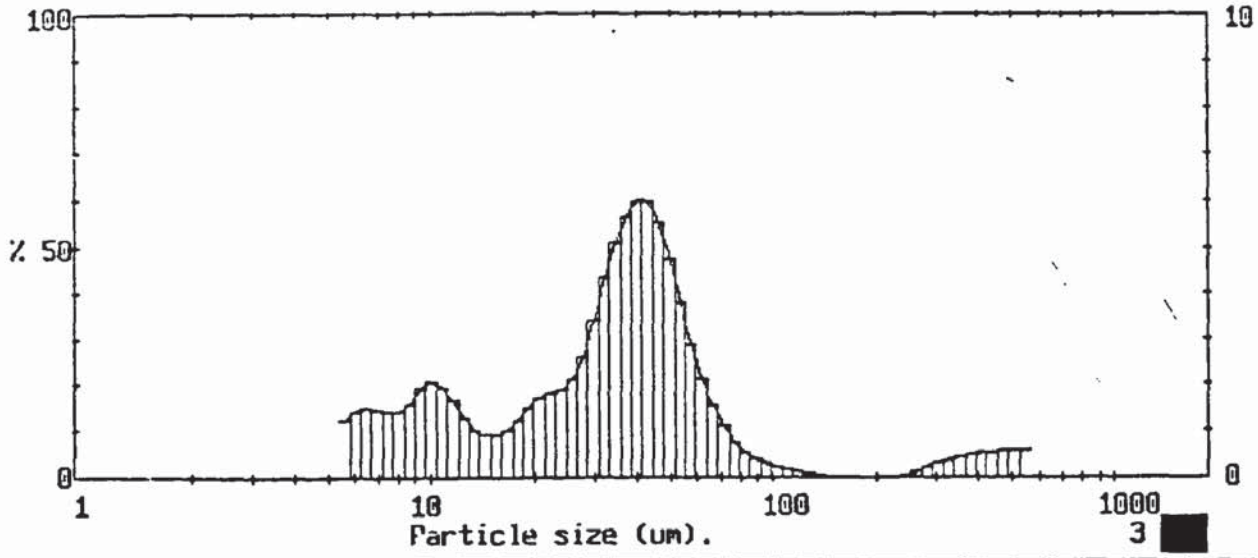

1598 pil 1DR459 / 0/ 0/0.00/1.00/
30% W/W salt Soln
600 rpm

000000384

MALVERN Series 2600 SB.20 Master Mode 25 Feb 1998 1:23 pm

High Size	Under %	High Size	Under %	High Size	Under %	High Size	Under %	High Size	Under %	High Size	Under %	Span 1.67
564	100	254	95.3	114	95.0	51.3	81.1	23.1	33.8	10.4	18.6	D[4,3] 50.30µm
524	99.4	236	95.3	106	94.8	47.7	76.4	21.4	31.9	9.64	16.5	
488	98.8	219	95.3	98.6	94.6	44.4	70.8	19.9	30.2	8.97	14.6	
454	98.3	204	95.3	91.7	94.3	41.2	64.9	18.5	28.7	8.34	13.0	D[3,2] 16.22µm
422	97.7	190	95.3	85.3	93.9	38.4	58.9	17.2	27.5	7.76	11.6	
392	97.2	176	95.3	79.3	93.4	35.7	53.2	16.0	26.4	7.21	10.2	
365	96.7	164	95.3	73.8	92.6	33.2	48.2	14.9	25.5	6.71	8.7	D[v,0.9] 63.95µm
339	96.3	153	95.3	68.6	91.5	30.8	43.8	13.9	24.6	6.24	7.2	
315	96.0	142	95.2	63.8	89.9	28.7	40.4	12.9	23.5	5.80	5.8	
293	95.6	132	95.2	59.3	87.8	26.7	37.8	12.0	22 2			D[v,0.1] 7.16µm
273	95.4	123	95.1	55.2	84.9	24.8	35.7	11.2	20.6			

Source = Data:p30v005	Beam length = 14.3 mm	Model indp	D[v,0.5] 34.10µm
Record No. = 6	Log. Diff. = 3.514		
Focal length = 300 mm	Obscuration = 0.2711	Volume Conc. = 0.0120%	
Presentation = pil	Volume distribution	Sp.S.A 0.3698 m²/cc.	Shape OFF

1598 pil 1DR459 / 0/ 0/0.00/1.00/
30% W/W salt Soln
600 rpm

000000384

MALVERN Series 2600 SB.20 Master Mode 25 Feb 1998 1:23 pm

Particle diameters		Volume percentiles		Distribution Moments.			
				Distbn	Mean	Stan.Dev.	Skewness
D(4,3)	50.30 µm	D[v,.10]	7.16				
D(4,2)	28.57 µm	D[v,.20]	10.91				
D(4,1)	17.16 µm	D[v,.30]	19.76	Volume	50.30	85.54	4.19
D(4,0)	11.78 µm	D[v,.40]	28.39	Surface	16.22	23.51	9.89
		D[v,.50]	34.10	Length	6.20	7.88	7.48
D(3,2)	16.22 µm	D[v,.60]	38.89	Number	3.81	3.02	8.15
D(3,1)	10.03 µm	D[v,.70]	43.89				
D(3,0)	7.26 µm	D[v,.80]	50.36				
		D[v,.90]	63.95				
D(2,1)	6.20 µm	D[v,.99]	498.06				
D(2,0)	4.86 µm			Source =Data:p30v005			
		Span	1.67	Record 6			
D(1,0)	3.81 µm	Unif.	0.99				

1598 pil 1DR459 / 0/ 0/0.00/1.00/
30% W/W salt Soln
600 rpm

000000384

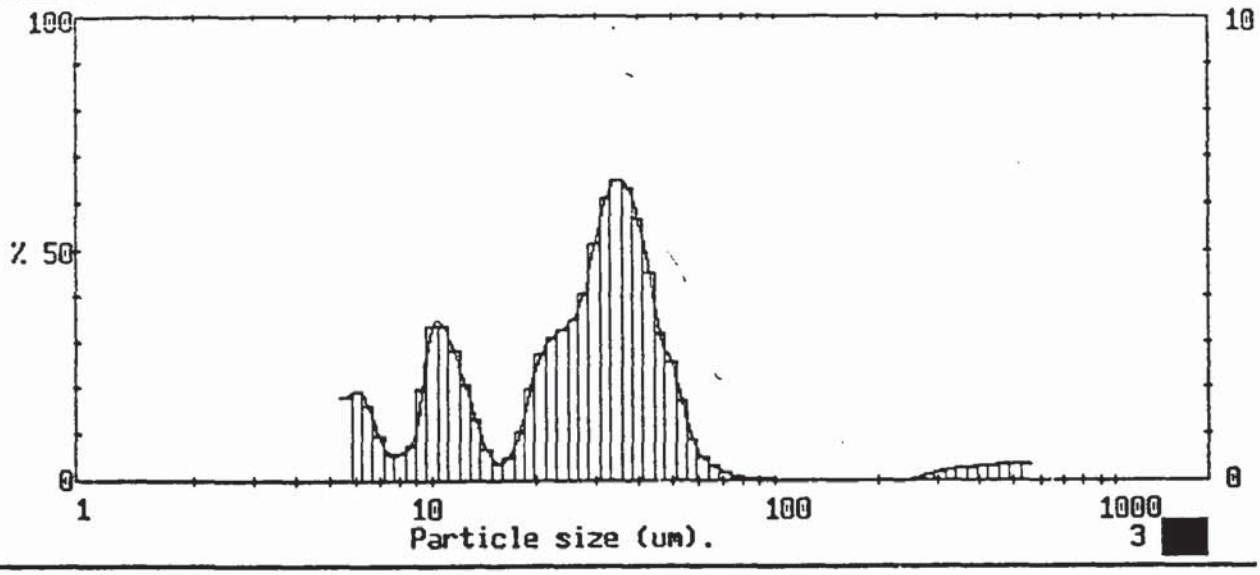

1598 pil 1DR459 / 0/ 0/0.00/1.00/
30% W/W salt Soln
700 rpm

000000385

MALVERN Series 2600 SB.20 Master Mode 25 Feb 1998 1:59 pm

High Size	Under %	High Size	Under %	High Size	Under %	High Size	Under %	High Size	Under %	High Size	Under %	Span 1.52
564	100	254	97.2	114	97.2	51.3	93.3	23.1	42.3	10.4	22.3	D[4,3] 36.39µm
524	99.6	236	97.2	106	97.1	47.7	90.7	21.4	39.2	9.64	19.0	
488	99.3	219	97.2	98.6	97.1	44.4	87.5	19.9	36.5	8.97	17.0	
454	99.0	204	97.2	91.7	97.1	41.2	83.0	18.5	34.5	8.34	16.2	D[3,2] 12.48µm
422	98.6	190	97.2	85.3	97.1	38.4	77.4	17.2	33.4	7.76	15.7	
392	98.3	176	97.2	79.3	97.0	35.7	71.0	16.0	32.9	7.21	15.1	
365	98.0	164	97.2	73.8	96.9	33.2	64.5	14.9	32.6	6.71	14.1	D[v,0.9] 46.81µm
339	97.8	153	97.2	68.6	96.7	30.8	58.4	13.9	31.9	6.24	12.5	
315	97.6	142	97.2	63.8	96.4	28.7	53.2	12.9	30.6	5.80	10.5	
293	97.4	132	97.2	59.3	96.0	26.7	49.2	12.0	28.5			D[v,0.1] 5.69µm
273	97.2	123	97.2	55.2	95.0	24.8	45.6	11.2	25.7			

Source = Data:p30v005	Beam length = 14.3 mm	Model indp	D[v,0.5] 27.11µm
Record No. = 9	Log. Diff. = 3.477		
Focal length = 300 mm	Obscuration = 0.3538	Volume Conc. = 0.0127%	Shape OFF
Presentation = pil	Volume distribution	Sp.S.A 0.4808 m²/cc.	

1598 pil 1DR459 / 0/ 0/0.00/1.00/
30% W/W salt Soln
700 rpm

000000385

MALVERN Series 2600 SB.20 Master Mode 25 Feb 1998 1:59 pm

Particle diameters		Volume percentiles	
D(4,3)	36.39 µm	D[v,.10]	5.69
D(4,2)	21.31 µm	D[v,.20]	9.88
D(4,1)	13.28 µm	D[v,.30]	12.59
D(4,0)	9.50 µm	D[v,.40]	21.85
		D[v,.50]	27.11
D(3,2)	12.48 µm	D[v,.60]	31.46
D(3,1)	8.02 µm	D[v,.70]	35.27
D(3,0)	6.07 µm	D[v,.80]	39.61
		D[v,.90]	46.81
D(2,1)	5.16 µm	D[v,.99]	458.04
D(2,0)	4.24 µm		
		Span	1.52
D(1,0)	3.48 µm	Unif.	0.87

Distribution Moments.			
Distbn	Mean	Stan.Dev.	Skewness
Volume	36.39	68.04	5.58
Surface	12.48	17.27	11.87
Length	5.16	6.15	6.98
Number	3.48	2.41	8.59

Source =Data:p30v005
Record 9

1598 pil 1DR459 / 0/ 0/0.00/1.00/
30% W/W salt Soln
700 rpm

000000385

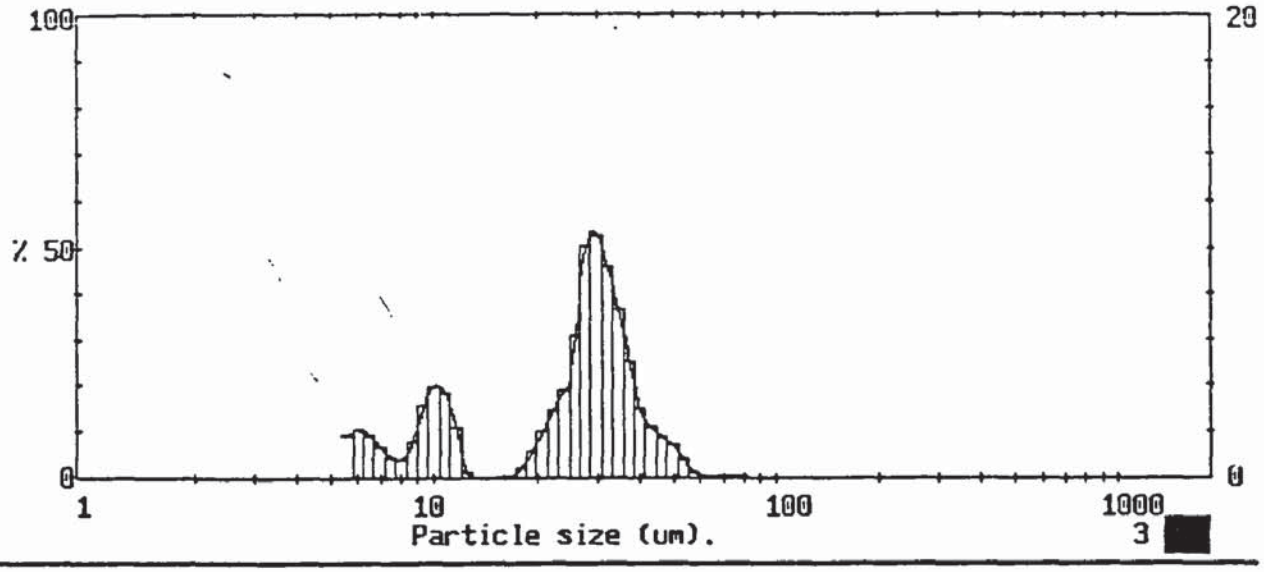

1598 pil 1DR459 / 0/ 0/0.00/1.00/
30% W/W salt Soln
800 rpm

000000386

MALVERN Series 2600 SB.20 Master Mode 25 Feb 1998 2:59 pm

High Size	Under %	High Size	Under %	High Size	Under %	High Size	Under %	High Size	Under %	High Size	Under %	Span 1.19
564	100	254	100	114	100	51.3	98.6	23.1	38.0	10.4	25.1	D[4,3] 23.91µm
524	100	236	100	106	100	47.7	97.2	21.4	35.0	9.64	21.1	
488	100	219	100	98.6	100	44.4	95.4	19.9	33.0	8.97	18.0	D[3,2] 12.48µm
454	100	204	100	91.7	100	41.2	93.2	18.5	31.8	8.34	16.4	
422	100	190	100	85.3	100	38.4	90.2	17.2	31.4	7.76	15.6	D[v,0.9] 38.18µm
392	100	176	100	79.3	99.9	35.7	85.2	16.0	31.4	7.21	14.7	
365	100	164	100	73.8	99.9	33.2	77.8	14.9	31.4	6.71	13.4	D[v,0.1] 5.92µm
339	100	153	100	68.6	99.8	30.8	68.6	13.9	31.4	6.24	11.5	
315	100	142	100	63.8	99.7	28.7	58.1	12.9	31.4	5.80	9.4	
293	100	132	100	59.3	99.7	26.7	48.0	12.0	31.1			
273	100	123	100	55.2	99.4	24.8	41.8	11.2	28.8			

Source =Data:p30v005	Beam length = 14.3 mm	Model indp	D[v,0.5] 27.10µm
Record No. = 11	Log. Diff. = 3.876		
Focal length = 300 mm	Obscuration = 0.4336	Volume Conc. = 0.0165%	
Presentation = pil	Volume distribution	Sp.S.A 0.4807 m²/cc.	Shape OFF

1598 pil 1DR459 / 0/ 0/0.00/1.00/
30% W/W salt Soln
800 rpm

000000386

MALVERN Series 2600 SB.20 Master Mode 25 Feb 1998 2:59 pm

Particle diameters		Volume percentiles	
D(4,3)	23.91 µm	D[v,.10]	5.92
D(4,2)	17.28 µm	D[v,.20]	9.43
D(4,1)	11.77 µm	D[v,.30]	11.49
D(4,0)	8.75 µm	D[v,.40]	24.01
		D[v,.50]	27.10
D(3,2)	12.48 µm	D[v,.60]	29.05
D(3,1)	8.25 µm	D[v,.70]	31.15
D(3,0)	6.25 µm	D[v,.80]	33.82
		D[v,.90]	38.18
D(2,1)	5.46 µm	D[v,.99]	52.85
D(2,0)	4.43 µm		
		Span	1.19
D(1,0)	3.59 µm	Unif.	0.38

Distribution Moments.			
Distbn	Mean	Stan.Dev.	Skewness
Volume	23.91	13.13	0.13
Surface	12.48	11.95	1.17
Length	5.46	6.19	3.53
Number	3.59	2.59	7.27

Source =Data:p30v005
Record 11

1598 pil 1DR459 / 0/ 0/0.00/1.00/
30% W/W salt Soln
800 rpm

000000386

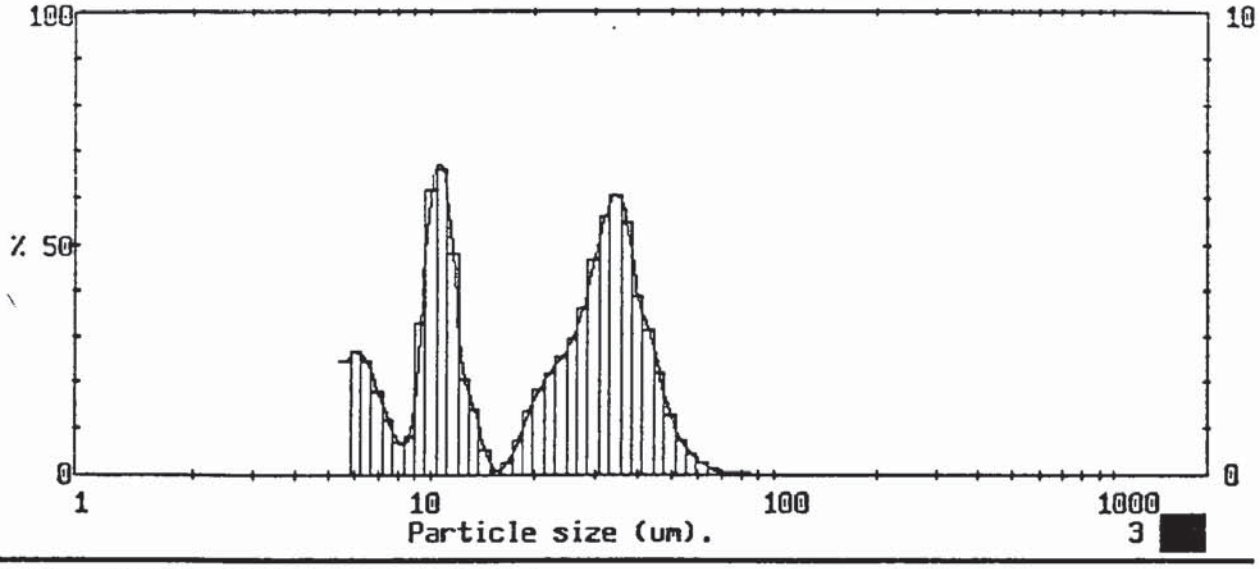

1598 pil lDR459 / 0/ 0/0.00/1.00/
30% W/W salt Soln
900 rpm

000000387

MALVERN Series 2600 SB.20 Master Mode 25 Feb 1998 5:24 pm

High Size	Under %	High Size	Under %	High Size	Under %	High Size	Under %	High Size	Under %	High Size	Under %	Span 2.40
564	100	254	100	114	100	51.3	98.3	23.1	56.7	10.4	34.6	D[4,3] 20.47µm
524	100	236	100	106	100	47.7	97.0	21.4	54.4	9.64	28.4	
488	100	219	100	98.6	100	44.4	94.8	19.9	52.5	8.97	25.0	D[3,2] 9.46µm
454	100	204	100	91.7	100	41.2	91.6	18.5	51.2	8.34	24.2	
422	100	190	100	85.3	100	38.4	87.7	17.2	50.4	7.76	23.5	
392	100	176	100	79.3	99.9	35.7	82.2	16.0	50.2	7.21	22.3	D[v,0.9] 39.89µm
365	100	164	100	73.8	99.9	33.2	76.2	14.9	50.1	6.71	20.5	
339	100	153	100	68.6	99.8	30.8	70.5	13.9	49.5	6.24	18.0	
315	100	142	100	63.8	99.7	28.7	65.8	12.9	48.1	5.80	15.3	D[v,0.1] 4.90µm
293	100	132	100	59.3	99.5	26.7	62.2	12.0	46.0			
273	100	123	100	55.2	99.0	24.8	59.2	11.2	41.2			

Source = Data:p30v005	Beam length = 14.3 mm	Model indp	D[v,0.5] 14.58µm
Record No. = 14	Log. Diff. = 3.537		
Focal length = 300 mm	Obscuration = 0.5329	Volume Conc. = 0.0168%	
Presentation = pil	Volume distribution	Sp.S.A 0.6340 m²/cc.	Shape OFF

1598 pil lDk459 / 0/ 0/0.00/1.00/
30% W/W salt Soln
900 rpm

000000387

MALVERN Series 2600 SB.20 Master Mode 25 Feb 1998 5:24 pm

Particle diameters		Volume percentiles		Distribution Moments.			
D(4,3)	20.47 µm	D[v,.10]	4.90	Distbn	Mean	Stan.Dev.	Skewness
D(4,2)	13.92 µm	D[v,.20]	6.60				
D(4,1)	9.69 µm	D[v,.30]	9.85	Volume	20.47	14.58	0.56
D(4,0)	7.48 µm	D[v,.40]	11.00	Surface	9.46	10.20	2.04
		D[v,.50]	14.58	Length	4.70	4.73	4.63
D(3,2)	9.46 µm	D[v,.60]	25.30	Number	3.45	2.07	7.58
D(3,1)	6.67 µm	D[v,.70]	30.61				
D(3,0)	5.35 µm	D[v,.80]	34.73				
		D[v,.90]	39.89				
D(2,1)	4.70 µm	D[v,.99]	55.14	Source =Data:p30v005			
D(2,0)	4.02 µm			Record 14			
		Span	2.40				
D(1,0)	3.45 µm	Unif.	0.88				

1598 pil lDR459 / 0/ 0/0.00/1.00/
30% W/W salt Soln
900 rpm

000000387

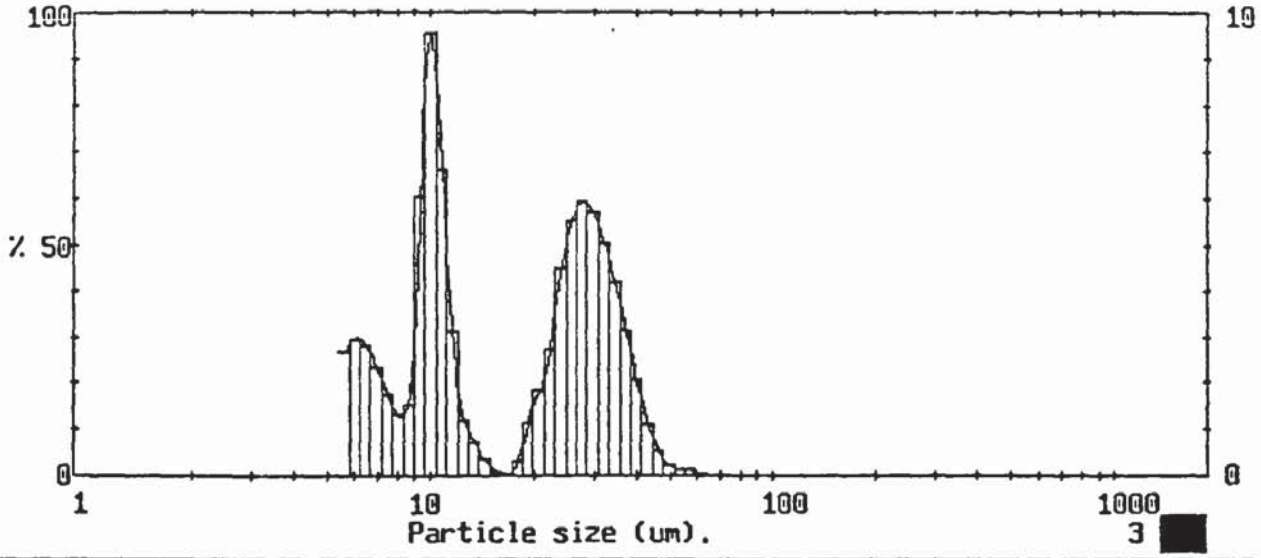

1598 pil lDR459 / 0/ 0/0.00/1.00/
30% W/W salt Soln
1000 rpm

000000388

MALVERN Series 2600 SB.20 Master Mode 25 Feb 1998 5:32 pm

High Size	Under %	High Size	Under %	High Size	Under %	High Size	Under %	High Size	Under %	High Size	Under %	Span 2.60
564	100	254	100	114	100	51.3	99.6	23.1	61.6	10.4	43.4	D[4,3] 17.48µm
524	100	236	100	106	100	47.7	99.4	21.4	58.8	9.64	33.8	
488	100	219	100	98.6	100	44.4	98.9	19.9	57.0	8.97	27.8	
454	100	204	100	91.7	100	41.2	97.7	18.5	55.8	8.34	26.2	D[3,2] 8.97µm
422	100	190	100	85.3	100	38.4	95.7	17.2	55.5	7.76	24.9	
392	100	176	100	79.3	100	35.7	92.5	16.0	55.5	7.21	23.1	
365	100	164	100	73.8	100	33.2	88.3	14.9	55.4	6.71	20.8	D[v,0.9] 34.08µm
339	100	153	100	68.6	100	30.8	83.2	13.9	55.1	6.24	17.9	
315	100	142	100	63.8	100	28.7	77.6	12.9	54.4	5.80	14.9	
293	100	132	100	59.3	99.9	26.7	71.6	12.0	53.1			D[v,0.1] 5.04µm
273	100	123	100	55.2	99.8	24.8	66.1	11.2	50.0			

Source = Data:p30v005	Beam length = 14.3 mm	Model indp	D[v,0.5] 11.15µm
Record No. = 15	Log. Diff. = 3.600		
Focal length = 300 mm	Obscuration = 0.5730	Volume Conc. = 0.0178%	
Presentation = pil	Volume distribution	Sp.S.A 0.6692 m²/cc.	Shape OFF

1598 pil lDR459 / 0/ 0/0.00/1.00/
30% W/W salt Soln
1000 rpm

000000388

MALVERN Series 2600 SB.20 Master Mode 25 Feb 1998 5:32 pm

Particle diameters		Volume percentiles		Distribution Moments.			
D(4,3)	17.48 µm	D[v,.10]	5.04	Distbn	Mean	Stan.Dev.	Skewness
D(4,2)	12.52 µm	D[v,.20]	6.57				
D(4,1)	9.12 µm	D[v,.30]	9.31	Volume	17.48	12.10	0.56
D(4,0)	7.20 µm	D[v,.40]	10.10	Surface	8.97	8.74	1.92
		D[v,.50]	11.15	Length	4.84	4.47	3.98
D(3,2)	8.97 µm	D[v,.60]	22.28	Number	3.55	2.14	6.16
D(3,1)	6.59 µm	D[v,.70]	26.13				
D(3,0)	5.36 µm	D[v,.80]	29.57				
		D[v,.90]	34.08				
D(2,1)	4.84 µm	D[v,.99]	44.94	Source =Data:p30v005			
D(2,0)	4.14 µm			Record 15			
		Span	2.60				
D(1,0)	3.55 µm	Unif.	0.93				

1598 pil lDR459 / 0/ 0/0.00/1.00/
30% W/W salt Soln
1000 rpm

000000388

30% w/w and 0.06% v/v

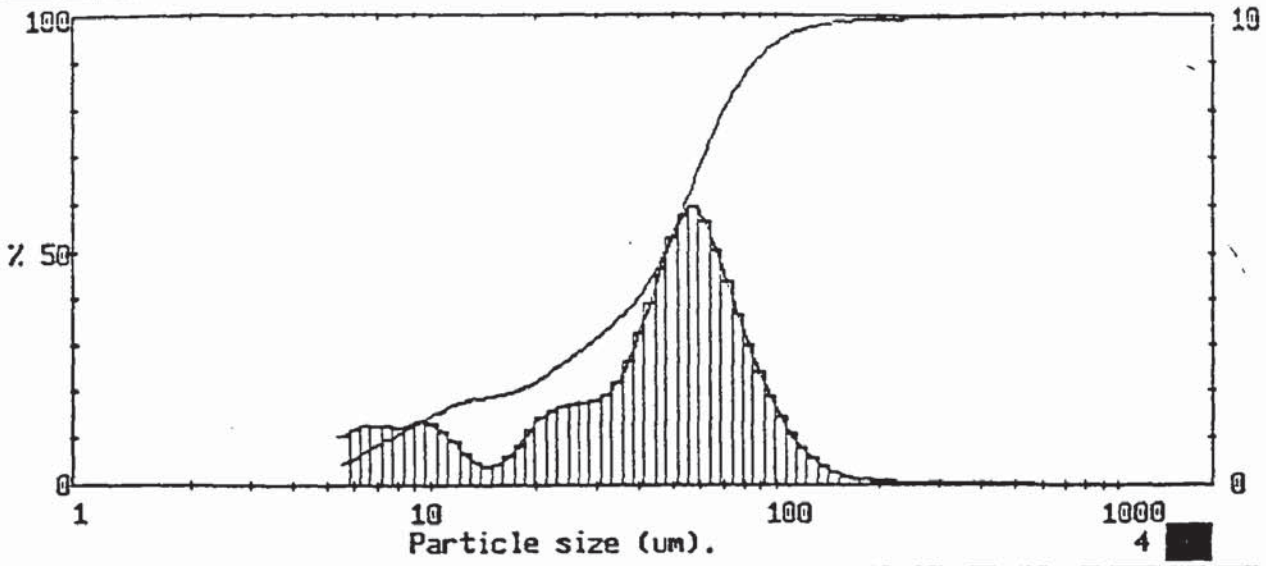

1598 pil 1DR459 / 0/ 0/0.00/1.00/
30% W/W salt Soln
500 rpm

000000305

MALVERN Series 2600 SB.20 Master Mode 26 Feb 1998 10:26 am

High Size	Under %	High Size	Under %	High Size	Under %	High Size	Under %	High Size	Under %	High Size	Under %	Span 1.66
564	100	254	99.5	114	96.7	51.3	56.3	23.1	25.3	10.4	15.5	D[4,3] 48.95µm
524	100	236	99.4	106	95.6	47.7	51.0	21.4	23.7	9.64	14.2	
488	99.9	219	99.4	98.6	94.1	44.4	46.4	19.9	22.2	8.97	12.8	D[3,2] 19.28µm
454	99.9	204	99.3	91.7	92.2	41.2	42.4	18.5	21.0	8.34	11.5	
422	99.8	190	99.2	85.3	89.8	38.4	39.1	17.2	20.2	7.76	10.3	D[v,0.9] 85.73µm
392	99.8	176	99.1	79.3	86.8	35.7	36.5	16.0	19.6	7.21	9.0	
365	99.7	164	98.9	73.8	83.1	33.2	34.3	14.9	19.1	6.71	7.7	D[v,0.1] 7.64µm
339	99.7	153	98.7	68.6	78.8	30.8	32.3	13.9	18.7	6.24	6.4	
315	99.6	142	98.5	63.8	73.7	28.7	30.5	12.9	18.2	5.80	5.2	
293	99.6	132	98.1	59.3	68.1	26.7	28.7	12.0	17.6			
273	99.6	123	97.5	55.2	62.1	24.8	27.0	11.2	16.6			

Source = Data:p30v006	Beam length = 14.3 mm	Model indp	D[v,0.5] 46.99µm
Record No. = 2	Log. Diff. = 4.171		
Focal length = 300 mm	Obscuration = 0.2727	Volume Conc. = 0.0143%	Shape OFF
Presentation = pil	Volume distribution	Sp.S.A 0.3113 m²/cc.	

1598 pil 1DR459 / 0/ 0/0.00/1.00/
30% W/W salt Soln
500 rpm

000000305

MALVERN Series 2600 SB.20 Master Mode 26 Feb 1998 10:26 am

Particle diameters		Volume percentiles	
D(4,3)	48.95 µm	D[v,.10]	7.64
D(4,2)	30.72 µm	D[v,.20]	16.93
D(4,1)	17.91 µm	D[v,.30]	28.11
D(4,0)	12.07 µm	D[v,.40]	39.15
		D[v,.50]	46.99
D(3,2)	19.28 µm	D[v,.60]	53.75
D(3,1)	10.83 µm	D[v,.70]	60.77
D(3,0)	7.57 µm	D[v,.80]	69.92
		D[v,.90]	85.73
D(2,1)	6.09 µm	D[v,.99]	169.23
D(2,0)	4.74 µm		
		Span	1.66
D(1,0)	3.69 µm	Unif.	0.55

Distribution Moments.			
Distbn	Mean	Stan.Dev.	Skewness
Volume	48.95	39.90	3.97
Surface	19.28	23.92	2.68
Length	6.09	8.96	5.63
Number	3.69	2.97	10.82

Source =Data:p30v006
Record 2

1598 pil 1DR459 / 0/ 0/0.00/1.00/
30% W/W salt Soln
500 rpm

000000305

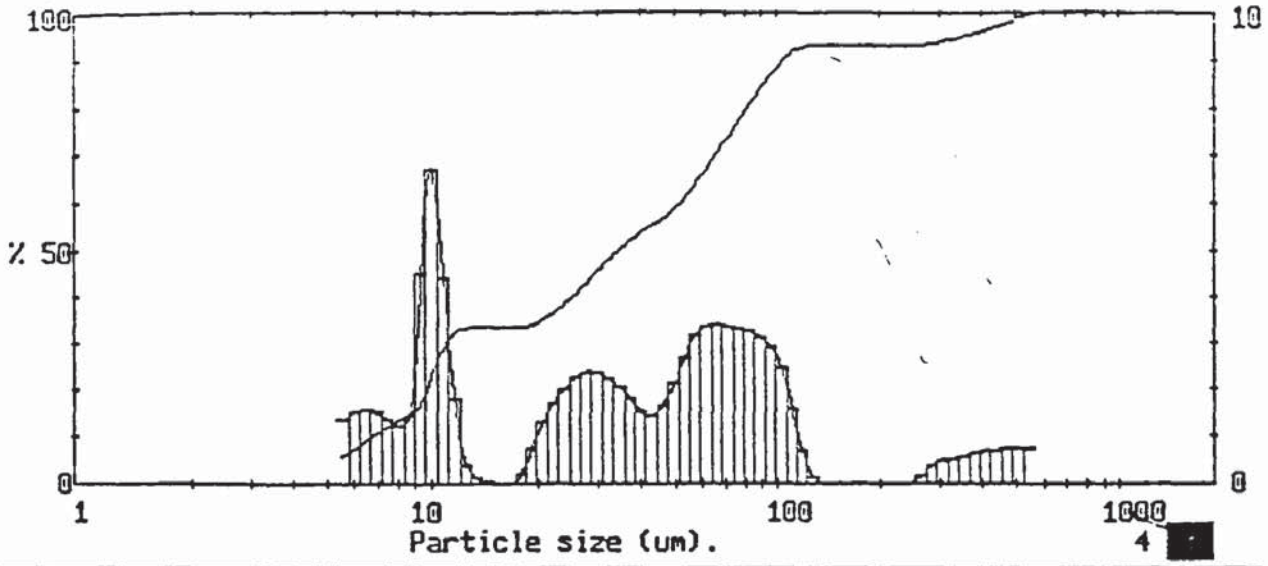

1598 pil 1DR459 / 0/ 0/0.00/1.00/
30% W/W salt Soln
600 rpm

000000313

MALVERN Series 2600 SB.20 Master Mode 26 Feb 1998 9:37 am

High Size	Under %	High Size	Under %	High Size	Under %	High Size	Under %	High Size	Under %	High Size	Under %	Span 2.80
564	100	254	93.5	114	92.6	51.3	59.8	23.1	37.6	10.4	26.8	D[4,3] 64.10µm
524	99.2	236	93.5	106	91.0	47.7	57.7	21.4	35.9	9.64	20.1	
488	98.5	219	93.5	98.6	88.6	44.4	56.0	19.9	34.6	8.97	15.5	
454	97.7	204	93.5	91.7	85.6	41.2	54.5	18.5	33.8	8.34	14.1	D[3,2] 15.06µm
422	97.0	190	93.5	85.3	82.5	38.4	52.9	17.2	33.6	7.76	12.8	
392	96.3	176	93.5	79.3	79.2	35.7	51.1	16.0	31.6	7.21	11.4	
365	95.7	164	93.5	73.8	75.9	33.2	49.1	14.9	31.6	6.71	9.9	D[v,0.9] 102.62µm
339	95.1	153	93.5	68.6	72.5	30.8	46.8	13.9	31.6	6.24	8.3	
315	94.5	142	93.5	63.8	69.1	28.7	44.4	12.9	33.4	5.80	6.8	
293	94.0	132	93.5	59.3	65.7	26.7	42.0	12.0	33.0			D[v,0.1] 6.74µm
273	93.7	123	93.3	55.2	62.5	24.8	39.7	11.2	31.2			

Source = Data:p30v006	Beam length = 14.3 mm	Model indp	D[v,0.5] 34.25µm
Record No. = 5	Log. Diff. = 3.700		
Focal length = 300 mm	Obscuration = 0.2963	Volume Conc. = 0.0123%	Shape OFF
Presentation = pil	Volume distribution	Sp.S.A 0.3983 m²/cc.	

1598 pil 1DR459 / 0/ 0/0.00/1.00/
30% W/W salt Soln
600 rpm

000000313

MALVERN Series 2600 SB.20 Master Mode 26 Feb 1998 9:37 am

Particle diameters		Volume percentiles		Distribution Moments.			
D(4,3)	64.10 µm	D[v,.10]	6.74	Distbn	Mean	Stan.Dev.	Skewness
D(4,2)	31.08 µm	D[v,.20]	9.64				
D(4,1)	17.66 µm	D[v,.30]	10.87	Volume	64.10	98.98	3.22
D(4,0)	12.02 µm	D[v,.40]	25.06	Surface	15.06	27.18	8.60
		D[v,.50]	34.25	Length	5.70	7.31	11.30
D(3,2)	15.06 µm	D[v,.60]	51.57	Number	3.79	2.69	9.69
D(3,1)	9.27 µm	D[v,.70]	64.99				
D(3,0)	6.88 µm	D[v,.80]	80.72				
		D[v,.90]	102.62				
D(2,1)	5.70 µm	D[v,.99]	513.15	Source =Data:p30v006			
D(2,0)	4.65 µm			Record 5			
		Span	2.80				
D(1,0)	3.79 µm	Unif.	1.46				

1598 pil 1DR459 / 0/ 0/0.00/1.00/
30% W/W salt Soln
600 rpm

000000313

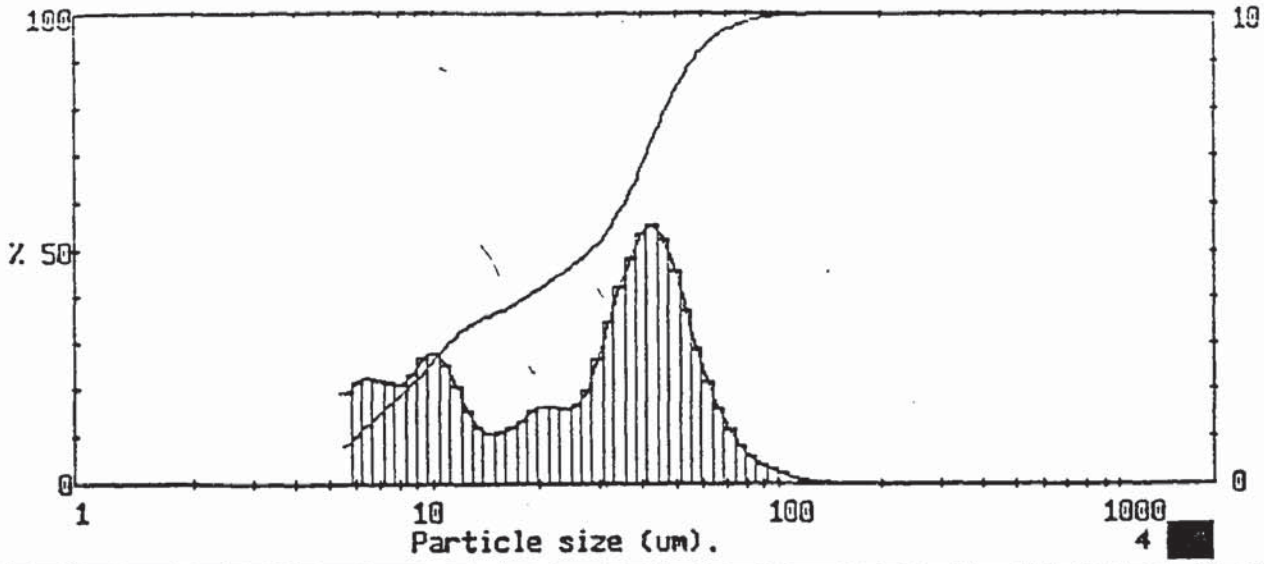

1598 pil lDR459 / 0/ 0/0.00/1.00/
30% W/W salt Soln
700 rpm

000000307

MALVERN Series 2600 SB.20 Master Mode 26 Feb 1998 1:11 pm

High Size	Under %	High Size	Under %	High Size	Under %	High Size	Under %	High Size	Under %	High Size	Under %	Span 1.73
564	100	254	100	114	99.8	51.3	85.9	23.1	44.8	10.4	27.9	D[4,3] 29.22µm
524	100	236	100	106	99.7	47.7	81.3	21.4	43.2	9.64	25.1	
488	100	219	100	98.6	99.5	44.4	76.1	19.9	41.6	8.97	22.4	D[3,2] 12.45µm
454	100	204	100	91.7	99.2	41.2	70.5	18.5	40.0	8.34	20.1	
422	100	190	100	85.3	98.8	38.4	65.2	17.2	38.7	7.76	18.0	D[v,0.9] 55.64µm
392	100	176	100	79.3	98.2	35.7	60.4	16.0	37.5	7.21	15.8	
365	100	164	100	73.8	97.4	33.2	56.2	14.9	36.4	6.71	13.6	D[v,0.1] 5.97µm
339	100	153	100	68.6	96.3	30.8	52.7	13.9	35.3	6.24	11.3	
315	100	142	100	63.8	94.6	28.7	50.1	12.9	34.2	5.80	9.2	D[v,0.5] 28.63µm
293	100	132	99.9	59.3	92.5	26.7	48.1	12.0	32.6			
273	100	123	99.9	55.2	89.6	24.8	46.4	11.2	30.5			Shape OFF

Source = Data:p30v006	Beam length = 14.3 mm	Model indp
Record No. = 7	Log. Diff. = 3.450	
Focal length = 300 mm	Obscuration = 0.4443	Volume Conc. = 0.0171%
Presentation = pil	Volume distribution	Sp.S.A 0.4817 m²/cc.

1598 pil lDR459 / 0/ 0/0.00/1.00/
30% W/W salt Soln
700 rpm

000000307

MALVERN Series 2600 SB.20 Master Mode 26 Feb 1998 1:11 pm

Particle diameters		Volume percentiles		Distribution Moments.			
D(4,3)	29.22 µm	D[v,.10]	5.97	Distbn	Mean	Stan.Dev.	Skewness
D(4,2)	19.08 µm	D[v,.20]	8.31				
D(4,1)	12.51 µm	D[v,.30]	10.99	Volume	29.22	21.20	0.82
D(4,0)	9.20 µm	D[v,.40]	18.53	Surface	12.45	14.45	2.15
		D[v,.50]	28.63	Length	5.38	6.17	5.06
D(3,2)	12.45 µm	D[v,.60]	35.46	Number	1.66	2.51	8.06
D(3,1)	8.19 µm	D[v,.70]	40.95				
D(3,0)	6.26 µm	D[v,.80]	46.81				
		D[v,.90]	55.64				
D(2,1)	5.38 µm	D[v,.99]	88.57				
D(2,0)	4.44 µm						
		Span	1.74				
D(1,0)	3.66 µm	Unif.	0.62				

Source =Data:p30v006
Record 7

1598 pil lDR459 / 0/ 0/0.00/1.00/
30% W/W salt Soln
700 rpm

000000307

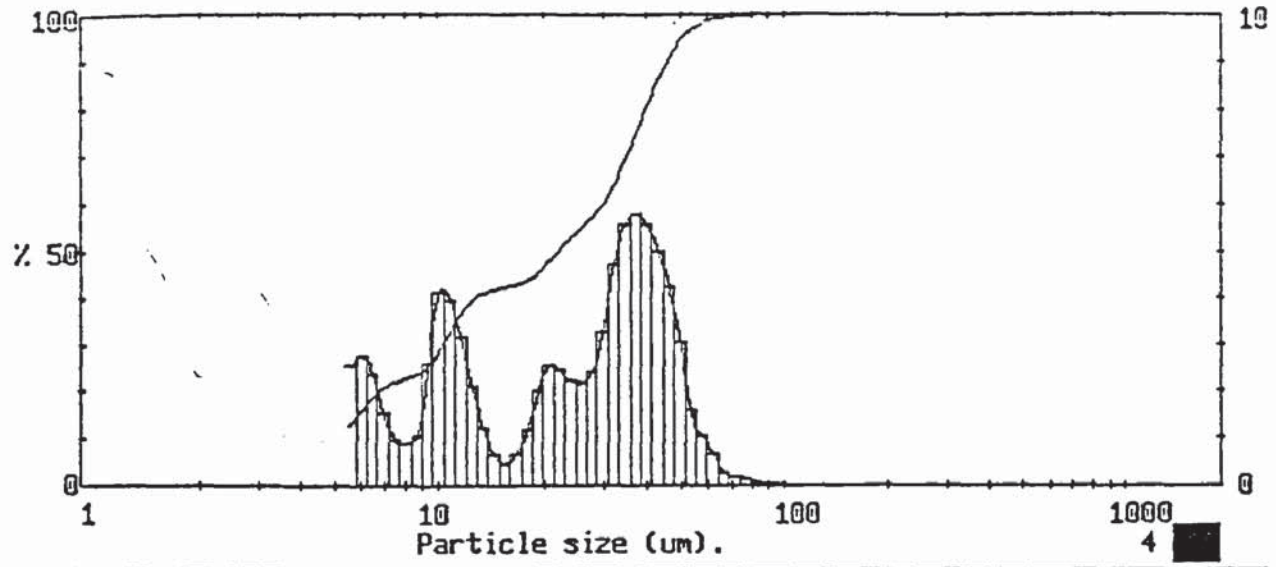

1598 pil 1DR459 / 0/ 0/0.00/1.00/
30% W/W salt Soln
800 rpm

000000308

MALVERN Series 2600 SB.20 Master Mode 26 Feb 1998 1:34 pm

High Size	Under %	High Size	Under %	High Size	Under %	High Size	Under %	High Size	Under %	High Size	Under %	Span 1.84
564	100	254	100	114	100	51.3	96.0	23.1	51.8	10.4	31.2	D[4,3] 23.53µm
524	100	236	100	106	100	47.7	92.9	21.4	49.3	9.64	27.1	
488	100	219	100	98.6	100	44.4	88.7	19.9	46.7	8.97	24.5	
454	100	204	100	91.7	99.9	41.2	83.7	18.5	44.7	8.34	23.4	D[3,2] 10.13µm
422	100	190	100	85.3	99.9	38.4	78.1	17.2	43.5	7.76	22.5	
392	100	176	100	79.3	99.9	35.7	72.2	16.0	42.8	7.21	21.5	
365	100	164	100	73.8	99.7	33.2	66.7	14.9	42.4	6.71	20.0	D[v,0.9] 45.30µm
339	100	153	100	68.6	99.5	30.8	61.9	13.9	41.7	6.24	17.6	
315	100	142	100	63.8	99.3	28.7	58.6	12.9	40.5	5.80	14.8	
293	100	132	100	59.3	98.6	26.7	56.2	12.0	38.4			D[v,0.1] 5.03µm
273	100	123	100	55.2	97.6	24.8	54.0	11.2	35.2			

Source = Data:p30v006	Beam length = 14.3 mm	Model indp	D[v,0.5] 21.88µm
Record No. = 9	Log. Diff. = 3.379		
Focal length = 300 mm	Obscuration = 0.5639	Volume Conc. = 0.0196%	Shape OFF
Presentation = pil	Volume distribution	Sp.S.A 0.5925 m²/cc.	

1598 pil 1DR459 / 0/ 0/0.00/1.00/
30% W/W salt Soln
800 rpm

000000308

MALVERN Series 2600 SB.20 Master Mode 26 Feb 1998 1:34 pm

Particle diameters		Volume percentiles	
D(4,3)	23.53 µm	D[v,.10]	5.03
D(4,2)	15.43 µm	D[v,.20]	6.71
D(4,1)	10.35 µm	D[v,.30]	10.16
D(4,0)	7.84 µm	D[v,.40]	12.63
		D[v,.50]	21.88
D(3,2)	10.13 µm	D[v,.60]	29.70
D(3,1)	6.86 µm	D[v,.70]	34.66
D(3,0)	5.43 µm	D[v,.80]	39.31
		D[v,.90]	45.30
D(2,1)	4.65 µm	D[v,.99]	61.54
D(2,0)	3.98 µm		
		Span	1.84
D(1,0)	3.40 µm	Unif.	0.66

Distribution Moments.			
Distbn	Mean	Stan.Dev.	Skewness
Volume	23.53	16.52	0.46
Surface	10.13	11.65	2.03
Length	4.65	5.05	5.07
Number	3.40	2.06	8.88

Source =Data:p30v006
Record 9

1598 pil 1DR459 / 0/ 0/0.00/1.00/
30% W/W salt Soln
800 rpm

000000308

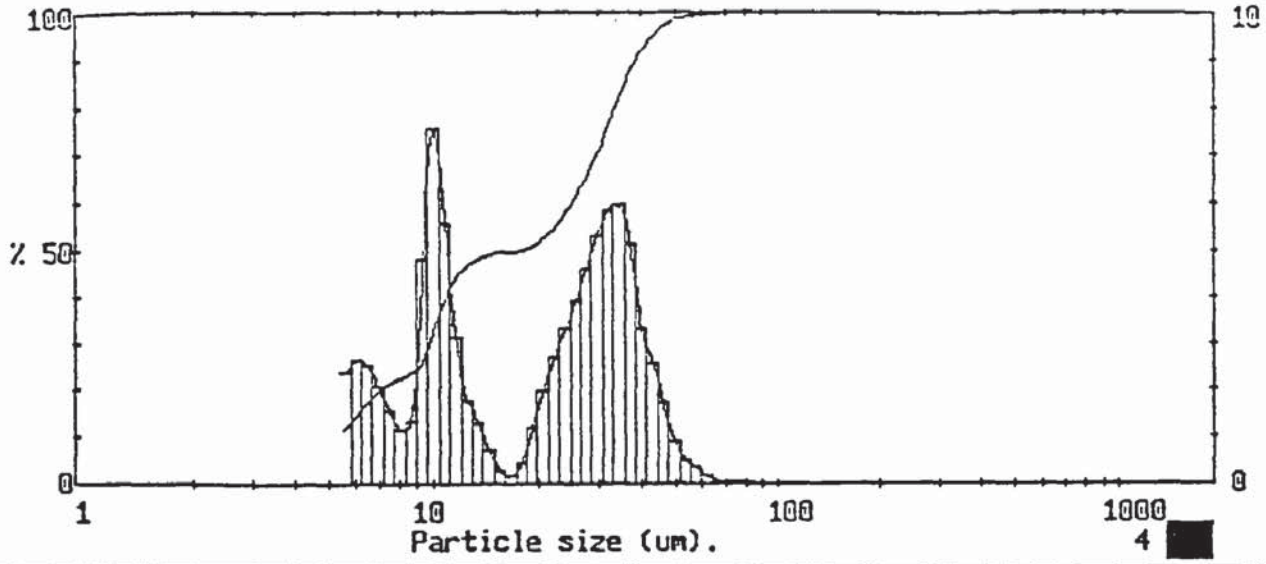

1598 pil 1DR459 / 0/ 0/0.00/1.00/
30% W/W salt Soln
900 rpm

000000309

MALVERN Series 2600 SB.20 Master Mode 26 Feb 1998 1:48 pm

High Size	Under %	High Size	Under %	High Size	Under %	High Size	Under %	High Size	Under %	High Size	Under %	Span 1.82
564	100	254	100	114	100	51.3	98.8	23.1	56.1	10.4	36.9	D[4,3] 20.10µm
524	100	236	100	106	100	47.7	97.9	21.4	53.4	9.64	29.3	
488	100	219	100	98.6	100	44.4	96.2	19.9	51.4	8.97	24.5	D[3,2] 9.86µm
454	100	204	100	91.7	100	41.2	93.6	18.5	50.2	8.34	23.1	
422	100	190	100	85.3	100	38.4	90.3	17.2	49.8	7.76	22.0	
392	100	176	100	79.3	100	35.7	85.2	16.0	49.6	7.21	20.4	D[v,0.9] 38.16µm
365	100	164	100	73.8	99.9	33.2	79.2	14.9	49.3	6.71	18.4	
339	100	153	100	68.6	99.9	30.8	73.3	13.9	48.6	6.24	15.8	
315	100	142	100	63.8	99.8	28.7	68.0	12.9	47.4	5.80	13.2	D[v,0.1] 5.25µm
293	100	132	100	59.3	99.6	26.7	63.4	12.0	45.6			
273	100	123	100	55.2	99.3	24.8	59.5	11.2	42.4			

Source = Data:p30v006	Beam length = 14.3 mm	Model indp	D[v,0.5] 18.10µm
Record No. = 11	Log. Diff. = 3.490		
Focal length = 300 mm	Obscuration = 0.6221	Volume Conc. = 0.0224%	Shape OFF
Presentation = pil	Volume distribution	Sp.S.A 0.6083 m²/cc.	

1598 pil 1DR459 / 0/ 0/0.00/1.00/
30% W/W salt Soln
900 rpm

000000309

MALVERN Series 2600 SB.20 Master Mode 26 Feb 1998 1:48 pm

Particle diameters		Volume percentiles	
D(4,3)	20.10 µm	D[v,.10]	5.25
D(4,2)	14.08 µm	D[v,.20]	7.09
D(4,1)	9.95 µm	D[v,.30]	9.72
D(4,0)	7.69 µm	D[v,.40]	10.75
		D[v,.50]	18.10
D(3,2)	9.86 µm	D[v,.60]	25.07
D(3,1)	7.00 µm	D[v,.70]	29.50
D(3,0)	5.59 µm	D[v,.80]	33.49
		D[v,.90]	38.16
D(2,1)	4.97 µm	D[v,.99]	52.63
D(2,0)	4.20 µm		
		Span	1.82
D(1,0)	3.56 µm	Unif.	0.67

Distribution Moments.			
Distbn	Mean	Stan.Dev.	Skewness
Volume	20.10	13.77	0.52
Surface	9.86	10.05	1.88
Length	4.97	4.93	4.17
Number	3.56	2.24	6.71

Source =Data:p30v006
Record 11

1598 pil 1DR459 / 0/ 0/0.00/1.00/
30% W/W salt Soln
900 rpm

000000309

30% w/w and 0.07% v/v

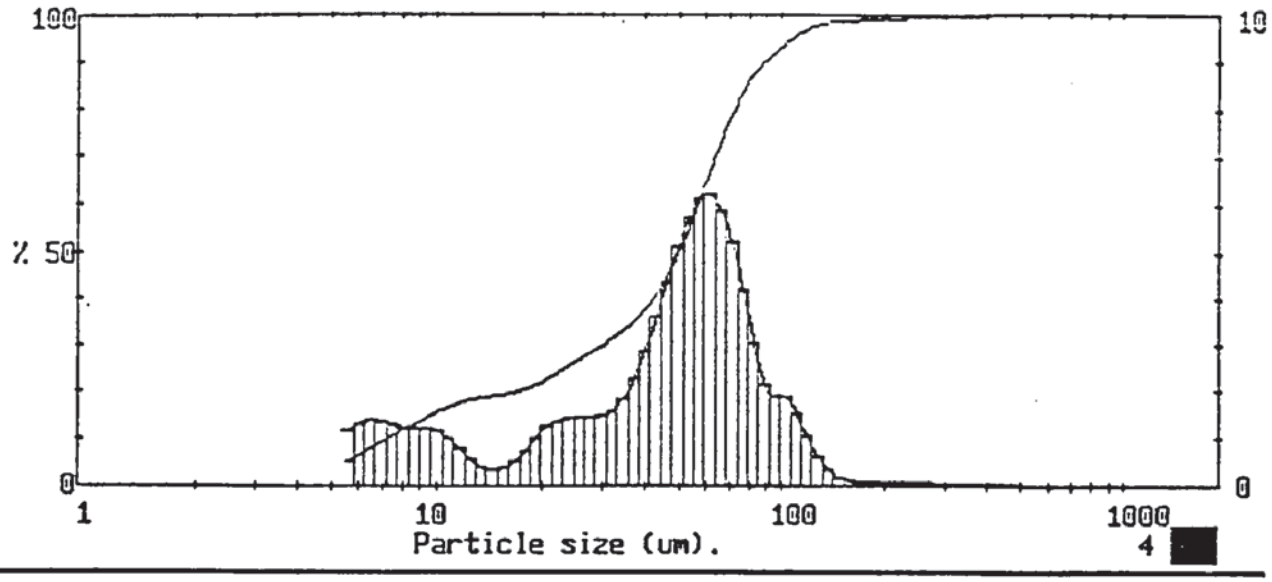

1598 pil lDR459 / 0/ 0/0.00/1.00/
30% W/W salt Soln
500 rpm

000000301

MALVERN Series 2600 SB.20 Master Mode 27 Feb 1998 1:29 pm

High Size	Under %	High Size	Under %	High Size	Under %	High Size	Under %	High Size	Under %	High Size	Under %	Span 1.63
564	100	254	99.6	114	96.6	51.3	52.5	23.1	24.8	10.4	16.3	D[4,3] 50.26µm
524	100	236	99.5	106	95.0	47.7	47.4	21.4	23.4	9.64	15.1	
488	100	219	99.4	98.6	93.1	44.4	43.0	19.9	22.2	8.97	13.9	
454	99.9	204	99.3	91.7	91.2	41.2	39.4	18.5	21.1	8.34	12.6	D[3,2] 18.73µm
422	99.9	190	99.2	85.3	89.0	38.4	36.5	17.2	20.4	7.76	11.4	
392	99.9	176	99.1	79.3	86.0	35.7	34.2	16.0	19.9	7.21	10.1	
365	99.8	164	99.0	73.8	81.8	33.2	32.3	14.9	19.5	6.71	8.7	D[v,0.9] 87.87µm
339	99.8	153	98.9	68.6	76.5	30.8	30.7	13.9	19.1	6.24	7.3	
315	99.8	142	98.7	63.8	70.6	28.7	29.2	12.9	18.7	5.80	6.0	
293	99.7	132	98.3	59.3	64.4	26.7	27.7	12.0	18.2			D[v,0.1] 7.19µm
273	99.6	123	97.7	55.2	58.2	24.8	26.3	11.2	17.4			

Source = Data:p30v007	Beam length = 14.3 mm	Model indp	D[v,0.5] 49.58µm
Record No. = 3	Log. Diff. = 4.161		
Focal length = 300 mm	Obscuration = 0.3057	Volume Conc. = 0.0159%	
Presentation = pil	Volume distribution	Sp.S.A 0.3204 m²/cc.	Shape OFF

1598 pil lDR459 / 0/ 0/0.00/1.00/
30% W/W salt Soln
500 rpm

000000301

MALVERN Series 2600 SB.20 Master Mode 27 Feb 1998 1:29 pm

Particle diameters		Volume percentiles		Distribution Moments.			
				Distbn	Mean	Stan.Dev.	Skewness
D(4,3)	50.26 µm	D[v,.10]	7.19				
D(4,2)	30.68 µm	D[v,.20]	16.39				
D(4,1)	17.51 µm	D[v,.30]	29.83	Volume	50.26	38.52	3.13
D(4,0)	11.78 µm	D[v,.40]	41.82	Surface	18.73	24.30	2.46
		D[v,.50]	49.58	Length	5.70	8.62	6.11
D(3,2)	18.73 µm	D[v,.60]	56.33	Number	3.59	2.75	12.23
D(3,1)	10.33 µm	D[v,.70]	63.30				
D(3,0)	7.26 µm	D[v,.80]	71.87				
		D[v,.90]	87.87				
D(2,1)	5.70 µm	D[v,.99]	167.15	Source =Data:p30v007			
D(2,0)	4.52 µm			Record 3			
		Span	1.63				
D(1,0)	3.59 µm	Unif.	0.53				

1598 pil lDR459 / 0/ 0/0.00/1.00/
30% W/W salt Soln
500 rpm

000000301

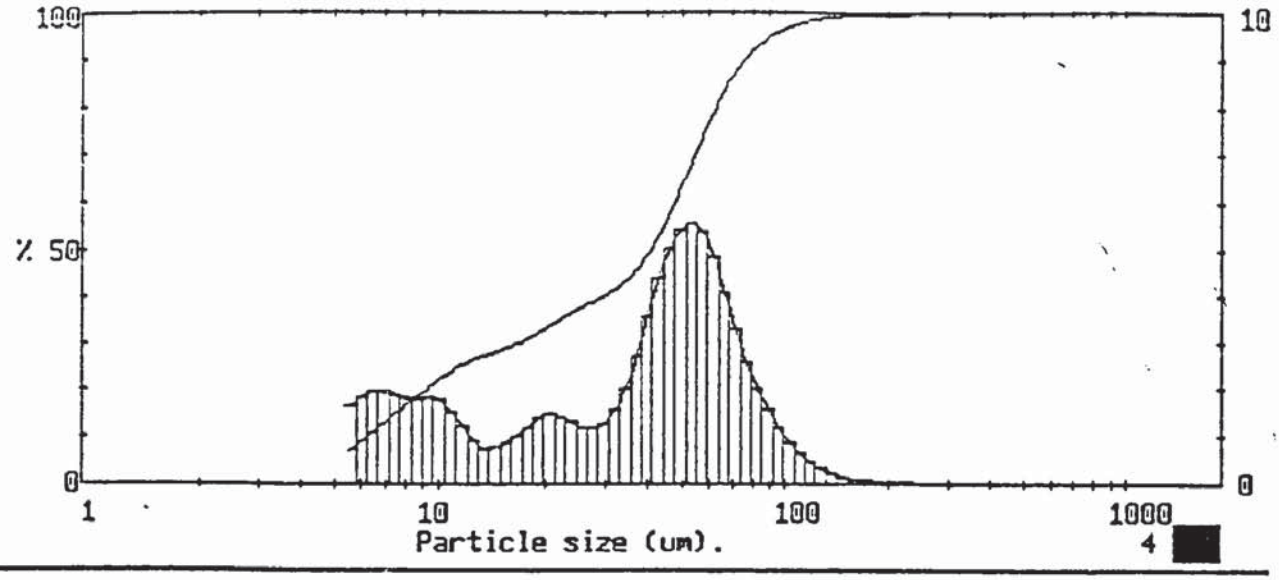

1598 pil 1DR459 / 0/ 0/0.00/1.00/
30% W/W salt Soln
600 rpm

000000302

MALVERN Series 2600 SB.20 Master Mode 27 Feb 1998 2:24 pm

High Size	Under %	High Size	Under %	High Size	Under %	High Size	Under %	High Size	Under %	High Size	Under %	Span 1.70
564	100	254	99.9	114	98.3	51.3	66.0	23.1	36.1	10.4	23.3	D[4,3] 40.03µm
524	100	236	99.9	106	97.7	47.7	60.6	21.4	34.6	9.64	21.5	
488	100	219	99.9	98.6	96.8	44.4	55.5	19.9	33.1	8.97	19.6	D[3,2] 14.50µm
454	100	204	99.8	91.7	95.6	41.2	51.1	18.5	31.7	8.34	17.8	
422	100	190	99.8	85.3	94.0	38.4	47.5	17.2	30.5	7.76	16.0	
392	100	176	99.7	79.3	91.9	35.7	44.7	16.0	29.5	7.21	14.1	D[v,0.9] 75.05µm
365	100	164	99.6	73.8	89.3	33.2	42.6	14.9	28.6	6.71	12.1	
339	99.9	153	99.5	68.6	86.0	30.8	41.1	13.9	27.8	6.24	10.1	
315	99.9	142	99.4	63.8	81.9	28.7	39.8	12.9	27.1	5.80	8.2	D[v,0.1] 6.21µm
293	99.9	132	99.2	59.3	77.0	26.7	38.6	12.0	26.1			
273	99.9	123	98.8	55.2	71.6	24.8	37.4	11.2	24.9			

Source = Data:p30v007	Beam length = 14.3 mm	Model indp	D[v,0.5] 40.44µm
Record No. = 6	Log. Diff. = 3.929		
Focal length = 300 mm	Obscuration = 0.4090	Volume Conc. = 0.0178%	Shape OFF
Presentation = pil	Volume distribution	Sp.S.A 0.4137 m²/cc.	

1598 pil 1DR459 / 0/ 0/0.00/1.00/
30% W/W salt Soln
600 rpm

000000302

MALVERN Series 2600 SB.20 Master Mode 27 Feb 1998 2:24 pm

Particle diameters		Volume percentiles	
D(4,3)	40.03 µm	D[v,.10]	6.21
D(4,2)	24.10 µm	D[v,.20]	9.09
D(4,1)	14.55 µm	D[v,.30]	16.64
D(4,0)	10.25 µm	D[v,.40]	29.07
		D[v,.50]	40.44
D(3,2)	14.50 µm	D[v,.60]	47.32
D(3,1)	8.77 µm	D[v,.70]	54.03
D(3,0)	6.51 µm	D[v,.80]	61.95
		D[v,.90]	75.05
D(2,1)	5.30 µm	D[v,.99]	127.10
D(2,0)	4.36 µm		
		Span	1.70
D(1,0)	3.59 µm	Unif.	0.59

Distribution Moments.

Distbn	Mean	Stan.Dev.	Skewness
Volume	40.03	31.13	2.16
Surface	14.50	19.24	2.55
Length	5.30	6.99	6.32
Number	3.59	2.48	10.69

Source =Data:p30v007
Record 6

1598 pil 1DR459 / 0/ 0/0.00/1.00/
30% W/W salt Soln
600 rpm

000000302

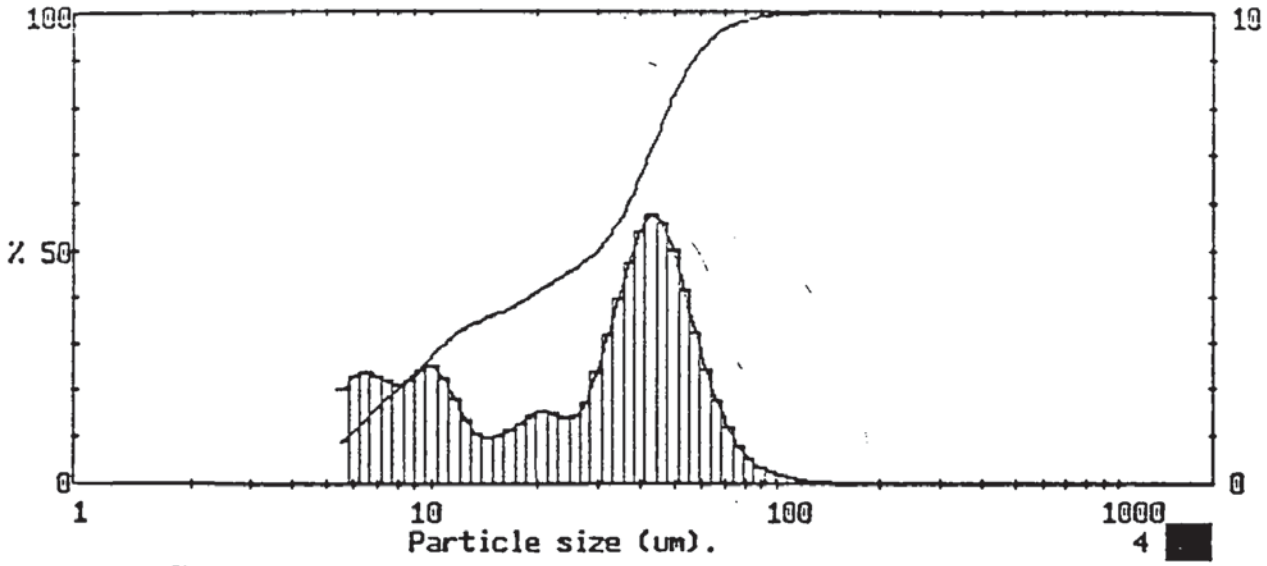

1598 pil 1DR459 / 0/ 0/0.00/1.00/
30% W/W salt Soln
700 rpm

000000303

MALVERN Series 2600 SB.20 Master Mode 27 Feb 1998 2:50 pm

High Size	Under %	High Size	Under %	High Size	Under %	High Size	Under %	High Size	Under %	High Size	Under %	Span 1.69
564	100	254	100	114	99.8	51.3	84.7	23.1	44.1	10.4	28.6	D[4,3] 29.72µm
524	100	236	100	106	99.7	47.7	79.7	21.4	42.6	9.64	26.1	
488	100	219	100	98.6	99.5	44.4	74.1	19.9	41.0	8.97	23.7	D[3,2] 12.15µm
454	100	204	100	91.7	99.2	41.2	68.4	18.5	39.6	8.34	21.5	
422	100	190	100	85.3	98.8	38.4	63.0	17.2	38.3	7.76	19.4	D[v,0.9] 56.48µm
392	100	176	100	79.3	98.3	35.7	58.2	16.0	37.1	7.21	17.2	
365	100	164	100	73.8	97.5	33.2	54.2	14.9	36.1	6.71	14.8	D[v,0.1] 5.78µm
339	100	153	100	68.6	96.3	30.8	51.0	13.9	35.1	6.24	12.4	
315	100	142	100	63.8	94.5	28.7	48.7	12.9	34.1	5.80	10.1	
293	100	132	99.9	59.3	92.1	26.7	46.9	12.0	32.7			
273	100	123	99.9	55.2	88.9	24.8	45.5	11.2	30.9			

Source = Data:p30v007	Beam length = 14.3 mm	Model indp	D[v,0.5] 29.96µm
Record No. = 8	Log. Diff. = 3.439		
Focal length = 300 mm	Obscuration = 0.5555	Volume Conc. = 0.0230%	
Presentation = pil	Volume distribution	Sp.S.A 0.4939 m²/cc.	Shape OFF

1598 pil 1DR459 / 0/ 0/0.00/1.00/
30% W/W salt Soln
700 rpm

000000303

MALVERN Series 2600 SB.20 Master Mode 27 Feb 1998 2:50 pm

Particle diameters		Volume percentiles		Distribution Moments.			
				Distbn	Mean	Stan.Dev.	Skewness
D(4,3)	29.72 µm	D[v,.10]	5.78				
D(4,2)	19.00 µm	D[v,.20]	7.93	Volume	29.72	21.54	0.74
D(4,1)	12.30 µm	D[v,.30]	10.83	Surface	12.15	14.61	2.18
D(4,0)	9.04 µm	D[v,.40]	18.98	Length	5.16	6.00	5.39
		D[v,.50]	29.96	Number	3.58	2.37	8.81
D(3,2)	12.15 µm	D[v,.60]	36.71				
D(3,1)	7.92 µm	D[v,.70]	42.10				
D(3,0)	6.08 µm	D[v,.80]	47.88				
		D[v,.90]	56.48				
D(2,1)	5.16 µm	D[v,.99]	87.65				
D(2,0)	4.30 µm			Source =Data:p30v007			
		Span	1.69	Record 8			
D(1,0)	3.58 µm	Unif.	0.61				

1598 pil 1DR459 / 0/ 0/0.00/1.00/
30% W/W salt Soln
700 rpm

000000303

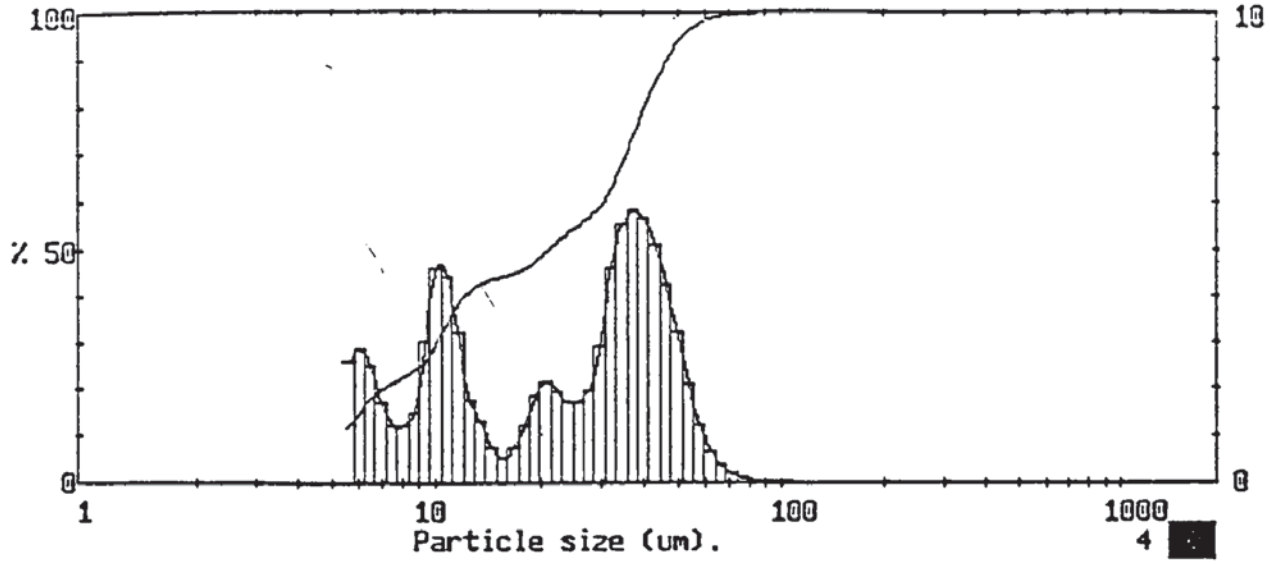

1598 pil 1DR459 / 0/ 0/0.00/1.00/
30% W/W salt Soln
800 rpm

000000304

MALVERN Series 2600 SB.20 Master Mode 27 Feb 1998 3:26 pm

High Size	Under %	High Size	Under %	High Size	Under %	High Size	Under %	High Size	Under %	High Size	Under %	Span 1.94
564	100	254	100	114	100	51.3	95.1	23.1	52.4	10.4	32.5	D[4,3] 23.69µm
524	100	236	100	106	100	47.7	91.8	21.4	50.4	9.64	27.9	
488	100	219	100	98.6	100	44.4	87.6	19.9	48.3	8.97	24.8	
454	100	204	100	91.7	99.9	41.2	82.5	18.5	46.4	8.34	23.3	D[3,2] 10.28µm
422	100	190	100	85.3	99.9	38.4	76.8	17.2	45.2	7.76	22.1	
392	100	176	100	79.3	99.8	35.7	71.0	16.0	44.5	7.21	20.8	
365	100	164	100	73.8	99.7	33.2	65.5	14.9	43.9	6.71	19.1	D[v,0.9] 46.13µm
339	100	153	100	68.6	99.5	30.8	60.8	13.9	43.2	6.24	16.5	
315	100	142	100	63.8	99.1	28.7	57.9	12.9	41.9	5.80	13.7	
293	100	132	100	59.3	98.4	26.7	55.9	12.0	40.1			D[v,0.1] 5.22µm
273	100	123	100	55.2	97.2	24.8	54.2	11.2	36.9			

Source = Data:p307007	Beam length = 14.3 mm	Model indp	D[v,0.5] 21.13µm
Record No. = 9	Log. Diff. = 3.266		
Focal length = 300 mm	Obscuration = 0.6297	Volume Conc. = 0.0238%	
Presentation = pil	Volume distribution	Sp.S.A 0.5838 m²/cc.	Shape OFF

1598 pil 1DR459 / 0/ 0/0.00/1.00/
30% W/W salt Soln
800 rpm

000000304

MALVERN Series 2600 SB.20 Master Mode 27 Feb 1998 3:26 pm

Particle diameters		Volume percentiles	
D(4,3)	23.69 µm	D[v,.10]	5.22
D(4,2)	15.61 µm	D[v,.20]	6.94
D(4,1)	10.52 µm	D[v,.30]	9.99
D(4,0)	7.97 µm	D[v,.40]	11.96
		D[v,.50]	21.13
D(3,2)	10.28 µm	D[v,.60]	30.34
D(3,1)	7.01 µm	D[v,.70]	35.23
D(3,0)	5.55 µm	D[v,.80]	39.94
		D[v,.90]	46.13
D(2,1)	4.79 µm	D[v,.99]	62.83
D(2,0)	4.07 µm		
		Span	1.94
D(1,0)	3.47 µm	Unif.	0.70

Distribution Moments.			
Distbn	Mean	Stan.Dev.	Skewness
Volume	23.69	16.93	0.50
Surface	10.23	11.74	2.09
Length	4.79	5.13	5.04
Number	3.47	2.14	8.32

Source =Data:p307007
Record 9

1598 pil 1DR459 / 0/ 0/0.00/1.00/
30% W/W salt Soln
800 rpm

000000304

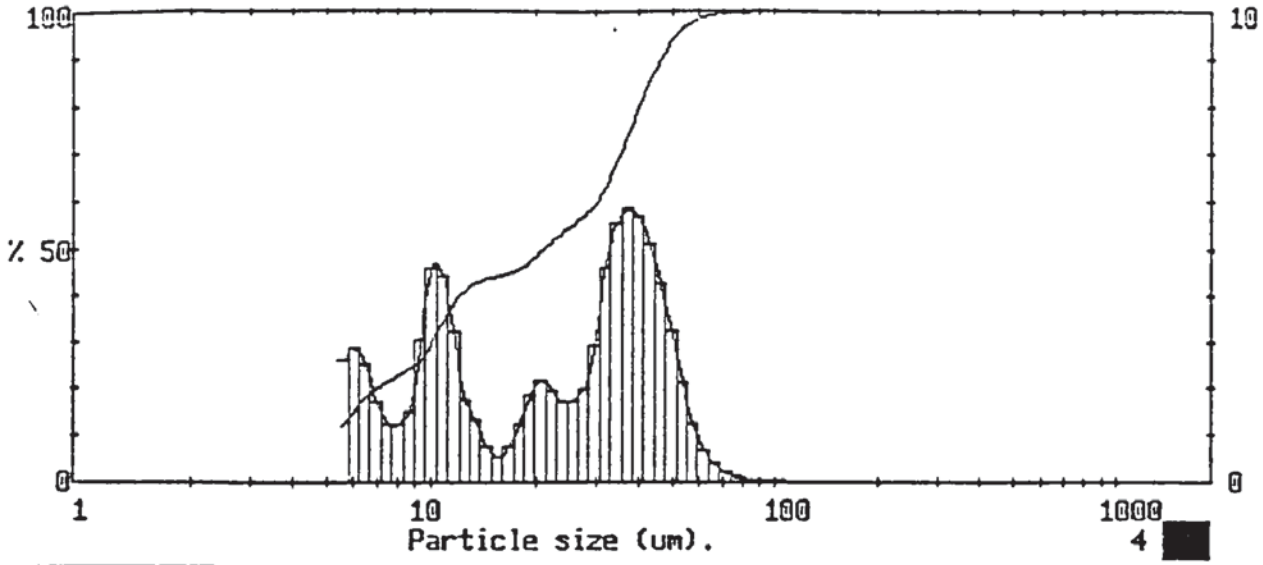

1598 pil lDR459 / 0/ 0/0.00/1.00/
30% W/W salt Soln
900 rpm

00000304

MALVERN Series 2600 SB.20 Master Mode 27 Feb 1998 3:26 pm

High Size	Under %	High Size	Under %	High Size	Under %	High Size	Under %	High Size	Under %	High Size	Under %	Span 1.94
564	100	254	100	114	100	51.3	95.1	23.1	52.4	10.4	32.5	D[4,3] 23.69µm
524	100	236	100	106	100	47.7	91.8	21.4	50.4	9.64	27.9	
488	100	219	100	98.6	100	44.4	87.6	19.9	48.3	8.97	24.8	D[3,2] 10.28µm
454	100	204	100	91.7	99.9	41.2	82.5	18.5	46.4	8.34	23.3	
422	100	190	100	85.3	99.9	38.4	76.8	17.2	45.2	7.76	22.1	D[v,0.9] 46.13µm
392	100	176	100	79.3	99.8	35.7	71.0	16.0	44.5	7.21	20.8	
365	100	164	100	73.8	99.7	33.2	65.5	14.9	43.9	6.71	19.1	D[v,0.1] 5.22µm
339	100	153	100	68.6	99.5	30.8	60.8	13.9	43.2	6.24	16.5	
315	100	142	100	63.8	99.1	28.7	57.9	12.9	41.9	5.80	13.7	
293	100	132	100	59.3	98.4	26.7	55.9	12.0	40.1			
273	100	123	100	55.2	97.2	24.8	54.2	11.2	36.9			

Source = Data:p30v007	Beam length = 14.3 mm	Model indp	D[v,0.5] 21.13µm
Record No. = 9	Log. Diff. = 3.266		
Focal length = 300 mm	Obscuration = 0.6297	Volume Conc. = 0.0238%	
Presentation = pil	Volume distribution	Sp.S.A 0.5838 m²/cc.	Shape OFF

1598 pil lDR459 / 0/ 0/0.00/1.00/
30% W/W salt Soln
900 rpm

00000304

MALVERN Series 2600 SB.20 Master Mode 27 Feb 1998 3:26 pm

Particle diameters		Volume percentiles	
D(4,3)	23.69 µm	D[v,.10]	5.22
D(4,2)	15.61 µm	D[v,.20]	6.94
D(4,1)	10.52 µm	D[v,.30]	9.99
D(4,0)	7.97 µm	D[v,.40]	11.96
		D[v,.50]	21.13
D(3,2)	10.28 µm	D[v,.60]	30.34
D(3,1)	7.01 µm	D[v,.70]	35.23
D(3,0)	5.55 µm	D[v,.80]	39.94
		D[v,.90]	46.13
D(2,1)	4.79 µm	D[v,.99]	62.83
D(2,0)	4.07 µm		
		Span	1.94
D(1,0)	3.47 µm	Unif.	0.70

Distribution Moments.			
Distbn	Mean	Stan.Dev.	Skewness
Volume	23.69	16.93	0.50
Surface	10.28	11.74	2.09
Length	4.79	5.13	5.04
Number	3.47	2.14	8.32

Source =Data:p30v007
Record 9

1598 pil lDR459 / 0/ 0/0.00/1.00/
30% W/W salt Soln
900 rpm

00000304

Appendix 7

Calculation of the power input per unit mass , ε , and the eddies length scale, respectively,

$$N_p = \frac{P}{\rho_c N^3 D^5}$$

Where

$$\varepsilon = \frac{P}{V_T \rho_c}$$

$$Eddy\ length = \left[\left(\frac{\mu_c}{\rho_c}\right)^3 / \varepsilon\right]^{\frac{1}{4}}$$

Phase Conc.	N (rps)	Re	P (W)	ε (W/kg)	Eddy length μm
20.0	5.0	8933	0.32	0.29	59
20.0	6.6	11911	0.78	0.70	47
20.0	8.3	14889	1.52	1.38	40
20.0	10.0	17866	2.63	2.39	35
20.0	11.6	20844	4.18	3.80	31
20.0	13.3	23822	6.25	5.67	28
20.0	15.0	26800	8.90	8.07	25
20.0	16.6	29778	12.20	11.07	23
25.0	5.0	7636	0.33	0.29	66
25.0	6.6	10182	0.80	0.70	53
25.0	8.3	12728	1.57	1.38	45
25.0	10.0	15273	2.71	2.39	39
25.0	11.6	17819	4.31	3.80	35
25.0	13.3	20364	6.44	5.67	31
25.0	15.0	22910	9.17	8.07	29
25.0	16.6	25456	12.58	11.07	26
30.0	5.0	7203	0.35	0.29	69
30.0	6.6	9604	0.83	0.70	56
30.0	8.3	12004	1.62	1.38	47
30.0	10.0	14406	2.81	2.39	41
30.0	11.6	16806	4.46	3.80	36
30.0	13.3	19208	6.67	5.67	33
30.0	15.0	21609	9.49	8.07	30
30.0	16.6	24009	13.02	11.07	28

Appendix 8

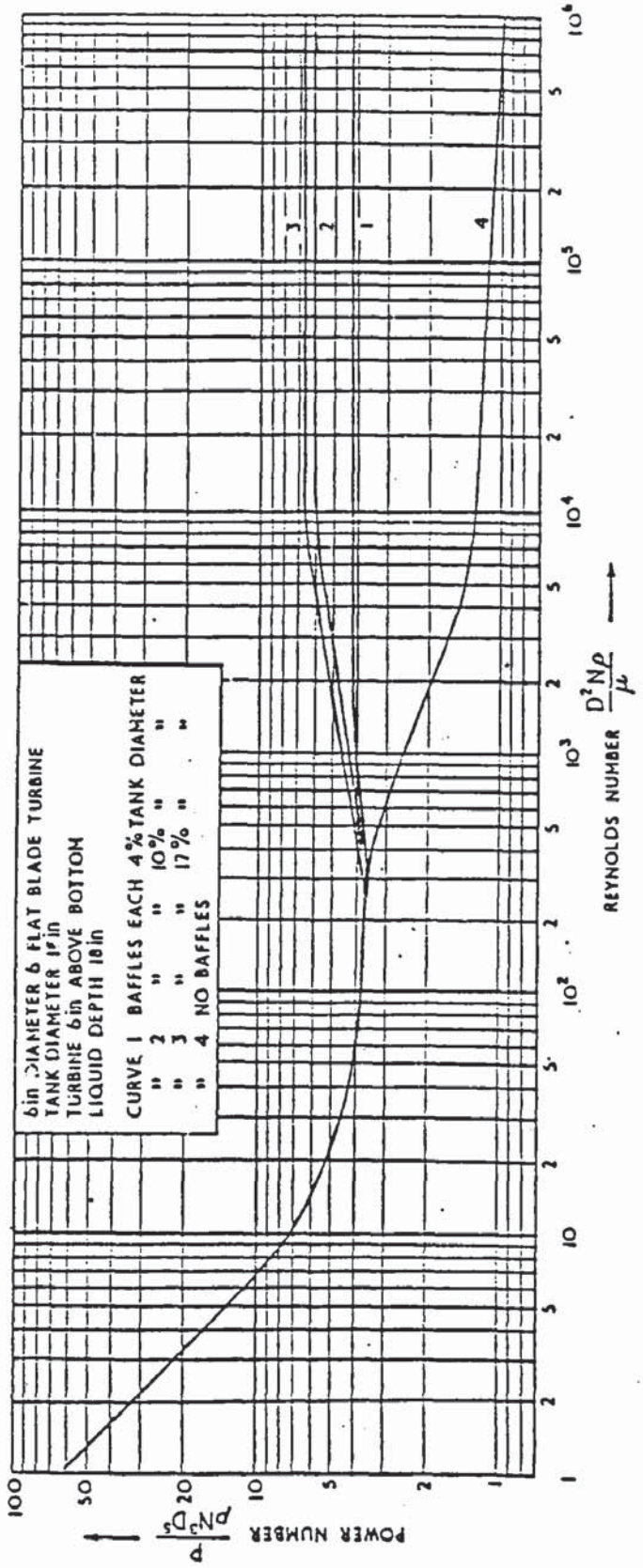

Power number as a function of Reynolds number for a turbine mixer

Publications

1. H. Al-Anzi, I.P.T. Moore (1995) "The Effect of Phase Compositions and Volume Ratios on The Settling Time for Two Aqueous-Phase Dispersions", *CHEMECA 95, 23rd Australasian Chemical Engineering Conference*, Vol. **3**, pp.92-97.

2. H. Al-Anzi, I.P.T. Moore, (1995), *I Chem E Research Event, First European Conference for Young Researchers in Chemical Engineering,* Vol. **2**, pp. 844-846.